UNDERSTANDING AND MODULATING SYNAPTIC DYSFUNCTION IN HUNTINGTON DISEASE

by

Mandi Elizabeth Schmidt

B.Sc., University of Waterloo, 2013

A THESIS SUBMITTED IN PARTIAL FULFILLMENT OF THE REQUIREMENTS FOR THE DEGREE OF

DOCTOR OF PHILOSOPHY

in

THE FACULTY OF GRADUATE AND POSTDOCTORAL STUDIES

(Neuroscience)

THE UNIVERSITY OF BRITISH COLUMBIA

(Vancouver)

October 2019

The following individuals certify that they have read, and recommend to the Faculty of Graduate and Postdoctoral Studies for acceptance, the dissertation entitled:

Understanding and Modulating Synaptic Dysfunction in Huntington Disease

submitted by Mandi Schmidt in partial fulfillment of the requirements for the degree of Doctor of Philosophy in Neuroscience

Examining Committee:

Michael Hayden (Medical Genetics)
Supervisor

Lynn Raymond (Psychiatry)
Supervisory Committee Member

Yu Tian Wang (Neurology)
University Examiner

Filip Van Petegem (Biochemistry and Molecular Biology)
University Examiner

Additional Supervisory Committee Members:

Ann Marie Craig (Psychiatry)
Supervisory Committee Member

Mahmoud Pouladi (Medicine – National University of Singapore)
Supervisory Committee Member

ABSTRACT

Huntington disease (HD) is a devastating neurodegenerative disorder caused by a CAG repeat expansion in the huntingtin gene. Early disrupted cortico-striatal (CS) transmission contributes to neuronal spine and synapse dysfunction primarily in striatal medium spiny neurons (MSNs), the most vulnerable cell type in HD, as well as in cortical neurons. Irreversible neurodegeneration of MSNs occurs with disease progression, leading to motor, cognitive, and psychiatric symptoms. However, synaptic dysfunction and spine loss are hypothesized to be therapeutically reversible before neuronal death occurs. One of the earliest alterations to occur in HD mouse models is enhanced striatal extrasynaptic (ex) N-methyl-D-aspartate receptor (NMDAR) expression and activity. This activity is mediated primarily through GluN2B subunit-containing receptors and is linked to increased activation of cell death pathways, inhibition of survival signaling, and greater susceptibility to excitotoxicity. Death-associated protein kinase 1 (DAPK1) is a pro-apoptotic kinase highly expressed in neurons during development. DAPK1 becomes re-activated and recruited to exNMDARs during ischemia where it phosphorylates GluN2B at S1303, amplifying receptor function. Approaches to reduce DAPK1 activity have demonstrated benefit in animal models of stroke, Alzheimer disease, Parkinson disease, and chronic stress, indicating that DAPK1 may be a novel target for neuroprotection. The overall hypothesis of this thesis was that aberrant DAPK1 activity contributes to exGluN2B dysfunction in HD, leading to early CS synaptic instability. An in vitro CS co-culture model was extensively optimized to allow rapid and robust detection of HD-like CS synaptic phenotypes, including MSN spine loss. Early dysregulation of DAPK1 was observed in the YAC128 HD mouse model, which was associated with elevated exGluN2B pS1303. Inhibition of DAPK1 normalized exGluN2B phosphorylation and surface expression, and completely prevented YAC128 MSN spine loss in CS co-culture. DAPK1 silencing restored nuclear CREB activation and partially rescued age-associated dendritic spine loss in vivo, thus validating DAPK1 as a target for synaptic protection in HD and warranting development of DAPK1-targeted therapies for neurodegeneration.

LAY SUMMARY

Huntington disease (HD) is a genetic disorder that causes physical, cognitive, and psychiatric symptoms. Dysfunctional transmission of the neurotransmitter glutamate occurs at synapses between cortical and striatal neurons in the brain, causing altered neuronal morphology and cell death. Specifically, glutamate receptors become mislocalized outside of synapses (extrasynaptic), and are linked to cell death signaling pathways. Death-associated protein kinase 1 (DAPK1) catalyzes the chemical addition of a phosphate group to proteins. DAPK1 phosphorylates extrasynaptic glutamate receptors, amplifying their function, and has been implicated in Alzheimer disease, Parkinson disease, stroke, and chronic stress. However, the potential role of DAPK1 in HD has not been evaluated. Here, a model of HD cortico-striatal synaptic dysfunction was optimized. DAPK1 was dysregulated early in HD mice, and inhibition of DAPK1 normalized glutamate receptor phosphorylation and localization in HD neurons. Reducing DAPK1 activity preserved synaptic morphology, indicating that DAPK1 may be a novel therapeutic target for HD.

PREFACE

Chapter 2

Chapter 2 has been published in *BMC Biology* 16:58. Schmidt ME, Buren C, Mackay JP, Cheung D, Dal Cengio L, Raymond LA, Hayden MR. (2018). Altering cortical input unmasks synaptic phenotypes in the YAC128 cortico-striatal co-culture model of Huntington disease. I designed, performed, and analysed all neuronal culture and Golgi-Cox imaging experiments, assisted with the design and interpretation of electrophysiological data, and wrote the entire manuscript. Caodu Buren and James P Mackay designed, performed, and analysed the electrophysiological experiments, and revised the manuscript. Daphne Cheung and Louisa Dal Cengio assisted in optimizing and performing immunofluorescence and Golgi-Cox staining experiments. Lynn A Raymond and Michael R Hayden assisted with interpretation of the data and revised the manuscript. The use of plural pronouns has been maintained from the original manuscript.

Chapters 3 & 4

Chapters 3 and 4 are in preparation to be combined and submitted for publication as one manuscript: Schmidt ME, Caron NS, Dal Cengio L, Ko Y, Lazic N, Anderson L, Raymond LA, Hayden MR. Death-associated protein kinase 1 promotes extrasynaptic GluN2B phosphorylation and striatal spine loss in Huntington disease. I designed all of the experiments and wrote the entire manuscript. Nicholas Caron advised on the design of the DAPK1 ASOs and in vivo cohorts, performed ICV ASO injections, assisted in results interpretation, and revised the manuscript. Louisa Dal Cengio performed RT-PCR experiments and perfusions, and assisted with tissue collection, neuronal cultures, and biochemistry. Nikola Lazic assisted with Western blots and co-immunoprecipitations. Yun Ko generated behavior data and assisted with memantine administration. Lisa Anderson sectioned and processed Golgi-Cox

samples. Lynn A Raymond and Michael R Hayden assisted with interpretation of the data and revised the manuscript. All other experiments and data analysis were performed by me.

Ethics approval

The studies described in this thesis have been approved by the Animal Care Committee at the University of British Columbia. All mice were handled according to institutional guidelines. Approval certificate numbers: A16-0130 and A16-0206.

TABLE OF CONTENTS

LIST OF TABLES

LIST OF FIGURES

LIST OF ABBREVIATIONS

Aβ	Amyloid-beta proteolytic product of amyloid precursor protein
AD	Alzheimer disease
AMPA	α-amino-3-hydroxy-5-methyl-4-isoxazolepropionic acid
AMPAR	AMPA receptor
AP2	Clathrin adaptor protein 2
APP	Amyloid precursor protein
ARD	Autoregulatory domain
ASO	Antisense oligonucleotide
ATP	Adenosine triphosphate
BACHD	Transgenic mouse model of Huntington disease made using a bacterial artificial chromosome containing the full-length human mutant huntingtin gene with 97 mixed CAA-CAG repeats
BDNF	Brain-derived neurotrophic factor
C6R	Transgenic mouse model expressing full-length human mutant huntingtin bearing a point mutation at the D586 caspase cleavage site
CAG140	Knock-in mouse model of Huntington disease with 140 CAG repeats
CaM	Calmodulin
CaMKII	Ca^{2+}/calmodulin-dependent protein kinase II
CaN	Calcineurin
CBD	Cytoskeletal binding domain
CBP	CREB-binding protein
Cdk5	Cyclin-dependent kinase 5
CICR	Calcium-induced calcium release
CK2	Casein kinase 2
CREB	Cyclic AMP response element-binding protein
CS	Cortico-striatal
CTX	Cortical/cortex
CUS	Chronic unpredictable stress
D1-type	Dopamine receptor 1-expressing medium spiny neurons
D2-type	Dopamine receptor 2-expressing medium spiny neurons
DAPK1	Death-associated protein kinase 1
DAPK1β	An alternatively-spliced isoform of DAPK1, containing a 12 amino acid extension of the C-terminus
DAPK2	Death-associated protein kinase 2, also called DAPK-related protein kinase 1 (DRP1)
DAPK3	Death-associated protein kinase 3, also called zipper-interacting protein kinase (ZIPK)
DARPP32	Dopamine- and cyclic AMP-regulated phosphoprotein 32
DD	Death domain
DiI	1,1'-dioctadecyl-3,3,3',3'-tetramethylindocarbocyanine perchlorate

DIV	Day in vitro
DKI	DAPK1 inhibitor; TC-DAPK6
DMSO	Dimethyl sulfoxide
DRAK1	DAPK-related apoptosis-inducing protein kinase 1
DRAK2	DAPK-related apoptosis-inducing protein kinase 2
EPSC	Excitatory post-synaptic current
ER	Endoplasmic reticulum
ERK	Extracellular signal-regulated kinase
ExGluN2B	Extrasynaptic GluN2B
ExNMDAR	Extrasynaptic NMDA receptor
GABA	Gamma-aminobutyric acid
GAPDH	Glyceraldehyde 3-phosphate dehydrogenase
GFAP	Glial fibrillary acidic protein
GFP	Green fluorescent protein
GluN2A	NMDA receptor subunit 2A
GluN2B	NMDA receptor subunit 2B
GTP	Guanosine triphosphate
HDAC1	Histone deacetylase 1
HD	Huntington disease
HI	Hypoxia-ischemia
HSP90	Heat shock protein 90
HTT	Huntingtin
ICV	Intracerebroventricular
IFNγ	Interferon gamma
IP3R	Inositol triphosphate receptor
iPSC	Induced pluripotent stem cell
JNK	c-Jun N-terminal kinase
LAR	Leukocyte common antigen-related protein
LNA	Locked nucleic acid
LOAD	Late-onset Alzheimer disease
LTD	Long-term depression
LTP	Long-term potentiation
MAP2	Microtubule-associated protein 2
MAPK	Mitogen-activated protein kinase
MARK1/2	Microtubule affinity-regulating kinase 1/2
MCAO	Middle cerebral artery occlusion
mEPSC	Miniature excitatory postsynaptic current
mHTT	Mutant huntingtin
mRNA	Messenger ribonucleic acid
MLC2	Myosin regulatory light chain 2
MLCK	Myosin light chain kinase
MOE	2’-O-methoxyethylribose
mPFC	Medial prefrontal cortex
MSN	Medium spiny neuron
MT	Microtubule

N171-82Q	N-terminal huntingtin fragment mouse model of Huntington disease with 82 CAG repeats
NDRG2	N-Myc Downstream-Regulated Gene 2 Protein
NMDA	N-methyl D-aspartate
NMDAR	NMDA receptor
nNOS	Neuronal nitric oxide synthase
OGD	Oxygen and glucose deprivation
P38 MAPK	P38 mitogen-activated protein kinase
PD	Parkinson disease
PKA	Protein kinase A
PKC	Protein kinase C
PP2A	Protein phosphatase 2A
PSD	Postsynaptic density
PSD95	Postsynaptic density protein 95
PTEN	Phosphatase and tensin homolog
Q175FDN	Knock-in mouse model of Huntington disease with 175 CAG repeats
R6/1	N-terminal huntingtin fragment mouse model of Huntington disease with 116 CAG repeats
R6/2	N-terminal HTT fragment mouse model of Huntington disease with 144-150 CAG repeats
RNAi	RNA interference
RNase H	Ribonuclease H
RSK	Ribosomal S6 kinase
ROC	Ras of complex proteins
RyR	Ryanodine receptor
SNP	Single nucleotide polymorphism
STEP	Striatal-enriched protein tyrosine phosphatase
STR	Striatal/striatum
TC-DAPK6	DAPK1 inhibitor; DKI
TNF	Tumor necrosis factor
TS	Thalamo-striatal
VGLUT1	Vesicular glutamate transporter 1
W13	Full-length transgenic mouse model expressing full-length human mutant huntingtin bearing a point mutation at the D586 caspase cleavage site; also referred to as C6R
WT	Wild-type
wtHTT	Wild-type huntingtin
YAC18	Transgenic mouse model containing a yeast artificial chromosome expressing the full-length human wild-type huntingtin gene encoding 18 glutamines
YAC128	Transgenic mouse model of Huntington disease made using a yeast artificial chromosome containing the full-length human mutant huntingtin gene encoding 125-128 glutamines
YFP	Yellow fluorescent protein

ACKNOWLEDGEMENTS

I would like to thank my supervisor, Dr. Michael Hayden, for seeing my potential as an inexperienced co-op student nearly eight years ago, and for consistently supporting my growth as a scientist and person since then. Thank you for keeping me focused on the ultimate goal of improving the lives of people affected by Huntington disease, and for giving me the freedom to explore new ideas and push the boundaries of our lab's expertise. Thank you to my advisory committee for your support: Dr. Mahmoud Pouladi, Dr. Ann Marie Craig, and Dr. Lynn Raymond. I would like to particularly acknowledge Lynn for reaching out to me to offer additional one-on-one support from the very beginning. After each of our meetings, I left with a renewed passion for my work and a refreshing clarity of mind. Thank you for going above and beyond as a mentor.

An enormous thank you to the many interesting, quirky, and brilliant people I have had the pleasure to work with over the years. Thank you to Dr. Shaun Sanders for taking me under your wing as an undergraduate student who had never done protein work before. I am so incredibly fortunate that I had you and Dr. Dale Martin as mentors during that critical period (neuroscience pun intended) to teach me how important it was to deeply understand every aspect of what I was doing. Thank you both for your continued support to this day. To the others in the lab who have offered support as colleagues and often also as friends: Dr. Fannie Lemarié, Dr. Amirah Aly, Louisa Dal Cengio, Helen Baddeley, Nikola Lazic, Dr. Nick Caron, Stefanie Butland, Katherine Mui, Erika Villanueva, Dr. Niels Skotte, Stephanie Bortnick, Enzo Casal, Betty Nguyen, Dr. Amber Southwell, Cassandra MacDonald, Mahsa Amirabbasi, and Seetha Kumaran. A special thank you to Louisa for consistently pumping out unbelievably beautiful data and for being so dedicated to our projects. Thank you as well to Sheng Yu, Qingwen Xia, Mark Wang, and Yun Ko for all the animal, genotyping, and neuronal culture support.

Thank you to my family, especially my brothers. Nate, thank you for being a younger brother that I can still look up to in so many ways. Thank you for your

advice, encouragement, and for just understanding my brain at times when nobody else does. Matt, ever since we were kids, you have urged me out of my comfort zone (usually against my will). Your ambition and free spirit inspire me. Thank you for forcing me to read the “Double Helix” mystery novel when I was 14, ultimately sparking my intense passion for Huntington disease. You started all of this! Thank you to Janet and Jamie for cheering me on and being there to celebrate all the little milestones along the way! To my Grandfather, Aunt Virginia, Uncle Murray, Aunt Patricia, and my dear Grandmother, words cannot describe how much I love you. Your support and encouragement have never wavered for an instant. Grandma, you were so incredibly strong right until the end – thank you for helping to remind me of the true purpose of my work and the reason I chose this path.

To my closest friends, especially Kelly Anne Jones and Catherine McNair, thank you for being my constant cheerleaders since day one, and for never once holding it against me if I went weeks without contact. Thank you, Sammy Wilson for literally never giving up on inviting me for a coffee break, even though I was almost always too busy to go. To the friends who have come and gone, but offered support, laughs, and fresh perspectives along the way, thank you as well.

To those who kept me active through beach volleyball, hiking, cycling, aerobics classes, bootcamps, and squat challenges, thank you for helping me maintain my physical health. To my counsellor, psychiatrist, and everyone who took time to sit down and talk during a hard day, thank you for openly supporting my mental health.

Finally, to Russell Bonaguro, my stable compass. Thank you for knowing that I could do this, even when I was convinced that I couldn’t. You somehow achieved the perfect balance between empowering my ambition and urging me to slow down and seek support. Thank you for being willing to come pick me up from the lab exhausted and in tears, and equally willing to drive me into the lab with a kidney stone and on morphine so that my neuronal cultures wouldn’t die. You are an amazing partner, friend, and person.

DEDICATION

IN MEMORY OF MY BELOVED GRANDMOTHER,

CLARA EMMA SCHMIDT

YOUR UNWAVERING SUPPORT, COURAGE, AND LOVE CONTINUE TO MOTIVATE AND INSPIRE ME EVERY DAY

1 INTRODUCTION

1.1 HUNTINGTON DISEASE

Huntington disease (HD) is an autosomal dominant neurodegenerative disorder which causes debilitating motor, cognitive, and psychiatric disturbances [1]. HD is most common in European and North American populations, affecting an estimated 1 in 7300 individuals, while the majority of Asian and African populations exhibit much lower prevalence rates [1, 2]. HD typically manifests in mid-life and is inherited in an autosomal dominant manner, resulting in inter-generational transmission of the disease within families. Due to the absence of disease-modifying therapies, supportive care is aimed at symptomatic relief in order to maximize quality of life and functional capacity. However, future therapeutic interventions will likely be most effective if administered early in the disease course.

1.1.1 Genetic basis of Huntington disease

HD is caused by the expansion of a naturally-occurring CAG trinucleotide repeat in exon 1 of the huntingtin (*HTT*) gene to 40 repeats or longer [3]. Age of onset is determined by the length of the mutant *HTT* CAG tract, with individuals possessing longer repeats manifesting earlier in life [4, 5]. Clinical diagnosis generally occurs between the age of 30-50, although a juvenile form exists and is associated with expansions over 55 repeats [6]. A reduced penetrance range encompasses repeat lengths between 36-39 [7]. Individuals with a reduced penetrance allele may or may not develop symptoms of HD, indicating the presence of other genetic or environmental modifiers of HD penetrance within this range.

1.1.2 Clinical presentation and neuropathology

HD is clinically diagnosed primarily based on motor symptom onset assessed by a neurological examination, although family history is usually incorporated into the diagnostic process and the result is confirmed with genetic testing [6]. Motor symptoms consist of chorea (involuntary movements), dystonia (sustained, involuntary muscle contractions), gait imbalance, and oculomotor disturbances [8]. Disease progression continues for approximately 15 years until death, and over this time leads to dementia as well as difficulty walking, speaking, and swallowing [9]. In late stages, bradykinesia becomes apparent as choreic symptoms diminish [9].

Despite motor symptoms being the driving factor for official clinical diagnosis of HD, cognitive and psychiatric symptoms are often the first signs of illness, and consist of agitation, cognitive impairment, loss of focus, memory problems, depression, apathy, sleep disturbances, and irritability [9]. In parallel with these findings, studies have reported altered cortical excitability and synaptic activity in premanifest HD individuals, indicating that neuronal dysfunction occurs prior to motor onset [10, 11]. In support of this, the large-scale observational study TRACK-HD demonstrated structural changes in the brains of HD mutation carriers as well as subtle cognitive and motor impairments well before expected disease onset [12, 13]. A prodromal phase usually occurs between the premanifest and manifest stages of HD, when subtle symptoms are apparent, but are not severe enough to meet the requirements for motor diagnosis. Once a patient has been diagnosed with HD, the Unified Huntington Disease Rating Scale is used to monitor disease progression and assign a disease stage (1-5). This scale consists of a series of sub-tests which are used to assess motor score, cognitive and psychiatric function, and Total Functional Capacity, a measure of the patient's ability to complete work and daily life tasks [8].

Neuropathologically, HD is characterized by the selective and progressive cell death of inhibitory striatal gamma-aminobutyric acid (GABA)-ergic medium spiny neurons (MSNs) [14–16]. Neuropathological studies were used to develop

the Vonsattel grading system, which assigns a disease severity (Grade 0-4) to a patient based on the degree of striatal atrophy [17]. Cortical degeneration also occurs in later grades, and the level of atrophy in various cortical regions (ie. motor vs. anterior cingulate) correlates with the relative severity of different motor vs. mood symptoms [18]. Cortico-striatal (CS) circuitry plays a critical role in the control of motor function. Specifically, MSNs receive significant glutamatergic input from the cortex and in turn, striatal output occurs through two pathways. Activity of direct pathway (D1-type) MSNs serves to ultimately enhance excitatory input to the cortex, promoting movement, while indirect pathway (D2-type) MSNs reduce excitatory input to the cortex, decreasing movement [19]. In early stages of HD, impairment of D2 MSNs in the indirect pathway in addition to altered transmission onto direct pathway D1 MSNs leads to disinhibition of the cortex and the primary motor symptom of chorea [14, 19, 20]. Later, impaired transmission occurs along the direct pathway as well, causing reduced movement and CS disconnect [14, 19, 20]. Much evidence indicates that impaired synaptic transmission at the glutamatergic CS synapse plays a critical role in dysfunction of this pathway. This will be discussed in Section 1.2.

1.1.3 Overview of molecular pathogenesis

Expansion of the *HTT* CAG repeat encodes for an abnormally long polyglutamine tract in the resulting mutant HTT (mHTT) protein, which undergoes both a partial loss of wild-type HTT (wtHTT) function, and a gain of toxic function.

wtHTT is ubiquitously expressed throughout the body and plays a major role in many essential cellular processes through its interactions with hundreds of identified binding partners [21, 22]. wtHTT is essential for survival and neuronal function; Deletion of *Htt* causes embryonic lethality in mice, *Htt* heterozygous knockout mice have motor and cognitive impairments, and *Htt* inactivation in the forebrain of adult mice leads to neurodegeneration [23–25]. By interacting with various vesicle-associated proteins, wtHTT controls the transport of organelles along axons and dendrites [26]. Of particular importance, wtHTT promotes the

transport and secretion of vesicles containing brain-derived neurotrophic factor (BDNF) in neurons, a function which is impaired with HTT deficiency or mutation [27–29]. wtHTT also acts as a scaffold for autophagy proteins [30]. Notably, mutation of HTT dysregulates autophagy, promoting the formation of empty autophagosomes and preventing proper degradation of autophagy substrates [31]. wtHTT partially localizes to the nucleus in cells where it binds to various transcription factors, impacting gene expression [26]. The *BDNF* gene is one of these targets influenced by wtHTT function and is downregulated in HD patients and mouse models, as are several other genes involved in synaptic dysfunction and neuronal health [32–36]. In addition to regulation of these genes, wtHTT itself has pro-survival functions and protects neurons from excitotoxic death [37].

Although loss of wtHTT function occurs in HD, symptoms and neuropathology are hypothesized to occur principally due to a toxic HTT gain-of-function as a result of the polyglutamine expansion. mHTT dysregulates vesicle trafficking, mitochondrial function, proteasomal protein degradation, autophagy, gene expression, and susceptibility to oxidative stress [38]. However, altered transmission, particularly at the CS synapse, is proposed to be a critical and highly upstream promoter of many of these processes, as mHTT directly and indirectly influences the localization and function of key proteins involved in both presynaptic neurotransmitter release and postsynaptic receptor responses [39, 40].

1.1.4 Mouse models of Huntington disease

Early models of HD were generated by the use of neurotoxic compounds, such as the mitochondrial toxin 3-nitroproprionic acid, which partially recapitulates the striatal neurodegeneration observed in HD when injected systemically [41]. Similarly, administration of glutamatergic agonists into rodent brains produces striatal lesions, suggesting that excitotoxicity (cell death due to over-activation of glutamate receptors) may play a role in HD pathogenesis [42–47]. After the discovery of the causative *HTT* mutation in 1993, genetic animal models largely

replaced the use of chemical models. These can be categorized into three main types: fragment, full-length, and knock-in.

Fragment mouse models of HD were engineered to transgenically express an N-terminal fragment of human mHTT and include the R6/1, R6/2, and N171-82Q models. The R6 models express exon 1 of mHTT with approximately 150 CAG repeats, while the N171-82Q expresses a longer N-terminal fragment with 82 repeats [48, 49]. Fragment mice tend to have a severe phenotype with rapid onset, displaying motor impairment, neuronal structural alterations, dysregulated gene expression, and neuropathology, although more global atrophy is observed in comparison to human HD or full-length mouse models which demonstrate selective striatal and cortical degeneration [48, 50–52]. The presence of observable phenotypes by 1-2 months of age in fragment models is advantageous for preclinical study design as results can be obtained quickly. However, their rapid progression may eliminate subtle or slowly-progressing HD-like features and makes presymptomatic interventions difficult.

Full-length HD mouse models contain the entire human mutant *HTT* gene on a yeast or bacterial artificial chromosome (YAC or BAC), including its various genetic regulatory elements. The most common of these models are the YAC128 (utilized in this thesis) and BACHD, which express mHTT with 128 and 97 glutamines, respectively [50, 53]. Both models progressively develop relevant motor, cognitive, psychiatric, transcriptional, and neuropathological features of HD [51]. These phenotypes have been well-established in multiple labs, allowing for the use of robust readouts in preclinical studies. However, most phenotypes require 6-12 months of age to become apparent and changes are generally not as dramatic as those observed in fragment models [54]. Regardless, these models remain highly relevant for studying HD pathogenesis due to their high genetic and biological resemblance to the human disease. Two variations of the full-length models have recently been generated to express both human wtHTT and mHTT on a murine *Htt*-null background [55, 56]. These humanized models thus recapitulate HD genetics more precisely than YAC128 or BACHD mice, and

will be valuable in the future for evaluation of human *HTT* silencing-based therapeutic strategies.

Knock-in HD mice, such as the CAG140 model, were developed by introducing a region of human DNA containing the CAG expansion into the mouse *Htt* locus [57]. Thus, mHTT is expressed under the endogenous mouse promoter, eliminating the potential confounding factor of transgenic human gene overexpression. In general, HD phenotypes in knock-in models are mild, inconsistent, and not observable until late ages, making them less ideal for preclinical studies than other models [54]. However, recent improvements have been made by increasing the CAG tract length and enhancing mHTT expression to create the Q175FDN line, which demonstrates early, robust, and relevant HD-like features [58].

1.1.5 Therapeutic strategies in development for Huntington disease

Current therapies for HD consist solely of those aimed at symptomatic relief. Due to the clear genetic nature of HD, one of the most promising strategies for preventing or slowing disease progression is silencing of the mutant *HTT* gene. Many efforts in this area of research are ongoing, and one strategy, using a nonselective antisense oligonucleotide (ASO) directed at pan-*HTT* (IONIS-HTT_{RX}) recently demonstrated tolerability in a Phase 1b/2a clinical trial and successfully reduced mHTT protein levels in HD patient cerebrospinal fluid [59, 60]. A large efficacy trial using this ASO is currently underway.

Aside from HTT-targeted approaches, strategies that have shown promise in recent clinical trials or are currently in development for HD are generally aimed at neuroprotection and restoration of synaptic function (ie. pridopidine, memantine, laquinimod) [61]. It is likely that a combinatorial approach, consisting of *HTT* lowering as well as neuroprotective or ‘synaptoprotective’ drugs, will prove most efficacious for halting disease progression. Ideally, these therapies will be given to premanifest individuals in order to promote maximum benefit.

1.2 SYNAPTIC DYSFUNCTION IN HUNTINGTON DISEASE

The striatum is the earliest and most severely affected brain region in HD. This is partly due to a number of intrinsic striatal MSN properties that cause greater susceptibility to toxic mHTT expression, including unique transcriptional patterns, enhanced mitochondrial sensitivity to Ca^{2+} dysregulation, high expression of particular N-methyl D-aspartate receptor (NMDAR) subunits, large amounts of glutamatergic innervation, and somatic instability of the CAG repeat [19, 39, 40]. However, altered cortical function, particularly aberrant excitatory cortical input to the striatum, is proposed to be a key extrinsic driver of striatal MSN dysfunction and degeneration in HD [39, 40].

1.2.1 Altered excitatory cortico-striatal synaptic transmission in Huntington disease

In multiple HD mouse models, a biphasic pattern of CS glutamatergic activity has been observed. At early ages (within the first few months of life), prior to behavioral phenotypes or neurodegeneration, glutamate release and spontaneous CS excitatory activity are increased in HD mice compared to wild-type (WT), reflecting altered presynaptic mechanisms [62–64]. Conversely, cortical glutamate release and the frequency of synaptic activity become impaired with disease progression (mid to late life) [62–67]. A similar biphasic pattern was identified for postsynaptic α-amino-3-hydroxy-5-methyl-4-isoxazolepropionic acid (AMPA) receptor activity in YAC128 mice – at early ages (1 month), increased numbers of postsynaptic AMPA receptors (AMPARs) caused elevated evoked currents, while responses at later symptomatic ages were reduced [62]. However, other studies found decreased or unaltered AMPAR function in young HD MSNs, which might be explained by different mouse models or electrophysiological recording conditions used [68, 69].

Synaptic activity promotes neuroprotective cell signaling and gene expression in neurons; thus, loss of CS connections with disease progression reduces these pro-survival effects in striatal MSNs, contributing to neuronal

death [70, 71]. Furthermore, since excitatory CS activity results in delivery of BDNF to the striatum through its release at active cortical terminals, this synaptic disconnect likely also leads to inadequate trophic support to striatal MSNs [28, 72]. Thus, increasing MSN trophic support is an important and promising therapeutic target for HD. The early increases in CS activity prior to emergence of disease phenotypes may reflect compensatory mechanisms activated to overcome deficits in normal transmission. In vitro CS co-culture studies tend to recapitulate phenotypes observed in aged HD mice, such as impaired CS connectivity, reduced MSN spine numbers, and loss of MSN dendritic complexity [73–76]. This may be a result of these in vitro studies being performed in the absence of other modulatory neurotransmitters such as dopamine, which has been shown to differentially filter CS glutamate activity in young versus aged YAC128 mice [62].

Further insight into the nature of CS synaptic dysfunction came from evidence in multiple HD mouse models showing enhanced excitotoxic susceptibility to NMDAR agonism in the striatum, with excitotoxic resistance occurring at relatively progressed disease stages [77–79]. Electrophysiological NMDAR responses are also larger in MSNs from young HD mice compared to WT, followed by decreased NMDAR currents with disease progression [68, 77], thus correlating with both loss of CS activity and resistance to excitotoxicity. Interestingly, the early increase in NMDAR responses is primarily due to elevated extrasynaptic (ex) NMDAR expression and activity in MSNs both in slices and in primary co-culture with cortical neurons, while synaptic NMDAR currents are similar to WT [80, 81]. The hyperactivity of exNMDARs in HD is hypothesized to play a critical role in disease pathogenesis. This will be discussed in Section 1.3.6.3.

1.2.2 Structural synaptic abnormalities in Huntington disease neurons

CS synaptic dysfunction in HD eventually leads to morphological degeneration of striatal MSNs as they lose cortical glutamatergic and trophic support with disease

progression. In late-stage HD patient brains, MSNs contain abnormal dendritic arbors and fewer spines compared to control MSNs [82, 83]. Similarly, spine loss, excitatory synapse loss, and dendritic alterations have been observed in MSNs and cortical neurons from aged HD mice or mature primary neuronal cultures, as well as a loss of glutamatergic terminals in the striatum [73, 74, 84–93].

At early time points, protective mechanisms are proposed to compensate for altered CS transmission. This is supported by observations of proliferative morphological changes (larger spines, more spines, altered dendritic branching patterns) in early stage human HD striatal MSNs and increased excitatory CS activity in presymptomatic HD mice [62–64, 82]. Ideally, a therapeutic intervention aimed at preserving spines, synapses, and dendritic structure would be delivered as early as possible in HD patients in order to normalize CS transmission and prevent morphological changes and eventual neuronal death from occurring. However, recent work has shown that spine loss in 12-month-old YAC128 mice can be restored by inhibition of endoplasmic reticulum (ER) store-operated Ca^{2+} entry (SOCE) starting at 10.5 months [74]. This likely occurs by preventing Ca^{2+}-dependent modulation of SOCE effector molecules that cause spine structure reorganization [74]. This exciting finding suggests that late-intervention approaches to reestablish normal synaptic function and balance intracellular Ca^{2+} signaling may be more efficacious than previously thought.

1.3 N-METHYL D-ASPARTATE RECEPTORS

NMDARs are transmembrane ionotropic receptors which are enriched at neuronal postsynapses and are involved in excitatory glutamatergic signaling and synaptic plasticity in the brain. In addition to their essential role in neurotransmission, aberrant activity of NMDARs has been linked to several major neurological disorders, resulting in the development of tools and therapies aimed at receptor modulation.

1.3.1 General structure and function of NMDA receptors

In comparison to the related glutamatergic AMPARs and kainate receptors, NMDARs possess high Ca^{2+} permeability, which contributes to long-term Ca^{2+}-dependent signaling essential for synaptic potentiation or depression in neurons [94, 95]. Under resting conditions, the pore of the NMDAR is voltage-dependently blocked by a Mg^{2+} ion [96]. Binding of presynaptically-released agonist (glutamate) as well as a co-agonist (glycine or D-serine) to the extracellular ligand-binding domain of the receptor, in addition to depolarization of the postsynaptic membrane results in extrusion of the Mg^{2+} ion from the channel pore and a conformational change of the receptor, allowing ion influx [97]. For this reason, NMDARs have been described as coincidence detectors, only opening when both presynaptic and postsynaptic neurons are active at the same time. This coincidence detection serves to strengthen synaptic connections between synchronously active neuronal pairs during development or learning [98].

Mature NMDARs exist as tetramers containing four subunits each, which assemble to yield extracellular N-terminal and agonist binding domains, a transmembrane pore-forming domain, and an intracellular C-terminal domain [94, 97]. The various subunits are encoded by different genes and include GluN1, GluN2A-D and GluN3A-B [94, 97]. A mature receptor may form as a di-heteromer (two obligatory GluN1 subunits combined with two GluN2 or GluN3 subunits of the same sub-type; ie. GluN1/GluN2A or GluN1/GluN2B) or a tri-heteromer (ie. GluN1/GluN2A/GluN2B or GluN1/GluN2B/GluN3A, among other combinations) [94, 97]. The different GluN2 and GluN3 subunits are incorporated into receptors during various developmental timepoints, activity patterns, or at specific subcellular membrane locations, and confer distinct properties to the receptor [94, 97].

1.3.2 GluN2A versus GluN2B subunits

GluN2A and GluN2B are the most widely-expressed GluN2 subunits throughout the brain and differ substantially from each other in their activation properties [94]. GluN2B-containing receptors have a lower maximal open probability, higher sensitivity to glutamate and glycine, slower deactivation, longer excitatory postsynaptic current (EPSC) decay, and greater overall Ca^{2+} influx during low-frequency stimulation compared to GluN2A-containing receptors [94]. Furthermore, in mature neurons, GluN2B-containing receptors are hypothesized to be preferentially (though not exclusively) enriched at extrasynaptic sites, while GluN2A-containing receptors are concentrated within the postsynaptic density (PSD) [99–101]. Importantly, however, some studies have disputed this model and it is likely that the methodology and developmental timepoints used have a great impact on the observed distribution of GluN2 subunits [102–105]. Furthermore, the pharmacological tools used in many of these studies were only able to primarily evaluate the localization of pure GluN1/GluN2B populations, and not tri-heteromeric GluN1/GluN2A/GluN2B receptors, which are now widely accepted to comprise a large proportion of synaptic NMDARs in the mature brain and possess intermediate activation kinetics compared to pure di-heteromeric GluN1/GluN2A and GluN1/GluN2B receptors [106].

In contrast to the high structural and sequence similarity between GluN2A and GluN2B within the extracellular and transmembrane domains, the intracellular C-terminal tails differ greatly, resulting in dissimilar networks of protein binding partners [107, 108]. These interactions influence downstream cell signaling, with several studies suggesting a pro-survival role for GluN2A and a pro-death function for GluN2B, although this signaling dichotomy is not fully discrete and interpretation of results is again limited by the inability to pharmacologically isolate tri-heteromeric GluN1/GluN2A/GluN2B receptors [100, 105, 109–113].

During neuronal development, NMDARs play a critical role in consolidation of synchronously active synaptic partners [95]. Early in development, high expression of GluN2B subunits allows for greater and longer ion influx through GluN1/GluN2B receptors, inducing long-term Ca^{2+}-dependent processes that strengthen newly-developing synapses and dendritic spines [114–118]. As development progresses, these receptors gradually become replaced in an activity-dependent manner with GluN2A-containing receptors, which possess quick kinetics essential for precise control over the timing of synaptic activity [115–119]. As mentioned above, tri-heteromeric receptors likely constitute a significant portion of this mature synaptic receptor population with estimates of this fraction ranging from 10-50% [106]. The C-terminal tail of GluN2B mediates interactions with proteins involved in synaptic plasticity, such as Ca^{2+}/calmodulin-dependent protein kinase II (CaMKII). Anchoring of CaMKII to GluN2B during long-term potentiation (LTP) allows it to phosphorylate nearby AMPARs, promoting their activity [120, 121]. Thus, in the mature brain, synaptic GluN2B may function within tri-heteromeric receptors as a structural link between fast GluN2A-mediated activity and AMPAR-mediated mechanisms of long-term plasticity [106]. Conversely, extrasynaptic GluN1/GluN2B di-heteromers have been proposed to localize to immature sites of excitatory activity [101].

1.3.3 Synaptic versus extrasynaptic NMDA receptor signaling

Although NMDARs are highly enriched at synapses, their presence is also found outside of synapses (extrasynaptic). These receptor populations may be defined electrophysiologically (activated only during high-frequency activity or glutamate spillover, but not during low-frequency stimulation), biochemically (soluble in 1% Triton-X, thus not incorporated into the Triton-insoluble PSD), or microscopically (>100 nm away from the PSD in electron micrographs) [80, 122, 123].

In addition to subunit composition discussed above, the subcellular localization of an NMDAR also plays a role in dictating the effect of its activation. In general, synaptic NMDAR activity promotes cell survival signaling, nuclear

Ca^{2+} entry, and expression of genes involved in neuroprotection and mitochondria resilience, while exNMDARs antagonize these same pathways in a dominant manner, resulting in cell death signaling, downregulation of survival genes, and mitochondria toxicity (**Fig. 1.1**) [124, 125]. Importantly, the acquisition of cell death-promoting functions by exNMDARs in vitro develops between DIV7 and DIV12, a time period characterized by major synaptogenesis as well as the shift in GluN2B-GluN2A NMDAR composition [126–128]. Thus, a unified hypothesis has emerged to explain the ultimate outcome of NMDAR activity in mature neurons, and considers both the composition and location of the receptor: synaptic GluN2A-containing receptors promote neuronal survival, while extrasynaptic GluN2B-containing receptors initiate cell death [129]. During early development (prior to coupling with cell death pathways), exNMDAR activity may contribute to the formation of new synapses by enhancing neuronal postsynaptic responses [102, 130]. With maturation, extrasynaptic GluN2B (exGluN2B)-containing receptors become linked to detrimental cellular pathways, possibly as a mechanism to eliminate imprecise or weak neuronal connections which have not undergone significant LTP and incorporation of GluN2A-containing NMDARs [125, 126]. ExGluN2B activity may also promote critical LTD processes [131, 132]. In adult neurons, exNMDARs are activated by physiological glutamate spillover and contribute to synaptic responses, LTD, or NMDAR spikes [130, 133–135]. Others have provided evidence that exNMDAR activation by glutamate released from nearby glial cells modulates synaptic function and neuronal network synchrony [136–138]. A delicate equilibrium between synaptic and exNMDAR activity is unquestionably critical in the brain, and disruption of this balance has been implicated in a number of acute and chronic neurological disorders, including HD (see Section 1.3.6).

1.3.4 Link between NMDA receptors and ER Ca^{2+} dynamics

Ca^{2+} influx through NMDARs is critical for receptor function – both for survival signaling in response to physiological stimulation, and for neuronal death after

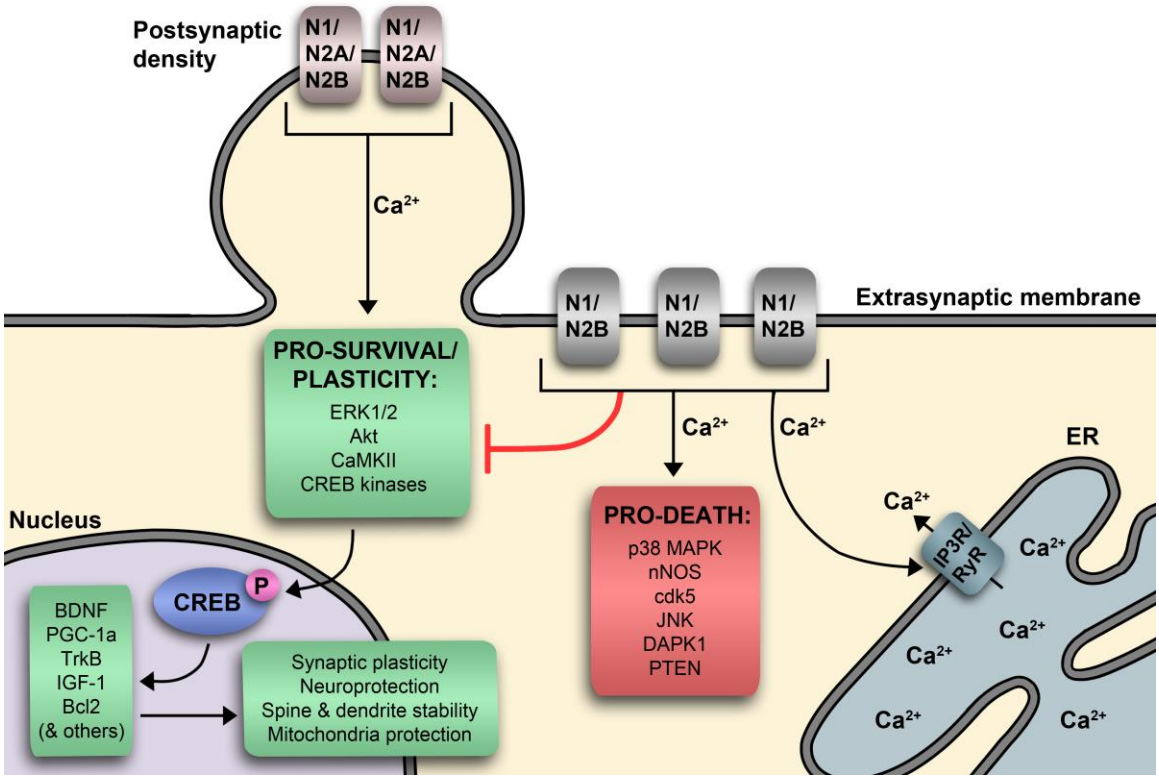

Figure 1.1: Synaptic and extrasynaptic NMDA receptor signaling. Ca^{2+} influx through synaptic NMDARs activates cell signaling pathways that promote neuronal survival and plasticity. Activation of nuclear CREB by S133 phosphorylation is a key component of this pathway, leading to transcription of a number of target genes involved in plasticity, neuronal protection, and spine stability. Extrasynaptic di-heteromeric GluN1/GluN2B NMDAR activity antagonizes synaptic signaling in a dominant fashion and promotes the activation of pro-death signaling. Additionally, Ca^{2+} influx through NMDARs can be further amplified by IP3R- and RyR-mediated ER Ca^{2+} release (Ca^{2+}-induced Ca^{2+} release, CICR). CICR may occur at both synaptic (not shown) or extrasynaptic subcellular compartments.

toxic NMDA treatment [125]. The ER is an important storage organelle for intracellular Ca^{2+} and can amplify cytosolic Ca^{2+} levels in response to receptor influx through a pathway termed Ca^{2+}-induced Ca^{2+} release (CICR) (**Fig. 1.1**) [139–144]. This occurs through activation of ER inositol triphosphate receptors (IP3Rs) and ryanodine receptors (RyRs) and while this contributes to physiological NMDAR function, a pathological increase in this process can lead to ER-to-mitochondria Ca^{2+} transfer, mitochondria depolarization, and neuronal death [144, 145]. Interestingly, IP3R-dependent Ca^{2+} “waves” through the ER network have been proposed to be the key component of fast synapse-to-

nucleus Ca^{2+} signaling in neurons, allowing synaptic activity to influence gene expression despite being physically localized far away from the nucleus [139]. In this way, NMDAR activity and ER Ca^{2+} store dynamics are tightly linked. In support of this hypothesis, inhibition of IP3R or RyR are protective against NMDA excitotoxicity in cultured neurons [144, 145]

1.3.5 Regulation of NMDA receptors by phosphorylation

NMDAR subunits undergo phosphorylation at multiple sites within their cytosolic C-terminal tails, influencing subcellular localization, surface expression, and activity of the assembled ion channel. Some of the key phosphorylation sites within GluN1, GluN2A, and GluN2B are depicted in **Fig. 1.2** and occur via a number of protein kinases, most commonly Src-family tyrosine kinases, protein kinase A (PKA), and protein kinase C (PKC) [146].

Phosphorylation of GluN2B at S1480 by casein kinase 2 (CK2) disrupts its stabilizing interaction with postsynaptic density protein 95 (PSD95), thus reducing surface expression and/or allowing diffusion of GluN2B-containing receptors away from the PSD [147–149]. This process is a key mechanism for GluN2B removal from synapses during the developmental activity-dependent GluN2A-GluN2B switch [149]. Phosphorylation at the nearby site Y1472, which lies within the clathrin adaptor protein 2 (AP2) binding domain, prevents AP2 binding, thus reducing clathrin-mediated endocytosis and promoting surface expression, particularly at the synapse [149–151]. Interestingly, pS1480 negatively regulates phosphorylation of Y1472, likely by preventing Src-family tyrosine kinases from associating with the receptor via PSD95 interactions [149, 152, 153]. Conversely, pY1472 is positively regulated by Y1070 phosphorylation, which enhances binding of the tyrosine kinase Fyn to GluN2B [154]. While Y1472 phosphorylation appears to play a major role in synaptic GluN2B localization, pY1336 has been linked to enrichment of GluN2B in extrasynaptic membrane compartments, and regulates cleavage of GluN2B subunits by calpain [155, 156].

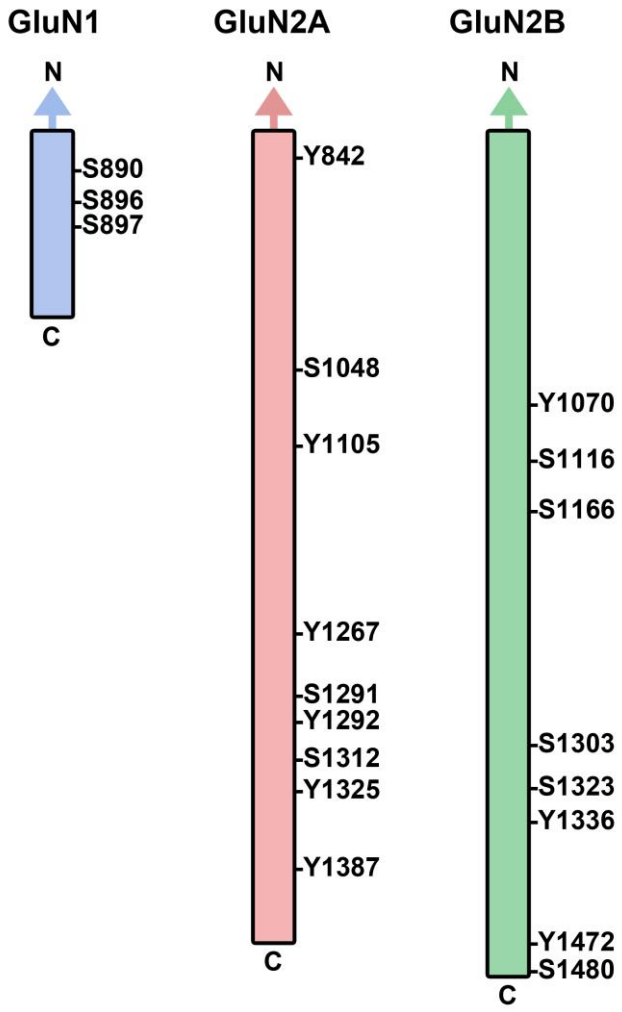

Figure 1.2: Key phosphorylation sites in the C-terminal domains of GluN1, GluN2A, and GluN2B. Various kinases and phosphatases regulate the phosphorylation of serine (S) and tyrosine (Y) residues within the C-terminal tails of NMDAR subunits in response to neuronal activity during development, learning, or pathology.

Potentiation of receptor currents also occurs through PKC-, CaMKII-, or DAPK1-mediated phosphorylation of GluN2B S1303 and S1323 [157–159]. Additionally, GluN2B S1166 phosphorylation enhances NMDAR synaptic currents and dendritic spine Ca^{2+} signaling, further fine-tuning receptor function [160].

In GluN2A, Y842 phosphorylation plays a major role in AP2 binding, while phosphorylation sites have been identified at Y1105, Y1267, Y1292, Y1325, and Y1387, most of which have been shown to potentiate receptor currents [161–163]. GluN2A sites S1291 and S1312 are analogous to GluN2B S1303 and

S1323, and phosphorylation of these residues also increases receptor currents [157, 158]. Phosphorylation at other sites, including GluN2A S1048 and GluN2B S1116 regulate surface expression [164, 165].

Phosphorylated serine residues exist within the GluN1 C-terminus and play a major role in receptor clustering and trafficking [166]. Specifically, phosphorylation at these sites masks a nearby ER retention motif, allowing exit from the ER and consequent trafficking to the cell surface [167].

These above phosphorylation events are modified in response to neuronal activity or toxic insult, and thus represent additional targets which may be exploited to develop therapies for neurological disease involving aberrant NMDAR activity.

1.3.6 Extrasynaptic NMDA receptor involvement in neurological disease

Glutamate excitotoxicity involving NMDARs has been implicated in a range of acute and chronic neurological disorders including stroke, traumatic brain injury, Alzheimer disease (AD), Parkinson disease (PD), amyotrophic lateral sclerosis, multiple sclerosis, and HD. Altered extracellular glutamate concentrations and/or redistribution of NMDARs in many of these conditions, along with evidence that synaptic and exNMDARs produce opposing signaling outcomes, suggests that neuronal death is driven by a shift from pro-survival to pro-death NMDAR function and that this is a convergent pathological mechanism despite different primary disease causes [124].

1.3.6.1 Excitotoxicity and ischemic stroke

Ischemic stroke causes neuronal death due to excitotoxicity as a result of a large increase in extracellular glutamate levels, which occurs due to excess neurotransmitter release as well as impaired uptake and reversal of glial glutamate transporters [168–171]. The resulting hyperactivation of exNMDARs and imbalance in Ca^{2+} homeostasis leads to the disruption of multiple signaling

pathways in neuronal culture or in vivo animal models of ischemia [172]. Specifically, excitotoxic or ischemic activation of primarily GluN2B-containing exNMDARs decreases protective cAMP response element-binding protein (CREB) and extracellular signal-regulated kinase (ERK) activation, consequently downregulating BDNF production and survival signaling (**Fig. 1.1**) [125, 173, 174]. It furthermore induces detrimental p38 mitogen-activated protein kinase (MAPK) activation downstream of both calpain-mediated striatal-enriched protein tyrosine phosphatase (STEP) cleavage and GluN2B-PSD95-coupled neuronal nitric oxide synthase (nNOS) activation [175, 176]. Additionally, ischemia leads to the pro-death activation of cyclin-dependent kinase 5 (cdk5), c-Jun N-terminal kinase (JNK), death-associated protein kinase 1 (DAPK1), and the nuclear translocation of phosphatase and tensin homolog (PTEN) (**Fig. 1.1**) [176–180]. Small-molecule inhibition of these downstream pro-death proteins or peptide-mediated blockade of their interaction with NMDARs protects neurons from excitotoxic death, indicating that targeting excitotoxicity at a level directly below the NMDAR itself may prove advantageous in human disease [172]. Despite the acute nature of ischemia, the knowledge obtained using these animal models of has encouraged further exploration into the commonality of pathogenic pathways between stroke and neurodegeneration, including HD.

1.3.6.2 Alzheimer disease

AD is the most prevalent form of dementia and is characterized by the formation of amyloid-beta (Aβ) plaques and hyperphosphorylated tau-containing neurofibrillary tangles [181]. However, evidence indicates that soluble Aβ oligomers and phosphorylated tau protein are the primary drivers of synaptic dysfunction and neuronal death in AD [181].

Soluble tau binds to Src-family tyrosine kinases, directing them to postsynaptic NMDARs where they regulate GluN2B surface expression via phosphorylation at Y1472 [182, 183]. This physiological function is altered by tau hyperphosphorylation or Aβ-induced tau mislocalization in AD mouse models

[182, 183]. Additionally, Aβ reduces synaptic NMDAR expression and decreases synaptic currents in primary neurons, thus shifting the synaptic-extrasynaptic NMDAR balance and reducing downstream phosphorylation of CREB [184–186]. Aβ also increases extracellular glutamate concentrations, possibly through reducing glial glutamate uptake, which further promotes the activation of exNMDARs [187, 188]. Notably, exNMDAR activation itself induces tau overexpression and Aβ generation in neurons, thus further amplifying synaptic dysfunction and neurodegeneration [189, 190].

As expected based on the subunit distribution of NMDARs, GluN2B-selective antagonists reverse some of the downstream molecular effects of Aβ in neurons, indicating a prominent role for receptors containing this subunit [185, 186, 191]. Similarly, selective blockade of exNMDARs protects neurons from Aβ-induced spine and synapse loss [188, 192]. Promisingly, memantine, an NMDAR open-channel blocker with preference for receptors in the extrasynaptic compartment at low concentrations, has shown benefit in some AD clinical trials, particularly when administered as part of combination therapy, and is approved for the treatment of moderate to severe AD [193].

1.3.6.3 Huntington disease

The role of extrasynaptic GluN2B-containing NMDAR excitotoxicity in the pathogenesis of HD has been particularly well-characterized. Studies in HD cellular and in vivo animal models have consistently demonstrated enhanced susceptibility to NMDAR agonists and increased NMDAR-mediated currents compared to WT [68, 77, 78, 81, 194–201]. Cell death in these experiments was primarily due to GluN1/GluN2B, but not GluN1/GluN2A receptor activation, as it was largely blocked by GluN2B-selective antagonism with ifenprodil [81, 196, 197, 200]. These elevated NMDAR currents were associated with increased intracellular Ca^{2+} responses in HD MSNs, resulting in mitochondrial membrane depolarization and caspase activation [68, 197, 199, 200, 202].

In 2007, Fan et al. observed enhanced forward trafficking of NMDAR subunits to the surface of HD MSNs, identifying a potential explanation for elevated receptor currents [203]. This mechanism was further elucidated by a study showing increased association between GluN2B and its scaffold protein PSD95 in YAC128 striatal tissue, which would be expected to stabilize GluN2B-containing receptors at the cell surface [194]. A GluN2B-PSD95 interference peptide perturbed this interaction, reduced NMDAR surface levels, and prevented NMDA-induced apoptosis in YAC128 MSNs [194]. Later work provided evidence that this protective effect was mediated by blocking p38 MAPK activation which was dependent on the PSD95-GluN2B interaction [204]. Additionally, small-molecule p38 MAPK inhibition was neuroprotective [204]. This provided some of the first evidence that reversing surface expression of GluN2B-containing receptors and/or inhibiting signaling directly downstream of exNMDAR activation may provide neuroprotection in HD.

Further support came from work demonstrating that preferential blockade of exNMDARs with low-dose memantine in YAC128 mice from 2-12 months of age restored striatal volume and improved motor function, while high-dose memantine (which would be expected to also inhibit synaptic NMDAR activity) worsened these phenotypes [205]. In a seminal 2010 study, Milnerwood et al. clearly demonstrated enhanced extrasynaptic GluN2B-containing NMDAR activity in YAC128 MSNs in vivo [80]. This was due to an increase in GluN2B protein levels in the extrasynaptic (non-PSD) membrane compartment [80]. Importantly, these changes were observed at 1 month of age – well before behavioral phenotypes, neurodegeneration, or MSN structural changes [80]. Remarkably, low-dose memantine treatment from 2-4 months of age restored YAC128 striatal nuclear CREB activity and motor learning at 4 months [80]. These findings were supported by a later study in which the same treatment paradigm restored the balance between cell survival (phospho-CREB; pCREB) and cell death (phospho-p38 MAPK) signaling in the YAC128 striatum, and normalized exGluN2B protein expression [206]. Furthermore, YAC128 MSNs co-cultured with cortical neurons exhibit elevated surface GluN2B expression as well

as enhanced exNMDAR current which is blocked by ifenprodil [81]. In these experiments, ifenprodil or memantine prevented NMDA-induced CREB shut-off and neuronal death, both of which were more severe in control-treated YAC128 MSNs compared to WT [81]. Altered exNMDAR function was later observed in both direct (D1) and indirect (D2) MSNs of YAC128 mice [207]. Further supporting a pathological role for GluN2B-containing NMDARs in HD, a mHTT knock-in mouse model generated to overexpress GluN2B develops exacerbated striatal neuropathology [208].

mHTT undergoes caspase-mediated cleavage at multiple sites, generating toxic N-terminal polyglutamine-containing fragments [209]. Mutation of a key mHTT cleavage site, D586, results in complete amelioration of disease pathology in YAC128 mice, including reversal of exNMDAR currents and MSN susceptibility to NMDAR agonism [80, 195, 210]. This indicates that mHTT cleavage at this site is essential for dysregulation of NMDARs, although the precise mechanism by which the aa1-586 mHTT fragment leads to enhanced exNMDAR activity remains unknown.

Altered NMDAR phosphorylation has been reported in HD mouse models. Downregulation of GluN1 phosphorylation at S897, which would be expected to reduce NMDAR surface expression [167], occurs in the N171-82Q striatum at all disease stages assessed [211]. In the R6/2 hippocampus, tyrosine phosphorylation of GluN2A is decreased [212]. In 2012, Gladding et al. observed reduced GluN2B pY1472 in YAC128 striatal tissue [213]. This was associated with greater synaptic activation of the Y1472 phosphatase STEP and reduced synaptic retention of GluN2B, resulting in receptor movement to extrasynaptic membranes [213]. Furthermore, elevated GluN2B calpain cleavage, which has been linked to Y1336 phosphorylation, promotes its localization at the extrasynaptic surface in the YAC128 striatum, possibly by decreasing endocytosis [156, 213]. In contrast, an earlier study reported enhanced mHTT-induced GluN2B tyrosine phosphorylation in transfected cells [214]. However, this study was not able to assess synaptic versus extrasynaptic phosphorylation, and the antibody used did not distinguish between Y1472 and the nearby

phosphorylation sites Y1336 and Y1252. Altogether these findings show that mHTT dysregulates post-translational modification of NMDARs, impacting their function and localization at the neuronal surface. Further investigation of phosphorylation levels at other GluN2B residues in HD mice, in addition to a deeper understanding of the mechanisms underlying these changes, will provide novel options for therapeutic regulation of NMDAR excitotoxicity in HD.

1.4 DEATH-ASSOCIATED PROTEIN KINASE 1 STRUCTURE AND FUNCTION

DAPK1 is a 160-kDa (1430-amino acid) Ca^{2+}/calmodulin (CaM)-dependent serine/threonine (S/T) kinase which is expressed highly in the brain, regulates GluN2B phosphorylation, and possesses pro-apoptotic functions. The orthologous human and mouse genes are located on chromosome 9 and chromosome 13, respectively, and share 95% amino acid sequence identity. Evolutionary conservation, particularly within the major functional domains of the protein, extends as far back as C. elegans, with the highest degree of similarity present within the N-terminal kinase domain.

1.4.1 Discovery of DAPK1 and characterization of its functional domains

DAPK1 was first discovered in an antisense cDNA expression library screen designed to identify genes that promote interferon gamma (IFNγ)-induced cell death in HeLa cells [215]. Sequence homology analysis and in vitro phosphorylation assays indicated the presence of a CaM binding domain (also called the autoregulatory domain, ARD) as well as an adjacent N-terminal S/T catalytic domain [215]. Furthermore, DAPK1 demonstrated autophosphorylation activity which was dependent on the presence of the adenosine triphosphate (ATP)-binding lysine residue at position 42, an amino acid which is conserved in essentially all kinases and important for proper structural conformation of the active site (**Fig. 1.3**) [215]. Subsequent work confirmed Ca^{2+}/CaM-dependent in

vitro kinase activity toward myosin light chain 2 (MLC2), which was abolished in a K42A catalytically-inactive mutant [216]. When the CaM binding domain was deleted (ΔCaM), constitutive Ca^{2+}/CaM-independent activity remained, indicating a negative regulatory role for this region [216]. This inhibitory feature is common to other CaM-regulated kinases, such as myosin light chain kinase (MLCK) and CaMKII, which also contain an ARD [217].

Soon after these initial studies, the site of DAPK1 autophosphorylation was mapped to the evolutionarily-conserved S308 residue within the ARD (**Fig. 1.3**) [218]. Addition of Ca^{2+}/CaM or introduction of a phosphodeficient mutation (S308A) reduced autophosphorylation of DAPK1 and enhanced its kinase activity toward MLC2 in vitro [218]. The S308A mutant also possessed higher binding affinity for CaM, and transfection of either the S308A or a ΔCaM construct into HEK293 cells promoted significant cell death compared to WT DAPK1, while mimicking phosphorylation with an S308D or S308E mutation reduced CaM binding affinity, decreased kinase activity and conferred protection [218]. Based on these findings and additional structural data, a model was proposed whereby phosphorylated S308 stabilizes the ARD within the catalytic ATP-binding pocket, blocking pro-apoptotic kinase activity. Dephosphorylation of S308 partially opens this autoinhibitory lock and in combination with high levels of Ca^{2+}, facilitates CaM binding to the ARD, release of the catalytic domain through a conformational change, and full activation of the kinase [218]. More recent crystal structure and biochemical analyses support this model, pointing to a multi-step DAPK1 activation process that requires both S308 dephosphorylation and binding of Ca^{2+}-activated CaM [219].

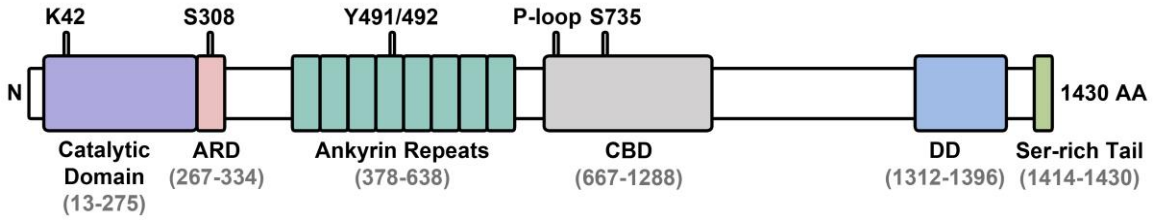

Figure 1.3: Human DAPK1 functional domains and key amino acid residues. DAPK1 contains multiple functional domains including a catalytic domain, an autoregulatory domain (ARD), eight ankyrin repeats, a cytoskeletal binding domain (CBD), a death domain (DD), and a serine-rich tail. Key motifs and post-translational modification sites are noted. Amino acid residue numbers are depicted in grey.

Positioned adjacent to the kinase and CaM binding domains are the ankyrin repeats and the cytoskeletal binding domain (CBD) (**Fig. 1.3**), both of which play critical roles in the localization of DAPK1 to the cytoskeletal network and undergo post-translational modifications which alter the function of the protein.

Near the C-terminus lies the death domain (DD) (**Fig. 1.3**), a sequence which is also found in other proteins involved in apoptosis and mediates interactions with a number of binding partners, such as ERK, p53, and tau [220]. The biological significance of these interactions, particularly in the context of excitotoxicity, will be discussed in Section 1.5.2. Deletion of the DD does not affect DAPK1 autophosphorylation or in vitro catalytic activity toward MLC2, but still impairs the maximum cell death-inducing function of the kinase, possibly by impairing critical interactions with other protein partners [216, 221, 222]. This hypothesis is supported by studies in which expression of a small DD protein blocked the ability of DAPK1 or other stressors to promote cell death, likely due to competition with the full-length kinase for its binding partners which normally interact through this domain [221, 223, 224].

Finally, the final 17 amino acid C-terminal tail of DAPK1 is unusually serine-rich (**Fig. 1.3**). A peptide corresponding to this sequence inhibited cell death induced by ceramide treatment or DAPK1 overexpression, suggesting a protective role for this region, and deletion of this sequence potentiated DAPK1-induced apoptosis in HEK293 cells without affecting its kinase activity [223, 225].

The authors proposed that the serine-rich tail may modulate DAPK1 activity in cis by folding over other protein domains, and that the protective effect of the peptide was due to inhibition in trans of the full DAPK1 protein by altering the folded structure of the protein and consequently its interaction with various binding partners.

1.4.2 DAPK1 isoforms and homologs

An alternatively-spliced isoform of DAPK1 (DAPK1β) has been described, and possesses a 12 amino acid extension of the C-terminus [226]. All structural domains of DAPK1 (differentiated in this sub-section by the term DAPK1α) are retained in DAPK1β [226]. As predicted, based on a nearly identical kinase domain to DAPK1α, DAPK1β shows in vitro Ca^{2+}/CaM-dependent kinase activity toward MLC2, and this is reliant on the presence of the conserved K42 residue within the kinase domain [226]. Unexpectedly, ectopic expression of DAPK1β in HeLa cells protected against tumor necrosis factor (TNF)-induced apoptosis and consequent caspase activation, and this effect required K42, indicating that DAPK1β kinase activity was cytoprotective [226]. Importantly, however, DAPK1α expression also provided a mild protective benefit in this study, which was discordant with several other reports demonstrating apoptosis in response to DAPK1α overexpression [216, 218, 221–223], and a later independent study observed pro-apoptotic function of DAPKβ [227]. Thus, additional work is required to determine exactly how the function of DAPK1α and DAPK1β differ from each other, and to assess whether these findings can be supported in an endogenous scenario. The C-terminal tail negatively regulates the activity of DAPK1, potentially involving post-translational phosphorylation of its many serine residues [223, 225]. Thus, it is possible that an extension of this region in DAPK1β enhances the inhibitory function of the C-terminal domain, leading to protective effects instead of promoting apoptosis.

A number of DAPK1 paralogs exist within the DAPK family: DAPK2 (DAPK-related protein kinase 1; DRP1), DAPK3 (Zipper-interacting protein

kinase; ZIPK), DRAK1 (DAPK-related apoptosis-inducing protein kinase 1), and DRAK2. DAPK2 and DAPK3 possess approximately 80% sequence identity to DAPK1 within the catalytic domain, while DRAK1 and DRAK2 share 50% identity. All 5 DAPK family members contain the catalytic domain but differ in the presence of the other functional domains, which may impact their localization and function (**Fig. 1.4**). Similar to DAPK1, kinase activity of DAPK2 and DAPK3 is reliant on the presence of the conserved ATP-binding lysine residue within the catalytic site, and both proteins also have roles in apoptosis [228–230]. Of all DAPK1 paralogs, only DAPK2 contains the Ca^{2+}/CaM-binding ARD with an autoinhibitory phospho-serine site, and as expected, deletion of this domain results in a constitutively active kinase [228, 230]. Kinase activity regulation of the ARD-lacking DAPK3 is hypothesized to instead occur via phosphorylation of various threonine residues in the catalytic domain [231].

All 5 DAPK family members contain short stretch of positively charged amino acid residues in the catalytic domain, called the basic loop [232]. This structure is not necessary for substrate phosphorylation, but instead mediates DAPK1 or DAPK2 homodimerization, as well as heterodimerization between DAPK1/DAPK2 and DAPK1/DAPK3 [233–236]. Dimerization may functionally contribute to DAPK activity regulation by influencing CaM binding and substrate accessibility to the catalytic site [235, 237, 238]. Furthermore, activation of DAPK3 through direct phosphorylation by DAPK1 within heterodimers has been reported [233]

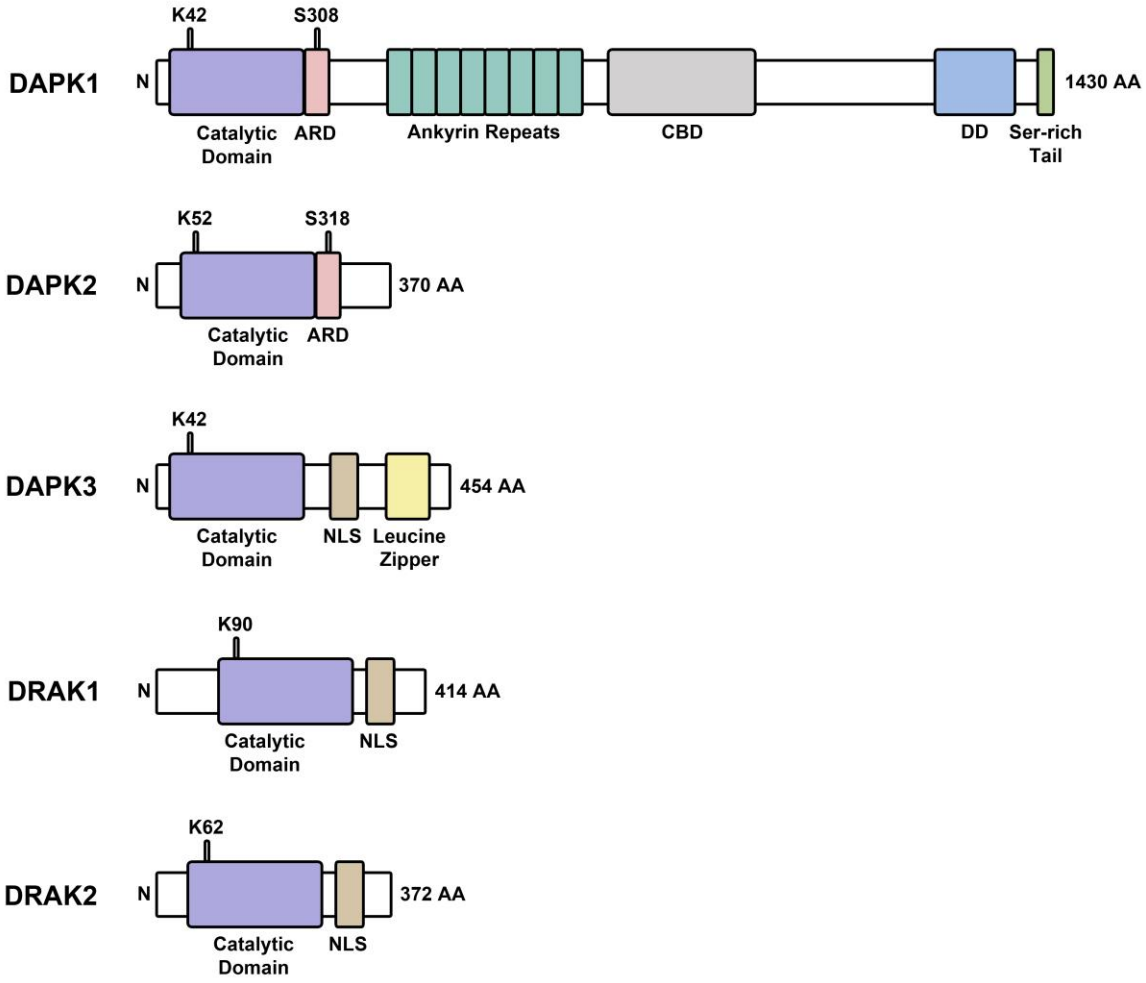

Figure 1.4: Functional domains of human DAPK family members. DAPK1 contains multiple functional domains including a catalytic domain, an autoregulatory domain (ARD), eight ankyrin repeats, a cytoskeletal binding domain (CBD), a death domain (DD), and a serine-rich tail. All other family members lack the domains C-terminal to the catalytic domain, with the exception of DAPK2, which possesses an ARD. DAPK3 contains a nuclear localization signal (NLS) and a leucine zipper domain, while the more distantly-related kinases DRAK1 and DRAK2 only contain an NLS C-terminal to their kinase domains. The highly-conserved catalytic lysine residue (K42 in DAPK1) and autoinhibitory phosphorylation site (S308 in DAPK1) are marked.

1.4.3 Tissue and cellular distribution of DAPK1

A small number of comprehensive studies of *Dapk1* mRNA tissue distribution in rodents have been performed to date. In 1999, Yamamoto et al. found that *Dapk1* was predominantly expressed at a comparable level in the brain and lung,

and to a lesser extent, the kidney and heart of adult rats [239]. *Dapk1* expression peaked in the brain at E20 and tapered quickly in the postnatal period [239]. At embryonic time points, *Dapk1* expression was found in nearly all brain regions, while expression in the adult rat was largely restricted to the cortex and hippocampus [239]. Interestingly, expression was observed almost exclusively in neurons, but not glia [239]. These results were supported by another study which also observed strong *Dapk1* mRNA expression in the brain and lung of adult rats, with brain expression peaking at approximately E18 [240]. In this study, adult mRNA expression was observed in neurons within multiple brain regions including the cortex, olfactory bulb, striatum, and thalamus [240]. Despite multiple studies reporting high expression in the lung, the primary function of DAPK1 in this organ is currently not well understood, but may play a role in regulating lung cell proliferation and inflammation [241, 242].

Together, these region- and time-specific expression patterns, in addition to evidence for its pro-apoptotic function, led to the hypothesis that DAPK1 plays a role in physiological neuronal death during mammalian nervous system development. Since then, others have observed DAPK1 protein expression in the cortex and hippocampus of adult rodents or in cultured primary embryonic neurons, but these studies were generally conducted in the context of a disease state and there still exists a limited understanding of the physiological function of DAPK1 in the mature brain.

Early studies of DAPK1 subcellular localization found it was associated with the cytoskeleton. Specifically, DAPK1 colocalizes with actin microfilaments as assessed by immunostaining and fractionation experiments [216]. Deletion of various regions of DAPK1 identified amino acids 641-835 (comprising part of what is now termed the CBD), as critical for this distribution [216]. Overexpression of active DAPK1 induced microfilament alterations similar to those occurring in response to apoptotic stimuli, indicating a role for cytoskeletal DAPK1 in promoting morphological changes during cell death [216]. These effects were later found to be associated with phosphorylation of the actin motor complex protein MLC2 at S19 by DAPK1, contributing to actin fiber contraction

and membrane blebbing [243]. In this study, deletion of either the CBD or the ankryin repeats impaired proper actin localization of DAPK1 [243]. Furthermore, DAPK1 also promotes membrane blebbing through an alternate pathway, by interacting with the microtubule-associated protein 1B [244].

In addition to cytoskeletal binding, DAPK1 has also been reported to interact with transmembrane NMDARs as well as localize to dendritic spines, mitochondria, and the nucleus, with these interactions being sensitive to the levels and/or patterns of neuronal activity [177, 245–247].

1.4.4 Regulation of DAPK1 expression and kinase activity

As previously discussed, DAPK1 becomes fully activated through a two-step mechanism involving S308 dephosphorylation and Ca^{2+}-activated CaM binding. The relationship between these two events is reciprocal: phosphorylation at S308 reduces CaM binding affinity, while CaM binding reduces S308 autophosphorylation, thus keeping the kinase in a tightly-regulated inactive state until an appropriate activation signal occurs [218]. Aside from this, a number of other transcriptional processes and post-translational modifications contribute to fine-tuning of DAPK1 protein levels and kinase activity.

1.4.4.1 Regulators of DAPK1 phosphorylation

As described above, DAPK1 is kept in an inactive state through S308 autophosphorylation within the CaM binding domain, which likely occurs through an intramolecular cis-transfer of a phosphate group from ATP bound to K42 in the catalytic site [248]. Various stimuli result in Ca^{2+}-dependent activation of DAPK1 by dephosphorylation at this residue, which can occur via calcineurin (CaN) or protein phosphatase 2A (PP2A) [177, 249–253]. Phosphorylation of the nearby site, S289, by ribosomal s6 kinase 1/2 (RSK1/2) has been reported by different groups to either inhibit or enhance DAPK1 activity, indicating that

various experimental conditions may influence the impact of phosphorylation at this site [254, 255].

Within the CBD exists a short P-loop sequence (amino acids 695-702) critical for cytoskeletal localization, which lies within a larger amino acid stretch with homology to the Ras of complex proteins (ROC) domain of the ROCO protein kinase family [216]. Binding of guanosine triphosphate (GTP) to the ROC domain influences kinase activity of these protein family members [256]. Carlessi et al. showed that DAPK1 homodimerizes via binding of its catalytic domain to the ROC domain of another DAPK1 molecule, and that GTP binding to the P-loop within the ROC domain inhibits DAPK1 kinase activity by upregulating S308 cis autophosphorylation [248]. Furthermore, DAPK1 was shown to possess intrinsic GTPase activity, leading the authors to hypothesize that hydrolysis of the bound GTP promotes activation of the kinase, thus fine-tuning its function [248].

Within the ankyrin repeats are two adjacent tyrosine residues, Y491/492 (**Fig. 1.3**) which are phosphorylated by Src kinase and dephosphorylated by leukocyte common antigen-related protein (LAR) [257]. Wang et al. observed that phosphorylation at Y491/492 results in DAPK1 inactivation, while dephosphorylation by LAR promotes its activity and pro-apoptotic function [257]. Similar to the ROC-catalytic domain interaction, the mechanism for this regulation involves binding of the ankyrin repeats to the catalytic domain, which is enhanced by phosphorylation at Y491/492 [257]. However, the potential modulatory effect of pY491/492 on pS308 was not investigated.

S735 lies within the fourth ankryin repeat of DAPK1 (**Fig. 1.3**), and can be phosphorylated by ERK [222]. This phosphorylation event increases DAPK1 catalytic activity and requires interaction of ERK with the DD of DAPK1 [222]. Again, it was not assessed whether this activation of DAPK1 by pS735 occurs via reduced pS308, but it is a plausible theory given the evidence that the ankyrin repeats can interact with the catalytic domain [257].

1.4.4.2 DAPK1 degradation and cleavage

In addition to phosphorylation, DAPK1 activity levels are also controlled by modulation of the protein level itself, which can occur via both degradative or cleavage mechanisms.

The presence of smaller 120-kDa and 60-kDa fragments of DAPK1 have been reported in multiple studies [226, 252, 258]. The levels of these fragments increase in response to ischemia or evoked seizures in rodents, indicating that pathological cleavage of DAPK1 occurs in the brain [252, 258]. Incubation of DAPK1 with cathepsin B produced a 60kDa fragment, and a cathepsin B inhibitor prevented oxygen and glucose deprivation (OGD)-induced generation of the 120-kDa fragment [252, 258, 259]. The minimal binding site on DAPK1 for cathepsin B was later mapped to amino acids 836-947 within the CBD, and inhibition of cathepsin B increased the steady-state levels of full-length DAPK1 in cells [259]. However, the specific location of these cleavage events within DAPK1 and the impact on its functional activity remain to be determined.

Polyubiquitination of DAPK1 targets it for proteasomal degradation, and is catalyzed by multiple E3 ligases [260–263]. Conversely, heat shock protein 90 (HSP90) interacts with DAPK1 and E3 ligases within heterocomplexes, preventing DAPK1 degradation by the ubiquitin proteasome pathway [263]. Thus, fine-tuning of DAPK1 protein turnover is achieved by modulation of the relative levels of HSP90 and various E3 ligases within DAPK1 chaperone complexes.

Other degradative pathways also contribute to regulation of DAPK1 protein levels. Interaction with the GTPase-activating protein tuberin promotes DAPK1 lysosomal degradation, independent of autophagic or proteasomal activity [264]. Furthermore, an alternative splice variant of DAPK1, termed s-DAPK1, has been described [265]. s-DAPK1 does not contain the kinase domain but consists of a portion of the ankyrin repeat region [265]. This s-DAPK1 protein is short-lived in cells and promotes degradation of full-length DAPK1 in a proteasome-independent manner [265]. However, further investigation is required to understand the mechanism of this regulatory process.

1.4.4.3 Transcriptional regulation of *DAPK1*

A number of regulatory processes influence the mRNA levels of *DAPK1.* Methylation of CpG islands in the *DAPK1* promoter result in downregulation of its expression levels [266]. This process has been linked to a number of human cancers, as will be discussed briefly in Section 1.5.6. *DAPK1* was identified as a target of p53, which binds to intron 1 of both the human and mouse genes in response to various cell stressors, increasing *DAPK1* transcription [267]. Interestingly, DAPK1 phosphorylates and activates p53 during ischemia, promoting its nuclear translocation and expression of pro-apoptotic target genes, suggesting a positive feedback loop between DAPK1 and p53 which is activated in neuronal death [220]. Other transcription factors shown to either positively or negatively regulate *DAPK1* transcription include C/EBP-β, Smad, STAT3, NF-kB, and HOXC9 [266, 268]. Finally, post-transcriptional regulation of *DAPK1* mRNA occurs through binding of miR-103 and miR-107 to the 3' UTR, which either blocks translation or promotes mRNA degradation [269]. miR-26a also regulates DAPK1 levels [270]. Further study of the transcriptional control of DAPK1 is warranted, particularly in the context of neurological disease.

1.4.5 DAPK1 substrates and interactors

In recent years, a number of key DAPK1 substrates have been identified and these phosphorylation events are involved in various physiological and pathogenic cellular processes. DAPK1 utilizes the same consensus sequence as all Ca^{2+}/CaM-regulated kinases (RXXS/TX), which has assisted in mapping the specific phosphorylation sites on some of its substrates [217]. A list of known DAPK1 substrates and interactors as well as brief summaries of the functional consequences of each reaction or interaction are shown in **Table 1.1.** Substrates of particular interest due to their potential involvement in neurological disease or neuronal death are discussed in greater detail in the following sub-sections.

Table 1.1: DAPK1 substrates and interactors

	Protein	Substrate phospho- site	DAPK1 interaction domains	Effect of phosphorylation or interaction	Ref.
Substrates	α-synuclein	S129	Unknown	pS129 influences α-synuclein turnover, localization, and protein interactions	[270, 271]
	Beclin-1	T119	Catalytic domain	Dissociation of beclin-1 from Bcl proteins and induction of autophagy	[272, 273]
	CaMKK	S511	Unknown	Attenuation of CaM-stimulated CaMKK autophosphorylation	[274]
	GluN2B	S1303	Catalytic domain	Increased GluN2B-containing NMDA receptor conductance and surface expression	[152, 177]
	MLC2	T18/S19	Unknown	Actin fiber contraction and membrane blebbing	[226, 243]
	NDRG2	S350	Cytoskeletal binding domain	Promotion of neuronal death in response to ceramide or Aβ	[275]
	P53	S23	Death domain	Translocation of p53 to nucleus and mitochondria; enhanced p53 pro-apoptotic function in both locations	[220]
	Pin1	S71	Cytoskeletal binding domain	Inhibition of Pin1 nuclear localization and function	[276]
	Syntaxin-1A	S188	Unknown	Reduction of syntaxin-1A binding to munc18-1	[277]
	Tau	S262	Catalytic domain, Death domain	Increased synaptic tau, decreased spine and synapse density	[220, 247]
Interactors	APP	N/A	Death domain	Promotion of APP phosphorylation at T688 by JNK	[278]
	DANGER	N/A	Unknown	Inhibition of DAPK1 activity	[279]
	ERK	N/A	Death domain	ERK-mediated phosphorylation of DAPK1 at S735 stimulates DAPK1 activity; DAPK1-mediated cytosolic sequestration of ERK reduces nuclear ERK activity	[222]
	LAR	N/A	Unknown	LAR-mediated dephosphorylation of DAPK1 at Y491/492 stimulates its catalytic pro-apoptotic function	[257]
	MAP1B	N/A	Unknown	Promotion of autophagy and membrane blebbing	[244]
	MARK1/2	N/A	Death domain	Stimulation of MARK1/2 phosphorylation of tau at S262 and inhibition of axon formation	[280]
	PKD	N/A	Unknown	H_2O_2-induced activation of JNK via PKD	[281]
	Src kinase	N/A	Unknown	Src-mediated phosphorylation at Y491/492 promotes DAPK1 inactivation	[257]
	UNC5H2	N/A	Death domain	Recruits DAPK1 to PP2A, promoting DAPK1 S308 dephosphorylation and activation	[250]

1.4.5.1 GluN2B

DAPK1 was identified as a predominant interactor recruited to GluN2B-containing NMDARs during ischemic stroke in response to pathological Ca^{2+} influx [177]. The GluN2B interaction site spans amino acids 1292-1304, and is phosphorylated by DAPK1 at S1303 within this region [177]. Interestingly, phosphorylation at S1303 further enhances the DAPK1-GluN2B interaction, as does introduction of a S308A phosphodeficient mutation in DAPK1, suggesting a positive amplification of binding between these two proteins once activated [246]. Through the use of phosphomimetic and phosphodeficient mutations, pS1303 was found to enhance GluN2B-containing receptor conductance as well as promote GluN2B surface expression [152, 177]. Like DAPK1, CaMKII also interacts with and phosphorylates GluN2B at S1303 [282]. However, instead of further promoting CaMKII binding, pS1303 may instead inhibit Ca^{2+}-independent binding of autonomously active CaMKII [283, 284]. This is proposed to comprise a key mechanism for the function of CaMKII in synaptic activity-induced long-term plasticity, whereby CaMKII interacts with GluN2B during synaptic activity, phosphorylates the receptor at S1303, and is then maintained in an autophosphorylated, autonomously active state once Ca^{2+} levels have dissipated [284, 285]. Interestingly, the effect of pS1303 on GluN2B surface expression is mediated through regulation of CaMKII binding. CaMKII anchors CK2 to GluN2B receptors, allowing it to subsequently phosphorylate GluN2B at S1480 and reduce NMDAR surface expression [152]. pS1480 disrupts the interaction between GluN2B and PSD95, an anchor protein responsible for stabilizing GluN2B at the cell surface [147]. This stabilization likely occurs through the PSD95-mediated recruitment of Src family kinases such as Fyn, which phosphorylate the GluN2B internalization motif at Y1472, preventing clathrin adaptor AP2 binding and subsequent endocytosis [150, 151, 153]. Therefore, phosphorylation of GluN2B at S1303 by DAPK1 could presumably increase receptor surface expression by preventing CaMKII binding, thus unlinking CK2 from GluN2B, decreasing pS1480, and enhancing the surface-stabilizing interaction between GluN2B and PSD95. This hypothesis is illustrated in **Fig. 1.5**.

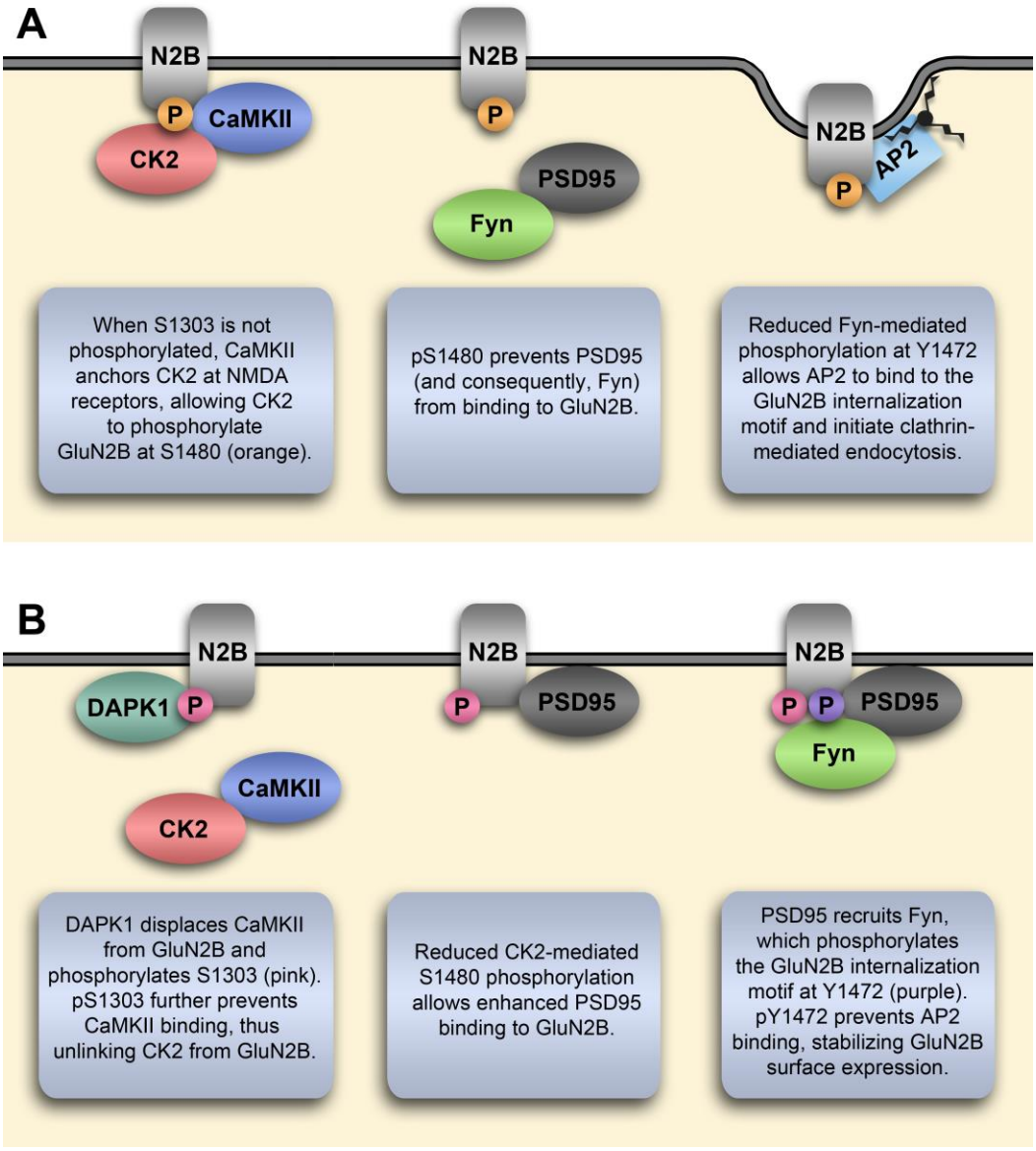

Figure 1.5: Hypothesis figure demonstrating the proposed interaction between DAPK1, pS1303, and GluN2B surface expression. (A) When S1303 is not phosphorylated, GluN2B surface expression is reduced through endocytosis. **(B)** Phosphorylation of GluN2B at S1303 by DAPK1 may promote surface stabilization by indirectly enhancing the GluN2B-PSD95 interaction.

In support of this, DAPK1 and CaMKII were recently found to directly compete for GluN2B binding, with the DAPK1 interaction prevailing under the low Ca^{2+} conditions present during long-term depression (LTD), and CaMKII binding more strongly during periods of high neuronal activity and LTP [246]. Thus, a delicate balance between DAPK1 and CaMKII interactions at the GluN2B receptor

complex may play a critical role in a neuron's homeostatic and plastic responses to activity or cellular stress.

1.4.5.2 ERK1/2

ERK1 and ERK2 are MAPKs involved in an array of signaling processes related to cell survival, cell cycle progression, and gene expression [286]. Bi-phosphorylation of ERK results in its activation, allowing it to phosphorylate cytosolic substrates such as the CREB kinases RSK1-4, as well as translocate to the nucleus where it phosphorylates various transcription factors, influencing gene expression [286].

A yeast two-hybrid screen designed to identify interacting partners with the DAPK1 DD pulled out ERK1 and ERK2, and these interactions were confirmed by co-immunoprecipitation with full-length DAPK1 in cells [222]. Further experiments demonstrated that ERK phosphorylates DAPK1 at S735, which enhances DAPK1 kinase activity in vitro [222]. Interestingly, it was shown that the interaction between DAPK1 and ERK sequestered ERK in the cytosol, preventing its nuclear translocation in response to serum stimulation in cells [222]. When DAPK1 was overexpressed, ERK signaling led to potentiation of cell death instead of anti-apoptotic effects [222]. The authors hypothesized the presence of a positive feedback loop between ERK and DAPK1 which acts to promote the apoptotic function of DAPK1 and alter the functional output of ERK if DAPK1 expression or activity reaches a particular threshold. Additionally, a human tumor-associated mutation in the death domain of DAPK1 (N1347S) prevents its interaction with ERK as well as impairs DAPK1/ERK-mediated apoptosis in cells [287]. Evidence for amplification of this DAPK1/ERK feedback loop in ischemic neuronal death exists and will be discussed further in Section 1.5.2.

Importantly, both ERK and its indirect downstream target CREB have been implicated in exNMDAR function and in HD. While synaptic NMDAR activity induces ERK and CREB phosphorylation, exNMDARs promote both ERK and

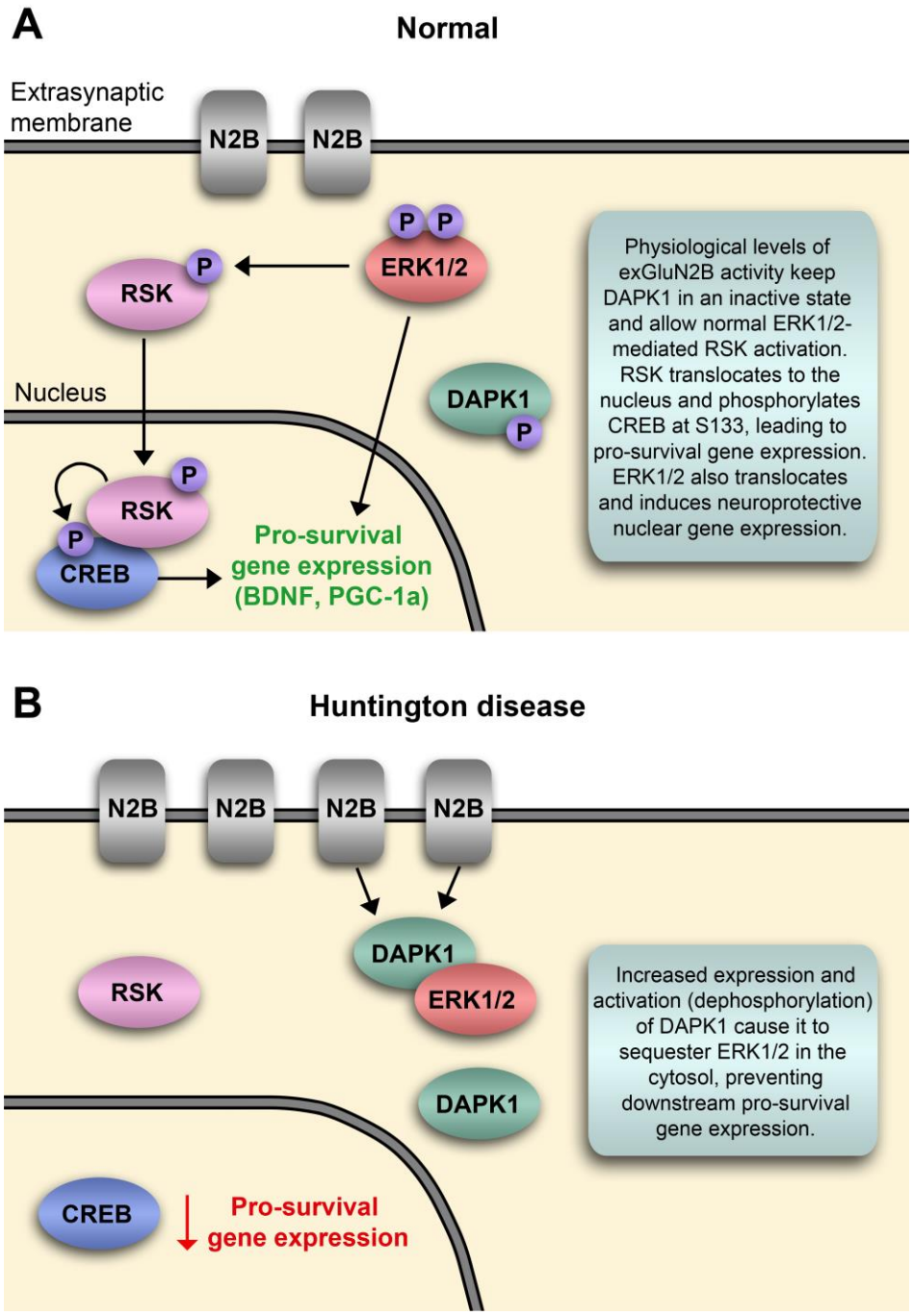

Figure 1.6: Hypothesis figure illustrating the proposed contribution of DAPK1 to exNMDAR-induced CREB and ERK shut-off in HD. (A) In normal conditions, ERK1/2 promotes nuclear pro-survival gene expression **(B)** Pathologically elevated and activated DAPK1 sequesters ERK in the cytosol, which prevents its nuclear translocation and may reduce its interaction with other cytosolic substrates or upstream ERK activators, leading to decreased CREB phosphorylation and a reduction in pro-survival gene expression.

CREB shut-off in a dominant manner [125, 173, 175]. As described earlier, exNMDAR activity is elevated at early stages in the YAC128 mouse model of HD, and this corresponds with reduced phosphorylation of striatal ERK and CREB [80, 206, 288]. It is plausible that activation of DAPK1 by increased exNMDAR function contributes to decreased phosphorylation of CREB and pro-survival gene expression in HD by sequestering ERK in the cytosol (**Fig. 1.6**). However, this hypothesis remains to be investigated.

1.4.5.3 Pin1 and Tau

Tau is a microtubule (MT)-associated protein which binds to and stabilizes the structure of MTs [289, 290]. Hyperphosphorylation of tau impacts its MT-associated functions and contributes to neuronal death in AD [181].

DAPK1 modulates tau phosphorylation and protein expression via multiple mechanisms. First, DAPK1 activates microtubule affinity regulating kinases 1/2 (MARK1/2) through a non-catalytic interaction, resulting in MARK1/2-induced phosphorylation of tau at S262 [280]. This process inhibits the assembly and stability of MTs, influencing axon formation and retinal degeneration in Drosophila [280]. Second, DAPK1 phosphorylates the peptidyl-prolyl cis-trans isomerase Pin1, thereby inactivating its function [276, 291]. Active Pin1 isomerizes the T231 phosphorylation site of tau from the cis to trans conformation [292, 293], and loss of Pin1 function has been linked to AD [294–296]. While cis-pT231 is associated with tau accumulation in AD and is unable to properly stabilize MTs, trans-pT231 can perform normal MT-associated functions [297]. Inactivation of Pin1 by DAPK1 thus increases cis-pT231 tau protein stability and phosphorylation, leading to impaired neurite outgrowth and MT assembly [291]. Finally, DAPK1 phosphorylates tau directly at S262 which, when phosphorylated, reduces tau affinity for MTs and destabilizes the cytoskeleton [247, 298]. This catalytic event not only plays a role in neurodegeneration in AD, but has also been linked to spine damage in ischemia, as will be discussed in Section 1.5.

1.4.6 Relationship between DAPK1 and CaMKII in synaptic plasticity

Recently, DAPK1 has been implicated in modulation of LTD and LTP via regulation of the subcellular localization of the related kinase CaMKII. CaMKII accumulates at excitatory synapses during LTP where it binds to GluN2B subunits within NMDAR complexes [121]. This relocalization and binding promotes phosphorylation of nearby AMPARs by CaMKII, increasing their conductance [120]. Furthermore, anchoring of CaMKII to GluN2B at synapses during LTP-inducing stimuli allows the interaction of CaMKII with other important contributors to synaptic plasticity, including actin cytoskeleton components and proteasomes [299, 300].

Based on the shared GluN2B substrate phosphorylation site (S1303) for both CaMKII and DAPK1, Goodell et al. sought to investigate the potential role of DAPK1 in chemical long-term plasticity in hippocampal slices. The authors found that DAPK1 and CaMKII compete for GluN2B binding, and that high Ca^{2+}/CaM levels during LTP conditions cause DAPK1 to be trafficked out of synapses, while LTD promotes DAPK1 activation and favors DAPK1 spine retention in a CaN-dependent manner [246]. Furthermore, the authors showed that overexpression of DAPK1 inhibits LTP-induced accumulation of CaMKII at synapses, and that small molecule inhibition of DAPK1 kinase activity blocks LTD [246]. Based on this work, DAPK1 is now hypothesized to possess a physiological role in modifying the direction of plasticity by controlling the level of CaMKII-GluN2B binding at the mature synapse. Thus, altered DAPK1 expression or activity in neurological disease could potentially contribute to aberrant synaptic plasticity.

1.4.7 Small molecule DAPK1 inhibitors

The first small molecule DAPK1 inhibitor was synthesized in 2003 by screening a compound library with a previously-developed in vitro DAPK1 enzyme assay [234, 301]. The only hit, an aminopyradazine, was subsequently modified to

improve potency (IC_{50} = 13μM) and selectivity for DAPK1 compared to PKC, PKA, and CaMKII [301]. Crystal structure analysis determined that the molecule occupied part of the ATP binding site within the DAPK1 catalytic domain, proximal to K42 [301]. This compound afforded neuroprotection in animal models of ischemia [252, 301].

In 2009, a structure-based virtual screening approach was used to achieve greater potency and selectivity for DAPK1 [302]. 400,000 compounds were initially screened with a docking algorithm and filtered to select compounds with appropriate characteristics for ATP site binding [302]. Further screening steps and in vitro kinase assays yielded a lead compound demonstrating potent inhibition of DAPK1 (IC_{50} = 69nM; 91% inhibition at 10 μM), as well as the related kinase DAPK3 (IC_{50} = 225 nM) (**Fig. 1.7**) [302]. Inhibition was ATP-competitive and highly selective for DAPK1/3 compared to 48 other S/T or tyrosine kinases [302]. This compound possesses the chemical name (4Z)-2-[(E)-2-Phenylethenyl)-4-(3-pyridinylmethylene)-5(4H)-oxazolone and was designated "TC-DAPK6." TC-DAPK6 has been widely used to investigate the involvement of DAPK1 in a number of neurological disease models, and was selected for experimental use in this thesis.

Recently, a fluorescent, high-throughput enzymatic screening assay for DAPK1 was used to identify another compound with ATP-competitive inhibitory activity toward DAPK1 (IC_{50} = 247 nM) [303]. Detailed crystal structure analysis found that the compound was held in position within the ATP-binding site through interactions with several amino acid residues, including K42 [303]. Based on these findings, it was proposed that potency and selectivity could be further improved in the future by extending the compound structure to interact more strongly with known DAPK1 substrate-recognition motifs [303]. This compound has not been tested in any disease models to date.

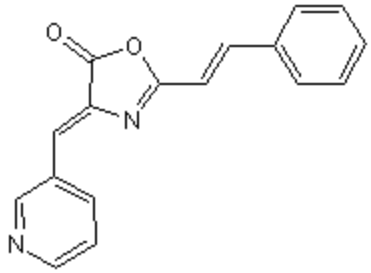

Figure 1.7 Molecular structure of TC-DAPK6. (4Z)-2-[(E)-2-Phenylethenyl)-4-(3-pyridinylmethylene)-5(4H)-oxazolone; IC_{50} for DAPK1 = 69nM.

1.5 ACTIVATION OF DAPK1 IN NEUROLOGICAL DISEASE AND NEUROPROTECTIVE EFFICACY OF DAPK1-TARGETING STRATEGIES

Over the past 20 years, numerous strategies designed to reduce DAPK1 expression or kinase activity have been designed and tested for their ability to alleviate cell death. Studies identifying a role for DAPK1 in neuronal death or neurological disease are summarized in **Table 1.2** and the effects of DAPK1-targeting approaches are listed in **Table 1.3**. Many of the earliest studies demonstrated protective benefits of targeting DAPK1 against various stressors in cells. Evidence for the involvement of DAPK1 in excitotoxicity and neuronal death began to emerge soon after, leading to a surge of interest in its potential as a novel therapeutic target. Consequently, aberrant DAPK1 activity and/or expression have consistently been linked to an increasing number of acute and chronic neurological disorders, as described below.

Table 1.2: Involvement of DAPK1 in neuronal death and neurological disease

Model/Treatment	Tissue/cell type	Effects	Ref.
Ceramide toxicity	Primary hippocampal neurons	Increased DAPK1 protein levels at 1-8h post-treatment	[225]
Kainic acid-induced seizure	Hippocampus	Increased DAPK1 protein levels	[258]
	Cortex & hippocampus	Increased number of DAPK1+ cells	[304]
Glioma-associated epilepsy	Peritumoral brain tissue	Increased DAPK1 protein expression compared to normal and tumoral tissue	[305]
Perinatal hypoxia-ischemia	Cerebrum	Increased DAPK1 activity 7h post-insult	[306]
Transient forebrain ischemia	Cortex	Gradually increased DAPK1 mRNA expression at 1-24h post-ischemia	[239]
Global ischemia	Cortex & hippocampus	Increased DAPK1 mRNA	[252]
Transient focal ischemia (MCAO)	Cortex & striatum	Reduced DAPK1 mRNA in ischemic core and penumbra; increased DAPK1 mRNA in surrounding striatal tissue	[252]
	Cortex	DAPK1 cleavage and dephosphorylation at S308	[252]
	Forebrain	DAPK1 activation 1-2h post-ischemia, increased DAPK1-GluN2B interaction and GluN2B pS1303	[177]
	Cortex	Increased DAPK1-tau interaction, DAPK1 activity, and tau pS262	[247]
	Cortex	Increased DAPK1-GluN2B interaction	[307]
	Cortex	Increased DAPK1-ERK interaction	[308]
In vitro ischemia (OGD)	Primary cortical neurons	DAPK1 dephosphorylation at S308 and cathepsin B-mediated cleavage	[252]
	Primary cortical neurons	Calcineurin-dependent DAPK1 dephosphorylation at S308 and increased activity	[177]
	Cortical neurons	Increased DAPK1 activity	[307]
	N2a cells	Increased DAPK1 protein level, decreased pS308, increased activity, enhanced DAPK1-ERK interaction	[308]
NMDA toxicity	Primary cortical neurons	DAPK1 dephosphorylation at S308	[252]
	Primary cortical neurons	Calcineurin-dependent DAPK1 dephosphorylation at S308 and increased activity	[177]
	Primary cortical neurons	Reduced total DAPK1 protein levels, dephosphorylation at S308, and enhanced interaction with GluN2B	[245]
	Primary cortical neurons	DAPK1 dephosphorylation at S308 and increased GluN2B pS1303	[309]
Aβ treatment	Hippocampal slices	Increased DAPK1 levels	[275]
AD (Tg2576 mice)	Brain lysates	Increased DAPK1 levels	[275]
	Entorhinal cortex	Increased DAPK1 activity	[310]
AD (hTau mice)	Hippocampus & cortex	Increased DAPK1 protein levels and tau pS262	[311]
Human AD	Genomic DNA	2 DAPK1 SNPs associated with late-onset AD; rs4878104 increases DAPK1 expression	[312, 313]
	Hippocampus	Increased DAPK1 protein levels and APP pT668	[275, 278, 291]
Chronic stress	mPFC	Increased DAPK1 protein levels, GluN2B-DAPK1 interaction, and GluN2B pS1303; decreased pS308, pCREB and BDNF	[314]
PD (MPTP mice)	Substantia nigra	Increased DAPK1 expression and α-synuclein pS129	[270]

Table 1.3: DAPK1-targeting strategies in models of neuronal death

Strategy	Disease model	Tissue/cell type	Effects	Ref.
RNAi	Ischemia/Excitotoxicity	Primary cortical neurons	Prevention of NMDA-induced GluN2B S1303 phosphorylation, current, and cell death	[309]
		N2a cells	Promotion of ERK nuclear translocation, increased pCREB, less cell death after ischemic insult	[308]
	AD/tauopathy	Primary hippocampal neurons	Reduced S262 tau phosphorylation by MARK2 and prevention of MARK2-induced impairment in axon formation	[280]
	Chronic stress	Prefrontal cortex	Antidepressant effects, reversal of stress-induced increase in GluN2B pS1303 and decrease in pCREB and BDNF	[314]
Dapk1-/-	Ischemia/Excitotoxicity	Retinal ganglion cells	Protection from glutamate toxicity	[315]
		Primary cortical neurons	Prevention of OGD- or NMDA-induced GluN2B S1303 phosphorylation, extrasynaptic NMDA receptor current and Ca2+ transients, and cell death	[177]
			Prevention of OGD-induced p53 activation	[220]
		Cortex, striatum, hippocampus	Fewer degenerating neurons after global ischemia	[177]
	AD/tauopathy	Cerebrum	Smaller MCAO-induced brain infarction and improved neurological score	[177]
		Hippocampus	Reduced number of apoptotic cells in Tg2576/Dapk1-null compared to Tg2576 mice	[275]
		Whole brain	Reduced levels of Aβ and less APP T668 phosphorylation in Tg2576/DAPK1-null compared to Tg2576 mice	[278]
		Hippocampal slices	Less Aβ -induced neuronal death	[275]
		Whole brain	Reduced APP T668 phosphorylation	[278]
		Primary cortical neurons	Reduced Aβ secretion	[278]
		Primary cortical neurons, brain slices	Reduced tau protein half-life	[291]
		Whole brain	Reduced tau protein levels and phosphorylation in aged mice	[291]
Kinase domain -/-	Ischemia/Excitotoxicity	Cortex	Smaller infarction area after MCAO, fewer degenerating neurons, less tau pS262, protection against loss of synaptic protein expression and spines, improved neurological score	[247]
	AD/tauopathy	Entorhinal cortex (EC)-hippocampal CA1 synapses	Reversal of impaired evoked EPSC amplitude, restoration of EC-CA1 synapse numbers and CA1 spines, normalization of action potential firing probability in CA1 cells, improved spatial learning and memory in Tg2576/DAPK1 kinase domain -/- compared to Tg2576 mice	[310]
	PD	Substantia nigra	Restored behavior phenotypes, prevented degeneration of dopaminergic neurons, reduced α-synuclein phosphorylation and aggregation in MPTP-injected mice	[270]

Strategy	Disease model	Tissue/cell type	Effects	Ref.
Small-molecule inhibition	Ischemia/Excitotoxicity	Whole brain	Prevention of hypoxia-ischemia-induced brain hemisphere weight loss and MAP2 protein decrease	[301]
		Primary cortical neurons	Protection against OGD-induced cell death	[252]
		Cerebrum	Reduced brain infarction volume after MCAO	[252]
		SH-SY57 cells	Protection against glutamate-induced cell death	[316]
	AD	Primary cortical neurons	Reduced Aβ secretion	[278]
	Chronic stress	Prefrontal cortex	Antidepressant effects, prevention of stress-induced increase in DAPK1 and GluN2B pS1303, reversal of stress-induced decrease in pCREB and BDNF	[314]
Peptide uncoupling	Ischemia/Excitotoxicity	Primary cortical neurons	(GluN2B) Prevention of OGD- or NMDA-induced GluN2B pS1303, extrasynaptic NMDA receptor current, Ca^{2+} transients, and cell death	[177]
			(P53) Protection against OGD-induced necrosis and apoptosis	[220]
		Cerebrum	(GluN2B) Smaller brain infarction, improved neurological score, and reduced GluN2B pS1303 after MCAO	[177]
		Cortex and striatum	(GluN2B) Reduced infarct area and number of degenerating neurons after MCAO	[245]
		Cortex and striatum	(P53) Reduced brain infarction volume and number of degenerating cells; improved neurological score after MCAO	[317]
		Cortex	(Tau) Smaller infarction volume, improved neurological score, and prevention of ischemia-induced tau pS262, synaptic protein loss, and altered synaptic transmission after MCAO	[247]
	Chronic stress	Prefrontal cortex	(GluN2B) Antidepressant effects	[314]
	PD	Substantia nigra	(α-synuclein) Restored behavior phenotypes, prevented degeneration of dopaminergic neurons, reduced α-synuclein phosphorylation and aggregation in MPTP-injected mice	[270]
Peptide-mediated knockdown	Ischemia/Excitotoxicity	Cortex and striatum	Reduced infarct area and number of degenerating neurons after MCAO	[245]
	Oxidative stress	Primary cortical neurons	Protection against H_2O_2 toxicity	[245]

1.5.1 Early studies of DAPK1 in cell death

Shortly after its initial identification as a positive mediator of TNF-induced apoptosis in HeLa cells, an additional study found that TNF specifically promotes rapid dephosphorylation of DAPK1 at S308 and enhanced catalytic activity, measured with an in vitro kinase assay [262]. Similar effects were observed in response to ceramide treatment in HeLa and PC12 cells [218, 262, 318], and this was associated with cell death. In primary hippocampal neurons, ceramide resulted in increased DAPK1 protein levels at 1-8 hours post-treatment, although S308 phosphorylation and kinase activity were not assessed [225]. RNA interference (RNAi) strategies targeting DAPK1 afforded protection against interferon gamma (IFNγ) and Fas-induced cell death in HeLa cells [221], and genetic deletion of DAPK1 conferred resistance to ceramide toxicity in primary neurons [225]. These early findings pointed toward a potentially significant role for DAPK1 activation in neuronal death.

1.5.2 The critical position of DAPK1 at the crossroads of multiple neuronal death pathways in ischemia

After the discovery and early characterization of DAPK1, its role in excitotoxicity and ischemic neuronal death became a major research focus. Although ischemic stroke is an acute condition, studies of DAPK1 in ischemia models were critical to understand the role of DAPK1 in neuronal death and have informed extensive follow-up research in models of neurodegeneration.

In 1999, Yamamoto et al. reported increased cortical *Dapk1* mRNA expression after transient forebrain ischemia in rodents [239]. This finding was supplemented by additional research in perinatal hypoxia-ischemia (HI) and renal ischemia models, both demonstrating increased DAPK1 activity in relevant tissues post-insult [306, 319]. Small molecule inhibition of DAPK1 prevented HI-induced loss of brain hemisphere weight, while genetic deletion of the DAPK1 kinase domain protected against ischemia-induced renal cell apoptosis and caspase-3 activation [301, 319]. In 2005, Shamloo et al. observed that transient

focal ischemia (middle cerebral artery occlusion; MCAO) caused *Dapk1* mRNA downregulation in the cortical ischemic core and upregulation in the nearby surviving striatal tissue [252]. This group also reported S308 dephosphorylation and proteolytic cleavage of cortical DAPK1 in response to ischemia [252]. These findings were validated in primary cortical neurons using the in vitro OGD model of ischemia, which also induced DAPK1 cleavage and S308 dephosphorylation in an NMDAR- and CaN-dependent manner [252]. Importantly, treatment with a DAPK1 inhibitor protected against OGD-induced neuronal death in vitro and reduced brain infarction volume in vivo after MCAO [252]. The beneficial effect of targeting DAPK1 was further demonstrated by improved survival of glutamate-treated retinal ganglion cells from DAPK1 knockout mice compared to WT [315], as well as protection against glutamate toxicity in cells treated with the DAPK1 inhibitor TC-DAPK6 [316].

Despite the growing body of evidence implicating DAPK1 in ischemia in the early 2000s, the mechanism by which DAPK1 contributes to neuronal death remained elusive. However, in 2010 Tu et al. identified DAPK1 as one of the major GluN2B interactors recruited to NMDAR complexes under ischemic conditions [177]. This group showed that MCAO activates DAPK1 in the mouse forebrain, and that active DAPK1 phosphorylates GluN2B at S1303, which consequently enhances GluN1/GluN2B channel conductance [177]. Interestingly, phosphorylation at S1303 may promote enhanced GluN2B surface expression in neurons, further contributing to receptor activity [152]. Tu et al. also demonstrated that both OGD and NMDA treatment of primary cortical neurons resulted in dephosphorylation of DAPK1 at S308 and increased catalytic activity [177]. However, these effects were blocked in CaN-null neurons, indicating that CaN is responsible for dephosphorylation of DAPK1 at S308 during ischemic stimuli [177]. OGD and NMDA treatment in primary neurons induced GluN2B S1303 phosphorylation, exNMDAR current, Ca^{2+} transients, and cell death, all of which were prevented by genetic deletion of the *Dapk1* gene [177]. Furthermore, *Dapk1*-null mice possessed fewer degenerating neurons in response to global ischemia compared to WT controls, as well as smaller brain infarction and

improved neurological score after MCAO [177]. Finally, the authors generated a DAPK1-GluN2B uncoupling peptide consisting of a short amino acid sequence of GluN2B in the DAPK1-binding region, and this also afforded beneficial effects on ischemia in vitro an in vivo [177]. However, it was recently demonstrated that the neuroprotective properties of this peptide are due to its activity as an open-channel NMDAR blocker, rather than due to blockade of the DAPK1-GluN2B interaction [320]. This recent study also failed to replicate some of the findings of Tu et al, indicating that further validation is required and methodological considerations must be taken into account for future DAPK1 studies [320]. Regardless of this discrepancy, Tu et al. hypothesized based on their findings that DAPK1 acts as a signal amplifier of extrasynaptic GluN2B-containing NMDAR excitotoxicity in ischemia, and follow-up studies from independent labs since then have supported this model and provided validation for DAPK1 as a novel neuroprotective therapeutic target. [245, 309]. Altogether, these findings indicate that recruitment and activation of DAPK1 in ischemia promotes the phosphorylation of exGluN2B, which results in amplification of excitotoxic stimuli.

In addition to this role in augmenting exGluN2B activity, much focus has centered on which other substrates of DAPK1 may become aberrantly activated and contribute to neuronal death in ischemia. A yeast two-hybrid screen using the C-terminal death domain of DAPK1 detected ERK, p53, and tau as interactors with this region, which is required for the full apoptotic activity of DAPK1 [220, 221].

As described in Section 1.4.5.2, DAPK1 is capable of sequestering ERK in the cytosol, preventing its translocation to the nucleus where it normally exerts pro-survival functions [222, 308]. Recently, Xiong et al. found that ischemia activated DAPK1 in N2a cells and enhanced the interaction between DAPK1 and ERK in cells and in vivo [308]. RNAi knockdown of DAPK1 promoted nuclear translocation of ERK, increased phosphorylation of CREB, and protected against ischemia-induced apoptosis [308]. Work from another group similarly observed improved cell survival and prevention of decreased phospho-ERK in response to OGD in DAPK1 shRNA-expressing cells [321].

The transcription factor p53 is a tumor suppressor protein with cell death-inducing functions [322]. Phosphorylation of p53 at its S23 activation site by DAPK1 induces its nuclear and mitochondrial translocation, leading respectively to downstream pro-apoptotic gene expression and necrotic activation of the permeability transition pore [220]. While OGD caused phosphorylation of p53 at S23 in WT primary neurons, this effect was blocked by genetic deletion of *Dapk1* [220]. Furthermore, a Tat peptide designed to block the DAPK1-p53 interaction protected OGD-treated neurons from both apoptosis and necrosis, and provided neuroprotection in vivo, indicating that DAPK1 converges multiple pathways of ischemic neuronal death via p53 [220, 317].

As stated previously, the tau protein binds to and stabilizes axonal MTs [289, 290]. Hyperphosphorylation of tau has been linked to synaptic dysfunction in both AD and ischemic stroke, possibly through altered interaction with NMDARs at the synapse [182, 183]. Tau phosphorylation at various sites, including S262, also reduces the affinity of tau for MTs, thus impacting MT stabilization [298]. Pei et al. discovered that activated DAPK1 interacts with and directly phosphorylates tau at S262 during induced ischemic stroke in rodents, leading to spine loss, reduced expression of synaptic proteins, and impaired synaptic transmission [247]. Genetic deletion of the DAPK1 catalytic domain or peptide-mediated uncoupling of the DAPK1-tau interaction prevented ischemia-induced tau S262 phosphorylation, spine loss, synapse dysfunction, neuronal death, and neurological impairments [247]. As will be described in the following sub-section, these findings point toward the presence of common pathogenic mechanisms involving DAPK1 and tau in both ischemic stroke and AD. Interestingly, exNMDAR activation (a primary feature of ischemia, AD, and HD) induces tau expression and phosphorylation at S262 in primary cortical neurons, which leads to ERK shut-off [189]. Thus, DAPK1 may function as an intermediate link between upstream exNMDAR excitotoxicity and downstream tau-mediated synaptic dysfunction and altered survival signaling.

Altogether, these recent studies indicate that DAPK1 interacts with multiple key molecular components of excitotoxicity and synaptic dysfunction in

ischemia. Many of these interactors are also DAPK1 substrates, influencing a range of downstream cellular functions. Promisingly, numerous genetic, pharmacological, and peptide-based therapeutic strategies to prevent DAPK1 activity are neuroprotective, necessitating further development of DAPK1-targeted therapies for preclinical and clinical trials, as well as the study of appropriate intervention time-points and treatment duration for acute versus chronic disorders of the nervous system.

1.5.3 DAPK1 in Alzheimer disease

Inheritance of certain common genetic variants influences risk for AD [323]. In 2006, Li et al. used genetic loci previously identified by multiple genome-wide analyses as a starting point to identify a single nucleotide polymorphism (SNP) (rs4878104) within the *DAPK1* gene which was significantly associated with late-onset AD (LOAD) in multiple sample populations [312]. Recently, this SNP was associated with increased *DAPK1* expression [313]. Consistent with these findings, studies have observed increased DAPK1 protein levels in the postmortem hippocampus of AD patients [275, 278, 291], although similar analyses from cortical tissue did not reach statistical significance, likely due to small sample numbers [324]. Interestingly, one of these studies observed increased hippocampal DAPK1 protein levels, but no change to mRNA expression, suggesting enhanced stability of the protein [291].

Two major pathological hallmarks of AD include the deposition of amyloid plaques containing the Aβ proteolytic product of the amyloid precursor protein (APP), and the formation of neurofibrillary tangles consisting of hyperphosphorylated tau [181]. As outlined in Section 1.3.6.2, interactions between soluble tau, Aβ, and exNMDARs ultimately contribute to spine/synapse loss and neurodegeneration in AD.

Similar to results from human AD hippocampal tissue, DAPK1 protein levels and activity are elevated in brains from transgenic AD mouse models [275, 310, 311]. This is associated with increased tau pS262, a site which is

phosphorylated by DAPK1 and promotes MT destabilization by reducing the binding affinity of tau [298, 311]. RNAi knockdown in cells or genetic deletion of *Dapk1* in mice reduced tau expression and phosphorylation, while small-molecule inhibition of DAPK1 enhanced primary cortical neurite maturation in vitro [280, 291, 311]. Although DAPK1 is not a direct kinase for APP, it indirectly promotes phosphorylation of APP at T668 by JNK3 [278]. pT668 levels, which are increased in the human AD hippocampus, promote Aβ generation via beta-secretase 1 cleavage [278, 325] Genetic deletion or small molecule inhibition of DAPK1 in primary cortical neurons reduced secretion of the Aβ peptide, while genetic *Dapk1* deletion normalized in vivo APP pT668 and Aβ levels in the brains of AD mice [278]. Furthermore, *Dapk1* deletion in these mice improved hippocampal synapse and spine survival, cortico-hippocampal EPSC amplitudes, and spatial learning and memory [275, 310]. These exciting studies highlight DAPK1 as an emerging therapeutic target with significant potential for synaptic and neuronal protection in chronic conditions such as AD, and suggest that these strategies may be translated to other neurodegenerative disorders including HD.

1.5.4 DAPK1 in chronic stress

Antidepressant effects of NMDAR (and particularly GluN2B) antagonism have been documented in rodents and humans, and likely occur by indirectly enhancing protein synthesis, synaptic AMPAR content, and excitatory transmission [326–329]. In rats, a 28-day chronic unpredictable stress (CUS) paradigm facilitates extrasynaptic GluN2B-containing NMDAR activation in response to high-frequency stimulation in medial prefrontal cortex (mPFC) slices [314]. This was associated with enhanced phosphorylation of GluN2B at S1303, an increased GluN2B-DAPK1 interaction by co-immunoprecipitation, elevated DAPK1 protein levels, as well as decreased levels of pS308-DAPK1, phospho-CREB (pCREB), and BDNF [314]. CUS also induced depressive-like behaviour in rats [314]. Infusion of the DAPK1 inhibitor TC-DAPK6 or a DAPK1-targeting AAV-short hairpin RNA into the mPFC reversed this depressive phenotype and

normalized CUS-induced changes in DAPK1, pS1303, pCREB, and BDNF [314]. Similarly, blocking the GluN2B-DAPK1 interaction with an interference peptide also provided antidepressant effects [314]. However, as described earlier, this peptide was found to exert therapeutic effects through direct modulation of NMDAR activity [320]. These findings indicate that DAPK1 may be a novel therapeutic target for the regulation of NMDAR activity in depression or other chronic neurological conditions.

1.5.5 DAPK1 in Huntington disease

The potential role of DAPK1 in HD pathogenesis has not yet been characterized. In 2006, high throughput mRNA microarray profiling on control and HD (grade 0-2) postmortem brains identified a number of differentially-expressed genes in the HD caudate [33]. These genes were enriched for biological processes involved predominantly in synaptic transmission, and tended to be downregulated in HD brains [33]. A significant decrease in caudate *DAPK1* mRNA levels was identified in the screen, although whether this is reflective of pathogenic or compensatory changes remains unknown [33]. Recent transcriptional profiling of WT and YAC128 striatal tissue at 6, 12, and 18 months of age did not pull out *Dapk1* as a differentially-expressed hit [330].

To date, two studies exist to link mHTT expression with DAPK1 activity. An immortalized mHTT knock-in striatal-like cell line ($STHdh^{Q111/Q111}$) is more sensitive to NMDA toxicity compared to control cells ($STHdh^{Q7/Q7}$), and this is associated with greater CaN activation and more rapid dephosphorylation of DAPK1 at S308 [253]. Additionally, co-expression of mHTT with GluN1/GluN2B in HEK293 cells causes upregulation of DAPK1 protein levels compared to cells co-expressing wtHTT [331]. However, no follow-up studies have been performed in relevant HD animal or neuronal culture models.

1.5.6 Link between DAPK1 and cancer: an important consideration for therapeutic development

DAPK1 is considered a tumor suppressor due to its known role as a positive mediator of apoptosis via substrates such as p53 and JNK [220, 281]. In support of this, hypermethylation of the *DAPK1* gene has been linked to a number of human cancers, while non-malignant tissues exhibit little to no *DAPK1* promoter methylation [266]. Interestingly, hyperphosphorylation of DAPK1 at Y491/492, which reduces DAPK1 activity, was observed in human colon tumor cell lines, indicating that in addition to epigenetic silencing of DAPK1, post-translational "silencing" can also occur in cancer cells [257]. Furthermore, autophagy, which may function in both tumor promotion and tumor suppression, is promoted by DAPK1 through phosphorylation of the autophagy-inducing protein beclin-1 [272, 332]. It is unknown whether downregulation of DAPK1 is causative of human cancers or simply an outcome of other dysregulated cellular pathways. Nevertheless, potentially serious consequences of reducing DAPK1 activity must be carefully considered in any future preclinical or clinical studies involving the administration of DAPK1-targeted therapies for neuroprotection. Of note, however, is the evidence for reduced cancer incidence in HD and related disorders [333–335]. Cancer and neurodegeneration have been proposed to involve similar molecular pathways which are disturbed in opposite directions – with cancer resulting from reduced cell death and neurodegeneration caused by increased cell death [333]. Thus, it is possible that a DAPK1-targeted therapy aimed to restore the balance between survival and death may pose a lower risk for cancer-related consequences in HD patients compared to the general population.

1.6 THESIS OBJECTIVES

Altered cortico-striatal synaptic transmission is a crucial pathogenic process which occurs early in HD and causes neuronal dysfunction and death. DAPK1 plays a critical role as a promoter of pro-death exNMDAR function and synaptic destabilization in multiple neurological disorders. However, no compelling evidence exists to provide rationale for the development of DAPK1-targeting strategies for synaptic and neuronal protection in HD. The main objectives of this thesis were as follows:

1. Develop a neuronal culture system for robust and reproducible elucidation of HD-like synaptic phenotypes in order to perform primary therapeutic target validation.
2. Assess whether DAPK1 disturbs exGluN2B function and synaptic integrity in the YAC128 HD mouse model and if so, evaluate potential mechanisms involved.
3. Determine if modulation of DAPK1 activity reverses YAC128 synaptic dysfunction and validate DAPK1 as a novel HD therapeutic target in vivo.

2 ALTERING CORTICAL INPUT UNMASKS SYNAPTIC PHENOTYPES IN THE CORTICO-STRIATAL CO-CULTURE MODEL OF HUNTINGTON DISEASE[1]

2.1 INTRODUCTION

Huntington disease (HD) is a devastating neurodegenerative disorder caused by a CAG repeat expansion in exon 1 of the huntingtin (*HTT*) gene [3]. The disease is characterized neuropathologically by progressive striatal atrophy and cortical degeneration, leading to impaired cognitive, psychiatric, and motor function [40]. Although overt disease onset occurs during mid-life, human and animal studies have collectively demonstrated that cortico-striatal (CS) synaptic dysfunction occurs early in HD and likely contributes to later neuronal loss [40, 336–338].

Medium spiny neurons (MSNs) make up the vast majority of the striatal neuronal population, and receive a high level of glutamatergic input from the cortex [339, 340]. MSNs are the earliest and most-affected neuronal population in HD, undergoing significant loss of dendritic structure and spines with disease progression in humans and animal models [74, 82, 85, 86, 88, 89]. Dysregulated glutamate release at CS synapses in addition to intrinsic MSN properties are hypothesized to ultimately cause selective vulnerability of this cell type [62, 64, 69, 80]. However, due to the plasticity of neural connections, CS synaptic dysfunction as well as MSN spine and synapse loss may be therapeutically reversible before neuronal death occurs [337].

The CS neuronal co-culture is a commonly-used in vitro model which consists of cortical and striatal neurons plated homogenously, generally at either a 1:1 or 1:3 cortical:striatal ratio [341]. This method partially recapitulates in vivo circuitry and MSN development, and permits functional CS synapses to be

---

[1] This chapter has been published in *BMC Biology* **16:**58. Schmidt ME, Buren C, Mackay JP, Cheung D, Dal Cengio L, Raymond LA, Hayden MR (2018). Altering cortical input unmasks synaptic phenotypes in the cortico-striatal co-culture model of Huntington disease. All experimental design, imaging, and analysis, except for electrophysiology, by MES. Electrophysiology by CB and JPM.

studied in relative isolation from other modulatory neurotransmitters or neuronal inputs [342, 343].

Previous characterization has been performed in 1:1 embryonic CS co-cultures from wild-type (WT) and YAC128 mice expressing full-length transgenic human mutant HTT (mHTT) [73, 81]. These studies demonstrated altered extrasynaptic NMDA receptor function in YAC128 co-cultured MSNs, accompanied by enhanced susceptibility to excitotoxicity as well as reduced CS excitatory synapse activity by 21 days in vitro (DIV), a phenotype undetectable in vivo until 6-7 months of age [62, 65]. Morphology was also evaluated by transfecting MSNs with yellow fluorescent protein (YFP) at the time of plating, and although this analysis showed stunted dendritic complexity in 1:1 co-cultured YAC128 MSNs compared to WT, no difference in spine numbers was observed [73]. This is in stark contrast to studies from another group, in which staining for dopamine- and cAMP-regulated phosphoprotein 32 (DARPP32), a marker of mature MSNs, was used for morphological analysis instead of transfected YFP to show dramatic spine loss in 1:3 CS co-cultured postnatal YAC128 MSNs [74, 75]. The methodological factors underlying the ability to observe this highly relevant HD phenotype remain unknown. DARPP32+ WT MSNs in 1:3 co-culture exhibit less dendritic complexity and fewer spines and synapses than in 1:1 co-culture, indicating that reducing cortical input impairs WT MSN development in vitro [341]. However, the impact of altering cortical input in the context of HD has not been evaluated.

In the present study, we have explored whether spine loss is a reproducible feature of HD in this model and investigated the potential methodological factors contributing to the emergence of this phenotype.

2.2 MATERIALS AND METHODS

2.2.1 Neuronal culture

Timed pregnancies were set up by mating wild-type FVB/N female mice with YAC128 (line 53) males. At E17.5, embryos were removed from anesthetized

mothers and brains were extracted and stored in a hibernate solution (Hibernate-E supplemented with L-glutamine and B27; Gibco) overnight while excess embryonic tissue was genotyped. Cortical and striatal tissues from both male and female embryos were dissected separately the following day in ice-cold Hank's Balanced Salt Solution, gently dissociated with a P1000 pipette, and incubated in 0.05% trypsin-EDTA (Gibco) at 37°C for 8 minutes. Cells were further dissociated with a short DNase treatment (0.08mg/mL) followed by resuspension in complete neurobasal medium (NBM supplemented with B27, penicillin-streptomycin, and L-glutamine; Gibco). Neurons from appropriate genotypes were combined at a 1:1, 1:2, 1:3 or 1:5 cortico:striatal ratio and plated on 12mm glass coverslips (Marienfeld Superior) in 24-well plates with a final density of 170,000 cells per well in 1mL complete NBM. Prior to plating, coverslips were treated overnight with 6N hydrochloric acid, washed thoroughly with sterile water and 70% ethanol, transferred to culture plates, and coated with sterile-filtered 50µg/mL poly-D-lysine hydrobromide (Sigma; P7886) in water overnight at room temperature. Coverslips were washed 4 times with sterile water and allowed to air dry before plating. For electrophysiological experiments, a YFP construct was transfected into striatal neurons at the time of plating to allow for MSN identification. Approximately 2 million striatal neurons were suspended in 100µL electroporation solution (Mirus Bio) prior to the final plating step, mixed with 2µg of DNA (YFP on a β-actin promoter; a gift from A.M. Craig, University of British Columbia) and nucleofected (Amaxa Nucleofector, Lonza Bio, program 05). Cells were diluted and plated in 500µL of 10% fetal bovine serum/DMEM. Media was replaced with 500µL complete NBM after 4 hours, and topped up to 1mL the following day. All cultures were supplemented with fresh NBM complete (20% well volume) every 3-7 days until fixation of coverslips at DIV14, 18 or 21.

2.2.2 Immunocytochemistry

Neurons on coverslips were fixed in 4% paraformaldehyde/PBS for 15 minutes at room temperature (RT), incubated in ice-cold methanol for 5 minutes at -20°C, permeabilized in 0.03% Triton-X/PBS for 5 minutes at RT, and blocked for 30

minutes at RT in 0.2% gelatin/PBS. Coverslips were incubated with primary antibody against dopamine- and cAMP-regulated phosphoprotein 32 (rat anti-DARPP32; R&D Systems Cat# MAB4230; 1:500) and microtubule-associated protein 2 (mouse anti-MAP2; Invitrogen Cat# MA5-12823; 1:200) in blocking buffer overnight at 4°C, washed in PBS, stained with secondary antibodies against rat IgG (Alexa Fluor 568 goat anti-rat IgG; Invitrogen Cat# A-11077; 1:500) or against mouse IgG (Alexa Fluor 488 goat anti-mouse IgG; Invitrogen Cat# A-11001; 1:500) for 1.5 hours at RT, washed in PBS, and mounted on slides using Prolong Gold Antifade Reagent with DAPI (Invitrogen). For spine and dendrite analysis, fluorescence images were acquired using a Leica TCS SP8 confocal laser scanning microscope at 63X objective magnification. Samples from different groups were interleaved and the researcher was blinded to experimental conditions during imaging and analysis. Image stacks of Z-step size 60µm were converted to 2D in Image J using the maximum intensity Z-projection function. Images were then background subtracted with a rolling ball radius of 35 pixels and de-speckled. Images were imported into NeuronStudio (Version 0.9.92) for semi-automated Sholl analysis as well as spine characterization using a minimum of 3 representative secondary or tertiary dendritic segments per cell. For analysis of DARPP32 and MAP2 staining intensity and cell survival counts, random fields of view were imaged at 20X objective magnification using identical laser intensities across samples. The number of MAP2+ or DARPP32+ with healthy nuclei in each field of view were counted, and staining intensity was measured within multiple secondary or tertiary dendrite regions from each neuron selected for analysis.

2.2.3 DiOlistic labeling

Cortical neurons were labeled in vitro with DiI stain (Invitrogen Cat# D282) as previously described [344], with minor alterations. Briefly, DIV21 cortical cultures were fixed in 2% PFA/PBS for 15 minutes at RT. 15-20 DiI crystals were sprinkled on top of coverslips, and a small volume of PBS was added to prevent cells from drying out. Coverslips were incubated in the dark for 10 minutes at RT,

followed by thorough PBS washing to remove crystals and incubation in the dark for an additional 6 hours in PBS. Coverslips were rinsed again in PBS and mounted on slides. Imaging and spine analysis were performed as described above with an excitation wavelength of 549nm.

2.2.4 Golgi-Cox staining

6- or 12-month mice were perfused with 2% paraformaldehyde/2% glutaraldehyde/PBS, post-fixed in the same solution overnight at 4°C and processed as previously described [345] with minor alterations. Briefly, brains were washed in PBS, incubated in Golgi-Cox solution (1% potassium dichromate, 1% mercuric chloride, 0.8% potassium chromate) for 5 days, and transferred to 30% sucrose/PBS. 100µm sections were cut on a vibratome and mounted on slides, which were dried overnight, washed in ddH_2O, incubated in 20% ammonium hydroxide for 10 minutes, washed in ddH_2O, passed through ascending grades of alcohol, and placed in xylene for 5 minutes. Coverslips were mounted on top of sections with Cytoseal mounting medium (Thermo Scientific). Transmitted light images were acquired with a Leica TCS SP8 confocal laser scanning microscope and a 63X objective lens. Images were imported into NeuronStudio and spines on dendritic segments from at least 15-20 neurons across multiple sections per animal were semi-automatically analysed.

2.2.5 Electrophysiology

Whole-cell patch-clamp electrophysiology was conducted as previously described [73]. Briefly, an Axon Instrument Axopatch B200B amplifier and pClamp 10.2 software (Molecular Devices) were used to collect data under voltage-clamp mode. Culture coverslips were perfused in a recording chamber with external recording solution containing picrotoxin and tetrodotoxin [73]. Miniature excitatory postsynaptic currents (mEPSCs) were recorded in YFP-positive neurons at a holding membrane potential of -70mV with the recording pipettes filled with K-gluconate internal solution [73]. Membrane capacitances

were measured within 2 minutes of patching each cell, and at least 30 synaptic events were analysed per cell with Clampfit 10.2 or 10.7.

2.2.6 Data analysis

All data is presented as mean ± SEM. Statistical analysis and graph generation were performed using GraphPad Prism 5, and figures were created in Adobe Photoshop CS5. *n* values for all experiments are recorded as the total number of cells analysed, with the number of independent cultures in parentheses. Student's t-test or 1- or 2-way ANOVA statistical tests with Bonferroni post-hoc analysis were used for all experiments. In some cases, t-tests were performed between specific groups after an ANOVA test when a planned comparison was established during the experimental design process. Significance for these tests is noted with the "#" symbol instead of "*".

2.3 RESULTS

2.3.1 Reducing cortical input elucidates robust YAC128 MSN spine loss in CS co-culture

We first sought to evaluate the effect of altered cortical input on HD-like phenotypes in vitro by culturing WT and YAC128 MSNs with cortical neurons side-by-side at both 1:1 and 1:3 CS ratios, using identical total cell densities. We utilized DARPP32 immunofluorescence staining for MSN morphological analysis in order to remain consistent with methodology used by Wu et al., 2016, as well as to avoid the requirement for YFP nucleofection, which we found to reduce the general health of neuronal cultures. Striatal DARPP32 is decreased in several models of HD, including YAC128 mice [50, 51, 346–350]. To confirm that potentially altered YAC128 DARPP32 expression levels would not interfere with accurate structural analysis, we measured immunofluorescence staining intensity in each culture condition at DIV21. We co-stained for the dendritic marker microtubule-associated protein 2 (MAP2) and imaged both channels at identical laser intensities across samples. We observed no differences in dendritic

DARPP32 intensity normalized to MAP2 intensity (**Fig. 2.1A, B**), indicating that MSN DARPP32 expression does not obviously differ between genotypes and that this is an appropriate method for dendritic and spine analysis in this model.

Using this approach, we observed a subtle reduction in MSN total spine density (90% of WT) and a nonsignificant decrease in mature mushroom spine density (88% of WT) in DIV21 1:1 YAC128 cultures (**Fig. 2.1C-E)**. Remarkably, limiting excitatory input using a 1:3 ratio dramatically enhanced this phenotype, such that the number of total and mature mushroom spines in YAC128 MSNs were reduced to approximately 78% and 63% of WT 1:3 levels, respectively (**Fig. 2.1C-E**). We did not observe significant differences in the density of immature (stubby, thin, and filopodia) spine types **(Fig. 2.1C, F**), suggesting a selective impairment in the stability of functionally mature spines.

A previous study using injection of Lucifer yellow fluorescent dye into striatal neurons in brain slices found YAC128 MSN spine loss at 12 months of age, but not at 6 months [74]. We confirmed this finding using a simple Golgi stain method and observe that spine density values and the degree of YAC128 total spine loss at 12 months in vivo (71% of WT) are accurately recapitulated in 1:3 CS co-cultures (**Fig. 2.1G, H**).

To further investigate the relationship between MSN spine density and cortical input, we compared two additional CS ratios (1:2 and 1:5) side-by-side with 1:1 and 1:3 conditions. In this set of experiments, there were no significant genotypic differences in either total or mature mushroom spine densities using a 1:1 ratio. We observed a negative correlation between total and mature mushroom spine densities versus the proportion of striatal cells at the time of plating in both genotypes (**Fig 2.1I, J**). Interestingly, there was a significant interaction between genotype and CS ratio, with the phenotype becoming more severe with increasing proportion of striatal cells at plating. This indicates that YAC128 MSN spine stability is progressively more sensitive than WT to reduced amounts of cortical input.

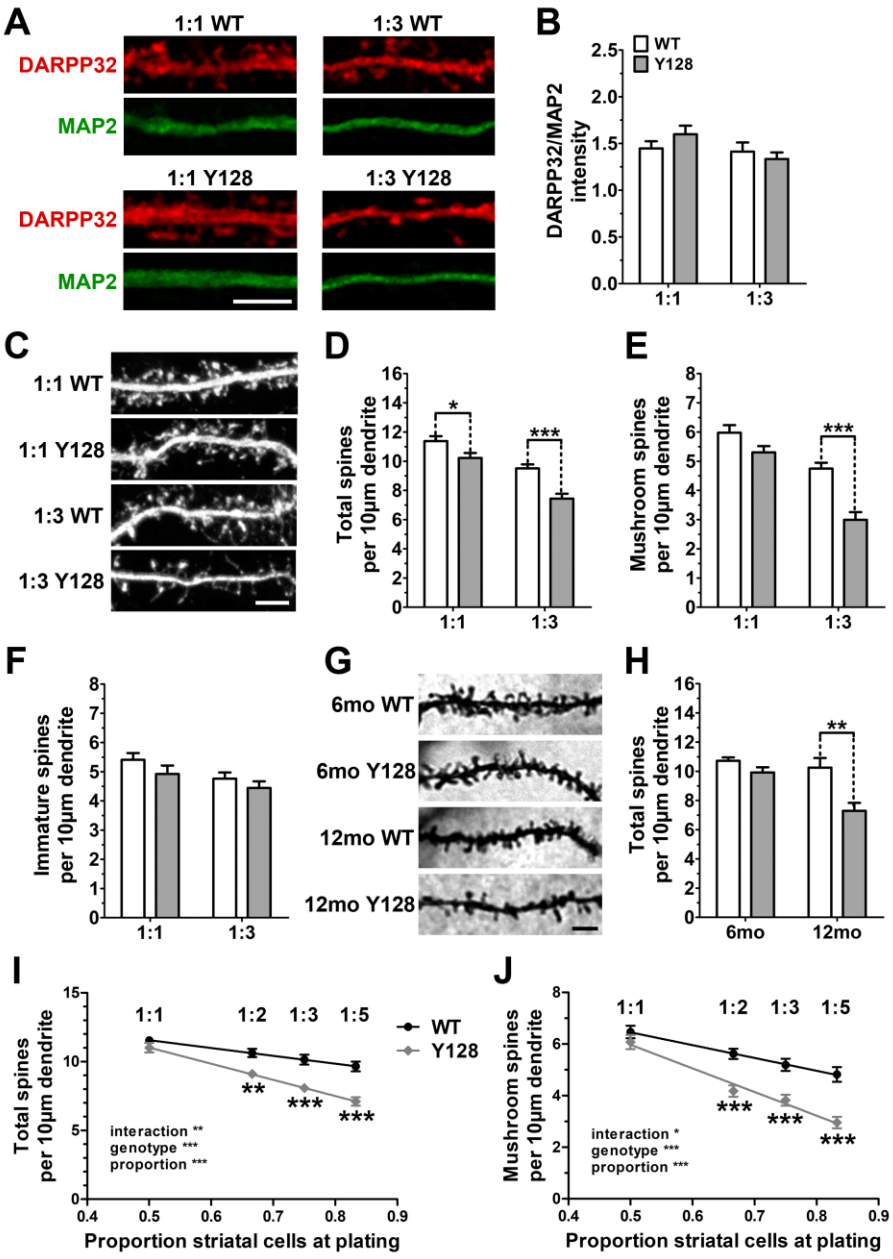

Figure 2.1: YAC128 MSNs co-cultured with cortical neurons at a 1:3 CS ratio recapitulate in vivo spine loss. WT and YAC128 (Y128) co-cultures were generated at either a 1:1 or 1:3 CS ratio and processed at DIV21 for DARPP32 and MAP2 immunocytochemistry, imaging, and spine analysis in NeuronStudio. **(A)** Sample images of DARPP32- and MAP2-stained dendrites in CS co-culture (scale bar = 5µm). **(B)** Quantification of DARPP32 staining intensity normalized to MAP2 intensity reveals no differences between genotypes or conditions [n=30(3); 2-way ANOVA with Bonferroni post-hoc analysis]. **(C)** Sample images of DARPP32-stained spines on secondary or tertiary dendrites in co-cultured MSNs at higher exposure (scale bar = 5µm). The differences in numbers of **(D)** total and **(E)** mature mushroom, but not **(F)** immature spines, are exacerbated in 1:3 co-cultured YAC128 MSNs [n=32(4); 2-way ANOVA with Bonferroni post-hoc analysis; *p<0.05, ***p<0.001]. **(G)** Representative Golgi staining of striatal MSNs in vivo (scale bar = 5µm). **(H)** Golgi analysis confirms that reduced MSN

total spine number occurs by 12 months of age in the YAC128 striatum, to a similar degree as in 1:3 co-cultures [n=4-5 6-month animals and 3 12-month animals per genotype; 2-way ANOVA with Bonferroni post-hoc analysis; **p<0.01]. A linear correlation exists between **(I)** total and **(J)** mushroom spines versus the proportion of striatal cells at plating. A significant interaction occurs between striatal proportion and genotype [n=30(3); 2-way ANOVA with Bonferroni post-hoc analysis; *p<0.05, **p<0.01, ***p<0.001].

Finally, we evaluated the impact of altering the total cell number per well (150,000, 170,000 or 230,000 in 24-well plates), keeping the CS ratio consistent at 1:3. There was no effect of initial plating density on the presence or severity of the YAC128 MSN spine phenotype at DIV21 (**Fig. 2.2A-C**).

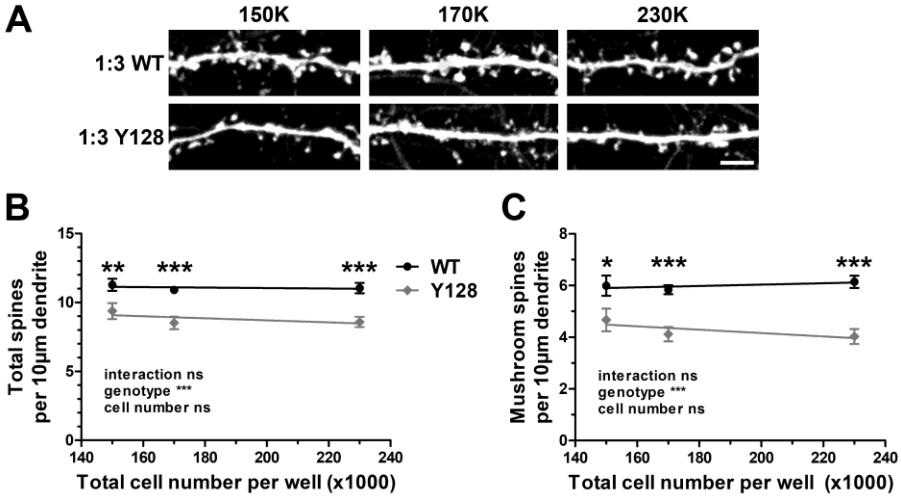

Figure 2.2: Initial plating density does not impact the presence or severity of YAC128 MSN spine instability. WT and YAC128 co-cultures were generated at a 1:3 CS ratio and plated at three different total cell numbers per well (150 000, 170 000, or 230 000 in 24-well plates). Coverslips were fixed at DIV21 and processed for DARPP32 immunocytochemistry, imaging, and spine analysis. **(A)** Sample images of DARPP32-stained spines on secondary or tertiary MSN dendrites (scale bar = 5µm). There was no effect of initial plating density on YAC128 **(B)** total or **(C)** mature mushroom spine density phenotypes [n=20(2); 2-way ANOVA with Bonferroni post-hoc analysis; *p<0.05, **p<0.01, ***p<0.001].

2.3.2 YAC128 spine instability is predominantly MSN-intrinsic

Previously, an impaired developmental increase in miniature excitatory post-synaptic current (mEPSC) frequency from DIV14 to DIV21 in 1:1 co-cultured YAC128 MSNs compared to WT was reported [73]. Chimeric co-cultures (WT striatal MSNs plated with YAC128 cortical neurons, or vice versa) exhibited an intermediate phenotype, indicating that altered excitatory functional connectivity is partially dependent on mHTT expression in both pre- and post-synaptic compartments [73]. We utilized a similar strategy to determine the relative contribution of each cell type to MSN spine stability in 1:3 co-cultures. We discovered that the difference in total spine numbers between WT and YAC128 was entirely dependent on mHTT expression in the MSN (**Fig. 2.3A, B**). When we specifically evaluated mature mushroom spines, we found a small contribution from cortical mHTT expression, with chimeric cultures demonstrating a trend to a more intermediate mushroom spine density (**Fig. 2.3A, C**). By t-test, WT MSNs co-cultured with YAC128 cortical neurons had fewer mushroom spines and a greater number of immature spines than those co-cultured with WT cortical neurons, despite similar total spine densities (**Fig. 2A-D**). Thus, cortical mHTT expression alters the ratio of mature/immature spines in WT neurons. These results suggest that mHTT expression primarily, but not exclusively, in the MSN impairs mechanisms of spine development or stability in response to reduced cortical input.

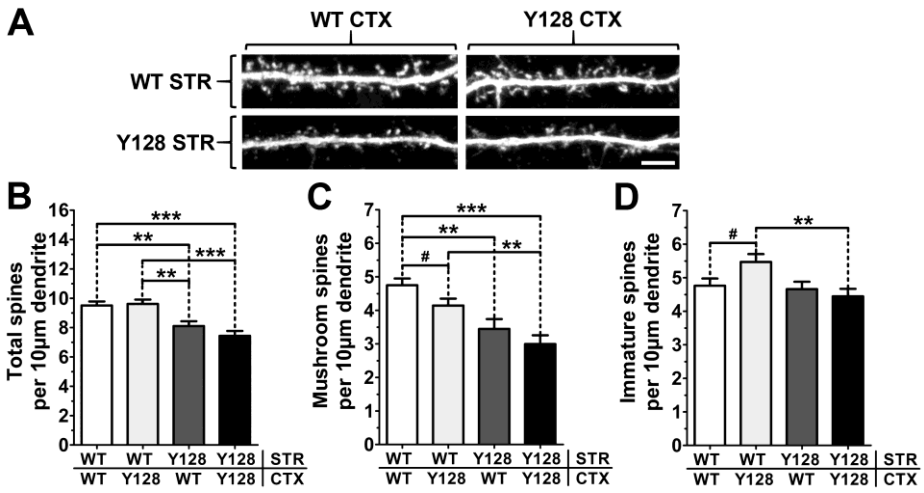

Figure 2.3: YAC128 spine instability is predominantly MSN-intrinsic. WT, YAC128, and chimeric co-cultures generated at a 1:3 CS ratio were processed at DIV21 for DARPP32 immunocytochemistry, imaging, and spine analysis. **(A)** Sample images of DARPP32-stained spines in pure or chimeric co-cultured MSNs (scale bar = 5µm). **(B)** Total spine density values in chimeric cultures are similar to pure cultures of the same MSN genotype. **(C)** Mature mushroom and **(D)** immature spine numbers are affected by both striatal (STR) and cortical (CTX) mHTT expression [n=32(4); 1-way ANOVA with Bonferroni post-hoc analysis; **p<0.01, ***p<0.001]. Student's t-test was used to compare WT STR/WT CTX and WT STR/Y128 CTX [n=32(4); Student's t-test; #p<0.05].

2.3.3 Decreasing cortical input masks the YAC128 MSN dendritic complexity phenotype in CS co-culture

Interestingly, in comparison to MSN spine density, we discovered an opposite effect of CS ratio on MSN dendritic structure by Sholl analysis. A robust impairment in total dendritic length and complexity was observed in DIV21 1:1 co-cultured YAC128 MSNs compared to WT (**Fig. 2.4A-C**), in agreement with previous results [73]. However, when a 1:3 CS ratio was utilized, WT MSN dendritic development became impaired, resulting in a much smaller genotypic difference between WT and YAC128 (**Fig. 2.4A-C**). Thus, differential elucidation of YAC128 MSN dendritic or spine phenotypes can be achieved by manipulation of the CS ratio.

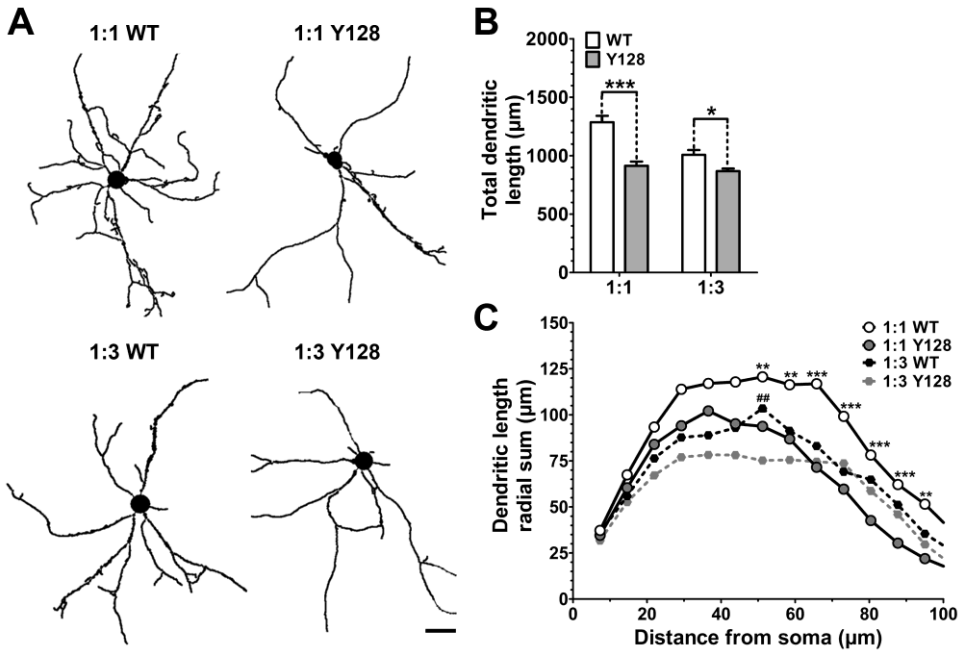

Figure 2.4: YAC128 MSNs in 1:1 CS co-culture demonstrate reduced dendritic length and complexity. WT and YAC128 co-cultures were generated at either a 1:1 or 1:3 CS ratio and processed at DIV21 for DARPP32 immunocytochemistry, imaging, and dendritic analysis. **(A)** Sample images of MSN dendritic traces generated in NeuronStudio (scale bar = 15µm). **(B)** Total length of the dendritic trace and **(C)** complexity by Sholl analysis are significantly reduced in 1:1 YAC128 MSNs compared to WT. Post-hoc statistical significance for Sholl analysis is shown only for WT 1:1 vs YAC128 1:1 (*) or WT 1:3 vs YAC128 1:3 (#) comparisons [n=32(4); 2-way ANOVA with Bonferroni post-hoc analysis; *p<0.05, **p<0.01, ***p<0.001].

2.3.4 YAC128 MSN dendritic and spine phenotypes are developmental in vitro

We next sought to determine at what timepoint the identified structural phenotypes are present in CS co-culture. When our DIV21 results were plotted over time along with DIV14 and DIV18 data from the same cultures, we observed that most of the identified YAC128 spine and dendrite alterations were present by DIV18 and all could be attributed to impaired development of YAC128 MSNs after DIV14, at which time there were no discernable phenotypes (**Fig. 2.5, 2.6**).

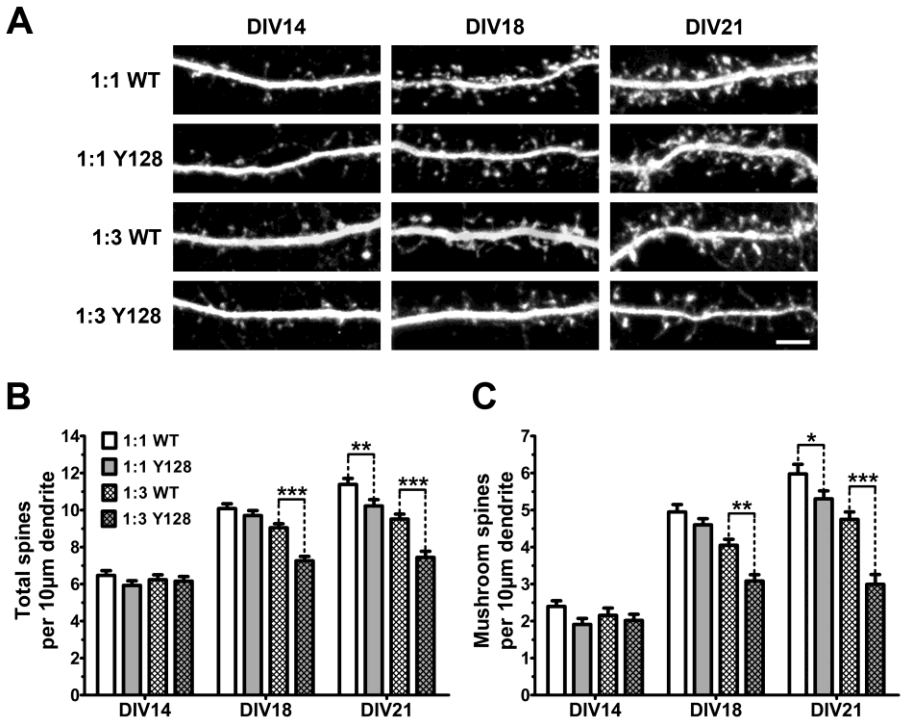

Figure 2.5: Reduced spine density in co-cultured YAC128 MSNs is a developmental phenotype. WT and YAC128 co-cultures were generated at either a 1:1 or 1:3 CS ratio and processed at DIV14, 18, or 21 for DARPP32 immunocytochemistry, imaging, and spine analysis. **(A)** Sample images of DARPP32-stained spines on secondary or tertiary MSN dendrites (scale bar = 5µm). A developmental increase in **(B)** total and **(C)** mature mushroom spine numbers is impaired after DIV14 in co-cultured YAC128 MSNs compared to WT [n=32(4); 2-way ANOVA with Bonferroni post-hoc analysis; *p<0.05, **p<0.01, ***p<0.001].

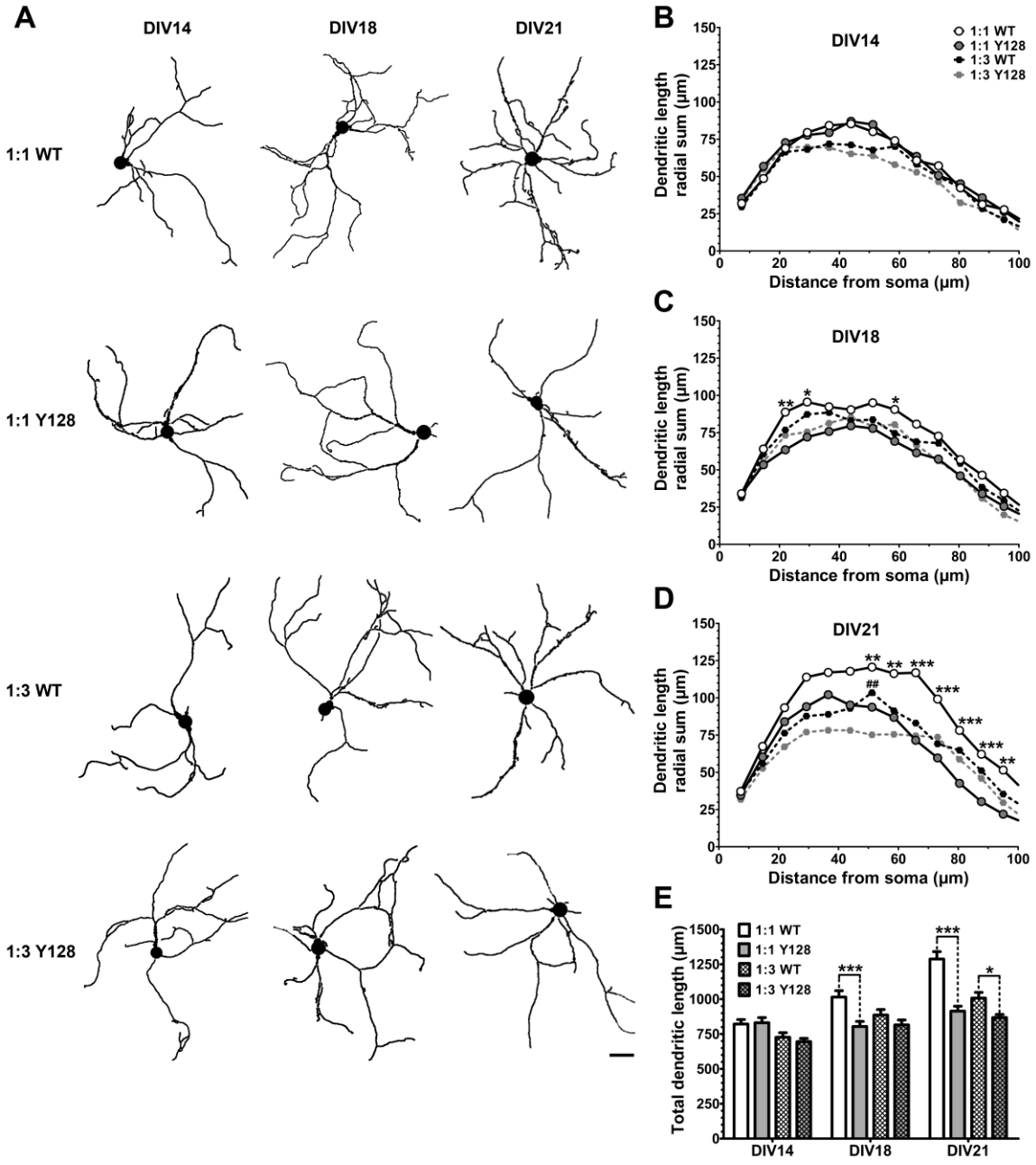

Figure 2.6: Reduced dendritic length and complexity in co-cultured YAC128 MSNs are developmental phenotypes. WT and YAC128 co-cultures were generated at either a 1:1 or 1:3 CS ratio and processed at DIV14, 18, and 21 for DARPP32 immunocytochemistry, imaging, and dendritic analysis. **(A)** Sample images of MSN dendritic traces generated in NeuronStudio (scale bar = 15µm). A developmental increase in **(B-D)** dendritic complexity by Sholl analysis and **(E)** total dendritic length are impaired after DIV14 in co-cultured YAC128 MSNs compared to WT. Post-hoc statistical significance for Sholl analysis is shown only for WT 1:1 vs YAC128 1:1 (*) or WT 1:3 vs YAC128 1:3 (#) comparisons [n=32(4); 2-way ANOVA with Bonferroni post-hoc analysis; *p<0.05, **p<0.01, ***p<0.001].

2.3.5 CS plating ratio influences electrophysiological phenotypes in YAC128 MSNs

To determine the functional impact of altering CS ratio, whole-cell patch-clamp electrophysiology was used to record mEPSCs and basal membrane capacitance from MSNs in 1:1 and 1:3 co-cultures at DIV14 and DIV21. Previously published data showed an increase in mEPSC frequency from DIV14 to DIV21 in 1:1 co-cultures, which was blunted in YAC128 MSNs [21]. We observed a similar trend in the current study, although there was no significant genotypic difference between WT and YAC128 at DIV21 (**Fig. 2.7A, B**). However, when a 1:3 ratio was utilized, there was only a small increase in mEPSC frequency from DIV14 to DIV21 for both WT and YAC128 such that there was no longer a trend to a difference between genotypes at DIV21 (**Fig. 2.7A, C**). This is consistent with a prior study which found reduced mEPSC frequency in DIV18 1:3 co-cultured WT MSNs compared to 1:1 [18]. Membrane capacitance, a measure of overall MSN size, increased with time in all culture conditions (**Fig. 2.7D, E**). However, the increase in 1:1 WT MSNs was more dramatic than in 1:1 YAC128 MSNs, elucidating a significant genotypic difference at DIV21 which was not observed in 1:3 co-cultures (**Fig. 2.7D, E**). This correlates well with our observation of a greater difference in dendritic arbor size and complexity between genotypes using a 1:1 CS ratio. These findings indicate that the previously published YAC128 mEPSC frequency and capacitance phenotypes are also CS ratio-dependent and that overall MSN functional connectivity correlates more closely with dendritic development than with spine density.

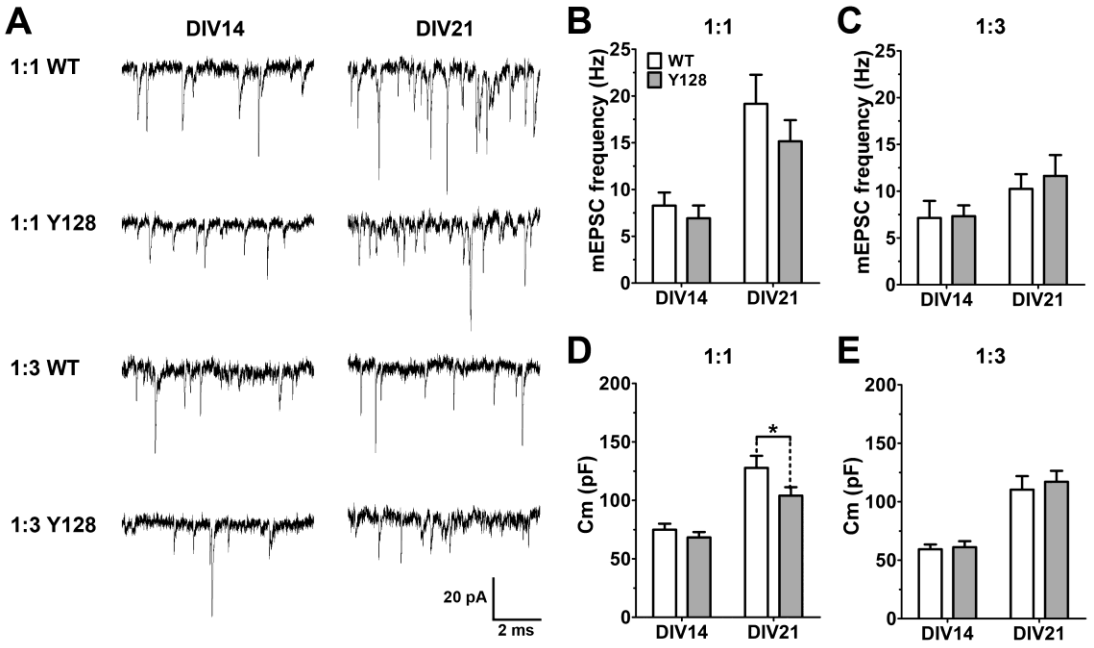

Figure 2.7: 1:1 co-cultured YAC128 MSNs exhibit an impaired increase in membrane capacitance with maturation. (A) Representative recording traces from WT and YAC128 MSNs in 1:1 or 1:3 co-culture at DIV14 and 21. **(B, C)** mEPSC frequency and **(D, E)** membrane capacitance (Cm) tend to increase with maturation, but a significant genotypic difference was only observed for Cm at DIV21 in 1:1 cultures [n=12-29(3); 2-way ANOVA with Bonferroni post-hoc analysis; *p<0.05].

2.3.6 Reducing cortical input promotes neuronal death in YAC128 CS co-culture

Previously, WT neurons (both cortical and striatal DARPP32+ MSNs) exhibited reduced basal survival at DIV18 when co-cultured at a 1:3 CS ratio versus 1:1 [341]. We used a similar approach to compare neuronal survival in DIV21 WT and YAC128 neurons at both CS ratios. We found significantly reduced survival of all neurons (MAP2+) as well as DARPP32+ MSNs in YAC128 1:3 co-cultures compared to WT 1:3 (**Fig. 2.8A-C**), despite being initially plated at identical live cell density. When we calculated the proportion of surviving MAP2+ neurons that were also DARPP32+, we found that neuronal loss in YAC128 1:3 co-cultures was partially selective for this cell population (**Fig. 2.8A, D**). This reveals an

additional CS ratio-dependent co-culture phenotype that may be useful for future studies of mHTT-induced neuronal death.

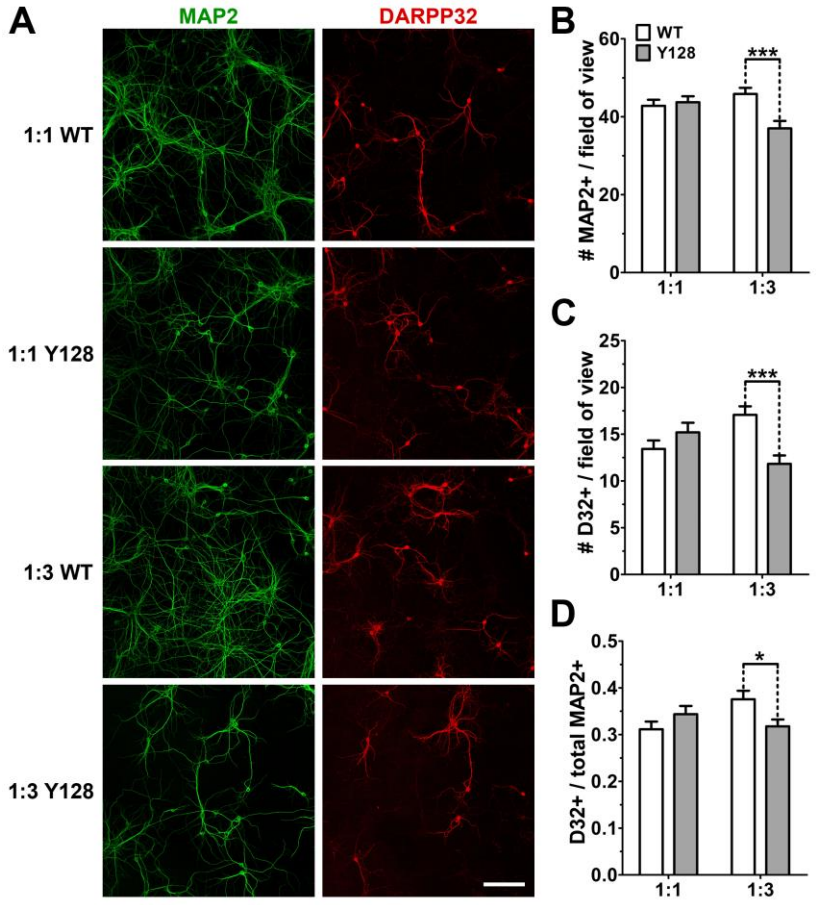

Figure 2.8: Neuronal survival is compromised in YAC128 1:3 CS co-cultures. WT and YAC128 co-cultures were fixed at DIV21 and stained for MAP2 and DARPP32 (D32). **(A)** Sample fields of view at 20X objective (scale bar = 100μm). The numbers of **(B)** MAP2+ and **(C)** DARPP32+ neurons per field of view were reduced in YAC128 1:3 co-cultures. **(D)** The proportion of DARPP32+ neurons (# DARPP32+ divided by # MAP2+) surviving at DIV21 was also significantly lower in YAC128 1:3 co-cultures [n=30 fields of view from 3 independent cultures; 2-way ANOVA with Bonferroni post-hoc analysis; *p<0.05, ***p<0.001].

2.3.7 In vitro diOlistic labeling reveals increased thin spines and reduced mushroom spine head size in mono-cultured YAC128 cortical neurons

Although striatal MSNs are the most severely-affected cell type in HD, there is evidence that mHTT causes neuronal and synaptic dysfunction in other brain regions as well, including the cortex and thalamus [338, 351, 352]. Thus, it may be desirable to utilize modified culture models for the study of these neuronal populations. For example, a YAC128 thalamo-striatal (TS) co-culture model was recently used to demonstrate mHTT-induced TS synaptic dysfunction [351].

We attempted to combine a previously-reported in vitro DiI diOlistic dye labeling protocol [344] with immunocytochemistry for glutamatergic markers in order to perform spine analysis on cortical neurons in CS co-culture. However, permeabilization of DiI-stained cells for internal staining resulted in release of DiI from cell membranes and poor filling of spines. Instead, we generated WT and YAC128 pure cortical monocultures for DiI spine analysis at DIV21. We did not observe any differences in total, mushroom, or stubby spine densities between genotypes, although there was an increased number of thin spines in YAC128 cortical neurons (**Fig. 2.9A-E**). Interestingly, we observed a significant 7% reduction in the diameter of YAC128 mushroom spines (**Fig. 2.9F**) indicating that subtle dysfunction in cortical neurons may also exist in vitro, which could contribute to CS synaptic alterations.

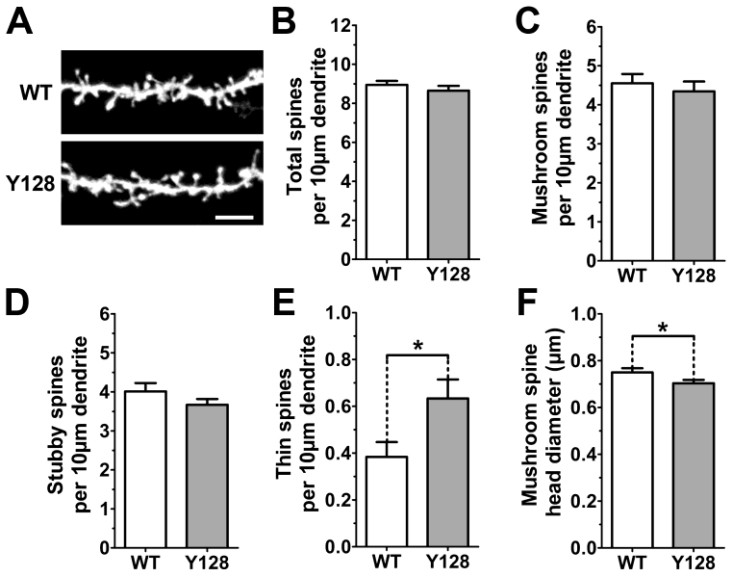

Figure 2.9: Thin spine density is increased and mushroom spine head diameter is reduced in DIV21 YAC128 cortical neurons. WT and YAC128 pure cortical cultures were fixed at DIV21 and subjected to in vitro DiI diOlistic dye labeling for spine analysis. **(A)** Sample images of DiI-stained spines on cortical dendrites (scale bar = 5µm). No significant differences in **(B)** total, **(C)** mushroom, or **(D)** stubby spine densities were observed in YAC128 cortical neurons. **(E)** Increased thin spine density and **(F)** reduced mushroom spine head diameter were measured in YAC128 cortical neurons compared to WT [n=30(3); Student's t-test; *p<0.05].

2.4 DISCUSSION

Optimization of the CS co-culture for elucidation of YAC128 synaptic phenotypes

The CS co-culture has become an attractive methodological option for the isolated study of both physiological and pathogenic mechanisms of CS synaptic function. This model allows direct assessment of neuronal morphology and synaptic transmission and can be used to quickly answer specific questions that are difficult to investigate using in vivo animal models. mHTT-expressing YAC128 CS co-cultures recapitulate many relevant in vivo synaptic phenotypes by 21 days in vitro [73], highlighting the practicality of this model as a primary tool for therapeutic target validation.

Spine instability, hypothesized to contribute to neuronal dysfunction in HD and other neurodegenerative disorders, has been observed in YAC128 MSNs in CS co-culture in some studies, but not others [73–75] . Recently, altering CS plating ratio was found to affect a number of functional and morphological characteristics of WT MSNs [341], leading us to hypothesize that modifying cortical input in YAC128 CS co-cultures may elucidate or exacerbate synaptic phenotypes, thus enhancing the utility of this culture system for HD research. In the present study we have clearly shown that modifying CS ratio in co-culture differentially elucidates YAC128 MSN synaptic phenotypes (summarized in **Table 2.1**). For future studies of therapeutic strategies to modify neurite growth or stability in HD, a 1:1 CS ratio is recommended. Conversely, for evaluation of potential neuroprotective or spine-stabilizing therapies, a 1:3 CS ratio is ideal, as this accurately recapitulates YAC128 age-associated in vivo MSN spine loss and neuronal death.

Table 2.1: Optimal CS ratios to elucidate YAC128 MSN phenotypes in co-culture

YAC128 MSN Phenotype	Optimal CS ratio
Spine loss	1:3
Impaired neuronal survival	1:3
Decreased dendritic length/complexity	1:1
Reduced mEPSC frequency	1:1
Reduced membrane capacitance	1:1

Intrinsic versus extrinsic effects of mHTT on MSN spine stability

Our result showing that decreasing the proportion of cortical neurons in CS co-culture promotes spine instability in YAC128 MSNs raises the interesting possibility that spine loss with disease progression in vivo is partially due to reduced cortical input. Indeed, studies support the hypothesis that progressive CS disconnect in HD results in loss of cortical excitatory support of MSNs and

reduced delivery of neurotrophic factors such as BDNF over time, causing striatal degeneration [336, 353]. However, in seeming contradiction, our experiments using chimeric cultures demonstrate that YAC128 MSN spine instability is primarily cell-autonomous (**Fig. 2.2**). We propose that mHTT expression in MSNs renders spines intrinsically more sensitive to low levels of cortical support, causing this phenotype to only emerge in the presence of reduced cortical input. There is evidence that depletion of endoplasmic reticulum (ER) Ca^{2+} stores and consequent enhanced store-operated Ca^{2+} entry in YAC128 MSNs contributes to spine loss in CS co-culture [74]. It is possible that reducing glutamatergic input with a 1:3 CS ratio exacerbates ER store depletion in YAC128 MSNs by limiting normal activity-induced extracellular Ca^{2+} influx, which might subsequently promote more dramatic spine loss.

A recent study investigated the contribution of cortical or striatal mHTT to synaptic dysfunction by crossing region-specific Cre-expressing mice to the transgenic full-length mHTT BACHD mouse model [354]. It was discovered that mHTT expression predominantly in the cortex was required for altered synaptic protein levels and reduced spontaneous EPSC frequency in the striatum of aged BACHD mice, while impaired evoked NMDA current was dependent on mHTT expression in both the striatum and cortex [354]. A follow-up study found improvement in striatal activity patterns and behavioral phenotypes in response to mHTT reduction in the cortex of BACHD mice [355]. Although our results in the present study showed that total spine density was determined entirely by mHTT expression in striatal neurons, we did observe a small effect of cortical expression on mushroom spine numbers. In particular, WT MSNs co-cultured with WT cortical neurons possessed similar total spine density as those co-cultured with YAC128 cortical neurons, but we observed fewer mushroom spines and a greater number of immature spines in MSNs from the chimeric cultures (**Fig. 2.2)**. Since mature and immature spines would be expected to have different functional properties, this indicates that cortical mHTT expression may contribute to altered CS synaptic readouts. In further support of this hypothesis,

we also report subtle spine morphology alterations in monocultured YAC128 cortical neurons (**Fig. 2.9**).

Spine and dendritic alterations in HD patients and animal models

Early reports using Golgi staining of postmortem HD patient brain samples demonstrated both proliferative and degenerative morphological alterations in striatal MSNs [82, 83]. These included an increase in the number and size of dendritic spines as well as altered dendritic branching in early stage (grade 2) HD [82]. In advanced HD brains, smaller dendritic arbors, spine loss, and dendritic swellings were observed [82]. It is hypothesized that early proliferative changes could reflect activation of compensatory mechanisms in response to synaptic dysfunction, which eventually become overwhelmed with disease progression and age. This is supported by observations of increased glutamate transmission onto striatal neurons at early time points in the YAC128 and BACHD mouse models, followed by reduced transmission at later ages [62, 63].

Multiple mouse models of HD recapitulate the structural degeneration observed in advanced HD brains. Both MSNs and cortical pyramidal neurons in the R6/1 mHTT fragment mouse model exhibit reduced spine density and spine length at symptomatic ages, and a later study also reported thinner apical dendrites in the somatosensory cortex [88, 90]. Similarly, symptomatic R6/2 mice demonstrate MSN spine loss in addition to thinner dendritic shafts [85, 91]. Studies in full-length mHTT models, including mHTT knock-in and BACHD mice, have also shown loss of dendritic spines in HD MSNs [92, 93]. Although we and others observed YAC128 MSN total spine loss at 12 months of age, but not at 6 months [74], a 15% reduction in secondary and tertiary dendrite spine density at 3 months of age has been reported [89], as well as diminished excitatory CS activity at 6-7 months [62, 65]. Thus, an effect of mHTT expression on spines and synapses is present in YAC128 mice but may be too subtle at early ages to be detected reliably by structural analysis in vivo.

Developmental synaptic phenotypes in YAC128 CS co-culture

We found that all of the identified DIV21 phenotypes were due to impaired development of YAC128 MSNs after DIV14 (**Fig. 2.5, 2.6**). In vivo, MSN spines and dendrites develop normally in WT and YAC128 animals when assessed by Golgi staining at 1 month of age [80]. Thus, our observation of developmental phenotypes in CS co-culture suggests that impaired synaptic function occurs early in vitro, before MSNs have reached a mature state. This is in agreement with previous work showing an impaired developmental increase in mEPSC frequency and stunted dendritic development after DIV14 using YFP transfection in co-cultured YAC128 MSNs [73]. However, our results are discordant with a recent study from Wu et al. showing degenerative spine loss from DIV14 to DIV21 in YAC128 CS co-cultured MSNs [74]. Differences in culture methodology might explain why Wu et al. observed a degenerative phenotype and we did not. If our culturing conditions were inherently more stressful to the neurons, their maturation by DIV14 may have been impaired, such that synaptic dysfunction occurred before spines or dendrites were fully developed. Alternatively, the use of postnatal cultures in Wu et al. might have promoted earlier maturation of MSNs by DIV14, either due to the later developmental age used or the presence of a greater number of supporting glial cells in the postnatal brain [356]. The existence of YAC128 dendritic and spine phenotypes at DIV18 but not at DIV14 is advantageous as it allows for in vitro testing of both preventative therapies (ie. from DIV14-21) or strategies aimed at phenotype reversal (ie. from DIV18-21).

Functional impact of altering cortical input in CS co-culture

Our electrophysiological results demonstrate that a 1:1 CS ratio is critical for the emergence of a YAC128 mEPSC frequency or membrane capacitance phenotype, which tend to correlate with total dendritic length (summarized in **Table 2.1**). Surprisingly, 1:3 co-cultured YAC128 MSNs had similar mEPSC frequencies to 1:3 WT MSNs, despite exhibiting significantly impaired spine stability. This finding raises the possibility that YAC128 cortical or striatal neurons in 1:3 cultures undergo compensatory upregulation of spontaneous CS activity,

potentially by increasing cortical glutamate release. It is also plausible that some of the additional spines on WT 1:3 MSNs possess NMDA receptor-containing silent synapses, which would not be active in our electrophysiological recording conditions, and thus may not result in an increased mEPSC frequency compared to YAC128 [357]. Alternatively, YAC128 1:3 MSNs could conceivably contain a higher number of active shaft synapses which likely constitute a large proportion of synapses in cultured neurons [127], and may be detected by electrophysiological recording, but would not be identifiable through spine analysis. One caveat in our interpretation of these results is that identification of MSNs for electrophysiological recording in CS co-culture requires a striatal YFP transfection step at the time of plating [73, 81], which could reduce overall culture health and thus impact the level of spontaneous activity observed. Furthermore, it is possible that YFP transfection and DARPP32 staining disproportionately identify MSN populations of different subtypes or maturity, leading to inconsistencies when comparing data obtained with each method.

Selective, age-associated loss of DARPP32+ MSNs in the YAC128 mouse model

Previous analysis of DARPP32+ MSN survival in WT CS co-cultures demonstrated that despite a 50% higher striatal plating density in 1:3 cultures versus 1:1, the number of DARPP32+ cells at DIV18 was similar in both conditions, suggesting selective vulnerability of this cell type [341]. In the present study, the density and proportion of WT DARPP32+ MSNs in 1:3 conditions at DIV21 increased by 27% and 21% respectively, compared to 1:1, although this was still less than the expected 50% increase (**Fig. 2.5**). It is possible that DARPP32 expression was higher after longer maturation to DIV21 in our study, potentially improving the sensitivity of this readout compared to the DIV18 study. Interestingly, YAC128 DARPP32+ MSNs in 1:3 CS co-culture exhibit reduced survival compared to WT when assessed at DIV21 (**Fig. 2.5**). This correlates well with our previously-established findings of striatal volume loss and reduced DARPP32+ MSN cell counts in 12-month old YAC128 brains [50, 346–348], as

well as decreased DARPP32 protein and mRNA levels at 10 months of age [51]. These in vivo alterations are associated with behavioral impairments which are less severe or not observable at earlier ages [50, 358]. Furthermore, decreased number and size of DARPP32+ neurons occurs in the human HD striatum, and is correlated with motor impairment [359]. Thus, we have enhanced our in vitro CS co-culture model to recapitulate age-associated MSN loss without the use of any acute stressors, such as glutamate, to induce cell death. This will prospectively be useful for preclinical testing of neuroprotective therapeutic approaches in a more representative model of chronic disease.

Conclusions

Altogether, we have optimized the CS co-culture system for broader and more reliable use in HD research and show that intrinsic MSN spine stability is highly sensitive to cortical input, thus providing both a clear explanation for inconsistent results from previous studies and a strategy to generate reproducible and disease-relevant findings in the future. The ability to observe a consistent spine phenotype in vitro is likely to be useful for preclinical HD drug development, because spine loss in YAC128 MSNs is dynamic, such that it can be modulated over relatively short periods of time [74, 75]. This provides a sensitive experimental readout for future studies of mHTT-induced synaptic dysfunction. Furthermore, the techniques we have utilized for morphological analysis are accessible, easy to establish, and can be used to generate results quickly compared to in vivo studies. Ultimately, our findings demonstrate that the CS co-culture system is amenable to modifications that allow differential elucidation of HD-like phenotypes in vitro, and provide a useful tool for future studies on mechanisms of synaptic dysfunction in HD. Ideally, this tool will be combined with other modeling and computational strategies in the future to more comprehensively understand the mechanisms underlying HD pathogenesis.

3 DAPK1 PROMOTES EXTRASYNAPTIC GLUN2B PHOSPHORYLATION AND STRIATAL SPINE LOSS IN HUNTINGTON DISEASE[2]

3.1 INTRODUCTION

Huntington disease (HD) is a debilitating and fatal neurodegenerative disorder caused by a CAG trinucleotide repeat expansion in huntingtin (HTT) [3]. The resulting mutant HTT (mHTT) protein disrupts multiple cell signaling pathways and protein-protein interactions, leading to altered cortico-striatal (CS) transmission, synaptic loss, and degeneration of GABA-ergic striatal medium spiny neurons (MSNs) [14–16, 19, 26, 40, 337].

MSNs receive high levels of excitatory glutamatergic input and trophic support (ie. brain-derived neurotrophic factor, BDNF) from cortical afferents [340]. mHTT causes both pre- and postsynaptic dysfunction at the CS synapse which, in addition to intrinsic MSN properties, contributes to their selective vulnerability in HD [337]. MSNs express N-methyl D-aspartate receptors (NMDARs) at CS postsynaptic sites. When activated, synaptic NMDARs initiate pro-survival signaling and upregulation of genes involved in synaptic maintenance and neuroprotection [124, 125]. Conversely, extrasynaptic GluN2B (exGluN2B) subunit-containing NMDAR activity promotes cell death processes and antagonism of synaptic signaling (**Fig. 1.1**) [124, 125]. Extensive research using the YAC128 full-length transgenic mouse model of HD has demonstrated enhanced exGluN2B surface expression, activity, and associated excitotoxic cell death signaling prior to neurodegeneration or synaptic spine loss in YAC128 MSNs [80, 81, 194, 203, 205, 213, 288]. Preferential blockade of exNMDARs in

[2] This chapter is in preparation to be combined with Chapter 4 and submitted for publication as one manuscript. Schmidt ME, Caron NS, Dal Cengio L, Ko Y, Lazic N, Anderson L, Raymond LA, Hayden MR. Death-associated protein kinase 1 promotes extrasynaptic GluN2B phosphorylation and striatal spine loss in Huntington disease.

vivo with low-dose memantine rescues motor deficits and neuropathology, restores striatal survival signaling, and normalizes exGluN2B levels in YAC128 mice [80, 205, 206].

Increased activation of exNMDARs is a common pathological event across other major neurological disorders, including AD and ischemic stroke [124]. This enhanced receptor activity causes activation of neuronal death signaling via p38, c-Jun terminal kinase (JNK), nNOS, caspases, and calpains, and shut-off of pro-survival ERK and nuclear phosphorylated CREB signaling, leading to synaptic dysfunction [360]. Despite these compelling data, direct therapeutic targeting of NMDARs has proven to be largely ineffective in clinical trials for ischemia, likely due to partial suppression of pro-survival synaptic NMDAR activity as a result of poor compound selectivity for exclusively extrasynaptic receptor populations [361]. For this same reason, chronic use of an NMDAR antagonist for the treatment of HD could produce adverse outcomes. These disappointing clinical trial results necessitate an alternate strategy to modulate pathological exGluN2B receptor activity while preserving synaptic function and survival signaling.

Death-associated protein kinase 1 (DAPK1) is a calcium/calmodulin-activated serine/threonine (S/T) kinase which is highly expressed during late embryonic development [215, 216, 239]. DAPK1 was initially identified as a positive mediator of apoptosis and later as a regulator of exGluN2B function [177, 215, 216]. Specifically, during ischemic excitoxicity in the adult mouse, DAPK1 becomes activated via S308 dephosphorylation and recruited to exGluN2B complexes, where it phosphorylates the intracellular GluN2B C-terminal domain at S1303, increasing receptor conductance [177]. S1303 phosphorylation has also been associated with enhanced GluN2B surface expression in neurons [152], suggesting that DAPK1 may act as a signal amplifier for exGluN2B under pathological conditions. Accordingly, numerous genetic and pharmacological DAPK1-targeting approaches have demonstrated neuroprotective and synapto-protective benefit in animal models of stroke, excitotoxicity, AD, PD, and chronic stress (**Table 1.3**).

In the present study, we have investigated whether DAPK1 contributes to enhanced exGluN2B function in HD. Furthermore, we assess whether small molecule DAPK1 inhibition prevents synaptic abnormalities in HD MSNs.

3.2 MATERIALS AND METHODS

3.2.1 Mice

Wild type (WT) and YAC128 mice were maintained on the FVB/N background and experiments were performed according to protocols approved by the University of British Columbia Animal Care Committee (Protocol numbers A16-0130 and A16-0206). Heterozygous line 53 YAC128 mice or line W13 C6R mice (YAC128 mice bearing a D586A point mutation rendering mHTT resistant to caspase cleavage at this site) and their WT littermates were used for all experiments with the exception of neuronal culture transfections. For these experiments, homozygous line 55 YAC128 and FVB/N mice were used in order to remain consistent with previously published work [81] as well as to improve culture health by avoiding an overnight genotyping step. For all cohorts, approximately equal numbers of male and female mice were used. All animals were sacrificed using CO_2.

3.2.2 Total cell lysis and Western blotting

Cortical or striatal total lysate was prepared by homogenizing snap-frozen tissue in stringent lysis buffer (20mM HEPES pH 7.4, 150mM NaCl, 40mM β-Glycerophosphate, 10mM NaF, 1% Triton-X, 1% SDS, 0.5% sodium deoxycholate) with protease and phosphatase inhibitors freshly added (1X Roche Complete Protease Inhibitor, 5μM zVAD, 1μg/mL Pepstatin A, 1mM sodium orthovanadate). Protein samples were sonicated, centrifuged to remove cellular debris, and quantified by DC assay. Equal amounts of protein from each sample were run by SDS-PAGE on 8% or 10% acrylamide gels and transferred to 0.45μm nitrocellulose membranes. Membranes were blocked in 5% skim milk

powder in TBST (0.1% Tween-20) for 1 hour at room temperature (RT), blotted in primary antibody in 3% BSA/TBST for 2 hours at RT, washed 4x in TBST, incubated with fluorescent secondary antibody for 1 hour at RT, washed, and scanned with a LI-COR imaging system. Band intensities were quantified using Image Studio Lite.

3.2.3 Subcellular fractionation

Subcellular fractionations from brain tissue were performed as previously described to isolate synaptic (post-synaptic density, PSD) and extrasynaptic (non-PSD) membrane fractions [80]. Striatal non-PSD preparations consistently produced low protein yield and unreliable detection of GluN2B phosphorylation. Therefore, we chose an alternate method for evaluation of striatal extrasynaptic pS1303 levels which has previously been utilized [288]. Tissue samples were homogenized in a gentle lysis buffer (20mM HEPES pH 7.4, 150mM NaCl, 40mM β-Glycerophosphate, 10mM NaF, 1% Triton-X) containing fresh protease and phosphatase inhibitors, but no SDS or sodium deoxycholate. This buffer is unable to lyse Triton-insoluble PSD membranes. Thus, after homogenization and high-speed centrifugation, the remaining supernatant was assumed to contain cytosol and “non-synaptic” membranes, including endosomes. Since GluN2B is a transmembrane protein, any GluN2B in the final protein sample was assumed to be localized to non-synaptic membranes. Synaptic and extrasynaptic/non-synaptic protein fractions were quantified and used for Western blotting as described above. Validation of this fractionation method as well as further isolation of cytosolic and nuclear compartments is depicted in **Fig. 3.1.** Antibodies and conditions used for Western blotting are listed in the following table:

Target	Host	Company	Catalogue #	Dilution
B-actin	Rabbit	Cell Signaling	4967	1:2000
CaMKIIα	Mouse	Cell Signaling	50049	1:2000
CaMKII-pT286	Rabbit	R&D Systems	PPS002	1:2000
DAPK1	Rabbit	Sigma	D1319	1:2000
DAPK1-pS308	Mouse	Sigma	D4941	1:400
GAPDH	Mouse	Millipore	MAB374	1:10,000
GluN2B	Mouse	Invitrogen	MA1-2014	1:1000
GluN2B-pS1303	Rabbit	Millipore	07-398	1:1000
HDAC1	Mouse	Santa Cruz	sc-81598	1:250
PSD95	Mouse	Thermo Fisher	MA1-046	1:2000
Synaptophysin	Mouse	BD Transduction	611880	1:10,000

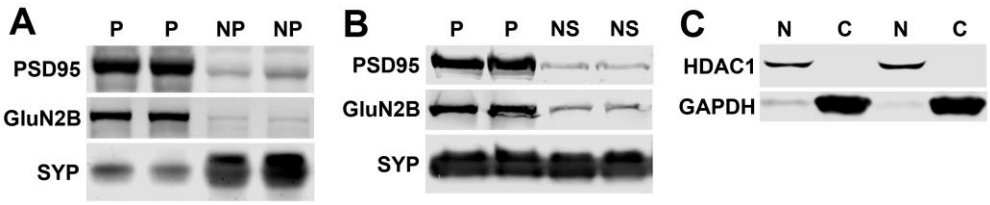

Figure 3.1: Western blot validation of subcellular fractionation method. (A) A standard subcellular fractionation protocol leads to enrichment of synaptic proteins PSD95 and GluN2B in the post-synaptic density (PSD) fraction, P, while the presynaptic marker synaptophysin (SYP) is enriched in the non-PSD compartment, NP. **(B)** A modified "non-synaptic," NS, lysis protocol using a gentle buffer followed by harsh lysis of the insoluble synaptic pellet, P, leads to a similar distribution profile for PSD95 and GluN2B as observed in (A). SYP was not enriched in the NS fraction, potentially due to the inclusion of cytosolic protein in this lysate which could dilute enrichment of presynaptic proteins. **(C)** Further fractionation steps allow clear distribution of the nuclear marker histone deacetylase 1 (HDAC1) into the nuclear compartment, N, and glyceraldehyde 3-phosphate dehydrogenase (GAPDH) into the cytosol, C.

3.2.4 Co-immunoprecipitation

Cortical tissue was homogenized in a gentle lysis buffer (50mM Tris, 150mM NaCl, 1% Igepal) with fresh protease inhibitors and pre-cleared with 10µL of Protein G Dynabeads (Invitrogen) for 1.5 hours at 4°C. During the pre-clear step, 15µL of Dynabeads per sample were washed once in lysis buffer, blocked with

3% BSA in lysis buffer, and conjugated to primary rabbit anti-DAPK1 antibody or control rabbit IgG (2.5µg per sample) in blocking solution for 1 hour at RT. Beads were washed twice in lysis buffer, added to pre-cleared lysates, and rotated overnight at 4°C. Beads were washed 3 times for 10 minutes in lysis buffer and protein was eluted in 1x LDS sample buffer (Invitrogen) with 100mM DTT at 70°C for 10 minutes. Samples were run by SDS-PAGE alongside previously set-aside input controls, transferred to nitrocellulose membranes, and blotted for DAPK1 and GluN2B using mouse primary antibodies. Co-immunoprecipitated GluN2B band intensity was normalized to the amount of immunoprecipitated DAPK1 for each sample.

3.2.5 In vivo memantine treatments

Male WT and female YAC128 (line 53) mice were set up in mating pairs and provided either regular drinking water or water containing memantine. The concentration of memantine was calculated based on the weight of the female mouse and an estimated average consumption of 5mL per day in order to administer a dose of 2mg/kg/day. Final memantine concentrations were approximately 12mg/L. Females were separated from males after 1 week, and pregnant females remained on either water or memantine treatment until pups were weaned at approximately P20. At this time, male and female pups were separated and the average pup weight per cage was used to calculate a 1 mg/kg/day dose, assuming an average consumption of 4mL per day per pup. Final memantine concentrations for pup treatment were approximately 2.5mg/L. At 1 month of age, mice were sacrificed and brain tissue was collected for subcellular fractionation and Western blotting.

3.2.6 Neuronal culture setup and transfections

Autoclaved glass coverslips (Marienfeld Superior) were shaken in 6N HCl overnight at RT, washed in ddH_2O and 70% ethanol, transferred to 24-well

plates, and allowed to air dry. Coverslips were coated with 100µg/mL high molecular weight poly-D-lysine (PDL) hydrobromide (Sigma; P6407) at RT overnight, washed 4 times thoroughly with water, and air dried before use. E17.5 embryos were removed from timed-pregnant female mice, and brains were kept overnight at 4°C in Hibernate-E supplemented with L-glutamine (0.5mM, Gibco) and B27 (Gibco) while excess embryonic tissue was used to perform genotyping. For dendritic spine experiments, cortical and striatal tissues were dissected separately in ice-cold Hank's Balanced Salt Solution (HBSS, Gibco). Dissected tissue was dissociated by gently pipetting once with a P1000 pipette, centrifuged, and enzymatically digested in 0.05% trypsin-EDTA (Gibco) for 8 minutes at 37°C. Tryspin was inactivated with 10% FBS in neurobasal medium (NBM, Gibco). Cells were then triturated gently 3-5 times in complete NBM (supplemented with L-glutamine, penicillin/streptomycin, and B27) containing DNase 1 (0.08mg/mL) for further dissociation. Cells were centrifuged, resuspended in complete NBM, counted, and plated at a 1:3 cortical:striatal ratio with a final density of 160,000 cells per well. For evaluation of exogenous YFP-GluN2B surface expression, striatal neurons were nucleofected with a YFP-GluN2B construct (2µg; a gift from Dr. Ann Marie Craig, University of British Columbia) prior to being mixed with cortical neurons at a 1:1 ratio and plated in 500µL 10% FBS/DMEM. Media was replaced with 500µL of warm complete NBM after 3-4 hours and topped up to 1mL the following day. For biochemical experiments, cortical and striatal tissue were kept together during the culture process and seeded in 6-well PDL-coated plates at a density of 1 million cells per well. All cultures were fed with fresh complete NBM (20% well volume) every 6-7 days until DIV14 and every 3-4 days afterwards, unless undergoing drug treatments.

3.2.7 Neuronal culture drug treatments and lysis

For imaging experiments, neurons grown on coverslips were treated every day from either DIV14 or DIV18 until DIV20 by diluting stock or control solution in 50µL of NBM complete which was added to each well with a final volume of 1mL.

Ifenprodil and memantine were dissolved in sterile H_2O and used at a final treatment concentration of 3µM. The DAPK1 inhibitor TC-DAPK6 (DKI; Tocris Bioscience) was dissolved in DMSO and used at a final concentration of 1µM (0.01% DMSO). Cultures were fixed and immunostained at DIV21.

For biochemistry, culture media was replaced with conditioned media containing 10µM DKI or DMSO (0.1%) for 1 hour. Cells were collected by scraping immediately following treatment, centrifuged, and frozen at -20°C for later processing. Pellets were lysed by pipetting in gentle lysis buffer to solubilize only non-synaptic proteins. Samples underwent SDS-PAGE and Western blotting as described above for detection of protein and phosphorylation levels.

3.2.8 Immunocytochemistry, microscopy, and image analysis

For spine experiments, neurons on coverslips were fixed at DIV21 for 15 minutes at RT in 4% paraformaldehyde/PBS. Coverslips were washed three times in PBS after fixation and between all subsequent incubation steps. Samples were incubated at -20°C in methanol for 5 minutes, permeabilized in 0.03% Triton-X/PBS at RT for 5 minutes, blocked in 0.2% gelatin/PBS at RT for 30 minutes, incubated with primary antibody against DARPP32 in blocking solution overnight at 4°C and fluorescent secondary antibody for 1.5 hours at RT. Coverslips were mounted on microscope slides using Prolong Gold Antifade Reagent with DAPI (Invitrogen). Z-stack images of step size 60 µm were acquired using a Leica SP8 confocal microscope with a 63x objective lens. Representative MSNs for imaging were selected based on a healthy nuclear appearance and high DARPP32 expression level. In Image J, files were converted to 2D images with the maximum intensity Z-projection option, background subtracted with a rolling ball radius of 35 pixels, and smoothed using the de-speckle function. De-speckling was necessary, as it dramatically improved the efficiency of automatic spine detection in NeuronStudio (Version 0.9.92). Images were imported into NeuronStudio for semi-automatic spine identification and classification using at least 3 different secondary or tertiary dendritic segments per neuron.

Exogenous YFP-GluN2B surface expression was assessed as previously described [81]. Transfected cultures grown on coverslips were live-stained at DIV21 by incubating with primary chicken GFP antibody in conditioned media for 10 minutes in a 37°C CO_2 incubator. Cells were rinsed once with warm conditioned media, fixed, and incubated with Alexa Fluor 488-conjugated goat anti-chicken secondary antibody for 1.5 hours at RT. Samples were subsequently permeabilized, blocked, and stained as described above for internal YFP and VGLUT1 using rabbit and guinea pig primary antibodies, respectively. This was followed by fluorescent secondary antibody staining (Alexa Fluor 568-conjugated goat anti-rabbit and Alexa Fluor 647-conjugated goat anti-guinea pig). Coverslips were mounted on slides and transfected cells were imaged at 63x objective magnification in three channels at constant laser intensity across samples. Three representative secondary or tertiary dendritic segments were selected and the mean intensity value from each GFP channel within each selection was measured and averaged to generate a surface-to-internal ratio value as a measure of surface expression. The numbers of total YFP-GluN2B punctae and punctae colocalized with VGLUT1 were counted manually and normalized to dendritic area to yield GluN2B punctae and synapse densities. For all imaging experiments, a total of at least 24 neurons from three individual culture batches were imaged. Primary antibodies and dilutions used for immunocytochemistry experiments are listed in the table below. Alexa Fluor goat secondary antibodies directed to the appropriate primary antibodies were used at a 1:500 dilution. All imaging and analyses were performed with the researcher blind to experiment conditions.

Target	Host	Company	Catalogue #	Dilution
DARPP32	Rat	R&D Systems	MAB4230	1:500
GFP	Chicken	Abcam	Ab13970	1:1000
GFP	Rabbit	Synaptic Systems	132 002	1:500
VGLUT1	Guinea Pig	Millipore	AB5905	1:4000

3.2.9 Data analysis

GraphPad Prism 5 was used for all statistical analysis and graph preparation. Figures were generated in Adobe Photoshop CS5. All data are presented as mean ± SEM. Student's t-test or 1- or 2-way ANOVA statistical tests with Bonferroni post-hoc analysis were used for all experiments. In some cases, t-tests were performed between specific groups after an ANOVA test when a planned comparison was established during the experimental design process. Significance for these tests is noted with the "#" symbol instead of "*".

3.3 RESULTS

3.3.1 DAPK1 expression and activation are dysregulated in the HD brain

Despite being predominantly expressed during neurodevelopment, DAPK1 becomes re-activated and expressed to a greater degree as a result of pathological conditions in the adult brain or in mature neurons [177, 225, 239, 245, 247, 252, 258, 275, 278, 291, 304, 306–311, 314]. Given the established role of NMDAR excitotoxicity in HD, we sought to evaluate whether DAPK1 is dysregulated in YAC128 mice. 1-month-old animals were used because this is the age at which YAC128 mice demonstrate enhanced excitotoxin sensitivity and elevated striatal exGluN2B, prior to behavioral or neuropathological phenotypes [77, 80]. We observed significantly increased DAPK1 protein levels in total lysates from both the cortex and striatum of YAC128 mice, as well as reduced site-specific phosphorylation at the autoinhibitory S308 residue (normalized to total protein level), indicating greater kinase activation (**Fig. 3.2A, B**). These changes were not observed in the cerebellum, which is largely spared in HD (**Fig. 3.2C**), nor in the cortex of human wtHTT-expressing YAC18 mice (**Fig. 3.3**), signifying that these changes are not due to transgenic overexpression of human HTT. When we evaluated *Dapk1* mRNA levels, we found no differences between genotypes (**Fig. 3.2D**), suggesting altered DAPK1 protein stability or turnover in YAC128 brains, as opposed to elevated transcription. Interestingly, in 1-month-old WT FVB animals, DAPK1 expression was significantly higher in cortical and

striatal tissues when compared directly to the cerebellum (**Fig. 3.2E**). Furthermore, phosphorylation of DAPK1 at S308 was reduced in the striatum compared to the cortex and was dramatically increased in the cerebellum (**Fig. 3.2E**). Thus, in the normal brain, DAPK1 expression and activation are highest in the regions most affected by HD.

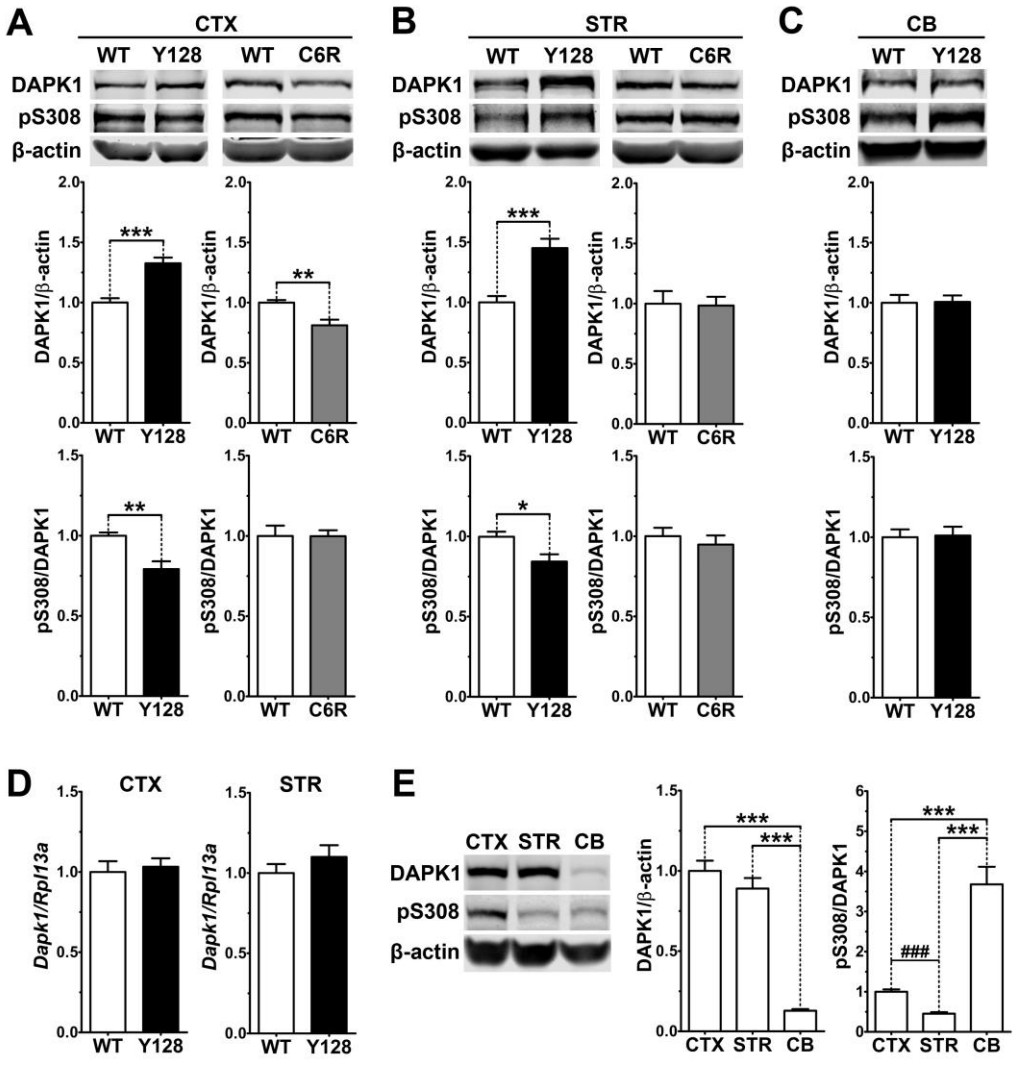

Figure 3.2: Increased DAPK1 protein expression and activation occur in affected regions of the YAC128 brain and require mHTT cleavage at D586. (A) Cortical (CTX), **(B)** striatal (STR), or **(C)** cerebellar (CB) tissues from 1-month-old WT, YAC128 (Y128; line 53), and C6R (line W13) mice were lysed in a stringent buffer and total lysate was run by SDS-PAGE followed by Western blotting for DAPK1, pS308, and β-actin. DAPK1 expression normalized to β-actin levels was increased in cortical and striatal YAC128 brain regions but not in the cerebellum or in C6R brains. DAPK1

phosphorylation at S308 normalized to total DAPK1 protein levels was reduced in the YAC128 cortex and striatum, indicating greater activation. No change to pS308 levels were observed in the YAC128 cerebellum or C6R brains. Data are normalized to WT values (n=6-12 biological replicates, 2 technical replicates each; student's t-test, *p<0.05, **p<0.01, ***p<0.001). **(D)** *Dapk1* mRNA expression quantified by qPCR is similar in WT and YAC128 brains at 1 month of age. Data are normalized to WT (n=6 biological replicates; student's t-test). **(E)** Tissues from 1-month-old WT FVB mice were lysed in a stringent buffer and total lysate was run by SDS-PAGE followed by Western blotting for DAPK1, pS308, and β-actin. DAPK1 expression is similar in the cortex and striatum, but significantly lower in the cerebellum. DAPK1 S308 phosphorylation is significantly reduced in the striatum compared to cortex by student's t-test indicating greater activation, while phosphorylation is dramatically higher in the cerebellum. Data are normalized to CTX values (n=8 biological replicates, 2 technical replicates each; student's t-test, ### p<0.001; 1-way ANOVA with Bonferroni post-hoc analysis, ***p<0.001).

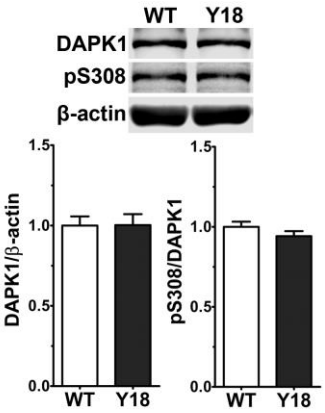

Figure 3.3: DAPK1 protein expression and activation are unaltered in the YAC18 cortex. Cortical tissues from 1-month-old WT and YAC18 (Y18; line 212) were lysed in a stringent buffer and total lysate was run by SDS-PAGE followed by Western blotting for DAPK1, pS308, and β-actin. DAPK1 expression and S308 phosphorylation were unchanged in YAC18 samples compared to WT littermates. Data are normalized to WT values (n=8 biological replicates, 2 technical replicates each; student's t-test).

The C6R mouse model expresses the YAC128 transgene bearing a point mutation at D586, rendering mHTT resistant to caspase cleavage at this site [195]. Unlike YAC128 mice, C6R mice are resistant to excitotoxicity, do not demonstrate enhanced exNMDAR activity, and display no motor deficits or neuropathology [80, 195]. We found that DAPK1 expression is reduced in the cortex and unaltered in the striatum of 1-month old C6R mice, and pS308 levels are comparable to WT in both brain regions (**Fig. 3.2A, B**), indicating that D586 cleavage is essential for mHTT-induced dysregulation of DAPK1. At 12 months

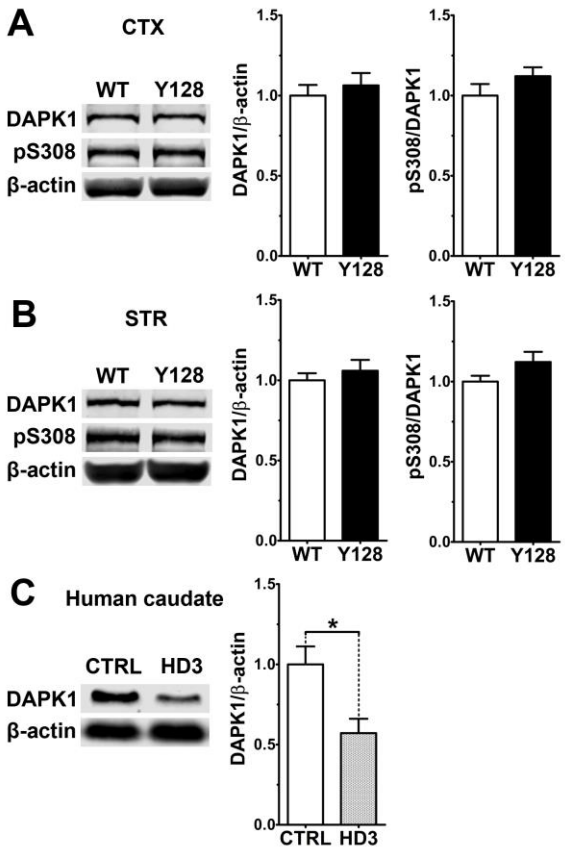

Figure 3.4: Increased DAPK1 protein expression and activation do not persist at late disease stages. (A) Cortical or **(B)** striatal tissues from 12-month-old mice were lysed in a stringent buffer and processed as described in Fig. 3.1. No differences in DAPK1 expression or phosphorylation level between WT and YAC128 brains were observed. Data are normalized to WT values (n=8 biological replicates, 2 technical replicates each; student's t-test). **(C)** Control (CTRL) or HD grade 3 (HD3) caudate samples of similar age and post-mortem interval were lysed and total protein was subjected to SDS-PAGE and Western blotting. Decreased DAPK1 expression was observed in HD3 brains compared to CTRL. Data are normalized to CTRL values (n=4-5 biological replicates, 2 technical replicates each; student's t-test, *p<0.05).

of age, YAC128 mice continue to exhibit increased exNMDAR currents, but have developed resistance to excitotoxicity, suggesting that compensatory protective mechanisms may be initiated with disease progression [77, 80]. In 12-month YAC128 mice, there was no observable difference in DAPK1 expression or phosphorylation compared to WT littermates (**Fig. 3.4A, B**). Furthermore, human postmortem caudate samples from late stage (Grade 3) HD patients contained significantly reduced levels of DAPK1 compared to control brains (**Fig. 3.4C**). Altogether, these findings provide evidence that mHTT causes upregulation of

DAPK1 expression and activity in the brain, at exclusively early disease stages prior to neurodegeneration, thus correlating with the time-course of previously observed synaptic dysfunction in this model.

3.3.2 Phosphorylation of exGluN2B at the DAPK1 site (S1303) is increased in the YAC128 brain

DAPK1 interacts with and phosphorylates exGluN2B at S1303, which contributes to amplification of receptor function and surface expression [152, 177]. We hypothesized that an increase in DAPK1 expression and activity in the YAC128 brain would correlate with enhanced phosphorylation at this GluN2B residue. Using subcellular fractionation (**Fig. 3.1**) and a site-specific antibody, we evaluated GluN2B and pS1303 levels in synaptic (post-synaptic density, PSD) and extrasynaptic (non-PSD) membrane compartments from 1-month-old WT and YAC128 tissues. We observed an increase in pS1303 in YAC128 cortices, which was specific to the extrasynaptic compartment, and not observed in synaptic fractions (**Fig. 3.5A, B**). We also did not detect altered GluN2B or pS1303 levels in YAC128 striatal synaptic fractions (**Fig. 3.5C**). Due to the length of the subcellular fractionation protocol and very low GluN2B protein yield obtained from the small amount of initial striatal tissue, we were unable to reliably detect S1303 phosphorylation in striatal extrasynaptic fractions. Therefore, we adopted a modified crude preparation method which involved lysing striatal samples in a gentle lysis buffer containing 1% Triton-X, which has been previously described and should be insufficient to solubilize the PSD [288], and immediately ran concentrated “non-synaptic” samples by SDS-PAGE and Western blot. Using this method, we detected a significant increase in non-synaptic pS1303 in the YAC128 striatum (**Fig. 3.5D**).

DAPK1 interacts more strongly with GluN2B receptors in vivo under pathological conditions and when S308 is dephosphorylated [177, 246]. Furthermore, phosphorylation of GluN2B at S1303 enhances the DAPK1-GluN2B interaction [246]. We hypothesized that a chronic elevation in DAPK1 expression,

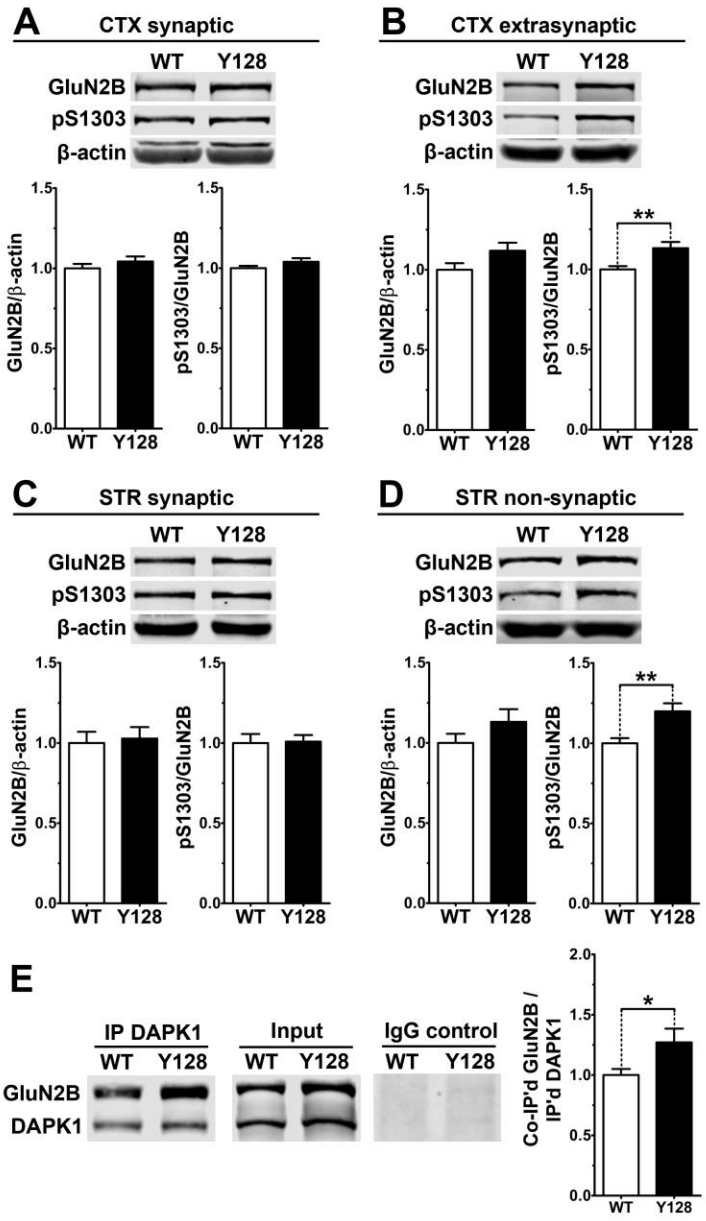

Figure 3.5: Extrasynaptic GluN2B S1303 phosphorylation and interaction with DAPK1 are elevated in the YAC128 brain. Cortical or striatal tissues were subjected to subcellular fractionation to yield **(A,C)** synaptic (PSD), **(B)** cortical extrasynaptic (non-PSD) or **(D)** striatal non-synaptic membrane fractions, which were run by SDS-PAGE and Western blotting for GluN2B expression and S1303 phosphorylation levels. Elevated pS1303 was specific to extrasynaptic/non-synaptic GluN2B in both brain regions. **(E)** The interaction between DAPK1 and non-synaptic GluN2B is increased in the 1-month YAC128 cortex. All sample blot images in (E) are cropped from the same Western blot membrane which contained multiple biological replicates run side-by-side. Data are normalized to WT values (n=6-14 biological replicates, 2 technical replicates each; student's t-test, *p<0.05, **p<0.01).

activation, and exGluN2B pS1303 levels would be associated with an enhanced basal DAPK1-GluN2B interaction in YAC128 brains. Using a gentle lysis buffer containing 1% NP-40 to preserve weak interactions and ensure solubilization of only non-PSD compartments, we observed an increase in the amount of non-synaptic GluN2B that co-immunoprecipitated with DAPK1 in the YAC128 cortex, signifying a greater level of interaction (**Fig. 3.5E**).

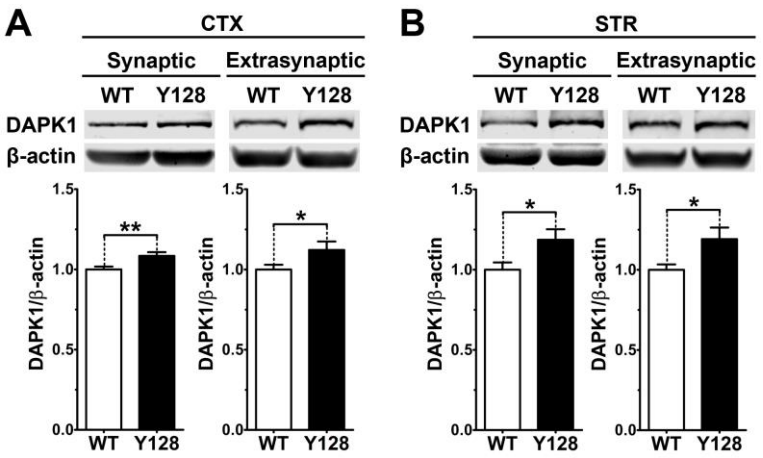

Figure 3.6: DAPK1 protein expression is elevated in both synaptic and extrasynaptic membrane fractions in the 1-month YAC128 brain. (A) Cortical or **(B)** striatal tissues were subjected to subcellular fractionation to isolate synaptic (PSD) and extrasynaptic (non-PSD) membranes, followed by SDS-PAGE and Western blotting for DAPK1 expression. Increased DAPK1 expression was observed in both compartments from both brain regions in YAC128 mice. Data are normalized to WT values (n=8-20 biological replicates; student's t-test, *p<0.05, **p<0.01).

Despite the specificity of elevated GluN2B pS1303 for the extrasynaptic compartment in YAC128 brains, we found that DAPK1 expression itself was significantly increased in both synaptic and extrasynaptic membrane fractions from the YAC128 cortex and striatum (**Fig. 3.6**). This suggests that altered DAPK1 function in HD may have as-of-yet undetermined consequences directly at the PSD, but its potential effect on S1303 phosphorylation of GluN2B is likely specific to the extrasynaptic receptor population.

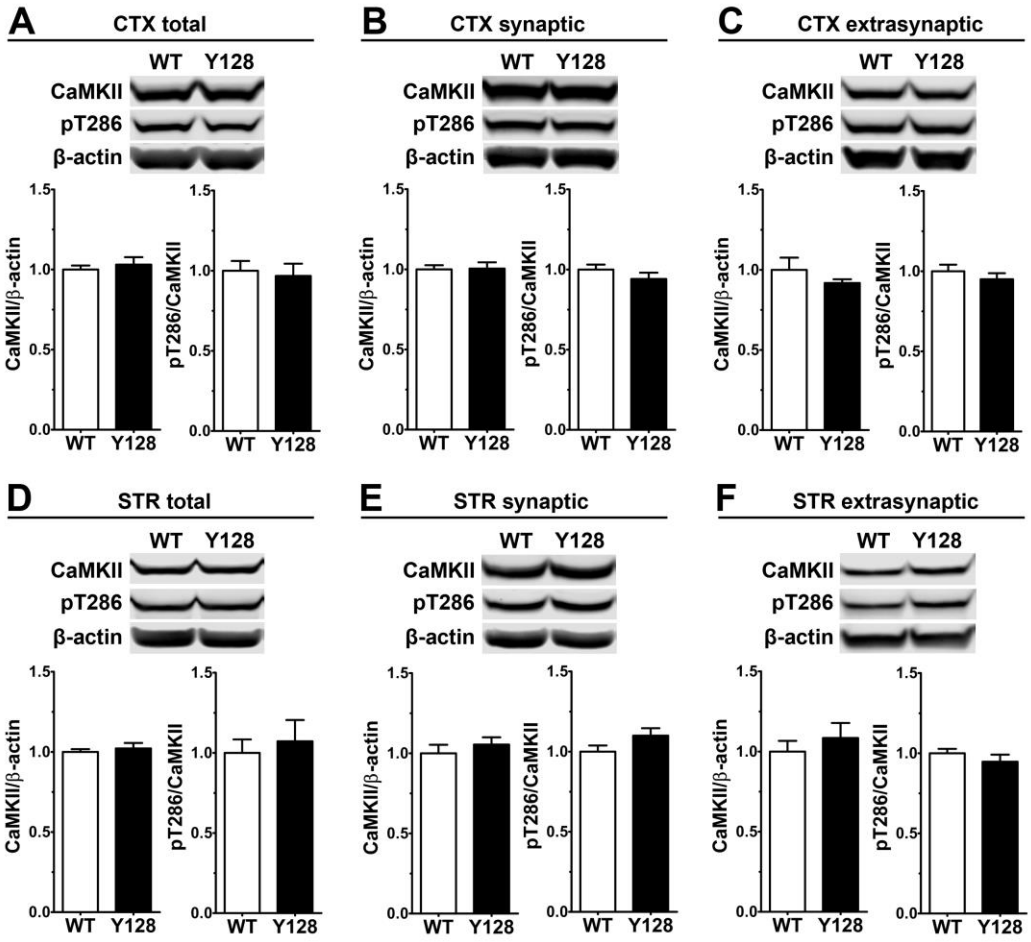

Figure 3.7: CaMKII protein expression and autonomous activation are unaltered in the 1-month YAC128 brain. Cortical or striatal tissues were lysed for **(A,D)** total protein or subjected to subcellular fractionation to isolate **(B,E)** synaptic (PSD) or **(C,F)** extrasynaptic (non-PSD) membranes. Samples were processed by SDS-PAGE and Western blotting for CaMKII expression and phosphorylation at the autonomous activation site T286. No differences in CaMKII protein level or phosphorylation were observed in YAC128 brains. Data are normalized to WT values and presented as mean ± SEM (n=8 biological replicates, 2 technical replicates each; student's t-test).

Calcium/calmodulin-dependent protein kinase II (CaMKII) is a DAPK1-related S/T kinase with established roles in synaptic signaling, neuronal plasticity, and receptor regulation [362]. Similar to DAPK1, CaMKII has been implicated in ischemic excitotoxicity related to NMDAR activation, and also phosphorylates GluN2B at S1303 [282, 363], influencing receptor surface expression [152]. Furthermore, DAPK1 mediates long-term depression (LTD) in hippocampal neurons by regulating the CaMKII-GluN2B interaction through competitive

binding [246]. Thus, it is possible that the observed increase in extrasynaptic pS1303 in YAC128 brains is due to altered CaMKII function instead of, or in addition to DAPK1 dysregulation. However, we found that CaMKII expression and autonomous activation measured by phosphorylation of T286 were unaltered in total, synaptic and extrasynaptic compartments of the YAC128 cortex and striatum (**Fig. 3.7**). These results suggest that the observed changes to pS1303 levels in YAC128 brains are more likely due to altered activity of DAPK1 rather than CaMKII.

3.3.3 In vivo exNMDAR blockade normalizes DAPK1 expression, activation, and exGluN2B pS1303 in the YAC128 cortex

Previously, treatment of cortical neurons with NMDA caused activation of DAPK1, and this was associated with elevated GluN2B pS1303 levels and exNMDAR-mediated calcium transients [177, 245]. The NMDAR antagonist AP5 or genetic deletion of DAPK1 abolished these effects, indicating that DAPK1 is activated downstream of NMDARs and subsequently augments exGluN2B phosphorylation and conductance [177]. In live YAC128 mice, low-dose treatment with memantine, which preferentially blocks exNMDAR channels, normalizes striatal cell survival (pCREB) and death (p-p38) signaling, returns exGluN2B expression to WT levels, and prevents motor function decline and neuropathology [80, 205, 206]. We thus hypothesized that a positive feedback loop may be pathologically amplified in HD, whereby elevated DAPK1 activation in YAC128 brains may both result from and contribute to increased exNMDAR function. To address the former, we treated WT and YAC128 mice with low-dose memantine from conception, and collected tissues for biochemistry at 1 month of age. We found that memantine treatment returned DAPK1 S308 phosphorylation in YAC128 total cortical lysate to WT levels (**Fig. 3.8A**). Unexpectedly, a significant interaction was observed between genotype and treatment group, such that DAPK1 protein levels were no longer significantly different between genotypes with memantine administration (**Fig. 3.8A**). We also observed normalization of elevated YAC128 exGluN2B S1303 phosphorylation with

treatment (**Fig. 3.8B**). These findings indicate that DAPK1 dephosphorylation and enhanced pS1303 levels may occur downstream of exNMDAR activity in the YAC128 cortex.

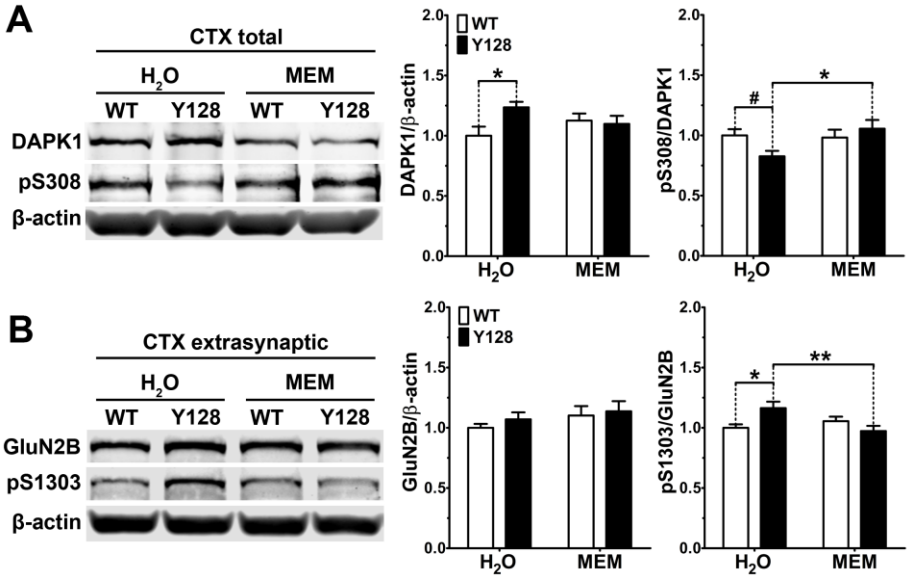

Figure 3.8: Low-dose memantine normalizes cortical DAPK1 activation and extrasynaptic pS1303 levels in YAC128 mice. Cortical tissues from 1-month-old WT and YAC128 mice treated with low-dose memantine from conception were processed to obtain **(A)** total or **(B)** extrasynaptic (non-PSD) membrane protein fractions. Samples were run by SDS-PAGE and Western blotting for DAPK1 or GluN2B protein expression and phosphorylation levels. Normalization of total DAPK1 pS308 and exGluN2B pS1303 was observed in YAC128 mice treated with memantine. Data are normalized to WT H2O values (n=8 biological replicates, 2 technical replicates each; 2-way ANOVA with Bonferroni post-hoc analysis, *p<0.05, **p<0.01; student's t-test, # p<0.05; 2-way ANOVA interaction *p<0.05 for DAPK1 protein level and pS308, 2-way ANOVA interaction **p<0.01 for pS1303).

3.3.4 DAPK1 kinase activity promotes exGluN2B phosphorylation and surface expression in YAC128 neurons

Our next experiments aimed to address whether DAPK1 contributes to increased exGluN2B phosphorylation or function in HD neurons. Consistent with the role of DAPK1 in amplifying exGluN2B function in ischemia, genetic manipulations eliminating DAPK1 expression or kinase activity promote neuroprotection and synaptic preservation in models of stroke, excitotoxicity, and AD (**Table 1.3**).

Furthermore, a selective, small-molecule DAPK1 inhibitor (TC-DAPK6, referred to here as “DKI”) protects against glutamate toxicity in SH-SY5Y cells, enhances maturation of primary cultured neurons, and prevents elevated GluN2B pS1303 and loss of pCREB and brain-derived neurotrophic factor (BDNF) levels in response to chronic stress in vivo [291, 314, 316]. TC-DAPK6 is highly selective for DAPK1 as well as the related kinase DAPK3 [302]. We used this same compound to evaluate the effect of targeting DAPK1 kinase activity on GluN2B receptors in YAC128 neurons. Primary YAC128 corticostriatal cultures exhibit increased endogenous pS1303, GluN2B, and DAPK1 levels at DIV21 compared to WT (**Fig. 3.9A**). These experiments were performed using a gentle lysis buffer as described above, in order to solubilize only non-synaptic proteins. Treatment with the DAPK1 inhibitor (DKI) normalized all of these measures to WT levels (**Fig. 3.9A**), indicating that DAPK1 activity contributes to pathologically elevated non-synaptic GluN2B and pS1303 in the presence of mHTT. Previously, an increase in surface expression of transfected YFP-GluN2B was observed in YAC128 MSNs co-cultured with cortical neurons at a 1:1 ratio, compared to WT [81]. We confirmed this phenotype in the present study and found that inhibition of DAPK1 reduced YFP-GluN2B surface expression in MSNs of both genotypes without affecting the number of receptor clusters, percent punctae colocalization with the presynaptic marker vesicular glutamate transporter 1 (VGLUT1), or number of synapses (YFP-GluN2B/VGLUT1 colocalized points) (**Fig. 3.9B**). These results demonstrate that DAPK1 kinase activity promotes elevated GluN2B phosphorylation in the presence of mHTT, and suggest that DAPK1-mediated phosphorylation of S1303 may be a key contributing factor to enhanced exGluN2B surface expression in YAC128 MSNs, which can be normalized with a DAPK1 inhibitor.

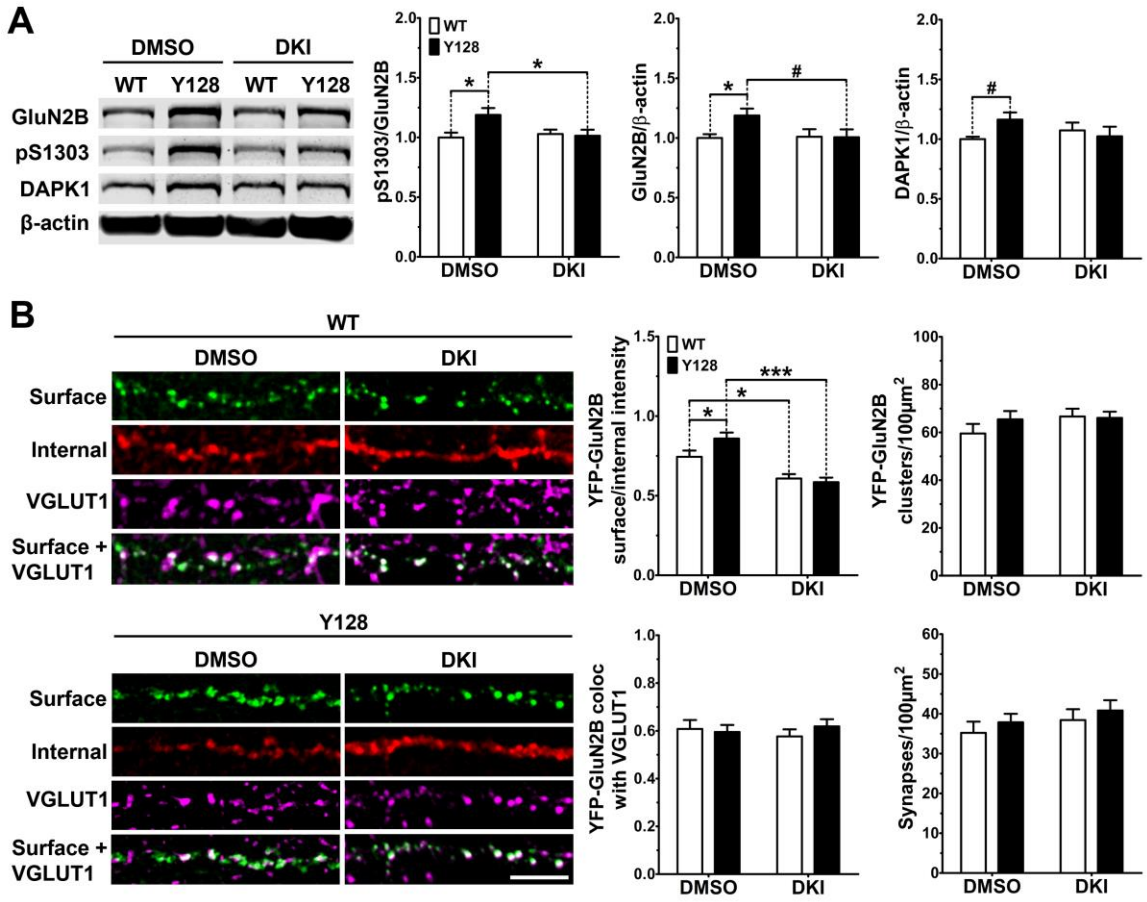

Figure 3.9: DAPK1 inhibition normalizes extrasynaptic GluN2B phosphorylation and surface expression in YAC128 neurons. (A) Corticostriatal primary cultures from WT and YAC128 embryos were treated at DIV21 with DMSO (0.1%) or a DAPK1 inhibitor (DKI, 10μM) for 1 h followed by lysis in a gentle buffer to solubilize non-synaptic protein. Lysates run by SDS-PAGE and Western blotting show increased YAC128 extrasynaptic GluN2B, pS1303, and DAPK1 levels, which are all normalized by DKI treatment. Data are normalized to WT DMSO values (n=8 biological replicates; 2-way ANOVA with Bonferroni post-hoc analysis, *p<0.05; student's t-test, #p<0.05). **(B)** Surface expression (surface/internal YFP fluorescence ratio) and cluster analysis of transfected YFP-GluN2B indicates increased GluN2B surface expression in 1:1 cortico-striatal co-cultured YAC128 MSNs and a reduction in both genotypes with DKI treatment (1μM for 3 days, 0.01% final DMSO concentration). No effect of genotype or treatment on YFP-GluN2B clustering, punctae colocalization with VGLUT1, or number of synapses were observed. Absolute values were used for punctae analysis (n=24-38 cells from 3 independent cultures; 2-way ANOVA with Bonferroni post-hoc analysis, *p<0.05, ***p<0.001). Scale bar = 5μm.

3.3.5 DAPK1 kinase activity promotes dendritic spine instability in YAC128 MSNs

MSN spine loss occurs with disease progression in HD patients and animal models [74, 82, 85, 86, 88, 89, 92, 93], as well as in DIV21 YAC128 MSNs co-cultured with cortical neurons at a 1:3 cortico:striatal (CS) ratio (Chapter 2). Recently, DAPK1 has been found to contribute to cortical spine and synapse degeneration after ischemia in vivo, and genetic deletion of the DAPK1 catalytic domain reverses hippocampal spine and synapse loss in Tg2576-APP AD mice [247, 310]. Therefore, we sought to determine if inhibiting DAPK1 could prevent or reverse striatal spine loss in YAC128 1:3 CS co-cultures. We used our established DARPP32 immunofluorescence staining method for MSN identification and morphological analysis. Similar to what we previously observed, YAC128 MSNs co-cultured with cortical neurons at a 1:3 ratio exhibited significantly reduced numbers of total spines at DIV21, and this was primarily due to a loss of mature mushroom-shaped spines with a small contribution of immature (stubby, thin, and filopodia) spine types (**Fig. 3.10A**). Treatment with DKI from DIV14-DIV21 completely rescued total, mature, and immature spine numbers in YAC128 MSNs to WT control levels (**Fig. 3.10A**).

Our previous work showed that YAC128 MSN spine instability in co-culture is apparent by DIV18, but not DIV14. Thus, DKI treatment from DIV14-21 prevented spine instability from occurring. We also wanted to determine if DKI treatment could reverse YAC128 spine loss after it had already occurred. To assess this, we performed a late-intervention treatment from DIV18-21 and observed complete reversal of total spine numbers, including near-complete rescue of mushroom spine density with DKI treatment (**Fig. 3.11**). We did not observe a basal genotypic difference in immature spine numbers in this batch of control-treated neurons (**Fig. 3.11**), indicating that this phenotype may show more culture-to-culture variation compared to the reliable and robust loss of mushroom spines observed in all experiments.

Next, we reasoned that if the beneficial effect of inhibiting DAPK1 on spine stability is mediated through its downregulation of exGluN2B function, then

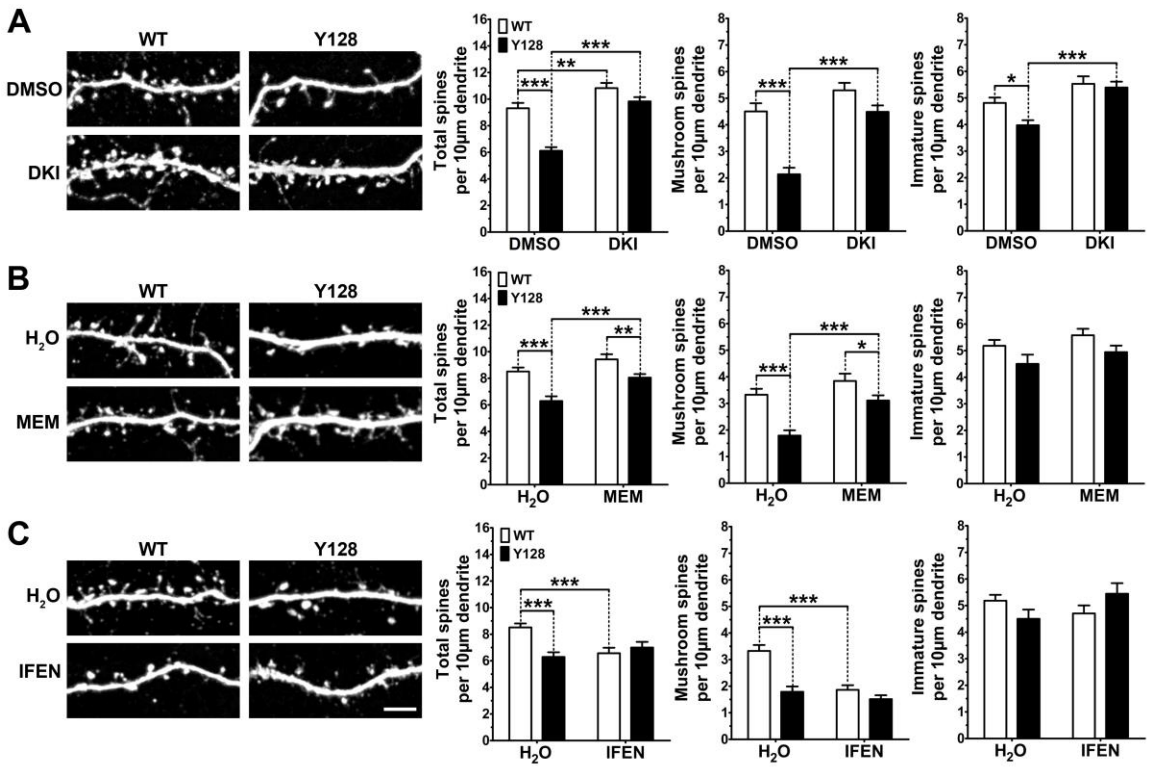

Figure 3.10: DAPK1 inhibition or extrasynaptic NMDAR blockade prevent spine instability in YAC128 MSNs. (A) WT and YAC128 1:3 CS co-cultures were treated from DIV14-21 with DMSO (0.01%) or a DAPK1 inhibitor (DKI, 1µM), followed by fixation and immunostaining for DARPP32. Semi-automated spine analysis in NeuronStudio demonstrates complete prevention of total, mushroom and immature spine loss in YAC128 MSNs. Co-cultures were treated with either water, memantine (MEM, 3µM) or ifenprodil (IFEN, 3µM) in the same way as for DKI. **(B)** Memantine rescued total and mushroom spine numbers in YAC128 MSNs. **(C)** Ifenprodil did not rescue total or mushroom YAC128 MSN spine numbers and reduced mushroom spine density in WT MSNs. **(B, C)** No genotypic difference in immature spine numbers was observed in these culture batches. Data are presented as non-normalized absolute values (n=24 cells from 3 independent cultures; 2-way ANOVA with Bonferroni post-hoc analysis, *p<0.05, **p<0.01, ***p<0.001). Scale bar = 5µm.

blockade of exNMDARs or GluN2B should have the same effect. Similar to DAPK1 inhibition, blockade of exNMDARs with low-dose memantine for 7 days completely rescued total and mature spine numbers in YAC128 MSNs (**Fig. 10B**). Surprisingly, GluN2B-selective antagonism with ifenprodil provided no benefit in YAC128 MSNs and significantly reduced mushroom spine density in WT MSNs (**Fig. 3.10C**), suggesting that ifenprodil may inhibit beneficial activity of GluN2B-containing synaptic NMDARs in this in vitro system. Ultimately, these

findings support our hypothesis that DAPK1 activity and consequent upregulation of exNMDAR function contribute to instability of MSN dendritic spines in HD.

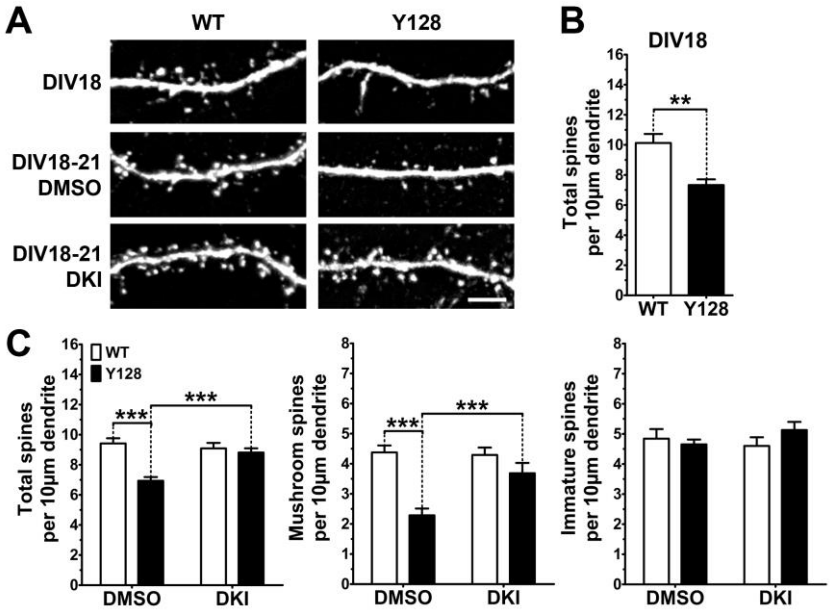

Figure 3.11: DAPK1 inhibition reverses spine instability in YAC128 MSNs. WT and YAC128 1:3 CS co-cultures were treated from DIV18-21 with DMSO (0.01%) or a DAPK1 inhibitor (DKI, 1 µM), followed by fixation, immunostaining for DARPP32, and semi-automated spine analysis in NeuronStudeo. **(A)** Representative dendritic images from each condition. **(B)** Total spine loss is apparent by DIV18. **(C)** DKI treatment reverses total and mushroom spine instability in YAC128 MSNs. Data are presented as non-normalized absolute values (n=24 cells from 3 independent cultures; 2-way ANOVA with Bonferroni post-hoc analysis, **p<0.01, ***p<0.001). Scale bar = 5µm.

3.4 DISCUSSION

Dysregulation of DAPK1 in early HD pathogenesis

In the present study, we have provided clear evidence that DAPK1 activity is altered in affected regions of the HD brain. This dysregulation follows a similar biphasic pattern to several other synaptic phenotypes in HD, with enhanced expression and activation observed at very early disease time points prior to neuropathology or behavioral deficits, but not at late stages [40, 62, 77]. The increase in DAPK1 protein expression and activation was associated with enhanced exGluN2B binding and phosphorylation at the DAPK1 site, S1303. Despite elevated protein levels, we did not observe altered *Dapk1* mRNA expression in the YAC128 brain compared to WT, suggesting stabilization of the protein. This phenomenon has previously been observed for DAPK1 in both AD and PD mouse models [270, 291]. To support this hypothesis, there is evidence that both activation (S308 dephosphorylation) of DAPK1 and phosphorylation of GluN2B at S1303 lead to a stronger GluN2B-DAPK1 interaction [246], which could presumably incorporate DAPK1 into NMDAR complexes, rendering it less accessible to degradation by proteasomes [262]. Thus, elevated DAPK1 levels may be secondary to activation of the protein.

Interestingly, DAPK1 protein levels and activity were unaffected in 12-month-old YAC128 mice (**Fig. 3.4**), Given the observed development of resistance to excitotoxicity in aged HD mice despite persistence of elevated exNMDAR currents [77, 80], this could represent uncoupling of GluN2B from downstream toxic signaling pathways and/or compensatory downregulation of those signal proteins as a protective strategy. In support of this, DAPK1 was dramatically reduced in late-stage (Grade 3) HD caudate tissue compared to controls, a finding corroborated by previously-published mRNA expression analysis in human HD patients [33]. Grade 3 HD patients generally exhibit 50-95% striatal volume and neuronal loss [364], compared to only 3-8% in 12-month YAC128 mice [348, 365]. Thus, our 12-month animal data may represent an intermediate phenotype while the human data sheds insight into more advanced

disease progression. DAPK1 is expressed primarily by neurons and not glia [239]. Furthermore, in this study we observed high expression of DAPK1 in the cortex and striatum compared to the cerebellum. Therefore, the ~43% decline in caudate DAPK1 levels in Grade 3 human HD brains may be caused by specific loss of neuronal cell types that highly express DAPK1.

Reciprocal positive feedback between exGluN2B activity, surface expression, DAPK1 activation, and pS1303

DAPK1 is activated and recruited to exGluN2B receptors during ischemia and phosphorylates the receptor at S1303, increasing current conductance and promoting neuronal death [177]. Thus, DAPK1 is a “signal amplifier” of pathological exGluN2B function. Prior evidence uncovered a potential mechanism whereby phosphorylation of GluN2B at S1303 may also enhance receptor surface expression (**Fig. 1.5**). When S1303 is in a dephosphorylated state, the CaMKII-GluN2B interaction is strengthened [283, 284], leading to CaMKII-mediated anchoring of casein kinase 2 (CK2) to the receptor complex [152]. CK2 phosphorylates GluN2B at S1480, which disrupts the PSD95-GluN2B interaction and destabilizes the receptor at the surface, resulting in clathrin-mediated endocytosis [147, 150–153]. It can be hypothesized that if extrasynaptic pS1303 levels are abnormally elevated, as has been demonstrated here, this could lead to reduced CaMKII anchoring of CK2, decreased pS1480, and thus greater postsynaptic density protein 95 (PSD95)-mediated stabilization of GluN2B at the surface. In fact, an increase in the PSD95-GluN2B interaction has been previously reported in extrasynaptic striatal fractions from YAC128 mice and was proposed to contribute to the elevated GluN2B surface expression consistently observed in this model [204]. It remains to be determined if pS1480 is decreased in YAC128 brains, as would be expected if this hypothesis holds true. Furthermore, although we only observed elevated GluN2B pS1303 in extrasynaptic fractions from YAC128 mice, DAPK1 was increased in both synaptic and extrasynaptic compartments (**Fig. 3.6**). DAPK1 and CaMKII, which

both phosphorylate S1303, were recently found to compete for GluN2B binding, and overexpression of DAPK1 inhibited long-term potentiation (LTP)-induced accumulation of CaMKII at synapses [246]. Thus, higher levels of synaptic DAPK1 in HD could potentially disrupt CaMKII-mediated synaptic plasticity. However, this remains to be investigated.

In the present study, blockade of exNMDARs with memantine rescued aberrant DAPK1 activation (pS308 levels) as well as exGluN2B pS1303 in the cortex of YAC128 mice (**Fig. 3.8**). This suggests that activation of DAPK1 and phosphorylation of S1303 are downstream consequences (either direct or indirect) of exNMDAR activity. Memantine treatment in YAC128 mice normalizes non-PSD GluN2B expression, indicating a direct correlation between activity and expression of the receptor in the extrasynaptic compartment [206]. Plausibly, the mechanism of this regulation could involve DAPK1-mediated phosphorylation of S1303 (**Fig. 3.12**). In support of this, we have shown that small-molecule inhibition of DAPK1 reduces S1303 phosphorylation and GluN2B surface expression in cultured YAC128 neurons (**Fig. 3.9**). Future experiments using GluN2B phosphodeficient and phosphomimetic mutants will be essential to confirm that this effect of DAPK1 inhibition on surface expression is dependent on the S1303 residue being dynamically phosphorylatable. Furthermore, since GluN2B phosphorylation at S1303 directly increases its binding affinity for DAPK1 [246] and may indirectly enhance binding to PSD95 (as described above) it will be important to determine if DAPK1 inhibition unlinks GluN2B from these two protein partners.

Synapto-protective effects of inhibiting DAPK1 kinase activity in vitro

We have utilized the 1:3 CS neuronal co-culture model previously optimized in Chapter 2 to evaluate the potential therapeutic benefit of inhibiting DAPK1 in HD. This “chronic” in vitro model naturally develops HD-like synaptic phenotypes over 3 weeks and is therefore advantageous over traditionally-used models of

NMDAR dysfunction which rely on acute toxic insult (ie. glutamate or NMDA) to induce rapid cell death.

We observed complete protection against spine instability in co-cultured YAC128 MSNs treated with a DAPK1 inhibitor (**Fig. 3.10**). Importantly, mature mushroom spines were preserved, suggesting the maintenance of functional activity, although this was not directly assessed. Low-dose memantine treatment had a similar beneficial effect on spine structure. While this suggests both compounds may be acting in the same pathway, an ideal future experiment to address this would be to treat cultures with both compounds to determine if there is an additive effect or not. Importantly, when we treated DIV18 cultures with the DAPK1 inhibitor, we successfully reversed spine loss after it had already occurred (**Fig. 3.11**). Thus, even though DAPK1 is exclusively dysregulated early in the YAC128 mouse model, it may still be a potentially attractive target for later intervention therapies aimed at restoring synaptic function of surviving neurons.

Although we did not probe the exact mechanism underlying the effect of DAPK1 inhibition on spine protection, there are a number of possibilities which could contribute. Given that heightened exNMDAR activity in YAC128 mice leads to CREB shut off by dephosphorylation at S133 [80, 81, 206], normalization of the balance between synaptic and extrasynaptic NMDAR signaling could restore CREB function, leading to downstream neuroprotection and synaptic strengthening. It is also possible that DAPK1 inhibition reduces its interaction with synaptic GluN2B, as described above, which could allow more CaMKII to bind in its place, promoting LTP and spine stability. Furthermore, DAPK1 is capable of sequestering ERK in the cytosol, thus limiting its nuclear translocation and consequent pro-survival signaling [222, 308], and reversal of this may be protective to spines. Finally, DAPK1 phosphorylates tau at S262 leading to spine damage in stroke [247]. Tau interacts with GluN2B-PSD95 complexes and phosphorylation at this site leads to destabilization of microtubules [298, 366]. Further investigation of tau S262 phosphorylation levels in HD and the potential contribution of this pathway to spine instability is warranted.

Potential involvement of ER calcium dysregulation in DAPK1-mediated spine loss in HD

NMDAR Ca^{2+} influx can induce further IP3R- or RyR-mediated Ca^{2+} release from the ER which, if occurring in excess, may result in mitochondria depolarization and neuronal death [144, 145]. ER Ca^{2+} stores are depleted in YAC128 neurons, causing enhanced store-operated Ca^{2+} entry (SOCE) and consequent spine degeneration [74]. This may occur via reduced SOCE-induced tonic activation of synaptic CaMKII, which normally maintains spine integrity [74, 367]. Blockade of SOCE restored intracellular Ca^{2+} dynamics and reversed MSN spine loss [74]. There is evidence for direct mHTT-induced sensitization of IP3Rs in YAC128 MSNs, as well as elevated RyR Ca^{2+} leakage from the ER, which contribute to ER store depletion and neuronal death [200, 368–370], but it remains to be determined if ER depletion is also linked to the increase in exGluN2B activity observed in this mouse model. Plausibly, potentiation of exGluN2B Ca^{2+} currents by DAPK1 could result in greater Ca^{2+} release from ER stores, thus promoting SOCE and spine degeneration.

Conclusions

In this study, we have provided compelling evidence that DAPK1 is a novel therapeutic target for synaptic protection in HD. DAPK1 is dysregulated early in YAC128 brains, contributes to aberrant exGluN2B phosphorylation and surface expression, and promotes spine loss in HD MSNs. We hypothesize that a positive feedback loop between exGluN2B and DAPK1 is amplified in the presence of mHTT, whereby exGluN2B surface expression and DAPK1 activity augment each other, ultimately leading to pathological exNMDAR-mediated CREB and ERK1/2 shut-off (**Fig. 3.12**). DAPK1 inhibition may restore synaptic function by breaking this amplification cycle and normalizing exGluN2B function. Importantly, it will be critical to validate these findings in vivo in order to rationalize further development of DAPK1-targeted therapies for HD.

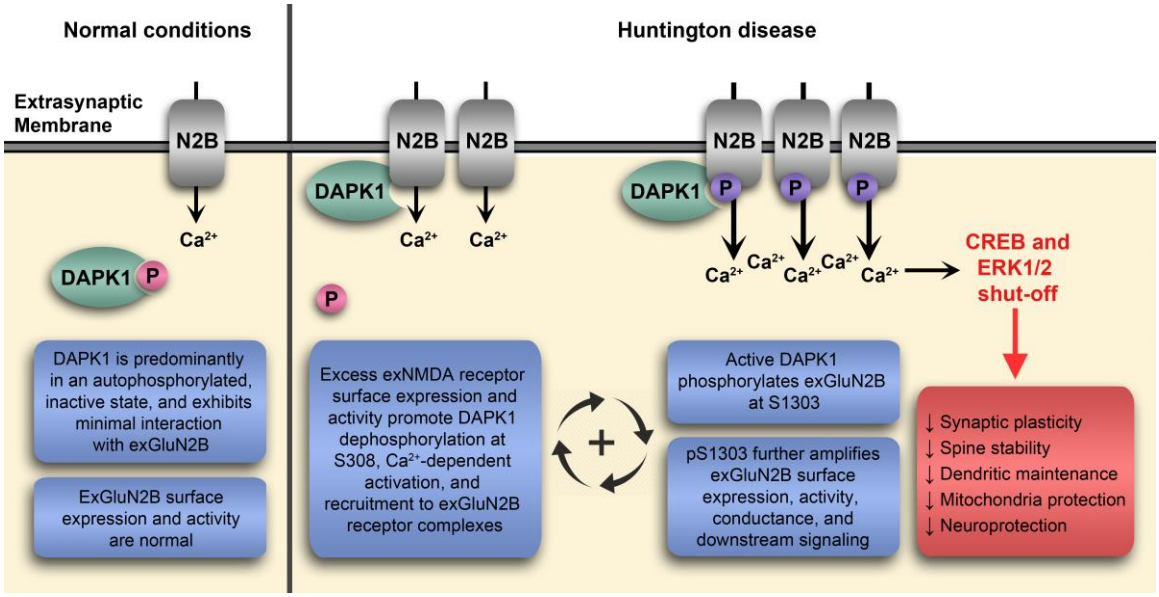

Figure 3.12: Hypothesis figure depicting the proposed role of DAPK1 in extrasynaptic GluN2B dysfunction in HD. DAPK1 and exGluN2B positively amplify each other's activity. Upregulation of this reciprocal pathway in HD leads to elevated exGluN2B surface expression and function, which promotes CREB and ERK1/2 shut-off and synaptic dysfunction.

4 IN VIVO VALIDATION OF DAPK1 AS A NOVEL THERAPEUTIC TARGET IN YAC128 MICE[3]

4.1 INTRODUCTION

Huntington disease (HD) diagnosis occurs during mid-life at the time of motor symptom emergence [6]. Despite this, studies show that psychiatric and synaptic abnormalities are present years before clinical onset in premanifest mutation carriers, and that by the time of overt motor disturbances, there is significant irreversible neuronal death in the striatum [12, 13, 17, 364]. Thus, it is critical that neuroprotective therapies be administered early in the disease time-course such that neuronal dysfunction can be corrected prior to cell death. Additionally, strategies aimed at restoring the proper function of surviving neurons at later disease stages may still offer additional benefit by delaying disease progression.

Enhanced exGluN2B surface expression and downstream shut-off of the nuclear pro-survival transcription factor CREB occur early in YAC128 HD mice [80, 81, 206]. Previously, we showed that DAPK1 activity is disturbed in YAC128 mice and that this is correlated with enhanced phosphorylation of exGluN2B at S1303 (Chapter 3). Importantly, these changes occurred at 1 month of age, prior to any behavioral or neuropathological phenotypes. Small molecule inhibition of DAPK1 restored GluN2B S1303 phosphorylation levels and normalized elevated GluN2B surface expression in YAC128 neurons. Inhibition also completely reversed spine instability in YAC128 MSNs in vitro, thus identifying DAPK1 as a potential novel neuroprotective target for HD. However, this requires in vivo validation to provide rationale for further development of DAPK1-targeted therapies.

---

[3] This chapter is in preparation to be combined with Chapter 3 and submitted for publication as one manuscript: Schmidt ME, Caron NS, Dal Cengio L, Ko Y, Lazic N, Anderson L, Raymond LA, Hayden MR. Death-associated protein kinase 1 promotes extrasynaptic GluN2B phosphorylation and striatal spine loss in Huntington disease.

Antisense oligonucleotides (ASOs) are synthetic, single-stranded, 8-50 nucleotide-long DNA molecules which bind to complementary mRNA, triggering ribonuclease H (RNase H) binding and consequent mRNA degradation, thus lowering target gene expression [371, 372]. Chemical modifications are regularly incorporated into the ASO backbone and sugar moieties to improve potency, tolerability, and pharmacokinetics [373]. For instance, replacement of the phosphate backbone with a phosphorothioate modification increases stability and distribution of the ASO by enhancing nuclease resistance and improving protein binding, while alterations to the sugar groups can also improve potency, stability, and toxicity profiles [373]. Furthermore, replacement of DNA nucleotides with constrained RNA analogs maintains the oligonucleotide in an ideal conformation for binding complementary sequences, thus improving affinity [373]. However, this locked nucleic acid (LNA) modification also confers resistance to RNase H cleavage [373]. To combat this problem, ASOs may be designed as “gapmers” to contain LNA wings flanking a central DNA gap which is still able to induce RNase H activity when bound to a target mRNA.

The use of an ASO-based approach to validate DAPK1 as an HD therapeutic target in vivo is advantageous in several ways over other RNA silencing methods or treatment with an inhibitor: (1) ASOs target unspliced pre-mRNA in addition to mRNA; thus, introns can be targeted, offering additional options for sequence design; (2) Although not permeable to the blood-brain barrier, ASOs are freely taken up by cells by endocytosis and therefore can be delivered directly to the brain ventricles in rodents or via the spinal fluid in humans without the need for a viral delivery vector [373–375]; (3) Due to the non-viral delivery method, the treatment dose and duration can be more tightly controlled or halted if adverse effects occur; (4) There is precedent in humans for tolerability and efficacy of ASOs for the treatment of genetic disorders of the nervous system [371]; and (5) Currently available small-molecule inhibitors may have as-of-yet undiscovered off-target protein binding partners which could contribute to treatment outcomes and compromise the validity of study conclusions.

Here, we have developed an ASO-based strategy to validate the potential neuroprotective efficacy of targeting DAPK1 in HD mice. Specifically, we evaluated the effect of in vivo DAPK1 lowering on extrasynaptic GluN2B phosphorylation, nuclear CREB activation, motor function, and dendritic spine density in YAC128 mice.

4.2 MATERIALS AND METHODS

4.2.1 Mice

Wild type (WT) and heterozygous YAC128 (line 53) mice were maintained on the FVB/N background and experiments were performed according to protocols approved by the University of British Columbia Animal Care Committee (Protocol numbers A16-0130 and A16-0206). For all cohorts, approximately equal numbers of male and female mice were used. All animals were sacrificed using CO_2.

4.2.2 Primary neuronal cultures

WT FVB E16.5 timed-pregnancy embryos were removed from anesthetized mothers and brains were extracted. Cortical and striatal tissues were kept together for dissections and culture setups because we found that this increased health of the resulting neurons compared to culturing cortical neurons alone. We estimate that the cortical:striatal ratio in these cultures was approximately 3:1 to 4:1. Tissue was dissected in ice-cold Hank's Balanced Salt Solution, gently dissociated with a P1000 pipette, and incubated in 0.05% trypsin-EDTA (Gibco) at 37°C for 8 minutes. Cells were further dissociated with a short DNase treatment (0.08mg/mL) followed by resuspension in complete neurobasal medium (NBM supplemented with B27, penicillin-streptomycin, and L-glutamine; Gibco). Neurons were seeded in 6-well plates previously coated with sterile-filtered 50µg/mL poly-D-lysine hydrobromide (Sigma; P7886) at a density of 1 million cells per well. Cultures were fed with fresh complete NBM (25% well volume) every 6-7 days.

4.2.3 Antisense oligonucleotide design and primary screen

Phosphorothioate-based antisense LNA gapmers (Exiqon) targeting the mouse *Dapk1* mRNA were designed using the online RNAxs siRNA design tool (http://rna.tbi.univie.ac.at/cgi-bin/RNAxs/RNAxs.cgi) as a guideline to prioritize target sequences based on mRNA accessibility. Five top hits were selected to minimize off-target complementarity and were converted to 17-mer antisense sequences. A primary screen was conducted by treating DIV7 corticostriatal FVB/N cultures directly in the culture media with 0, 100, or 1000nM of each ASO diluted in complete NBM. Cells were harvested at DIV14, lysed in a stringent buffer, and run by SDS-PAGE and Western blotting as described below for total DAPK1 protein expression levels.

4.2.4 In vivo ASO treatments

Mice (13 weeks old) were anesthetized using 3% isoflurane and secured on a stereotaxic frame. Mice were given pre-operative subcutaneous buprenorphine (0.1mg/kg) and 0.25% bupivacaine at the site of incision. A midline incision was made in the scalp to expose the skull. Then, a 50µL Hamilton syringe with a 26-gauge needle was oriented to the bregma and moved 0.3mm anterior, 1mm lateral, and 3mm ventral. An injection volume of 10µL was delivered into the lateral ventricle at a rate of 5µL/minute. The needle was left in place for 2 minutes after injection, before being slowly retracted. The scalp was closed with sutures and Vetbond tissue adhesive. Animals were then placed in a recovery cage with a heating pad, hydrogel, and food on the cage floor. Mice were given post-operative buprenorphine as needed and monitored for 72 hours.

4.2.5 Total lysis, subcellular fractionation, SDS-PAGE, and Western blotting

Total lysates from cortical tissue or neuronal culture cell pellets were prepared by lysing in stringent buffer (20mM HEPES pH 7.4, 150mM NaCl, 40mM β-

Glycerophosphate, 10mM NaF, 1% Triton-X, 1% SDS, 0.5% sodium deoxycholate) with additional protease and phosphatase inhibitors freshly added (1X Roche Complete Protease Inhibitor, 5μM zVAD, 1μg/mL Pepstatin A, 1mM sodium orthovanadate). Protein samples were sonicated, centrifuged to remove cellular debris, and quantified by DC assay. Equal amounts of protein from each sample were run by SDS-PAGE on 8% or 10% acrylamide gels and transferred to 0.45μm nitrocellulose membranes. Membranes were blocked in 5% skim milk powder in TBST (0.1% Tween-20) for 1 hour at room temperature (RT), blotted in primary antibody in 3% BSA/TBST for 2 hours at RT, washed 4x in TBST, incubated with fluorescent secondary antibody for 1 hour at RT, washed, and scanned using the LI-COR blot imaging system. Band intensities were quantified using Image Studio Lite.

Subcellular fractionations from cortical tissue were performed as previously described to isolate synaptic (post-synaptic density, PSD) and extrasynaptic (non-PSD) membrane fractions, as well as nuclear extracts (method validated in **Fig. 3.1**) [80]. Fractions were quantified and subjected to SDS-PAGE and Western blotting as described above. Antibodies and conditions used for Western blotting are listed in the following table:

Target	Host	Company	Catalogue #	Dilution
B-actin	Rabbit	Cell Signaling	4967	1:2000
CREB	Rabbit	Cell Signaling	9197	1:1000
CREB-pS133	Rabbit	Millipore	06-519	1:2000
DAPK1	Rabbit	Sigma	D1319	1:2000
DAPK1-pS308	Mouse	Sigma	D4941	1:400
GluN2B	Mouse	Invitrogen	MA1-2014	1:1000
GluN2B-pS1303	Rabbit	Millipore	07-398	1:1000
TBP	Mouse	Abcam	61411	1:1000

4.2.6 RNA extraction, cDNA synthesis, and qPCR

To assess gene expression, a small piece of anterior cortical tissue was cut and RNA was extracted using the Qiagen RNeasy Mini Kit (Cat# 74106) and RNase-free DNase set (Cat# 79254). cDNA was synthesized with the Superscript III First-Strand system according to manufacturer instructions (Life Technologies Cat# 18080-051). Quantitative RT-PCR reactions were prepared in MicroAmp Fast optical 96-well reaction plates (Applied Biosystems Cat# 4346907) with Power SYBR™ Green PCR Master Mix (Thermo Fisher Cat# 4368706), and run on the Applied Biosystems 7500 Fast Real-Time system. *Dapk1* and *GFAP* expression were quantified based on ΔΔCt values using the housekeeping gene *Rpl13a. Dapk1* primer sequences: 5'- GTCCGCTACCTCTGTTTGATG-3' and 5'-GTGTCCTTCCGCAGTCTTG-3'. *Rpl13a* primer sequences: 5'-GGAGGAGAAACGGAAGGAAAAG-3' and 5'-CCGTAACCTCAAGATCTGCTTCTT-3'. *GFAP* primer sequences: 5'-GAAAACCGCATCACCATTCC-3' and 5'-CTTAATGACCTCACCATCCCG-3'.

4.2.7 Behavior testing

To evaluate climbing behavior, mice were familiarized with the climbing apparatus (an inverted mesh pencil holder) by allowing them to explore the apparatus for 5 minutes at the age of 2 and 3 months. At 4 months of age, after a 3-week treatment period, mice were once again placed in the climbing apparatus and filmed for 5 minutes. Videos were manually scored to determine latency to begin climbing, number of climbing events, total time spent climbing, and number of rearing events. A climbing event was defined as all four paws off the ground, while a rearing event was classified as only the two front paws off the ground (with the exception of grooming behavior).

Motor learning and function were also assessed using the rotarod test. Mice were trained on a fixed-speed (18 rpm) rotarod for three two-minute trials per day (spaced 1 hour apart) for 3 consecutive days. On the 4th day, mice were subjected to an accelerating (5-40 rpm) rotarod for three five-minute tests,

spaced 1 hour apart. Mice were manually scored to determine the number of falls and the initial latency to fall.

For all behavior tests and analysis, the researcher was blind to genotypes and treatment conditions.

4.2.8 Golgi-Cox staining

3 weeks post-injection, PBS- or ASO-treated mice (approximately 12 months of age) were anesthetized with avertin, perfused with 2% paraformaldehyde/2% glutaraldehyde/PBS, and post-fixed in fixative overnight at 4°C. Brains were washed in PBS, incubated in Golgi-Cox solution (1% potassium dichromate, 1% mercuric chloride, 0.8% potassium chromate) for 5 days, and transferred to 30% sucrose/PBS. 100µm sections were cut on a vibratome and mounted on slides, which were dried overnight, washed in ddH_2O, incubated in 20% ammonium hydroxide for 10 minutes, washed in ddH_2O, passed through ascending grades of alcohol, and placed in xylene for 5 minutes. Coverslips were mounted on top of sections with Cytoseal mounting medium (Thermo Scientific). Transmitted light images were acquired with a Leica TCS SP8 confocal laser scanning microscope and a 63X objective lens. Images were imported into NeuronStudio and spines on dendritic segments from 12-15 neurons across multiple sections per animal were semi-automatically analysed.

4.2.9 Data analysis

GraphPad Prism 5 was used for all statistical analysis and graph preparation. Figures were generated in Adobe Photoshop CS5. All data are presented as mean ± SEM. In some cases, t-tests were performed between specific groups after an ANOVA test when a planned comparison was established during the experimental design process. Significance for these tests is noted with the “#” symbol instead of “*”.

4.3 RESULTS

4.3.1 Antisense oligonucleotides potently silence DAPK1 expression

To validate DAPK1 as a novel therapeutic target for synaptic protection in YAC128 mice, we developed a panel of LNA gapmer ASOs targeting the mouse *Dapk1* mRNA. Five ASOs targeting different regions of the *Dapk1* transcript were screened in FVB corticostriatal primary neurons by treating once at DIV7. Analysis of total cell lysates at DIV14 shows potent lowering of DAPK1 protein levels (to 10-20% of untreated) with both ASO3 and 5 at high doses (**Fig. 4.1**). ASO1 and 4 demonstrated less dramatic DAPK1 lowering to 39% and 65% of untreated, respectively (**Fig. 4.1**). Neurons treated with ASO2 exhibited high levels of cell death and therefore were not processed.

ASO3 and 5 were selected to test for in vivo target engagement in YAC128 mice. Mice were treated via intracerebroventricular (ICV) injection with PBS vehicle control or varying doses of either ASO3 or ASO5, and sacrificed 3 weeks post-injection for assessment of DAPK1 protein and mRNA levels in the brain. These doses and timepoints were chosen based on initial pilot studies (data not shown). Both ASOs demonstrated dose-dependent lowering of cortical *Dapk1* mRNA levels, with the high dose of ASO3 achieving the greatest level of knockdown (57% of control) (**Fig. 4.2A**). This was associated with a reduction in the protein level to 48% of control in the cortex and 71% of control in the striatum (**Fig. 4.2B, C**). Although ASO5 also significantly reduced DAPK1 levels at the tested doses (**Fig. 4.2A-C**), all treated mice lost significant body weight over the course of treatment and most reached a humane endpoint prior to the end of the 3-week period. Toxicity of ASO5 was confirmed by an increase in cortical glial fibrillary acidic protein (*GFAP)* mRNA expression in these mice (**Fig. 4.2D**), signifying poor tolerability and/or unintended off-target effects of this molecule. For this reason, ASO3 at a dose of 75µg per mouse was used for subsequent experimental cohorts, and is referred to hereafter as “ASO”.

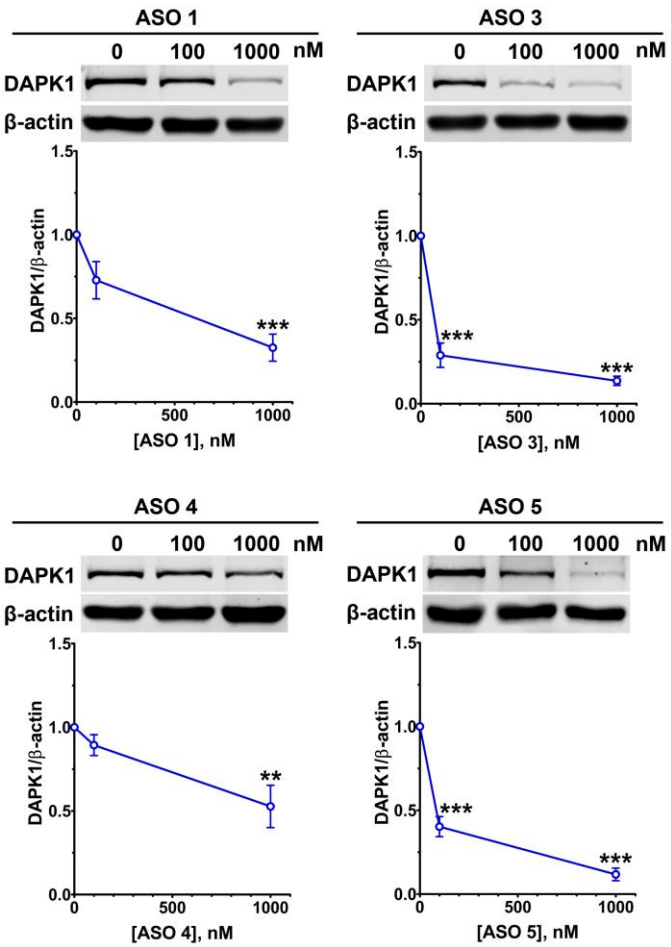

Figure 4.1: Antisense oligonucleotides potently lower DAPK1 protein levels in cultured primary neurons. FVB corticostriatal neuronal cultures were treated at DIV7 directly in the culture media, harvested at DIV14, lysed in a stringent lysis buffer, and run by SDS-PAGE and Western blotting to quantify total DAPK1 protein levels normalized to β-actin. ASO1 and 4 produced moderate DAPK1 lowering, while ASO3 and 5 were most potent. Data are normalized to 0 nM treatment conditions (n=4 independent cultures; 1-way ANOVA with Bonferroni post-hoc analysis; **p<0.01. ***p<0.001 compared to 0 nM).

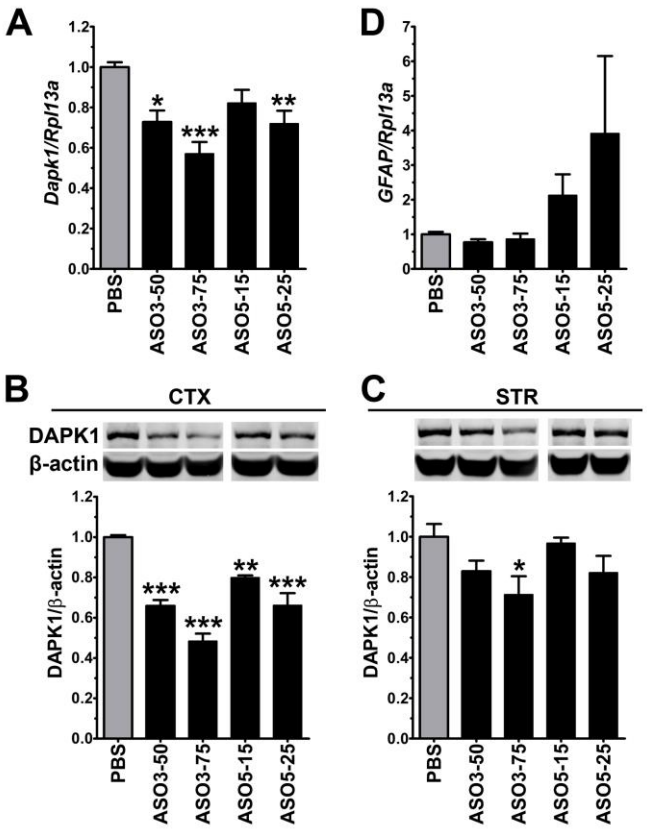

Figure 4.2: A single 75µg ICV dose of ASO3 is well-tolerated and significantly lowers DAPK1 levels at 3 weeks post-injection in YAC128 brains. 4-month-old YAC128 mice were injected ICV with PBS or various doses of ASO3 and 5 (ASO3-50µg, ASO3-75µg, ASO5-15µg, or ASO5-25µg) and sacrificed after 3 weeks to assess protein and gene expression levels. Both ASO3 and 5 successfully lowered **(A)** *Dapk1* mRNA expression and **(B)** total lysate DAPK1 protein levels in the cortex (CTX). **(C)** Only the high dose of ASO3 significantly reduced DAPK1 protein in the striatum (STR). **(D)** ASO5 produced undesirable side effects and a trend to increased cortical *GFAP* expression levels (n=4 mice per group; 1-way ANOVA with Dunnett post-hoc analysis; *p<0.05, **p<0.01, ***p<0.001 compared to PBS control). All Western blot samples within each panel were processed together and blot images were clipped from a single image file with identical brightness and contrast adjustments.

4.3.2 Short-term DAPK1 lowering normalizes cortical CREB expression and activation through a GluN2B pS1303-independent mechanism

We first sought to assess the impact of DAPK1 lowering on biochemical readouts of synaptic function and neuroprotection. To do so, we treated WT and YAC128 mice with PBS or ASO at 3 months and 1 week of age. After a 3-week treatment, mice were sacrificed and tissues were processed for biochemistry. This

experimental paradigm was selected because it allowed us to utilize the same cohort for both biochemistry and behavior testing at 4 months of age, one of the earliest timepoints that a reliable YAC128 motor phenotype exists [51, 376, 377].

Although not statistically significant, DAPK1 protein levels were greater in PBS-treated YAC128 total cortical lysates compared to WT (118% of WT PBS-treated) (**Fig. 4.3B, C**). With ASO treatment, we observed a significant reduction in YAC128 DAPK1 at the mRNA and protein level to 79% and 89% of WT PBS controls, respectively (**Fig. 4.3A, C**). Interestingly, we observed less knockdown in WT animals, causing both genotypes to have nearly identical DAPK1 mRNA and protein levels after treatment (**Fig. 4.3A, C**). Three out of 20 ASO-treated mice (15%; one WT and two YAC128 animals) did not exhibit appreciable DAPK1 lowering (ie. DAPK1 protein levels were ≥1.0 when normalized to the mean of the WT PBS group) due to unknown reasons. These data points are included in **Figure 4.3** to demonstrate overall efficacy of DAPK1 knockdown with this ASO. However, to specifically evaluate the impact of DAPK1 lowering on other readouts, only animals that responded to treatment were included; thus, the three aforementioned mice were excluded from subsequent biochemistry and behavior analysis. It is possible that lowering of DAPK1 protein levels induces activation of remaining DAPK1 as a homeostatic mechanism. Therefore, cortical pS308 levels were also assessed. We observed the expected reduction in pS308 levels in YAC128 PBS-treated animals compared to WT, indicating greater activation (**Fig. 4.3D**). Interestingly, there was a significant increase in YAC128 pS308 with ASO treatment (**Fig. 4.3D**). Of note, when pS308 levels were normalized to β-actin instead of DAPK1, there were no differences between groups (**Fig. 4.3E**), implying that there may be a stable pool of phosphorylated, inactive DAPK1 which is unaffected by mHTT or DAPK1 lowering.

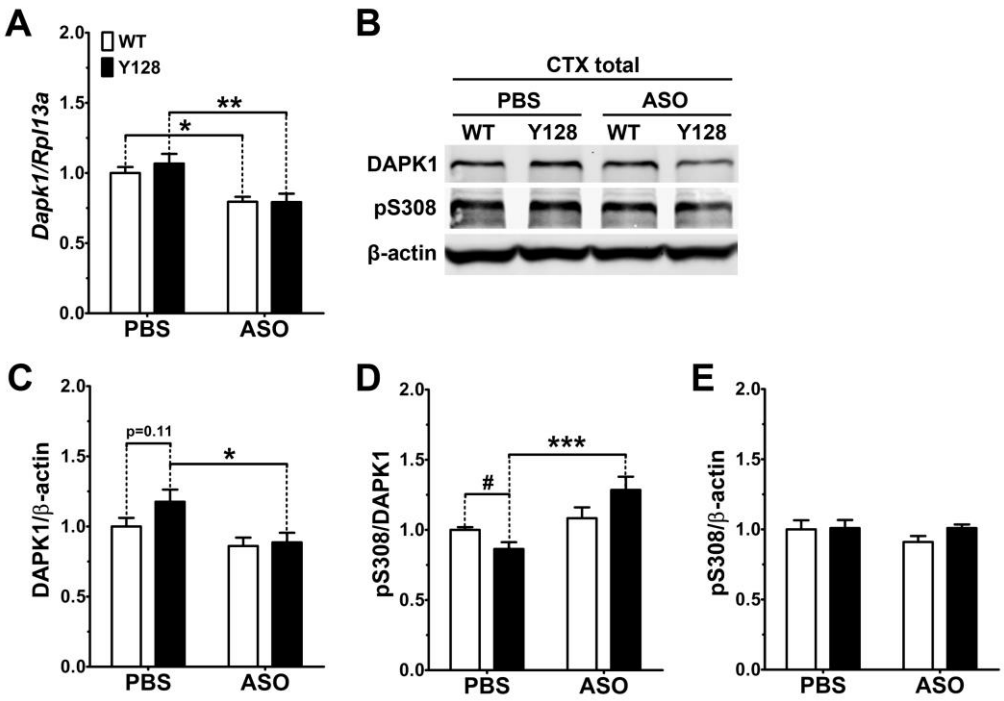

Figure 4.3: Cortical DAPK1 levels in 4-month-old WT and YAC128 mice are decreased with ASO treatment. WT and YAC128 littermates were injected ICV with PBS or ASO at 3 months and 1 week of age, followed by tissue collection for mRNA and protein analysis after 3 weeks. **(A)** A significant reduction in cortical (CTX) *Dapk1* mRNA was observed in both genotypes. **(B,C)** Total cortical DAPK1 protein levels were decreased to a similar degree. **(D,E)** pS308 was elevated following ASO treatment in YAC128 mice when normalized to DAPK1 protein level, but remained consistent compared to the β-actin loading control (n=10 biological replicates, 2 technical replicates each; 2-way ANOVA with Bonferroni post-hoc analysis, *p<0.05, **p<0.01, ***p<0.001; student's t-test, #p<0.05).

YAC128 mice undergo loss of striatal nuclear activity of the pro-survival transcription factor CREB by 1 month of age, which persists at 4 months and is indicated by reduced phosphorylation at S133 normalized to CREB protein level [80, 206]. CREB activation is a key contributor to neuronal protection and synaptic plasticity [378]. We observed a small but significant reduction in the cortical nuclear pS133/CREB ratio in PBS-treated YAC128 mice compared to WT littermates by t-test (**Fig. 4.4A, B**). Interestingly, this was associated with a large increase in the levels of nuclear CREB itself (**Fig. 4.4A, C**), suggesting that upregulated expression of nuclear CREB may occur as a compensatory mechanism to offset impaired activity. DAPK1 knockdown with ASO treatment

increased the pS133/CREB ratio to greater than that of WT PBS animals and almost completely normalized nuclear CREB levels (**Fig. 4.4B, C, D**), indicating a restored balance in nuclear CREB signaling.

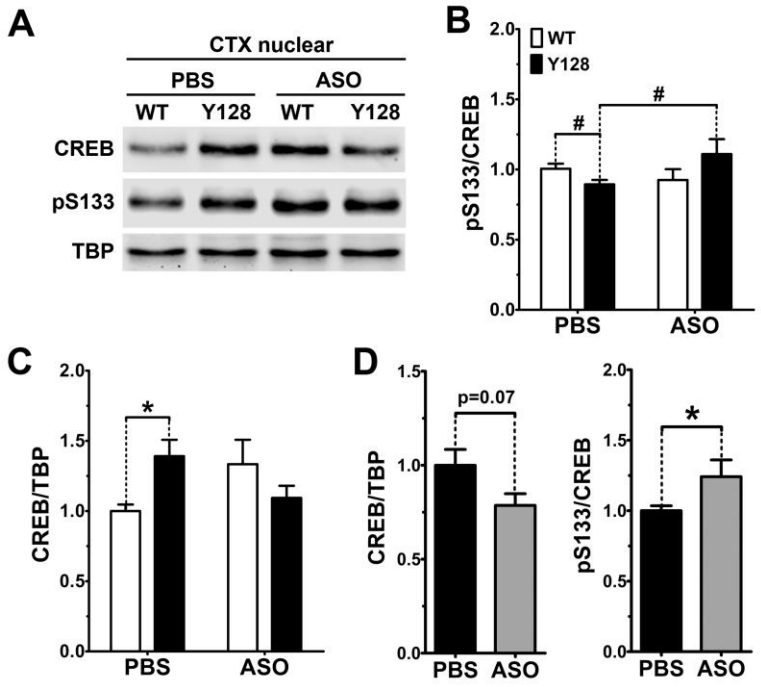

Figure 4.4: DAPK1 lowering normalizes cortical nuclear CREB expression and S133 phosphorylation in YAC128 mice. Cortical nuclear fractions were isolated from PBS- or ASO-treated 4-month-old WT and YAC128 mice. Samples were subjected to SDS-PAGE and Western blotting for CREB protein levels and phosphorylation at S133. **(A,B)** The nuclear ratio of pS133/CREB is normalized in YAC128 mice with DAPK1 lowering (ns by 2-way ANOVA Bonferroni post-hoc analysis; student's t-test #p<0.05). **(A,C)** Elevated YAC128 nuclear CREB levels (normalized to TBP, TATA-binding protein) are largely rescued with DAPK1 lowering. **(D)** Data from B and C were re-normalized and plotted for YAC128 PBS and ASO conditions only (n=10 biological replicates, 2 technical replicates each; 2-way ANOVA Bonferroni post-hoc analysis, *p<0.05).

We further assessed the effect of DAPK1 knockdown on exGluN2B pS1303. Previously, cortical non-PSD pS1303 levels were increased in 1-month YAC128 brains and a DAPK1 inhibitor normalized non-synaptic GluN2B and pS1303 levels in corticostriatal neuronal cultures (Chapter 3). Unexpectedly, we no longer observed a basal genotypic difference in extrasynaptic pS1303 levels at 4 months of age and there was no effect of the DAPK1 ASO on this measure

(**Fig. 4.5**). Although it has been previously shown that increased exGluN2B activity promotes CREB shut-off in YAC128 mice [80, 81], this result indicates that the effect of DAPK1 lowering on CREB phosphorylation is mediated through a mechanism not involving the phosphorylation level of exGluN2B at pS1303, at least using this experimental paradigm and mice of this particular age.

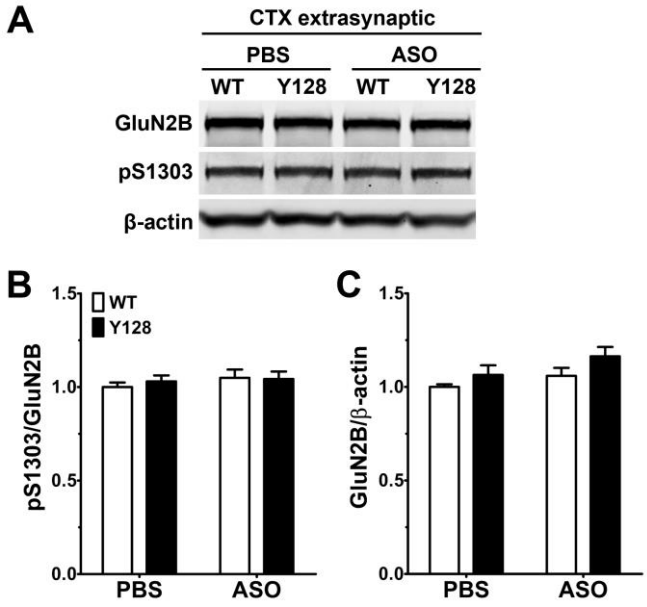

Figure 4.5: DAPK1 lowering does not alter cortical extrasynaptic GluN2B expression or S1303 phosphorylation. Cortical non-PSD fractions were isolated from PBS- or ASO-treated 4-month-old WT and YAC128 mice. Samples were subjected to SDS-PAGE and Western blotting for GluN2B protein levels and phosphorylation at S1303. Neither **(A,B)** pS1303, nor **(A,C)** GluN2B levels were altered between genotypes or with ASO treatment (n=8 biological replicates, 2 technical replicates each; 2-way ANOVA Bonferroni post-hoc analysis).

4.3.3 Short-term DAPK1 lowering does not improve YAC128 motor dysfunction

Next, we evaluated whether DAPK1 lowering could result in improved motor function in YAC128 mice. At 4 months of age, YAC128 mice display impaired motor learning and motor function compared to WT littermates assessed by rotarod and climbing tests [51, 376, 377]. Previous exposure to the climbing apparatus (**Fig. 4.6A**) improves the likelihood of observing a basal YAC128

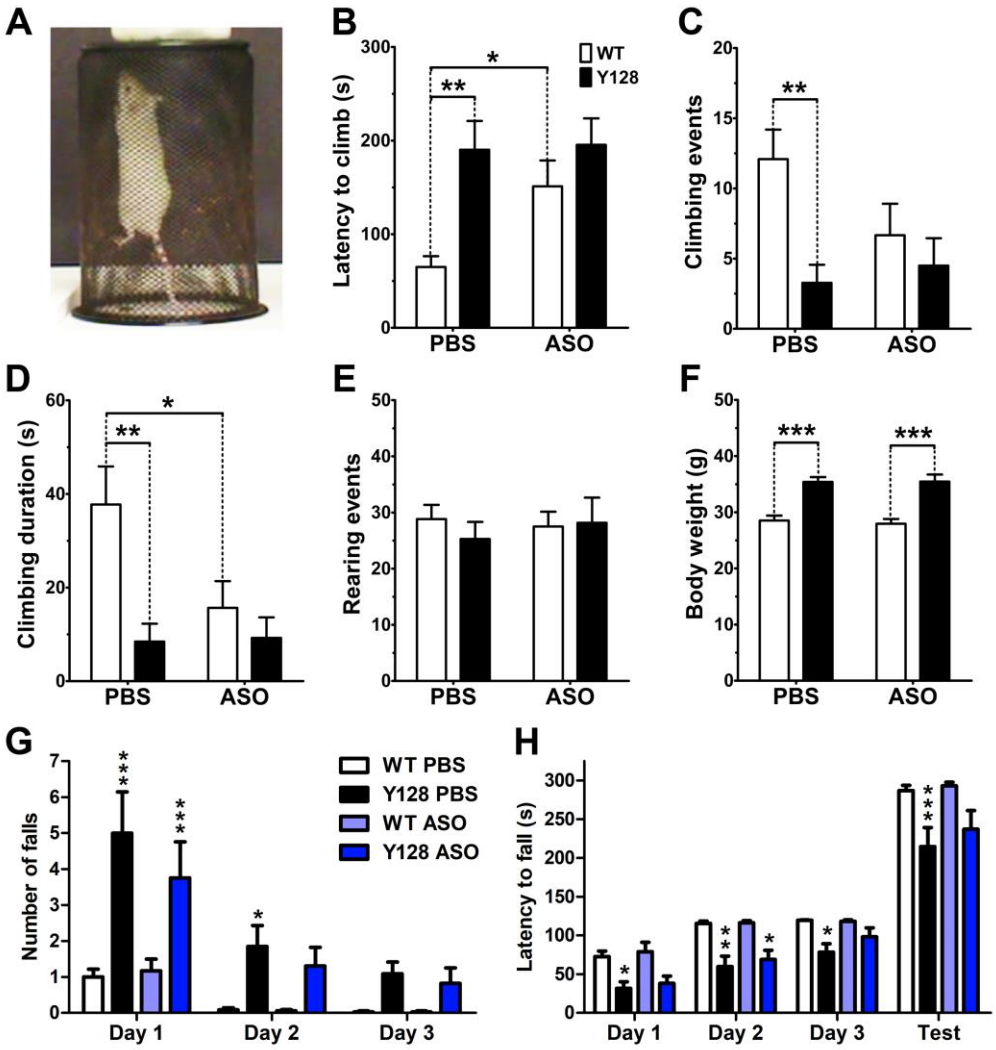

Figure 4.6: DAPK1 lowering does not improve motor performance in YAC128 mice. 4-month WT and YAC128 mice injected with PBS or ASO were subjected to motor testing 3 weeks post-treatment. **(A)** Climbing was evaluated over a 5-minute period using an inverted mesh pencil holder. DAPK1 lowering did not improve YAC128 **(B)** latency to climb, **(C)** number of climbing events, or **(D)** total time spent climbing, while WT mice demonstrated worsening of these measures. **(E)** The number of rearing events was unaltered between genotypes or treatment conditions. **(F)** Body weight was significantly higher in YAC128 animals and was not affected by DAPK1 lowering. Mice were also subjected to three days of fixed-speed rotarod training followed by a test day on an accelerating rotarod. **(G)** DAPK1 lowering in YAC128 mice did not improve elevated number of falls during training compared to WT littermates, and had no effect in WT mice. **(H)** Similarly, YAC128 decreased latency to fall during both training and testing was unaffected by DAPK1 lowering (n=10-12 mice per group; 2-way ANOVA with Bonferroni post-hoc analysis, *p<0.05, **p<0.01, ***p<0.001; in panel G and H, post-hoc comparisons are only depicted for WT PBS versus YAC128 PBS or WT ASO versus YAC128 ASO).

deficit compared to WT mice. Therefore, the cohort was subjected to 5 minutes of climbing at both 2 months and 3 months of age. Mice were then treated with either PBS or ASO one week later so that they could be behavior tested at the age of 4 months after a 3-week treatment. As expected, we observed a significant increase in latency to climb in PBS-treated YAC128 mice compared to WT at 4 months, as well as dramatically reduced climbing events and total climbing duration (**Fig. 4.6B-D**). The number of rearing events was not altered, indicating these differences were not due to a lack of interest in exploring the climbing apparatus (**Fig. 4.6E**). However, YAC128 mice were significantly heavier than WT (**Fig. 4.6F**), which could have an unintended impact on climbing ability. We found no effect of DAPK1 lowering on YAC128 body weight or climbing scores (**Fig. 4.6B-F**). Unexpectedly, ASO treatment impaired the performance of WT mice on the climbing test (**Fig. 4.6B-D).**

To assess the effect of DAPK1 lowering on motor learning, mice were trained every day for 3 days on a fixed-speed rotarod, followed by a test day on an accelerating rotarod (motor function). YAC128 PBS-treated mice consistently exhibited increased numbers of falls during training compared to WT PBS mice, as well as reduced latency to fall during both training and testing (**Fig. 4.6G, H**). DAPK1 lowering had no effect on these motor readouts in either genotype.

4.3.4 Short-term DAPK1 lowering partially rescues in vivo age-associated YAC128 striatal and cortical spine loss

Results from Section 3.3.5 demonstrated that small molecule inhibition of DAPK1 completely rescues MSN spine loss in YAC128 CS co-cultures, a feature that recapitulates age-associated in vivo spine loss in YAC128 mice. Furthermore, genetic deletion of the DAPK1 kinase domain is protective against spine loss in models of ischemia and AD [247, 310]. We sought to assess whether acute antisense DAPK1 lowering could reverse YAC128 spine loss in vivo by treating approximately 11-month-old mice with PBS or ASO, followed by Golgi-Cox staining 3 weeks later. We observed the expected reduction in total and

mushroom spine density in the striatum of YAC128 PBS mice compared to WT PBS (**Fig. 4.7A**). Treatment of YAC128 mice with the DAPK1 ASO resulted in a partial normalization of both measures, with a 39% recovery of total spine density and a 77% recovery of mushroom spine density (**Fig. 4.7A**). The effect of DAPK1 knockdown on spine density was even more apparent in the cortex. We observed a significant reduction in the density of all cortical spine types in YAC128 mice (**Fig. 4.7B**). DAPK1 knockdown provided partial rescue of total cortical spine numbers and complete normalization of cortical mushroom spines in YAC128 mice (**Fig. 4.7B**). No effect on immature spines was observed in either region.

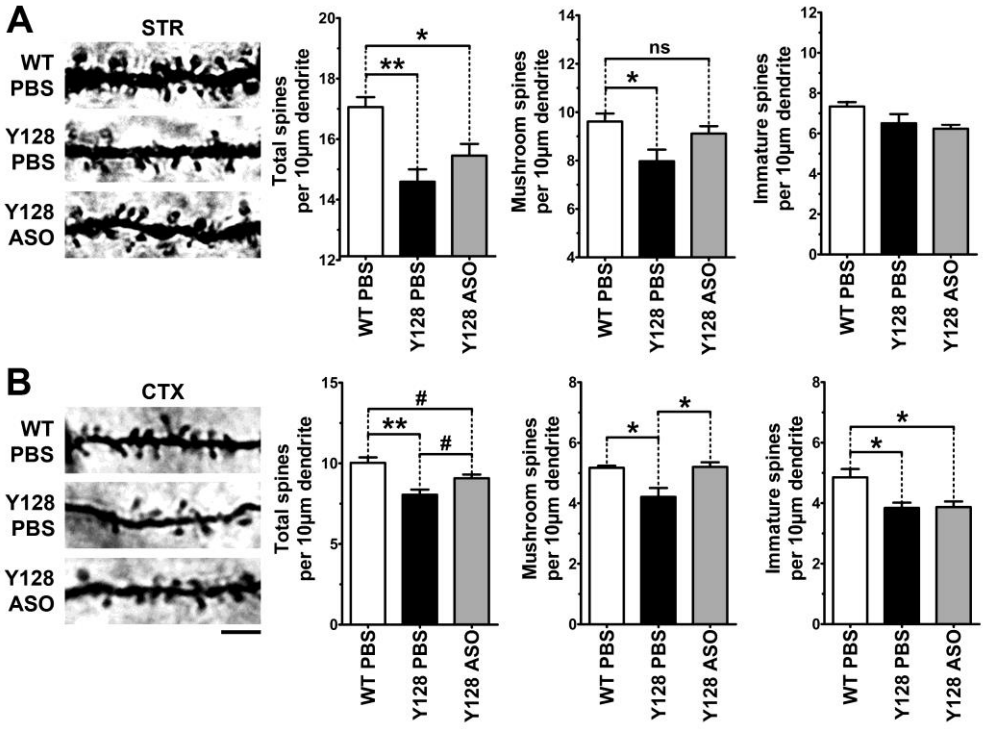

Figure 4.7: DAPK1 lowering partially rescues YAC128 spine loss in vivo. Mice were treated at approximately 11 months of age with PBS or DAPK1 ASO and perfused 3 weeks later. Brains were processed using a modified Golgi-Cox method and confocal microscopy to evaluate **(A)** striatal and **(B)** cortical spine density. Total spine density is partially rescued in both brain regions with treatment, specifically due to an increase in mushroom spine numbers. Immature spines were largely unaffected by DAPK1 lowering. Note adjusted y-axis scales in panel A to show effects more clearly (n=4-5 mice per group; 12-15 dendritic segments from individual cells analysed per animal; 1-way ANOVA with Bonferroni post-hoc analysis, *p<0.05, **p<0.01; student's t-test, #p<0.05, ##p<0.01). Scale bar = 5µm.

4.4 DISCUSSION

Development of an in vivo ASO-mediated DAPK1 knockdown approach

In the present work, we describe a novel ASO-based strategy to reduce DAPK1 activity in YAC128 HD mice. Despite treating with a relatively high dose (75 µg per mouse), we only achieved modest levels of mRNA and protein knockdown (**Fig. 4.3**). Our observation that DAPK1 protein was reduced to the same level in WT and YAC128 mice despite being higher in YAC128 mice to begin with suggests that there may be regulatory mechanisms keeping DAPK1 at a particular level despite ASO treatment. Alternatively, ASOs targeting different sequences may have improved potency and may be tolerated at even higher doses than our current molecule design.

We found that ICV-delivered ASO3 was tolerated in vivo, but ASO5 was not. Hepatotoxicity and significant weight loss have been described in mice administered with LNA-containing ASOs via intraperitoneal injection [379]. Although ASOs cannot cross the blood-brain barrier, they can be partially transferred from the cerebrospinal fluid to systemic circulation [380]. We did not assess hepatic function in our ASO5-treated group, but all mice exhibited extreme weight loss, requiring early termination of the cohort. Studies have shown that LNA-induced hepatotoxicity results from the binding of high-affinity gapmers to partially mismatched long pre-mRNA targets in the liver, and that gapmers containing TCC or TGC sequence motifs in any position within the molecule bind more strongly to cellular proteins and are significantly more likely to cause hepatotoxicity [379, 381–383]. Upon re-evaluation of our sequence designs, we discovered that ASO5 has two TCC motifs, while ASO3 contained neither TCC nor TGC, potentially explaining the differential tolerability observed.

For future optimization of DAPK1-targeted ASOs, a number of factors may be taken into consideration. TCC and TGC sequence motifs should be avoided [381]. Shortening the length of ASO molecules has been shown to either increase or decrease the risk of hepatotoxicity, meaning this parameter can be manipulated if toxicity is observed with a particular sequence [384, 385].

Alternate chemical modifications may also improve tolerability. Similar to LNAs, 2'-O-methoxyethylribose (MOE) modifications can be incorporated into the "wings" of a gapmer ASO to dramatically improve target binding affinity and pharmacokinetics. However, in a direct comparison with LNA gapmers in mice, MOE-based ASOs caused no hepatotoxicity [379]. Furthermore, a *HTT*-targeted MOE-containing ASO was successful in a recent phase 1b/2a HD clinical trial without adverse effects [59]. Recently, introduction of a 2'-O-methyl modification at gap position 2 within gapmer ASOs decreased protein binding and hepatotoxicity in mice [386]. Our results provide rationale for the design and screening of a more diverse panel of DAPK1-targeted ASOs.

Normalization of nuclear CREB activation in the YAC128 cortex after DAPK1 knockdown without changes to extrasynaptic GluN2B pS1303 or YAC128 motor dysfunction

We found that DAPK1 knockdown normalized nuclear CREB levels and rescued CREB S133 phosphorylation in YAC128 cortices (**Fig. 4.4**). Phosphorylation at S133 activates CREB, allowing it to bind to its nuclear coactivators and initiate pro-survival expression of neurotransmitter, growth factor, and signaling genes, including *BDNF, TRKB, IGF-1, and PGC-1α* [378, 387]. pS133 is decreased in various models of neurological disease and excitotoxicity, including HD, and therapies aimed at increasing its levels are neuroprotective [80, 81, 125, 378, 388]. Phosphorylation of CREB at S133 is essential for proper spine formation, spine remodeling, and LTP during learning and memory formation [378, 389–392]. Furthermore, overexpression of wild-type CREB induces pro-survival gene expression and neuroprotection in hippocampal cultures, while overexpression of a S133A mutant instead promotes neuronal death [393]. Therefore, an increase in relative pS133/CREB levels in ASO-treated YAC128 mice would be expected to be beneficial. Our observation of elevated basal nuclear CREB levels in YAC128 brains was unexpected. We hypothesize that increased nuclear CREB expression could occur as a compensatory mechanism to overcome deficient

pS133 phosphorylation, and that this upregulation may no longer be required when DAPK1 is knocked down due to rescue of pS133. CREB-binding protein (CBP) is a CREB co-activator which can be sequestered by nuclear mHTT and undergoes depletion in HD cell models [394, 395], meaning that even if nuclear CREB levels are high, its transcriptional activity may still be impaired. Though predominantly nuclear, CREB also localizes to the mitochondria [396]; thus, the basal increase in nuclear CREB in YAC128 brains could reflect altered localization as opposed to upregulated expression.

Enhanced exGluN2B signaling in YAC128 mice leads to CREB shut-off [80, 81]. Therefore, we initially hypothesized that re-balancing of nuclear CREB signaling with DAPK1 ASO treatment could be due to normalization of exGluN2B function via reduced pS1303. However, extrasynaptic pS1303 was not increased in YAC128 mice at 4 months of age, despite elevated levels observed at 1 month (**Fig. 4.5**). This suggests that some compensatory mechanism could be activated between these two time points leading to rescue of exGluN2B phosphorylation. This phenomenon has been described previously for striatal calpain activation, which occurs downstream of exNMDAR activity and promotes exGluN2B surface expression in 1.5-month YAC128 mice [175, 213, 397]. Calpain activation is increased in YAC128 mice compared to WT at 1.5 months of age, but not at 4 months, even though exGluN2B expression remains elevated [206], indicating multiple age-dependent mechanisms contributing to exGluN2B dysfunction. We also observed no effect of DAPK1 lowering on extrasynaptic pS1303 levels in either genotype (**Fig. 4.5**). It is possible that by 4 months of age, DAPK1 has been unlinked from exGluN2B signaling and therefore no longer influences phosphorylation at this site. Alternatively, another kinase may be able to compensate in its place. We did not observe altered CaMKII expression or autonomous phosphorylation with DAPK1 ASO treatment (data not shown), but this does not rule out regulation of S1303 phosphorylation by other kinases (such as PKC [159]) or phosphatases.

Our results indicate an exGluN2B pS1303-independent mechanism leading to CREB normalization with DAPK1 lowering. ERK can be sequestered in

the cytosol by DAPK1, which may prevent its activation and subsequent activity toward the CREB-kinase RSK (**Fig. 1.6**) [222, 286]. DAPK1 lowering may thus release ERK to indirectly promote CREB phosphorylation, but this remains to be investigated. Alternatively, although we did not observe effects of ASO lowering on CaMKII expression or autonomous activation, we did not assess its interaction with GluN2B or phosphorylation of its other downstream targets. Furthermore, there are additional regulatory post-translational modifications and cellular factors aside from pT286 that can influence CaMKII activity as well as dictate whether it promotes LTP or LTD processes [362, 398]. CaMKII has also been shown to mediate CREB S133 phosphorylation [399, 400]. Since DAPK1 overexpression inhibits synaptic CaMKII localization and interaction with GluN2B [246], it is possible that DAPK1 lowering influences CREB activity by enhancing GluN2B/CaMKII-mediated signaling.

It remains to be determined if DAPK1 lowering can restore GluN2B phosphorylation at an age when pS1303 is increased in YAC128 brains, which could potentially prevent synaptic dysfunction early in disease pathogenesis. The youngest age that an ICV treatment can be administered in mice is roughly 2 months of age, due to the coordinate requirements of the stereotaxic frame and the size of the mice prior to this age. Delivery of the DAPK1 inhibitor (DKI; TC-DAPK6) is another option which can be done at 1 month of age (via intravenous or intranasal administration), and is a promising method to evaluate the effect of blocking DAPK1 kinase activity, which could cause different outcomes than knockdown of the entire protein with all of its domains. TC-DAPK6 has been administered in rodents previously, although only one study has delivered the compound to the central nervous system and this was done via direct microinjection into the brain parenchyma [314]. Another strategy to test the efficacy of inhibiting DAPK1 kinase activity at earlier time points involves the use of a mouse model with a genetic deletion of the kinase domain, which has been utilized in other neurological disease models [247, 310], and could be crossed to the YAC128 line for analysis of extrasynaptic pS1303 at 1 month of age.

We did not observe improved motor performance in YAC128 mice treated with the DAPK1 ASO, despite normalization of nuclear CREB signaling (**Fig. 4.6**). It is likely that an intervention longer than three weeks may be necessary in order to see biochemical changes reflected in behavioral outcomes.

Impairment of WT motor performance with DAPK1 ASO treatment

Unexpectedly, we observed impaired climbing activity in WT, but not YAC128 mice with DAPK1 knockdown (**Fig. 4.6**). This could potentially indicate subtle toxicity of ASO3, which has been reported previously for LNA molecules in vivo, as described above, although we observed no overt signs of illness or *GFAP* induction in these mice after recovery from surgery. The ASO could also be binding to an unintended mRNA target in the brain due to the extremely high affinity of LNAs, resulting in dysfunction or toxicity. Although YAC128 mice are more susceptible to toxic insults [77] and might therefore be expected to demonstrate even more dramatic motor decline than WT animals if the ASO were toxic, it is possible that negative effects were masked by the already-present severe climbing phenotype in YAC128 mice. However, since we observed benefit of our ASO on YAC128 nuclear CREB activation and spine density, we hypothesize that a more plausible explanation is that disturbing an unperturbed system (ie. acutely lowering DAPK1 in a normal adult mouse brain) may offset the synaptic/extrasynaptic cell signaling balance in the opposite direction, which could be equally detrimental to motor learning and synaptic function. To address these possibilities, multiple optimized DAPK1-targeted ASOs with more well-tolerated chemical modifications will need to be tested.

Partial rescue of YAC128 striatal and cortical dendritic spine loss after short-term DAPK1 lowering

DAPK1 lowering for 3 weeks partially rescued total and mature dendritic spine loss in both the striatum and cortex of YAC128 mice (**Fig. 4.7**). Age-associated

spine loss occurs in multiple mouse models of HD as well as human HD patients and is hypothesized to be a consequence of synaptic dysfunction and cortico-striatal disconnect [73, 74, 82, 83, 88, 89, 92, 93]. Striatal MSNs and cortical pyramidal neurons undergo dendritic spine loss in symptomatic R6/1 and R6/2 HD fragment model mice [85, 88, 91]. Additionally, striatal MSN spines are lost in transgenic BACHD and mHTT knock-in mice [92, 93], as well as in 12-month YAC128 mice [74], which we have confirmed here and independently in Chapter 2. There is clear evidence of cortical neuron dysfunction in HD [338], and morphological Golgi assessment of HD postmortem cortical samples revealed a proportion of pyramidal neurons with degenerative changes to dendrites and spines, as well as an upregulation of dendritic complexity in remaining neurons, hypothesized to be a compensatory response [401]. However, to our knowledge, this is the first report demonstrating cortical spine loss in a full-length transgenic HD mouse model. Interestingly, we observed more efficient spine rescue in the cortex compared to the striatum, with complete normalization of mature mushroom spine numbers. This correlates with the higher level of DAPK1 knockdown that we obtained in this brain region. Our results highlight the dynamic nature of spine loss in HD, and support the hypothesis that late intervention therapies may be effective at reversing HD spine pathogenesis after it has already emerged, as has been suggested by previous reports in the YAC128 model [74, 402]. It will be critical to determine if these structural improvements translate to a rescue in functional CS synaptic transmission. Given our biochemical results and the involvement of CREB in promoting neuroprotection and spine stability, it is possible that rescuing nuclear pCREB with DAPK1 lowering is a contributing factor to the spine rescue we observed. Further investigation into this potential therapeutic mechanism is warranted.

Conclusions

Although there were no overt benefits of short-term DAPK1 lowering on YAC128 motor function, sensitive measures of spine structure demonstrated significant

rescue of cortical and striatal spine loss, which could plausibly occur via restoration of nuclear CREB signaling. These findings support DAPK1 as a novel therapeutic target for HD and warrant the testing of a longer intervention strategy and/or a more potent DAPK1 ASO, as well as deeper investigation into the precise mechanisms underlying the contribution of DAPK1 to spine loss in HD.

5 DISCUSSION AND CONCLUSIONS

5.1 OVERVIEW OF MAJOR FINDINGS

The overall goal of this thesis was to determine the role of DAPK1 in exGluN2B dysfunction in HD and to validate DAPK1 as a potential therapeutic target for synaptic protection. ExNMDAR hyperactivity plays a critical role in early synaptic dysfunction and phenotype onset in HD mice, making it an ideal highly-upstream target for neuroprotection [80, 81, 206]. GluN2B forms a key component of the NMDAR signaling hub, interacting with over 70 cytosolic and membrane proteins to influence neuronal activity and function [403]. Furthermore, the subunit is subjected to many post-translational processes which may be exploited to modify its function [146]. Despite the complexity of GluN2B regulation, its highly unique relationship with DAPK1 provides the opportunity for an innovative therapeutic approach. As depicted in **Fig. 3.12**, the conclusions from this thesis support a model whereby exGluN2B and DAPK1 positively reinforce one another's activity under conditions of pathological stress. Reducing DAPK1 activity breaks this amplification process, leading to normalization of mHTT-induced exGluN2B function as well as restoration of its own activity level. In vitro and in vivo targeting of DAPK1 produce a striking rescue of YAC128 dendritic spine loss in affected brain regions, thus validating DAPK1 as an exciting novel pre-clinical therapeutic target for HD.

The first specific aim of this thesis was to optimize a CS co-culture system to reliably detect HD-like synaptic phenotypes in vitro, with the ultimate goal of generating a tool for therapeutic target validation. Results showed that the relative level of cortical input in this model plays a critical role in the emergence of YAC128 spine, dendrite, and neuronal survival phenotypes. This finding is significant because it provides an explanation for existing discrepancies in the HD literature, offers insight into potential mechanisms of synaptic dysfunction in HD, and also demonstrates how the co-culture system can be methodologically adapted to answer specific questions. A major potential application of this work is the integration of this system into neuroprotective drug discovery pipelines.

The second specific aim of this thesis was to determine if and how DAPK1 disrupts exGluN2B function and synaptic integrity in HD. The major findings indicated that DAPK1 is dysregulated in the presence of mHTT, and that this contributes to enhanced S1303 phosphorylation and surface expression of exGluN2B. Excitingly, a small molecule inhibitor of DAPK1 completely reversed YAC128 MSN dendritic spine loss in the co-culture screening system described above, providing strong evidence for therapeutic potential of this compound or other DAPK1-targeting strategies in HD.

The third specific aim of this thesis was to validate DAPK1 as a novel HD therapeutic target in vivo using an antisense silencing approach. Results from this study showed that although DAPK1 knockdown did not improve behavioral outcomes in YAC128 mice, it did normalize cortical nuclear CREB activation and partially rescued in vivo age-associated dendritic spine loss in the cortex and striatum. These changes were independent of exGluN2B S1303 phosphorylation, implicating additional as-of-yet undetermined mechanisms of neuroprotection. Additional validation and further development of DAPK1-targeted therapies for neurodegeneration, including long-term treatment with a DAPK1 inhibitor, are now warranted.

5.2 FUTURE DIRECTIONS

5.2.1 Further development of in vitro modeling of HD CS synaptic dysfunction

5.2.1.1 Does impaired cortical input contribute to pathologically elevated exNMDAR function in YAC128 MSNs, and is this a key mechanism of spine loss?

Results from Chapter 2 demonstrated that reducing cortical input exacerbates striatal MSN spine loss in vitro. In Chapter 3, it was shown that DAPK1 contributes to exGluN2B phosphorylation, and that DAPK1 inhibition or blockade of exNMDARs with memantine both restore MSN spine numbers in this in vitro

model. Furthermore, previous work found that reducing cortical input to WT MSNs in CS co-culture increases MSN exNMDAR currents [341]. Together, these findings suggest a close relationship between (A) the level of cortical input to MSNs, (B) exNMDAR activity, and (C) spine stability. Thus, a key remaining question is whether impaired cortical input promotes YAC128 MSN spine loss by exacerbating exNMDAR activity, which is now linked to both DAPK1 activation and CREB shut-off in HD [80, 81, 206]. To address this question, an ideal experiment will be to compare exNMDAR currents in co-cultured WT and YAC128 MSNs at both 1:1 and 1:3 CS ratios. Also, DAPK1 inhibition would be expected to reduce electrophysiological MSN exNMDAR currents in this model, but this has not yet been assessed. Furthermore, endogenous synaptic transmission can be pharmacologically stimulated, and this has been shown to increase nuclear pCREB in CS co-culture [342]. This same strategy can be utilized to determine if there is also a resulting impact on spine stability and/or the level of exNMDAR and DAPK1 activity. Low-dose memantine rescues Aβ-induced hippocampal spine loss in vitro and in vivo [192, 404], and prevents CREB shut-off and neuropathology in YAC128 mice [80, 205, 206]. It will therefore be informative to determine if chronic memantine treatment also protects against in vivo spine loss in HD mice. Conversely, increasing exNMDAR activity in vitro by blocking glial glutamate uptake may exacerbate spine loss.

5.2.1.2 Can gene expression profiling or synaptic proteome analysis be used to identify dysregulated cellular programs involved in HD spine loss?

The use of high-throughput techniques will be critical to provide an unbiased understanding of the mechanisms underlying synaptic dysfunction in HD. To identify novel gene or protein drug targets for neuroprotection, the cellular programs affected by mHTT (in both cortical and striatal neurons) must be elucidated. To do this, gene expression profiling could be performed on CS co-cultures from different CS ratios and genotypes. Furthermore, analysis of the synaptic proteome composition may provide insight into potential mislocalized or

dysregulated proteins contributing to spine loss. A major limitation concerning these next steps lies in the 2D homogenous nature of the CS co-culture system, thus preventing cortical and striatal cell types from being analyzed independently or being distributed into in vivo-like higher-order structures. However, recent work has identified HD-like synaptic phenotypes in cortical and striatal YAC128 neurons grown in microfluidic chambers designed to maintain separation between cell types and the synaptic compartment [76]. Additionally, the use of 3D brain organoids to more accurately recapitulate in vivo circuitry is an exciting new research frontier that will allow region-specific analysis of disease pathogenesis without the use of live animals [405].

5.2.1.3 Can the CS co-culture model be combined with machine learning and high-throughput screening to rapidly identify novel neuroprotective candidate drugs?

Ultimately, the goal of creating a relevant in vitro model of HD synaptic dysfunction is to facilitate the development and testing of neuroprotective therapies for patients. While this can be done using low-throughput methods (such as what has been done in this thesis with the DAPK1 inhibitor TC-DAPK6), advancements in computer technology may dramatically improve the efficiency of this process. Machine learning is becoming increasingly integrated into the neuroscience field as a method to reliably classify and quantify the morphology of different neuronal types [406, 407]. By training algorithms on sets of manually-classified digitally reconstructed neurons, massive amounts of information pertaining to dendritic and spine structure can be obtained. This approach could theoretically be combined with a robotic cell culture system and an unbiased automated imaging program to create an essentially fully-autonomous drug discovery pipeline to identify candidate molecules that improve spine or synaptic strength in HD. Furthermore, machine learning algorithms can be trained to differentiate between neuronal sub-types based on morphology, potentially

allowing analysis of both cortical and striatal neurons from the same CS co-culture sample without the requirement for cell type markers such as DARPP32.

5.2.1.4 Do human HD patient iPSC-derived neurons recapitulate the morphological and biochemical synaptic abnormalities observed in HD brains and primary cultures from rodent models?

Animal models are invaluable tools for understanding disease pathogenesis and developing novel therapies. However, a vast majority of potential drug candidates that perform well in rodents have failed in human clinical trials for neurological disease, signifying critical differences between organisms that are impeding successful drug development (among other challenges). A key limitation to the study of neurodegenerative disease processes is the difficulty in obtaining relevant human brain tissues from early time points in pathogenesis, as well as appropriate matched control samples. By the time of death in HD patients, the majority of striatal volume has been lost [17, 364], and compensatory protective mechanisms to minimize further damage or inflammation in the brain have likely been activated. Studying postmortem HD tissues thus only gives a glimpse into the severe end-stage of disease which, as we know from animal studies, has different features than therapeutically-relevant periods earlier in life. With the advancement of induced pluripotent stem cell (iPSC) technology, it is now possible to generate stem cells from HD patient and healthy control fibroblasts and to differentiate these into glia and different neuronal subtypes. This provides the exciting option to characterize synaptic dysfunction in human HD neurons using robust experimental methods already developed for animal models. If reliable morphological and biochemical phenotypes can be detected in iPSC-derived HD neurons, candidate neuroprotective drugs identified by screening pipelines may demonstrate greater success once translated to human clinical trials.

5.2.2 Understanding the mechanisms linking DAPK1 to spine loss in HD and identifying cellular pathways affected by DAPK1 inhibition

5.2.2.1 Can "-omics" studies contribute to the understanding of DAPK1 dysfunction in HD and the effects of therapeutically targeting it?

As discussed above, high-throughput techniques are useful for the unbiased determination of molecular pathways involved in disease or drug responses. The results in this thesis have shed partial light on the potential mechanisms (ie. exGluN2B phosphorylation, CREB activation) linking DAPK1 to spine loss in HD. However, for a fuller understanding of how DAPK1 fits into HD pathogenesis, various transcriptomic and proteomic methods may be useful. Enriched biological processes and gene expression patterns may be identified by comparing the synaptic proteome, phospho-proteome, DAPK1 interactome, and transcriptome of WT and YAC128 brains, with or without a DAPK1-modifying intervention. This could also be done in WT versus *Dapk1*-null mice. This would contribute to understanding: (A) which pathways are dysregulated by mHTT, (B) which pathways are influenced by DAPK1 activity, (C) whether a DAPK1 ASO or small molecule inhibitor is effective in reinstating a healthy cellular program, and (D) whether additional related targets exist for which therapies have already been developed and tested in humans, thus rapidly accelerating drug discovery.

5.2.2.2 Are other known DAPK1 substrates or interactors aside from GluN2B dysregulated in HD mice, potentially contributing to spine loss and neuronal death?

This thesis focused on the relationship between DAPK1 and GluN2B in HD. However, many other DAPK1 substrates and interactors (listed in **Table 1.1**) have been linked to neuronal death and the pathogenesis of neurodegenerative disease, including α-synuclein, NDRG2, p53, Pin1, APP, and tau (see Section 1.4.5 and Section 1.5). Therefore, it will be of importance to assess whether these proteins undergo enhanced interaction with or phosphorylation by DAPK1 in the presence of mHTT. Of particular interest is the DAPK1-tau relationship.

DAPK1 promotes spine loss in acute ischemia by phosphorylation of tau at S262, causing destabilization of the cytoskeleton [247]. Tau hyperphosphorylation and deposition is a primary hallmark of AD pathogenesis and may also occur in HD [408–411]. Investigation into the potential involvement of this pathway in HD spine loss is warranted. Additionally, DAPK1 sequesters ERK1/2 in the cytosol during ischemia, preventing its nuclear translocation and pro-survival functions [222, 308]. It is also possible that this sequestration prevents activation of ERK1/2 by its upstream kinases. ERK1/2 is an indirect upstream activator of CREB [286], and both ERK1/2 and CREB are activated by synaptic NMDAR activity and dominantly shut off by extrasynaptic NMDARs (**Fig. 1.1**) [125, 173]. In presymptomatic YAC128 mice (1-2 months of age), both CREB and ERK1/2 exhibit reduced activation levels compared to WT mice [80, 288]. Therefore, it will be important to understand whether elevated DAPK1 in HD is a direct link between elevated exGluN2B activity and CREB shut-off via ERK1/2, and to assess if DAPK1 inhibition normalizes early cell survival signaling phenotypes in YAC128 mice.

5.2.2.3 Does increased DAPK1 activity contribute to disturbed ER Ca^{2+} store dynamics in YAC128 MSNs?

Intracellular Ca^{2+} signaling is disturbed in YAC128 neurons. In particular, cytosolic Ca^{2+} dynamics are altered in response to NMDAR stimulation. [68, 199, 200, 202]. Furthermore, ER Ca^{2+} stores are depleted, leading to enhanced SOCE and spine degeneration [74]. NMDAR-mediated Ca^{2+}-induced Ca^{2+} release can cause ER Ca^{2+} store depletion [143]. However, it is currently not known whether pathological NMDAR activity contributes to this occurrence in HD, and if so, whether there is a differential effect in synaptic versus extrasynaptic compartments. The present work has demonstrated that DAPK1 positively regulates exGluN2B phosphorylation and surface expression in HD, and that DAPK1 inhibition is protective against spine loss in YAC128 MSNs. Therefore, a critical remaining question is whether this protective effect is

mediated through normalization of intracellular Ca^{2+} dynamics. Specifically, does DAPK1 inhibition result in less Ca^{2+} influx through exGluN2B, and does this prevent ER Ca^{2+} store depletion in HD MSNs, thus protecting against downstream spine loss? These questions can be addressed through the use of well-established live Ca^{2+} imaging techniques.

5.2.3 Approaches to further validate DAPK1 as a novel HD target and to therapeutically inhibit its kinase activity in vivo

In Section 4.4, strategies to improve the potency, knockdown duration, and tolerability of DAPK1 ASOs were discussed. Ideally, knockdown of the DAPK1 protein would be improved to persist for several months, as has been achieved for highly-optimized HTT ASOs [412, 413], so that full motor, cognitive, psychiatric, neuropathological, and biochemical characterization can be done in YAC128 mice. Most evidence specifically implicates DAPK1 kinase activity in neuronal death, but it remains to be determined if the DAPK1 protein-interacting ankyrin repeats, cytoskeletal binding domain, and the C-terminal death domain are also therapeutically relevant in HD.

Hypermethylation and inactivation of the *DAPK1* gene are associated with various human cancers [266]. Therefore, any therapy aimed at reducing DAPK1 activity must be carefully considered for potential cancerous effects. However, there is a reduced risk of cancer in HD patients, which may provide partial protection against this risk [333, 335]. Furthermore, inactivation of *DAPK1* through promoter hypermethylation or ASO-mediated knockdown would result in loss of activity or function of all domains of the protein. It will therefore be important to distinguish between neuroprotective outcomes that are a result of reducing the total protein level versus inhibiting its kinase activity alone. It is likely that regions aside from the kinase domain play important roles in other cellular processes, such as autophagy [414], which may be protective in certain situations. The development and administration of selective small-molecule

DAPK1 inhibitors in vivo or deletion of specific DAPK1 functional domains in HD mice will be critical to address these questions, as detailed below.

5.2.3.1 Does genetic deletion of the DAPK1 kinase domain restore synaptic function in YAC128 mice?

A constitutive total *Dapk1* knockout mouse exists, and is protected against ischemic and Aβ-induced neuronal death compared to WT *Dapk1*+/+ mice [177, 275]. More recently, mice with specific deletions of the DAPK1 kinase domain (*KD-/-*) or death domain (*DD-/-)* have been developed. Deletion of the kinase domain in Tg2576 AD mice reverses hippocampal spine and synapse loss and improves spatial learning and memory [310]. *KD-/-* mice are also protected against neuronal loss, spine degeneration, and neurological impairments after ischemic insult [247]. It would be useful to determine if kinase domain deletion in YAC128 mice influences exGluN2B pS1303, nuclear pCREB, BDNF levels, dendritic spine loss, as well as behavioral and neuropathological phenotypes. If so, this would support the further development of small molecule DAPK1 kinase inhibitors. In parallel, characterization of a YAC128x*DD-/-* cross would inform whether the death domain may also be targetable (for instance, through the use of peptides or small molecule peptide mimics to prevent interactions between DAPK1 and its death domain binding partners).

5.2.3.2 Does in vivo small molecule inhibition of DAPK1 restore synaptic function in YAC128 mice?

Although multiple DAPK1 small molecule inhibitors have been developed, TC-DAPK6 (referred to in this thesis as DKI) is by far the most widely-used and well-characterized. This compound competes with ATP binding to the DAPK1 catalytic domain and has the lowest IC_{50} (69 nM) of all DAPK1 inhibitors described to date [302]. A number of studies (including those in this thesis) have utilized TC-DAPK6 to probe the role of DAPK1 in various neurological disease

models, and these works have identified neuroprotective and antidepressant properties of the drug (**Table 1.3**). To our knowledge, only one report has described the delivery of TC-DAPK6 to the rodent brain in vivo. In this case, the compound was microinjected directly into the cortex, and restoration of stress-induced GluN2B pS1303 and pCREB alterations were observed two days post-treatment, while antidepressant effects persisted at seven days [314]. For a chronic disease such as HD, an ideal treatment will be non-invasive and therefore allow for repeated dosing, which may be essential to produce a long-term therapeutic benefit. Thus, direct injection into the brain parenchyma is not a feasible option. Prediction analyses based on the structure of TC-DAPK6 indicate that it may be orally available and possess blood-brain barrier permeability, although these predictions need to be confirmed in vivo. Therefore, it may be possible to deliver TC-DAPK6 to the brain by repeated oral, intravenous, or intranasal administration. Nanoparticle-based delivery technologies may also be useful to facilitate access of the compound to the central nervous system for pre-clinical studies. A major question is whether TC-DAPK6 treatment can reverse exGluN2B phosphorylation and function in YAC128 mice, and whether this translates to long-term normalization of synaptic transmission, neuroprotection, and behavior outcomes. In this thesis, crude biochemical fractionation was used to separate synaptic (PSD) from extrasynaptic (non-PSD) GluN2B. However, this method retains internalized receptors as well as surface receptors within the membrane fractions [206, 415]. To specifically assess the effect of DAPK1 inhibition on exGluN2B surface expression in vivo, brain slices may be subjected to surface biotinylation prior to biochemical analysis [416]. Additionally, a two-step live-staining protocol was recently used to assess dynamic turnover of surface GluN2B in cultured neurons [416]. This technique could be used in YAC128 co-cultured MSNs to directly address the hypothesis that DAPK1 inhibition causes internalization and normalization of surface exGluN2B.

Although TC-DAPK6 is likely the most well-understood DAPK1 inhibitor currently available for research use, ongoing virtual screening efforts and crystal structure analysis are being used to further characterize the catalytic domain of

DAPK1 and to identify new inhibitory compounds with high potency and selectivity [303, 417, 418]. Lead compounds from these methods can be further modified and screened to select those that are most likely to have ideal safety profiles and pharmacokinetics.

5.3 CONCLUSIONS

Heightened exNMDAR activity and disturbed synaptic transmission are shared pathogenic features across essentially all major neurodegenerative disorders, despite differences in primary disease causes and affected brain regions [124]. Thus, common therapeutic approaches to modulate this pathway may be effective not only in HD, but in other conditions as well. DAPK1 is an exemplary therapeutic target with multiple overlapping potential clinical applications which remain to be explored in greater depth. Initially linked to acute ischemic neuronal death in 2010, aberrant DAPK1 activity has since been observed in animal models of AD, tauopathy, PD, chronic stress, and now for the first time, HD. Importantly, however, HD is a desirable central model for all forms of neuronal degeneration due to its definitive genetic cause, the wide selection of available animal models, and the ability to generate well-defined clinical trial treatment groups given the option for genetic diagnosis and predictive testing in at-risk individuals. Therefore, it will be ideal to use HD as a model for further development of DAPK1-targeted neuroprotective therapies.

REFERENCES

1. Bates GP, Dorsey R, Gusella JF, Hayden MR, Kay C, Leavitt BR, et al. Huntington disease. Nat Rev Dis Primers. 2015;1:15005.

2. Fisher ER, Hayden MR. Multisource ascertainment of Huntington disease in Canada: prevalence and population at risk. Mov Disord. 2014;29:105–14.

3. Huntington's Disease Collaborative Research Group. A novel gene containing a trinucleotide repeat that is expanded and unstable on Huntington's disease chromosomes. The Huntington's Disease Collaborative Research Group. Cell. 1993;72:971–83.

4. Lee J-M, Ramos EM, Lee J-H, Gillis T, Mysore JS, Hayden MR, et al. CAG repeat expansion in Huntington disease determines age at onset in a fully dominant fashion. Neurology. 2012;78:690–5.

5. Andrew SE, Goldberg YP, Kremer B, Telenius H, Theilmann J, Adam S, et al. The relationship between trinucleotide (CAG) repeat length and clinical features of Huntington's disease. Nat Genet. 1993;4:398–403.

6. Roos RA. Huntington's disease: a clinical review. Orphanet J Rare Dis. 2010;5:40.

7. ACMG/ASHG statement. Laboratory guidelines for Huntington disease genetic testing. The American College of Medical Genetics/American Society of Human Genetics Huntington Disease Genetic Testing Working Group. Am J Hum Genet. 1998;62:1243–7.

8. Unified Huntington's Disease Rating Scale: reliability and consistency. Huntington Study Group. Mov Disord. 1996;11:136–42.

9. Kirkwood SC, Su JL, Conneally PM, Foroud T. Progression of Symptoms in the Early and Middle Stages of Huntington Disease. Arch Neurol. 2001;58:273–8.

10. Schippling S, Schneider SA, Bhatia KP, Münchau A, Rothwell JC, Tabrizi SJ, et al. Abnormal motor cortex excitability in preclinical and very early Huntington's disease. Biol Psychiatry. 2009;65:959–65.

11. Orth M, Schippling S, Schneider SA, Bhatia KP, Talelli P, Tabrizi SJ, et al. Abnormal motor cortex plasticity in premanifest and very early manifest Huntington disease. J Neurol Neurosurg Psychiatry. 2010;81:267–70.

12. Tabrizi SJ, Langbehn DR, Leavitt BR, Roos RA, Durr A, Craufurd D, et al. Biological and clinical manifestations of Huntington's disease in the longitudinal TRACK-HD study: cross-sectional analysis of baseline data. Lancet Neurol. 2009;8:791–801.

13. Tabrizi SJ, Scahill RI, Durr A, Roos RA, Leavitt BR, Jones R, et al. Biological and clinical changes in premanifest and early stage Huntington's disease in the TRACK-HD study: the 12-month longitudinal analysis. Lancet Neurol. 2011;10:31–42.

14. Reiner A, Albin RL, Anderson KD, D'Amato CJ, Penney JB, Young AB. Differential loss of striatal projection neurons in Huntington disease. Proc Natl Acad Sci U S A. 1988;85:5733–7.

15. Albin RL, Reiner A, Anderson KD, Dure LS, Handelin B, Balfour R, et al. Preferential loss of striato-external pallidal projection neurons in presymptomatic Huntington's disease. Ann Neurol. 1992;31:425–30.

16. Richfield EK, Maguire-Zeiss KA, Vonkeman HE, Voorn P. Preferential loss of preproenkephalin versus preprotachykinin neurons from the striatum of Huntington's disease patients. Ann Neurol. 1995;38:852–61.

17. Vonsattel JP, Myers RH, Stevens TJ, Ferrante RJ, Bird ED, Richardson EP. Neuropathological classification of Huntington's disease. J Neuropathol Exp Neurol. 1985;44:559–77.

18. Thu DCV, Oorschot DE, Tippett LJ, Nana AL, Hogg VM, Synek BJ, et al. Cell loss in the motor and cingulate cortex correlates with symptomatology in Huntington's disease. Brain. 2010;133:1094–110.

19. Raymond LA. Striatal synaptic dysfunction and altered calcium regulation in Huntington disease. Biochem Biophys Res Commun. 2017;483:1051–62.

20. André VM, Fisher YE, Levine MS. Altered Balance of Activity in the Striatal Direct and Indirect Pathways in Mouse Models of Huntington's Disease. Front Syst Neurosci. 2011;5:46.

21. Marques Sousa C, Humbert S. Huntingtin: here, there, everywhere! J Huntingtons Dis. 2013;2:395–403.

22. Shirasaki DI, Greiner ER, Al-Ramahi I, Gray M, Boontheung P, Geschwind DH, et al. Network organization of the huntingtin proteomic interactome in mammalian brain. Neuron. 2012;75:41–57.

23. Nasir J, Floresco SB, O'Kusky JR, Diewert VM, Richman JM, Zeisler J, et al. Targeted disruption of the Huntington's disease gene results in embryonic lethality and behavioral and morphological changes in heterozygotes. Cell. 1995;81:811–23.

24. Zeitlin S, Liu JP, Chapman DL, Papaioannou VE, Efstratiadis A. Increased apoptosis and early embryonic lethality in mice nullizygous for the Huntington's disease gene homologue. Nat Genet. 1995;11:155–63.

25. Dragatsis I, Levine MS, Zeitlin S. Inactivation of Hdh in the brain and testis results in progressive neurodegeneration and sterility in mice. Nat Genet. 2000;26:300–6.

26. Saudou F, Humbert S. The Biology of Huntingtin. Neuron. 2016;89:910–26.

27. Gauthier LR, Charrin BC, Borrell-Pagès M, Dompierre JP, Rangone H, Cordelières FP, et al. Huntingtin controls neurotrophic support and survival of neurons by enhancing BDNF vesicular transport along microtubules. Cell. 2004;118:127–38.

28. Park H. Cortical Axonal Secretion of BDNF in the Striatum Is Disrupted in the Mutant-huntingtin Knock-in Mouse Model of Huntington's Disease. Exp Neurobiol. 2018;27:217–25.

29. Yu C, Li CH, Chen S, Yoo H, Qin X, Park H. Decreased BDNF Release in Cortical Neurons of a Knock-in Mouse Model of Huntington's Disease. Sci Rep. 2018;8:16976.

30. Rui Y-N, Xu Z, Patel B, Chen Z, Chen D, Tito A, et al. Huntingtin functions as a scaffold for selective macroautophagy. Nat Cell Biol. 2015;17:262–75.

31. Martinez–Vicente M, Talloczy Z, Wong E, Tang G, Koga H, Kaushik S, et al. CARGO RECOGNITION FAILURE IS RESPONSIBLE FOR INEFFICIENT AUTOPHAGY IN HUNTINGTON'S DISEASE. Nat Neurosci. 2010;13:567–76.

32. Zuccato C, Tartari M, Crotti A, Goffredo D, Valenza M, Conti L, et al. Huntingtin interacts with REST/NRSF to modulate the transcription of NRSE-controlled neuronal genes. Nat Genet. 2003;35:76–83.

33. Hodges A, Strand AD, Aragaki AK, Kuhn A, Sengstag T, Hughes G, et al. Regional and cellular gene expression changes in human Huntington's disease brain. Hum Mol Genet. 2006;15:965–77.

34. Ferrer I, Goutan E, Marín C, Rey MJ, Ribalta T. Brain-derived neurotrophic factor in Huntington disease. Brain Res. 2000;866:257–61.

35. Spires TL, Grote HE, Varshney NK, Cordery PM, van Dellen A, Blakemore C, et al. Environmental enrichment rescues protein deficits in a mouse model of Huntington's disease, indicating a possible disease mechanism. J Neurosci. 2004;24:2270–6.

36. Zuccato C, Ciammola A, Rigamonti D, Leavitt BR, Goffredo D, Conti L, et al. Loss of huntingtin-mediated BDNF gene transcription in Huntington's disease. Science. 2001;293:493–8.

37. Leavitt BR, van Raamsdonk JM, Shehadeh J, Fernandes H, Murphy Z, Graham RK, et al. Wild-type huntingtin protects neurons from excitotoxicity. J Neurochem. 2006;96:1121–9.

38. Labbadia J, Morimoto RI. Huntington's disease: underlying molecular mechanisms and emerging concepts. Trends Biochem Sci. 2013;38:378–85.

39. Ehrlich ME. Huntington's Disease and the Striatal Medium Spiny Neuron: Cell-Autonomous and Non-Cell-Autonomous Mechanisms of Disease. Neurotherapeutics. 2012;9:270–84.

40. Raymond LA, André VM, Cepeda C, Gladding CM, Milnerwood AJ, Levine MS. Pathophysiology of Huntington's disease: time-dependent alterations in synaptic and receptor function. Neuroscience. 2011;198:252–73.

41. Beal MF, Brouillet E, Jenkins BG, Ferrante RJ, Kowall NW, Miller JM, et al. Neurochemical and histologic characterization of striatal excitotoxic lesions produced by the mitochondrial toxin 3-nitropropionic acid. J Neurosci. 1993;13:4181–92.

42. Coyle JT, Schwarcz R. Lesion of striatal neurones with kainic acid provides a model for Huntington's chorea. Nature. 1976;263:244–6.

43. Ferrante RJ, Kowall NW, Cipolloni PB, Storey E, Beal MF. Excitotoxin lesions in primates as a model for Huntington's disease: histopathologic and neurochemical characterization. Exp Neurol. 1993;119:46–71.

44. Beal MF, Ferrante RJ, Swartz KJ, Kowall NW. Chronic quinolinic acid lesions in rats closely resemble Huntington's disease. J Neurosci. 1991;11:1649–59.

45. Roberts RC, Ahn A, Swartz KJ, Beal MF, DiFiglia M. Intrastriatal injections of quinolinic acid or kainic acid: differential patterns of cell survival and the effects of data analysis on outcome. Exp Neurol. 1993;124:274–82.

46. Beal MF, Kowall NW, Swartz KJ, Ferrante RJ, Martin JB. Differential sparing of somatostatin-neuropeptide Y and cholinergic neurons following striatal excitotoxin lesions. Synapse. 1989;3:38–47.

47. Beal MF, Kowall NW, Ellison DW, Mazurek MF, Swartz KJ, Martin JB. Replication of the neurochemical characteristics of Huntington's disease by quinolinic acid. Nature. 1986;321:168–71.

48. Mangiarini L, Sathasivam K, Seller M, Cozens B, Harper A, Hetherington C, et al. Exon 1 of the HD Gene with an Expanded CAG Repeat Is Sufficient to Cause a Progressive Neurological Phenotype in Transgenic Mice. Cell. 1996;87:493–506.

49. Schilling G, Becher MW, Sharp AH, Jinnah HA, Duan K, Kotzuk JA, et al. Intranuclear Inclusions and Neuritic Aggregates in Transgenic Mice Expressing a Mutant N-Terminal Fragment of Huntingtin. Hum Mol Genet. 1999;8:397–407.

50. Slow EJ, van Raamsdonk J, Rogers D, Coleman SH, Graham RK, Deng Y, et al. Selective striatal neuronal loss in a YAC128 mouse model of Huntington disease. Hum Mol Genet. 2003;12:1555–67.

51. Pouladi MA, Stanek LM, Xie Y, Franciosi S, Southwell AL, Deng Y, et al. Marked differences in neurochemistry and aggregates despite similar behavioural and neuropathological features of Huntington disease in the full-length BACHD and YAC128 mice. Hum Mol Genet. 2012;21:2219–32.

52. Rattray I, Smith E, Gale R, Matsumoto K, Bates GP, Modo M. Correlations of Behavioral Deficits with Brain Pathology Assessed through Longitudinal MRI and Histopathology in the R6/2 Mouse Model of HD. PLoS One. 2013;8. doi:10.1371/journal.pone.0060012.

53. Gray M, Shirasaki DI, Cepeda C, Andre VM, Wilburn B, Lu X-H, et al. Full Length Human Mutant Huntingtin with a Stable Polyglutamine Repeat Can Elicit Progressive and Selective Neuropathogenesis in BACHD Mice. J Neurosci. 2008;28:6182–95.

54. Kosior N, Leavitt BR. Murine Models of Huntington's Disease for Evaluating Therapeutics. Methods Mol Biol. 2018;1780:179–207.

55. Southwell AL, Warby SC, Carroll JB, Doty CN, Skotte NH, Zhang W, et al. A fully humanized transgenic mouse model of Huntington disease. Hum Mol Genet. 2013;22:18–34.

56. Southwell AL, Skotte NH, Villanueva EB, Østergaard ME, Gu X, Kordasiewicz HB, et al. A novel humanized mouse model of Huntington disease for preclinical development of therapeutics targeting mutant huntingtin alleles. Hum Mol Genet. 2017;26:1115–32.

57. Menalled LB, Sison JD, Dragatsis I, Zeitlin S, Chesselet M-F. Time course of early motor and neuropathological anomalies in a knock-in mouse model of Huntington's disease with 140 CAG repeats. J Comp Neurol. 2003;465:11–26.

58. Southwell AL, Smith-Dijak A, Kay C, Sepers M, Villanueva EB, Parsons MP, et al. An enhanced Q175 knock-in mouse model of Huntington disease with higher mutant huntingtin levels and accelerated disease phenotypes. Hum Mol Genet. 2016;25:3654–75.

59. Rodrigues FB, Wild EJ. Huntington's Disease Clinical Trials Corner: February 2018. J Huntingtons Dis. 7:89–98.

60. Tabrizi SJ, Leavitt BR, Landwehrmeyer GB, Wild EJ, Saft C, Barker RA, et al. Targeting Huntingtin Expression in Patients with Huntington's Disease. N Engl J Med. 2019.

61. Caron NS, Dorsey ER, Hayden MR. Therapeutic approaches to Huntington disease: from the bench to the clinic. Nat Rev Drug Discov. 2018;17:729–50.

62. Joshi PR, Wu N-P, André VM, Cummings DM, Cepeda C, Joyce JA, et al. Age-dependent alterations of corticostriatal activity in the YAC128 mouse model of Huntington disease. J Neurosci. 2009;29:2414–27.

63. André VM, Cepeda C, Fisher YE, Huynh M, Bardakjian N, Singh S, et al. Differential electrophysiological changes in striatal output neurons in Huntington's disease. J Neurosci. 2011;31:1170–82.

64. Cepeda C, Hurst RS, Calvert CR, Hernández-Echeagaray E, Nguyen OK, Jocoy E, et al. Transient and progressive electrophysiological alterations in the corticostriatal pathway in a mouse model of Huntington's disease. J Neurosci. 2003;23:961–9.

65. Cummings DM, Cepeda C, Levine MS. Alterations in striatal synaptic transmission are consistent across genetic mouse models of Huntington's disease. ASN Neuro. 2010;2:e00036.

66. Kolodziejczyk K, Parsons MP, Southwell AL, Hayden MR, Raymond LA. Striatal synaptic dysfunction and hippocampal plasticity deficits in the Hu97/18 mouse model of Huntington disease. PLoS ONE. 2014;9:e94562.

67. Heikkinen T, Lehtimäki K, Vartiainen N, Puoliväli J, Hendricks SJ, Glaser JR, et al. Characterization of neurophysiological and behavioral changes, MRI brain volumetry and 1H MRS in zQ175 knock-in mouse model of Huntington's disease. PLoS ONE. 2012;7:e50717.

68. Cepeda C, Ariano MA, Calvert CR, Flores-Hernández J, Chandler SH, Leavitt BR, et al. NMDA receptor function in mouse models of Huntington disease. J Neurosci Res. 2001;66:525–39.

69. Milnerwood AJ, Raymond LA. Corticostriatal synaptic function in mouse models of Huntington's disease: early effects of huntingtin repeat length and protein load. J Physiol (Lond). 2007;585 Pt 3:817–31.

70. Bell KFS, Hardingham GE. The influence of synaptic activity on neuronal health. Curr Opin Neurobiol. 2011;21:299–305.

71. Milnerwood AJ, Raymond LA. Early synaptic pathophysiology in neurodegeneration: insights from Huntington's disease. Trends Neurosci. 2010;33:513–23.

72. Altar CA, Cai N, Bliven T, Juhasz M, Conner JM, Acheson AL, et al. Anterograde transport of brain-derived neurotrophic factor and its role in the brain. Nature. 1997;389:856–60.

73. Buren C, Parsons MP, Smith-Dijak A, Raymond LA. Impaired development of cortico-striatal synaptic connectivity in a cell culture model of Huntington's disease. Neurobiol Dis. 2016;87:80–90.

74. Wu J, Ryskamp DA, Liang X, Egorova P, Zakharova O, Hung G, et al. Enhanced Store-Operated Calcium Entry Leads to Striatal Synaptic Loss in a Huntington's Disease Mouse Model. J Neurosci. 2016;36:125–41.

75. Ryskamp D, Wu J, Geva M, Kusko R, Grossman I, Hayden M, et al. The sigma-1 receptor mediates the beneficial effects of pridopidine in a mouse model of Huntington disease. Neurobiol Dis. 2017;97 Pt A:46–59.

76. Virlogeux A, Moutaux E, Christaller W, Genoux A, Bruyère J, Fino E, et al. Reconstituting Corticostriatal Network on-a-Chip Reveals the Contribution of the Presynaptic Compartment to Huntington's Disease. Cell Rep. 2018;22:110–22.

77. Graham RK, Pouladi MA, Joshi P, Lu G, Deng Y, Wu N-P, et al. Differential susceptibility to excitotoxic stress in YAC128 mouse models of Huntington disease between initiation and progression of disease. J Neurosci. 2009;29:2193–204.

78. Levine MS, Klapstein GJ, Koppel A, Gruen E, Cepeda C, Vargas ME, et al. Enhanced sensitivity to N-methyl-D-aspartate receptor activation in transgenic and knockin mouse models of Huntington's disease. Journal of Neuroscience Research. 1999;58:515–32.

79. Hansson O, Petersén Å, Leist M, Nicotera P, Castilho RF, Brundin P. Transgenic mice expressing a Huntington's disease mutation are resistant to quinolinic acid-induced striatal excitotoxicity. PNAS. 1999;96:8727–32.

80. Milnerwood AJ, Gladding CM, Pouladi MA, Kaufman AM, Hines RM, Boyd JD, et al. Early increase in extrasynaptic NMDA receptor signaling and expression contributes to phenotype onset in Huntington's disease mice. Neuron. 2010;65:178–90.

81. Milnerwood AJ, Kaufman AM, Sepers MD, Gladding CM, Zhang L, Wang L, et al. Mitigation of augmented extrasynaptic NMDAR signaling and apoptosis in cortico-striatal co-cultures from Huntington's disease mice. Neurobiol Dis. 2012;48:40–51.

82. Ferrante RJ, Kowall NW, Richardson EP. Proliferative and degenerative changes in striatal spiny neurons in Huntington's disease: a combined study using the section-Golgi method and calbindin D28k immunocytochemistry. J Neurosci. 1991;11:3877–87.

83. Graveland GA, Williams RS, DiFiglia M. Evidence for degenerative and regenerative changes in neostriatal spiny neurons in Huntington's disease. Science. 1985;227:770–3.

84. Singaraja RR, Huang K, Sanders SS, Milnerwood AJ, Hines R, Lerch JP, et al. Altered palmitoylation and neuropathological deficits in mice lacking HIP14. Hum Mol Genet. 2011;20:3899–909.

85. Klapstein GJ, Fisher RS, Zanjani H, Cepeda C, Jokel ES, Chesselet MF, et al. Electrophysiological and morphological changes in striatal spiny neurons in R6/2 Huntington's disease transgenic mice. J Neurophysiol. 2001;86:2667–77.

86. Laforet GA, Sapp E, Chase K, McIntyre C, Boyce FM, Campbell M, et al. Changes in cortical and striatal neurons predict behavioral and electrophysiological abnormalities in a transgenic murine model of Huntington's disease. J Neurosci. 2001;21:9112–23.

87. Deng YP, Wong T, Bricker-Anthony C, Deng B, Reiner A. Loss of corticostriatal and thalamostriatal synaptic terminals precedes striatal projection neuron pathology in heterozygous Q140 Huntington's disease mice. Neurobiol Dis. 2013;60:89–107.

88. Spires TL, Grote HE, Garry S, Cordery PM, Van Dellen A, Blakemore C, et al. Dendritic spine pathology and deficits in experience-dependent dendritic plasticity in R6/1 Huntington's disease transgenic mice. Eur J Neurosci. 2004;19:2799–807.

89. Marco S, Giralt A, Petrovic MM, Pouladi MA, Martínez-Turrillas R, Martínez-Hernández J, et al. Suppressing aberrant GluN3A expression rescues NMDA receptor dysfunction, synapse loss and motor and cognitive decline in Huntington's disease models. Nat Med. 2013;19:1030–8.

90. Nithianantharajah J, Barkus C, Vijiaratnam N, Clement O, Hannan AJ. Modeling brain reserve: experience-dependent neuronal plasticity in healthy and Huntington's disease transgenic mice. Am J Geriatr Psychiatry. 2009;17:196–209.

91. Murmu RP, Li W, Holtmaat A, Li J-Y. Dendritic spine instability leads to progressive neocortical spine loss in a mouse model of Huntington's disease. J Neurosci. 2013;33:12997–3009.

92. Lerner RP, Trejo Martinez LDCG, Zhu C, Chesselet M-F, Hickey MA. Striatal atrophy and dendritic alterations in a knock-in mouse model of Huntington's disease. Brain Res Bull. 2012;87:571–8.

93. Rocher AB, Gubellini P, Merienne N, Boussicault L, Petit F, Gipchtein P, et al. Synaptic scaling up in medium spiny neurons of aged BACHD mice: A slow-progression model of Huntington's disease. Neurobiol Dis. 2016;86:131–9.

94. Paoletti P, Bellone C, Zhou Q. NMDA receptor subunit diversity: impact on receptor properties, synaptic plasticity and disease. Nat Rev Neurosci. 2013;14:383–400.

95. Lohmann C, Kessels HW. The developmental stages of synaptic plasticity. J Physiol (Lond). 2014;592:13–31.

96. Mayer ML, Westbrook GL, Guthrie PB. Voltage-dependent block by Mg2+ of NMDA responses in spinal cord neurones. Nature. 1984;309:261–3.

97. Sanz-Clemente A, Nicoll RA, Roche KW. Diversity in NMDA receptor composition: many regulators, many consequences. Neuroscientist. 2013;19:62–75.

98. Cooke SF, Bliss TVP. Plasticity in the human central nervous system. Brain. 2006;129 Pt 7:1659–73.

99. Groc L, Heine M, Cousins SL, Stephenson FA, Lounis B, Cognet L, et al. NMDA receptor surface mobility depends on NR2A-2B subunits. Proc Natl Acad Sci USA. 2006;103:18769–74.

100. Martel M-A, Wyllie DJA, Hardingham GE. In developing hippocampal neurons, NR2B-containing N-methyl-D-aspartate receptors (NMDARs) can mediate signaling to neuronal survival and synaptic potentiation, as well as neuronal death. Neuroscience. 2009;158:334–43.

101. Tovar KR, Westbrook GL. The Incorporation of NMDA Receptors with a Distinct Subunit Composition at Nascent Hippocampal Synapses In Vitro. J Neurosci. 1999;19:4180–8.

102. Petralia RS, Wang YX, Hua F, Yi Z, Zhou A, Ge L, et al. Organization of NMDA receptors at extrasynaptic locations. Neuroscience. 2010;167:68–87.

103. Harris AZ, Pettit DL. Extrasynaptic and synaptic NMDA receptors form stable and uniform pools in rat hippocampal slices. J Physiol (Lond). 2007;584 Pt 2:509–19.

104. Thomas CG, Miller AJ, Westbrook GL. Synaptic and extrasynaptic NMDA receptor NR2 subunits in cultured hippocampal neurons. J Neurophysiol. 2006;95:1727–34.

105. Liu Y, Wong TP, Aarts M, Rooyakkers A, Liu L, Lai TW, et al. NMDA receptor subunits have differential roles in mediating excitotoxic neuronal death both in vitro and in vivo. J Neurosci. 2007;27:2846–57.

106. Stroebel D, Casado M, Paoletti P. Triheteromeric NMDA receptors: from structure to synaptic physiology. Current Opinion in Physiology. 2018;2:1–12.

107. Sun Y, Xu Y, Cheng X, Chen X, Xie Y, Zhang L, et al. The differences between GluN2A and GluN2B signaling in the brain. J Neurosci Res. 2018;96:1430–43.

108. Ryan TJ, Emes RD, Grant SG, Komiyama NH. Evolution of NMDA receptor cytoplasmic interaction domains: implications for organisation of synaptic signalling complexes. BMC Neurosci. 2008;9:6.

109. von Engelhardt J, Coserea I, Pawlak V, Fuchs EC, Köhr G, Seeburg PH, et al. Excitotoxicity in vitro by NR2A- and NR2B-containing NMDA receptors. Neuropharmacology. 2007;53:10–7.

110. Chen M, Lu T-J, Chen X-J, Zhou Y, Chen Q, Feng X-Y, et al. Differential roles of NMDA receptor subtypes in ischemic neuronal cell death and ischemic tolerance. Stroke. 2008;39:3042–8.

111. Zhou M, Baudry M. Developmental changes in NMDA neurotoxicity reflect developmental changes in subunit composition of NMDA receptors. J Neurosci. 2006;26:2956–63.

112. DeRidder MN, Simon MJ, Siman R, Auberson YP, Raghupathi R, Meaney DF. Traumatic mechanical injury to the hippocampus in vitro causes regional caspase-3 and calpain activation that is influenced by NMDA receptor subunit composition. Neurobiol Dis. 2006;22:165–76.

113. Terasaki Y, Sasaki T, Yagita Y, Okazaki S, Sugiyama Y, Oyama N, et al. Activation of NR2A receptors induces ischemic tolerance through CREB signaling. J Cereb Blood Flow Metab. 2010;30:1441–9.

114. Gambrill AC, Barria A. NMDA receptor subunit composition controls synaptogenesis and synapse stabilization. Proc Natl Acad Sci USA. 2011;108:5855–60.

115. Kirson ED, Schirra C, Konnerth A, Yaari Y. Early postnatal switch in magnesium sensitivity of NMDA receptors in rat CA1 pyramidal cells. J Physiol (Lond). 1999;521 Pt 1:99–111.

116. Sans N, Petralia RS, Wang YX, Blahos J, Hell JW, Wenthold RJ. A developmental change in NMDA receptor-associated proteins at hippocampal synapses. J Neurosci. 2000;20:1260–71.

117. Sheng M, Cummings J, Roldan LA, Jan YN, Jan LY. Changing subunit composition of heteromeric NMDA receptors during development of rat cortex. Nature. 1994;368:144–7.

118. Quinlan EM, Olstein DH, Bear MF. Bidirectional, experience-dependent regulation of N-methyl-D-aspartate receptor subunit composition in the rat visual

cortex during postnatal development. Proc Natl Acad Sci USA. 1999;96:12876–80.

119. Bellone C, Nicoll RA. Rapid bidirectional switching of synaptic NMDA receptors. Neuron. 2007;55:779–85.

120. Kristensen AS, Jenkins MA, Banke TG, Schousboe A, Makino Y, Johnson RC, et al. Mechanism of Ca2+/calmodulin-dependent kinase II regulation of AMPA receptor gating. Nat Neurosci. 2011;14:727–35.

121. Strack S, Colbran RJ. Autophosphorylation-dependent targeting of calcium/calmodulin-dependent protein kinase II by the NR2B subunit of the N-methyl- D-aspartate receptor. J Biol Chem. 1998;273:20689–92.

122. Hardingham GE, Bading H. Synaptic versus extrasynaptic NMDA receptor signalling: implications for neurodegenerative disorders. Nat Rev Neurosci. 2010;11:682–96.

123. Papouin T, Oliet SH. Organization, control and function of extrasynaptic NMDA receptors., Organization, control and function of extrasynaptic NMDA receptors. Philos Trans R Soc Lond B Biol Sci. 2014;369, 369:20130601–20130601.

124. Bading H. Therapeutic targeting of the pathological triad of extrasynaptic NMDA receptor signaling in neurodegenerations. J Exp Med. 2017;214:569–78.

125. Hardingham GE, Fukunaga Y, Bading H. Extrasynaptic NMDARs oppose synaptic NMDARs by triggering CREB shut-off and cell death pathways. Nat Neurosci. 2002;5:405–14.

126. Hardingham GE, Bading H. Coupling of extrasynaptic NMDA receptors to a CREB shut-off pathway is developmentally regulated. Biochim Biophys Acta. 2002;1600:148–53.

127. Boyer C, Schikorski T, Stevens CF. Comparison of Hippocampal Dendritic Spines in Culture and in Brain. J Neurosci. 1998;18:5294–300.

128. Hoffmann H, Gremme T, Hatt H, Gottmann K. Synaptic activity-dependent developmental regulation of NMDA receptor subunit expression in cultured neocortical neurons. J Neurochem. 2000;75:1590–9.

129. Lai TW, Shyu W-C, Wang YT. Stroke intervention pathways: NMDA receptors and beyond. Trends Mol Med. 2011;17:266–75.

130. Harris AZ, Pettit DL. Recruiting extrasynaptic NMDA receptors augments synaptic signaling. J Neurophysiol. 2008;99:524–33.

131. Massey PV, Johnson BE, Moult PR, Auberson YP, Brown MW, Molnar E, et al. Differential roles of NR2A and NR2B-containing NMDA receptors in cortical long-term potentiation and long-term depression. J Neurosci. 2004;24:7821–8.

132. Delgado JY, Fink AE, Grant SGN, O'Dell TJ, Opazo P. Rapid homeostatic downregulation of LTP by extrasynaptic GluN2B receptors. J Neurophysiol. 2018;120:2351–7.

133. Chalifoux JR, Carter AG. Glutamate spillover promotes the generation of NMDA spikes. J Neurosci. 2011;31:16435–46.

134. Oikonomou KD, Short SM, Rich MT, Antic SD. Extrasynaptic glutamate receptor activation as cellular bases for dynamic range compression in pyramidal neurons. Front Physiol. 2012;3:334.

135. Papouin T, Ladépêche L, Ruel J, Sacchi S, Labasque M, Hanini M, et al. Synaptic and extrasynaptic NMDA receptors are gated by different endogenous coagonists. Cell. 2012;150:633–46.

136. Fellin T, Pascual O, Gobbo S, Pozzan T, Haydon PG, Carmignoto G. Neuronal synchrony mediated by astrocytic glutamate through activation of extrasynaptic NMDA receptors. Neuron. 2004;43:729–43.

137. Angulo MC, Kozlov AS, Charpak S, Audinat E. Glutamate released from glial cells synchronizes neuronal activity in the hippocampus. J Neurosci. 2004;24:6920–7.

138. Jourdain P, Bergersen LH, Bhaukaurally K, Bezzi P, Santello M, Domercq M, et al. Glutamate exocytosis from astrocytes controls synaptic strength. Nat Neurosci. 2007;10:331–9.

139. Hagenston AM, Bading H. Calcium signaling in synapse-to-nucleus communication. Cold Spring Harb Perspect Biol. 2011;3:a004564.

140. Emptage N, Bliss TV, Fine A. Single synaptic events evoke NMDA receptor-mediated release of calcium from internal stores in hippocampal dendritic spines. Neuron. 1999;22:115–24.

141. Solovyova N, Veselovsky N, Toescu EC, Verkhratsky A. Ca(2+) dynamics in the lumen of the endoplasmic reticulum in sensory neurons: direct visualization of Ca(2+)-induced Ca(2+) release triggered by physiological Ca(2+) entry. EMBO J. 2002;21:622–30.

142. Yamamoto K, Hashimoto K, Isomura Y, Shimohama S, Kato N. An IP3-assisted form of Ca2+-induced Ca2+ release in neocortical neurons. Neuroreport. 2000;11:535–9.

143. Dittmer PJ, Wild AR, Dell'Acqua ML, Sather WA. STIM1 Ca2+ Sensor Control of L-type Ca2+-Channel-Dependent Dendritic Spine Structural Plasticity and Nuclear Signaling. Cell Rep. 2017;19:321–34.

144. Ferreira IL, Ferreiro E, Schmidt J, Cardoso JM, Pereira CMF, Carvalho AL, et al. Aβ and NMDAR activation cause mitochondrial dysfunction involving ER calcium release. Neurobiol Aging. 2015;36:680–92.

145. Ruiz A, Matute C, Alberdi E. Endoplasmic reticulum Ca(2+) release through ryanodine and IP(3) receptors contributes to neuronal excitotoxicity. Cell Calcium. 2009;46:273–81.

146. Lussier MP, Sanz-Clemente A, Roche KW. Dynamic Regulation of N-Methyl-d-aspartate (NMDA) and α-Amino-3-hydroxy-5-methyl-4-isoxazolepropionic Acid (AMPA) Receptors by Posttranslational Modifications. J Biol Chem. 2015;290:28596–603.

147. Chung HJ, Huang YH, Lau L-F, Huganir RL. Regulation of the NMDA receptor complex and trafficking by activity-dependent phosphorylation of the NR2B subunit PDZ ligand. J Neurosci. 2004;24:10248–59.

148. Chen B-S, Gray JA, Sanz-Clemente A, Wei Z, Thomas EV, Nicoll RA, et al. SAP102 mediates synaptic clearance of NMDA receptors. Cell Rep. 2012;2:1120–8.

149. Sanz-Clemente A, Matta JA, Isaac JTR, Roche KW. Casein kinase 2 regulates the NR2 subunit composition of synaptic NMDA receptors. Neuron. 2010;67:984–96.

150. Lavezzari G, McCallum J, Lee R, Roche KW. Differential binding of the AP-2 adaptor complex and PSD-95 to the C-terminus of the NMDA receptor subunit NR2B regulates surface expression. Neuropharmacology. 2003;45:729–37.

151. Prybylowski K, Chang K, Kan L, Vicini S, Wenthold RJ. The synaptic localization of NR2B-containing NMDA receptors is controlled by interactions with PDZ proteins and AP-2. Neuron. 2005;47:845–57.

152. Sanz-Clemente A, Gray JA, Ogilvie KA, Nicoll RA, Roche KW. Activated CaMKII Couples GluN2B and Casein Kinase 2 to Control Synaptic NMDA Receptors. Cell Reports. 2013;3:607–14.

153. Nakazawa T, Komai S, Tezuka T, Hisatsune C, Umemori H, Semba K, et al. Characterization of Fyn-mediated tyrosine phosphorylation sites on GluR epsilon 2 (NR2B) subunit of the N-methyl-D-aspartate receptor. J Biol Chem. 2001;276:693–9.

154. Lu W, Fang W, Li J, Zhang B, Yang Q, Yan X, et al. Phosphorylation of tyrosine Y1070 at the GluN2B subunit is regulated by synaptic activity and critical for surface expression of NMDA receptors. J Biol Chem. 2015;:jbc.M115.663450.

155. Goebel-Goody SM, Davies KD, Alvestad Linger RM, Freund RK, Browning MD. Phospho-regulation of synaptic and extrasynaptic N-methyl-d-aspartate receptors in adult hippocampal slices. Neuroscience. 2009;158:1446–59.

156. Wu H-Y, Hsu F-C, Gleichman AJ, Baconguis I, Coulter DA, Lynch DR. Fyn-mediated phosphorylation of NR2B Tyr-1336 controls calpain-mediated NR2B cleavage in neurons and heterologous systems. J Biol Chem. 2007;282:20075–87.

157. Jones ML, Leonard JP. PKC site mutations reveal differential modulation by insulin of NMDA receptors containing NR2A or NR2B subunits. Journal of Neurochemistry. 2005;92:1431–8.

158. Liao GY, Leonard JP. Insulin modulation of cloned mouse NMDA receptor currents in Xenopus oocytes. J Neurochem. 1999;73:1510–9.

159. Liao GY, Wagner DA, Hsu MH, Leonard JP. Evidence for direct protein kinase-C mediated modulation of N-methyl-D-aspartate receptor current. Mol Pharmacol. 2001;59:960–4.

160. Murphy JA, Stein IS, Lau CG, Peixoto RT, Aman TK, Kaneko N, et al. Phosphorylation of Ser1166 on GluN2B by PKA Is Critical to Synaptic NMDA Receptor Function and Ca2+ Signaling in Spines. J Neurosci. 2014;34:869–79.

161. Vissel B, Krupp JJ, Heinemann SF, Westbrook GL. A use-dependent tyrosine dephosphorylation of NMDA receptors is independent of ion flux. Nat Neurosci. 2001;4:587–96.

162. Yang M, Leonard JP. Identification of mouse NMDA receptor subunit NR2A C-terminal tyrosine sites phosphorylated by coexpression with v-Src. J Neurochem. 2001;77:580–8.

163. Zheng F, Gingrich MB, Traynelis SF, Conn PJ. Tyrosine kinase potentiates NMDA receptor currents by reducing tonic zinc inhibition. Nat Neurosci. 1998;1:185–91.

164. Grau C, Arató K, Fernández-Fernández JM, Valderrama A, Sindreu C, Fillat C, et al. DYRK1A-mediated phosphorylation of GluN2A at Ser(1048) regulates the surface expression and channel activity of GluN1/GluN2A receptors. Front Cell Neurosci. 2014;8:331.

165. Plattner F, Hernandéz A, Kistler TM, Pozo K, Zhong P, Yuen EY, et al. Memory Enhancement by Targeting Cdk5 Regulation of NR2B. Neuron. 2014;81:1070–83.

166. Tingley WG, Ehlers MD, Kameyama K, Doherty C, Ptak JB, Riley CT, et al. Characterization of protein kinase A and protein kinase C phosphorylation of the N-methyl-D-aspartate receptor NR1 subunit using phosphorylation site-specific antibodies. J Biol Chem. 1997;272:5157–66.

167. Scott DB, Blanpied TA, Swanson GT, Zhang C, Ehlers MD. An NMDA receptor ER retention signal regulated by phosphorylation and alternative splicing. J Neurosci. 2001;21:3063–72.

168. Bosley TM, Woodhams PL, Gordon RD, Balázs R. Effects of anoxia on the stimulated release of amino acid neurotransmitters in the cerebellum in vitro. J Neurochem. 1983;40:189–201.

169. Drejer J, Benveniste H, Diemer NH, Schousboe A. Cellular origin of ischemia-induced glutamate release from brain tissue in vivo and in vitro. J Neurochem. 1985;45:145–51.

170. Silverstein FS, Buchanan K, Johnston MV. Perinatal hypoxia-ischemia disrupts striatal high-affinity [3H]glutamate uptake into synaptosomes. J Neurochem. 1986;47:1614–9.

171. Dawson LA, Djali S, Gonzales C, Vinegra MA, Zaleska MM. Characterization of transient focal ischemia-induced increases in extracellular glutamate and aspartate in spontaneously hypertensive rats. Brain Res Bull. 2000;53:767–76.

172. Lai TW, Zhang S, Wang YT. Excitotoxicity and stroke: identifying novel targets for neuroprotection. Prog Neurobiol. 2014;115:157–88.

173. Ivanov A, Pellegrino C, Rama S, Dumalska I, Salyha Y, Ben-Ari Y, et al. Opposing role of synaptic and extrasynaptic NMDA receptors in regulation of the extracellular signal-regulated kinases (ERK) activity in cultured rat hippocampal neurons. J Physiol (Lond). 2006;572 Pt 3:789–98.

174. Tao X, Finkbeiner S, Arnold DB, Shaywitz AJ, Greenberg ME. Ca2+ influx regulates BDNF transcription by a CREB family transcription factor-dependent mechanism. Neuron. 1998;20:709–26.

175. Xu J, Kurup P, Zhang Y, Goebel-Goody SM, Wu PH, Hawasli AH, et al. Extrasynaptic NMDA receptors couple preferentially to excitotoxicity via calpain-mediated cleavage of STEP. J Neurosci. 2009;29:9330–43.

176. Soriano FX, Martel M-A, Papadia S, Vaslin A, Baxter P, Rickman C, et al. Specific targeting of pro-death NMDA receptor signals with differing reliance on the NR2B PDZ ligand. J Neurosci. 2008;28:10696–710.

177. Tu W, Xu X, Peng L, Zhong X, Zhang W, Soundarapandian MM, et al. DAPK1 interaction with NMDA receptor NR2B subunits mediates brain damage in stroke. Cell. 2010;140:222–34.

178. Zhang S, Taghibiglou C, Girling K, Dong Z, Lin S-Z, Lee W, et al. Critical role of increased PTEN nuclear translocation in excitotoxic and ischemic neuronal injuries. J Neurosci. 2013;33:7997–8008.

179. O'Hare MJ, Kushwaha N, Zhang Y, Aleyasin H, Callaghan SM, Slack RS, et al. Differential roles of nuclear and cytoplasmic cyclin-dependent kinase 5 in apoptotic and excitotoxic neuronal death. J Neurosci. 2005;25:8954–66.

180. Rashidian J, Rousseaux MW, Venderova K, Qu D, Callaghan SM, Phillips M, et al. Essential role of cytoplasmic cdk5 and Prx2 in multiple ischemic injury models, in vivo. J Neurosci. 2009;29:12497–505.

181. Bloom GS. Amyloid-β and tau: the trigger and bullet in Alzheimer disease pathogenesis. JAMA Neurol. 2014;71:505–8.

182. Ittner LM, Ke YD, Delerue F, Bi M, Gladbach A, van Eersel J, et al. Dendritic function of tau mediates amyloid-beta toxicity in Alzheimer's disease mouse models. Cell. 2010;142:387–97.

183. Burnouf S, Martire A, Derisbourg M, Laurent C, Belarbi K, Leboucher A, et al. NMDA receptor dysfunction contributes to impaired brain-derived neurotrophic factor-induced facilitation of hippocampal synaptic transmission in a Tau transgenic model. Aging Cell. 2013;12:11–23.

184. Snyder EM, Nong Y, Almeida CG, Paul S, Moran T, Choi EY, et al. Regulation of NMDA receptor trafficking by amyloid-beta. Nat Neurosci. 2005;8:1051–8.

185. Li S, Jin M, Koeglsperger T, Shepardson NE, Shankar GM, Selkoe DJ. Soluble Aβ oligomers inhibit long-term potentiation through a mechanism involving excessive activation of extrasynaptic NR2B-containing NMDA receptors. J Neurosci. 2011;31:6627–38.

186. Rönicke R, Mikhaylova M, Rönicke S, Meinhardt J, Schröder UH, Fändrich M, et al. Early neuronal dysfunction by amyloid β oligomers depends on activation of NR2B-containing NMDA receptors. Neurobiol Aging. 2011;32:2219–28.

187. Scimemi A, Meabon JS, Woltjer RL, Sullivan JM, Diamond JS, Cook DG. Amyloid-β1-42 slows clearance of synaptically released glutamate by mislocalizing astrocytic GLT-1. J Neurosci. 2013;33:5312–8.

188. Talantova M, Sanz-Blasco S, Zhang X, Xia P, Akhtar MW, Okamoto S, et al. Aβ induces astrocytic glutamate release, extrasynaptic NMDA receptor activation, and synaptic loss. Proc Natl Acad Sci USA. 2013;110:E2518-2527.

189. Sun X-Y, Tuo Q-Z, Liuyang Z-Y, Xie A-J, Feng X-L, Yan X, et al. Extrasynaptic NMDA receptor-induced tau overexpression mediates neuronal death through suppressing survival signaling ERK phosphorylation. Cell Death Dis. 2016;7:e2449.

190. Bordji K, Becerril-Ortega J, Nicole O, Buisson A. Activation of extrasynaptic, but not synaptic, NMDA receptors modifies amyloid precursor protein expression pattern and increases amyloid-ß production. J Neurosci. 2010;30:15927–42.

191. Roselli F, Tirard M, Lu J, Hutzler P, Lamberti P, Livrea P, et al. Soluble beta-amyloid1-40 induces NMDA-dependent degradation of postsynaptic density-95 at glutamatergic synapses. J Neurosci. 2005;25:11061–70.

192. Savchenko A, Braun GB, Molokanova E. Nanostructured Antagonist of Extrasynaptic NMDA Receptors. Nano Lett. 2016;16:5495–502.

193. Folch J, Busquets O, Ettcheto M, Sánchez-López E, Castro-Torres RD, Verdaguer E, et al. Memantine for the Treatment of Dementia: A Review on its Current and Future Applications. J Alzheimers Dis. 62:1223–40.

194. Fan J, Cowan CM, Zhang LYJ, Hayden MR, Raymond LA. Interaction of postsynaptic density protein-95 with NMDA receptors influences excitotoxicity in the yeast artificial chromosome mouse model of Huntington's disease. J Neurosci. 2009;29:10928–38.

195. Graham RK, Deng Y, Slow EJ, Haigh B, Bissada N, Lu G, et al. Cleavage at the caspase-6 site is required for neuronal dysfunction and degeneration due to mutant huntingtin. Cell. 2006;125:1179–91.

196. Zeron MM, Chen N, Moshaver A, Lee AT, Wellington CL, Hayden MR, et al. Mutant huntingtin enhances excitotoxic cell death. Mol Cell Neurosci. 2001;17:41–53.

197. Zeron MM, Hansson O, Chen N, Wellington CL, Leavitt BR, Brundin P, et al. Increased sensitivity to N-methyl-D-aspartate receptor-mediated excitotoxicity in a mouse model of Huntington's disease. Neuron. 2002;33:849–60.

198. Chen N, Luo T, Wellington C, Metzler M, McCutcheon K, Hayden MR, et al. Subtype-specific enhancement of NMDA receptor currents by mutant huntingtin. J Neurochem. 1999;72:1890–8.

199. Zeron MM, Fernandes HB, Krebs C, Shehadeh J, Wellington CL, Leavitt BR, et al. Potentiation of NMDA receptor-mediated excitotoxicity linked with

intrinsic apoptotic pathway in YAC transgenic mouse model of Huntington's disease. Mol Cell Neurosci. 2004;25:469–79.

200. Tang T-S, Slow E, Lupu V, Stavrovskaya IG, Sugimori M, Llinás R, et al. Disturbed Ca2+ signaling and apoptosis of medium spiny neurons in Huntington's disease. Proc Natl Acad Sci USA. 2005;102:2602–7.

201. Shehadeh J, Fernandes HB, Zeron Mullins MM, Graham RK, Leavitt BR, Hayden MR, et al. Striatal neuronal apoptosis is preferentially enhanced by NMDA receptor activation in YAC transgenic mouse model of Huntington disease. Neurobiol Dis. 2006;21:392–403.

202. Fernandes HB, Baimbridge KG, Church J, Hayden MR, Raymond LA. Mitochondrial sensitivity and altered calcium handling underlie enhanced NMDA-induced apoptosis in YAC128 model of Huntington's disease. J Neurosci. 2007;27:13614–23.

203. Fan MMY, Fernandes HB, Zhang LYJ, Hayden MR, Raymond LA. Altered NMDA receptor trafficking in a yeast artificial chromosome transgenic mouse model of Huntington's disease. J Neurosci. 2007;27:3768–79.

204. Fan J, Gladding CM, Wang L, Zhang LYJ, Kaufman AM, Milnerwood AJ, et al. P38 MAPK is involved in enhanced NMDA receptor-dependent excitotoxicity in YAC transgenic mouse model of Huntington disease. Neurobiol Dis. 2012;45:999–1009.

205. Okamoto S, Pouladi MA, Talantova M, Yao D, Xia P, Ehrnhoefer DE, et al. Balance between synaptic versus extrasynaptic NMDA receptor activity influences inclusions and neurotoxicity of mutant huntingtin. Nat Med. 2009;15:1407–13.

206. Dau A, Gladding CM, Sepers MD, Raymond LA. Chronic blockade of extrasynaptic NMDA receptors ameliorates synaptic dysfunction and pro-death signaling in Huntington disease transgenic mice. Neurobiol Dis. 2014;62:533–42.

207. Botelho EP, Wang E, Chen JY, Holley S, Andre V, Cepeda C, et al. Differential Synaptic and Extrasynaptic Glutamate-Receptor Alterations in Striatal Medium-Sized Spiny Neurons of Aged YAC128 Huntington's Disease Mice. PLoS Curr. 2014;6.

208. Heng MY, Detloff PJ, Wang PL, Tsien JZ, Albin RL. In Vivo Evidence for NMDA Receptor-Mediated Excitotoxicity in a Murine Genetic Model of Huntington Disease. J Neurosci. 2009;29:3200–5.

209. Wellington CL, Singaraja R, Ellerby L, Savill J, Roy S, Leavitt B, et al. Inhibiting caspase cleavage of huntingtin reduces toxicity and aggregate formation in neuronal and nonneuronal cells. J Biol Chem. 2000;275:19831–8.

210. Graham RK, Deng Y, Carroll J, Vaid K, Cowan C, Pouladi MA, et al. Cleavage at the 586aa caspase-6 site in mutant huntingtin influences caspase-6 activation in vivo. J Neurosci. 2010;30:15019–29.

211. Jarabek BR, Yasuda RP, Wolfe BB. Regulation of proteins affecting NMDA receptor-induced excitotoxicity in a Huntington's mouse model. Brain. 2004;127 Pt 3:505–16.

212. Luthi-Carter R, Apostol BL, Dunah AW, DeJohn MM, Farrell LA, Bates GP, et al. Complex alteration of NMDA receptors in transgenic Huntington's disease mouse brain: analysis of mRNA and protein expression, plasma membrane association, interacting proteins, and phosphorylation. Neurobiol Dis. 2003;14:624–36.

213. Gladding CM, Sepers MD, Xu J, Zhang LYJ, Milnerwood AJ, Lombroso PJ, et al. Calpain and STriatal-Enriched protein tyrosine Phosphatase (STEP) activation contribute to extrasynaptic NMDA receptor localization in a Huntington's disease mouse model. Hum Mol Genet. 2012;21:3739–52.

214. Song C, Zhang Y, Parsons CG, Liu YF. Expression of polyglutamine-expanded huntingtin induces tyrosine phosphorylation of N-methyl-D-aspartate receptors. J Biol Chem. 2003;278:33364–9.

215. Deiss LP, Feinstein E, Berissi H, Cohen O, Kimchi A. Identification of a novel serine/threonine kinase and a novel 15-kD protein as potential mediators of the gamma interferon-induced cell death. Genes Dev. 1995;9:15–30.

216. Cohen O, Feinstein E, Kimchi A. DAP-kinase is a Ca2+/calmodulin-dependent, cytoskeletal-associated protein kinase, with cell death-inducing functions that depend on its catalytic activity. EMBO J. 1997;16:998–1008.

217. Swulius MT, Waxham MN. Ca2+/Calmodulin-dependent Protein Kinases. Cell Mol Life Sci. 2008;65:2637–57.

218. Shohat G, Spivak-Kroizman T, Cohen O, Bialik S, Shani G, Berrisi H, et al. The pro-apoptotic function of death-associated protein kinase is controlled by a unique inhibitory autophosphorylation-based mechanism. J Biol Chem. 2001;276:47460–7.

219. de Diego I, Kuper J, Bakalova N, Kursula P, Wilmanns M. Molecular basis of the death-associated protein kinase-calcium/calmodulin regulator complex. Sci Signal. 2010;3:ra6.

220. Pei L, Shang Y, Jin H, Wang S, Wei N, Yan H, et al. DAPK1-p53 interaction converges necrotic and apoptotic pathways of ischemic neuronal death. J Neurosci. 2014;34:6546–56.

221. Cohen O, Inbal B, Kissil JL, Raveh T, Berissi H, Spivak-Kroizaman T, et al. Dap-Kinase Participates in TNF-α–And FAS-Induced Apoptosis and Its Function Requires the Death Domain. J Cell Biol. 1999;146:141–8.

222. Chen C-H, Wang W-J, Kuo J-C, Tsai H-C, Lin J-R, Chang Z-F, et al. Bidirectional signals transduced by DAPK–ERK interaction promote the apoptotic effect of DAPK. EMBO J. 2005;24:294–304.

223. Raveh T, Berissi H, Eisenstein M, Spivak T, Kimchi A. A functional genetic screen identifies regions at the C-terminal tail and death-domain of death-associated protein kinase that are critical for its proapoptotic activity. Proc Natl Acad Sci U S A. 2000;97:1572–7.

224. Jang C-W, Chen C-H, Chen C-C, Chen J, Su Y-H, Chen R-H. TGF-beta induces apoptosis through Smad-mediated expression of DAP-kinase. Nat Cell Biol. 2002;4:51–8.

225. Pelled D, Raveh T, Riebeling C, Fridkin M, Berissi H, Futerman AH, et al. Death-associated Protein (DAP) Kinase Plays a Central Role in Ceramide-induced Apoptosis in Cultured Hippocampal Neurons. J Biol Chem. 2002;277:1957–61.

226. Jin Y, Blue EK, Dixon S, Hou L, Wysolmerski RB, Gallagher PJ. Identification of a New Form of Death-associated Protein Kinase That Promotes Cell Survival. J Biol Chem. 2001;276:39667–78.

227. Bialik S, Kimchi A. The death-associated protein kinases: structure, function, and beyond. Annu Rev Biochem. 2006;75:189–210.

228. Kawai T, Nomura F, Hoshino K, Copeland NG, Gilbert DJ, Jenkins NA, et al. Death-associated protein kinase 2 is a new calcium/calmodulin-dependent protein kinase that signals apoptosis through its catalytic activity. Oncogene. 1999;18:3471–80.

229. Kawai T, Matsumoto M, Takeda K, Sanjo H, Akira S. ZIP Kinase, a Novel Serine/Threonine Kinase Which Mediates Apoptosis. Mol Cell Biol. 1998;18:1642–51.

230. Inbal B, Shani G, Cohen O, Kissil JL, Kimchi A. Death-associated protein kinase-related protein 1, a novel serine/threonine kinase involved in apoptosis. Mol Cell Biol. 2000;20:1044–54.

231. Graves PR, Winkfield KM, Haystead TAJ. Regulation of zipper-interacting protein kinase activity in vitro and in vivo by multisite phosphorylation. J Biol Chem. 2005;280:9363–74.

232. Tereshko V, Teplova M, Brunzelle J, Watterson DM, Egli M. Crystal structures of the catalytic domain of human protein kinase associated with

apoptosis and tumor suppression. Nature Structural & Molecular Biology. 2001;8:899–907.

233. Shani G, Marash L, Gozuacik D, Bialik S, Teitelbaum L, Shohat G, et al. Death-associated protein kinase phosphorylates ZIP kinase, forming a unique kinase hierarchy to activate its cell death functions. Mol Cell Biol. 2004;24:8611–26.

234. Velentza AV, Schumacher AM, Weiss C, Egli M, Watterson DM. A protein kinase associated with apoptosis and tumor suppression: structure, activity, and discovery of peptide substrates. J Biol Chem. 2001;276:38956–65.

235. Patel AK, Yadav RP, Majava V, Kursula I, Kursula P. Structure of the dimeric autoinhibited conformation of DAPK2, a pro-apoptotic protein kinase. J Mol Biol. 2011;409:369–83.

236. Zimmermann M, Atmanene C, Xu Q, Fouillen L, Van Dorsselaer A, Bonnet D, et al. Homodimerization of the death-associated protein kinase catalytic domain: development of a new small molecule fluorescent reporter. PLoS ONE. 2010;5:e14120.

237. Shani G, Henis-Korenblit S, Jona G, Gileadi O, Eisenstein M, Ziv T, et al. Autophosphorylation restrains the apoptotic activity of DRP-1 kinase by controlling dimerization and calmodulin binding. EMBO J. 2001;20:1099–113.

238. Shiloh R, Bialik S, Kimchi A. The DAPK family: a structure–function analysis. Apoptosis. 2014;19:286–97.

239. Yamamoto M, Takahashi H, Nakamura T, Hioki T, Nagayama S, Ooashi N, et al. Developmental changes in distribution of death-associated protein kinase mRNAs. Journal of Neuroscience Research. 1999;58:674–83.

240. Sakagami H, Kondo H. Molecular cloning and developmental expression of a rat homologue of death-associated protein kinase in the nervous system. Brain Res Mol Brain Res. 1997;52:249–56.

241. Li Y, Zhu M, Zhang X, Cheng D, Ma X. Clinical significance of DAPK promoter hypermethylation in lung cancer: a meta-analysis. Drug Des Devel Ther. 2015;9:1785–96.

242. Nakav S, Cohen S, Feigelson SW, Bialik S, Shoseyov D, Kimchi A, et al. Tumor suppressor death-associated protein kinase attenuates inflammatory responses in the lung. Am J Respir Cell Mol Biol. 2012;46:313–22.

243. Bialik S, Bresnick AR, Kimchi A. DAP-kinase-mediated morphological changes are localization dependent and involve myosin-II phosphorylation. Cell Death Differ. 2004;11:631–44.

244. Harrison B, Kraus M, Burch L, Stevens C, Craig A, Gordon-Weeks P, et al. DAPK-1 binding to a linear peptide motif in MAP1B stimulates autophagy and membrane blebbing. J Biol Chem. 2008;283:9999–10014.

245. Fan X, Jin WY, Lu J, Wang J, Wang YT. Rapid and reversible knockdown of endogenous proteins by peptide-directed lysosomal degradation. Nat Neurosci. 2014;17:471–80.

246. Goodell DJ, Zaegel V, Coultrap SJ, Hell JW, Bayer KU. DAPK1 Mediates LTD by Making CaMKII/GluN2B Binding LTP Specific. Cell Reports. 2017;19:2231–43.

247. Pei L, Wang S, Jin H, Bi L, Wei N, Yan H, et al. A Novel Mechanism of Spine Damages in Stroke via DAPK1 and Tau. Cereb Cortex. 2015;25:4559–71.

248. Carlessi R, Levin-Salomon V, Ciprut S, Bialik S, Berissi H, Albeck S, et al. GTP binding to the ROC domain of DAP-kinase regulates its function through intramolecular signalling. EMBO Rep. 2011;12:917–23.

249. Widau RC, Jin Y, Dixon SA, Wadzinski BE, Gallagher PJ. Protein phosphatase 2A (PP2A) holoenzymes regulate death-associated protein kinase (DAPK) in ceramide-induced anoikis. J Biol Chem. 2010;285:13827–38.

250. Guenebeaud C, Goldschneider D, Castets M, Guix C, Chazot G, Delloye-Bourgeois C, et al. The dependence receptor UNC5H2/B triggers apoptosis via PP2A-mediated dephosphorylation of DAP kinase. Mol Cell. 2010;40:863–76.

251. Gozuacik D, Bialik S, Raveh T, Mitou G, Shohat G, Sabanay H, et al. DAP-kinase is a mediator of endoplasmic reticulum stress-induced caspase activation and autophagic cell death. Cell Death Differ. 2008;15:1875–86.

252. Shamloo M, Soriano L, Wieloch T, Nikolich K, Urfer R, Oksenberg D. Death-associated protein kinase is activated by dephosphorylation in response to cerebral ischemia. J Biol Chem. 2005;280:42290–9.

253. Xifró X, García-Martínez JM, Del Toro D, Alberch J, Pérez-Navarro E. Calcineurin is involved in the early activation of NMDA-mediated cell death in mutant huntingtin knock-in striatal cells. J Neurochem. 2008;105:1596–612.

254. Anjum R, Roux PP, Ballif BA, Gygi SP, Blenis J. The tumor suppressor DAP kinase is a target of RSK-mediated survival signaling. Curr Biol. 2005;15:1762–7.

255. Shiloh R, Bialik S, Kimchi A. Ser289 phosphorylation activates both DAPK1 and DAPK2 but in response to different intracellular signaling pathways. Cell Cycle. 2019;18:1169–76.

256. Marín I, van Egmond WN, van Haastert PJM. The Roco protein family: a functional perspective. FASEB J. 2008;22:3103–10.

257. Wang W-J, Kuo J-C, Ku W, Lee Y-R, Lin F-C, Chang Y-L, et al. The tumor suppressor DAPK is reciprocally regulated by tyrosine kinase Src and phosphatase LAR. Mol Cell. 2007;27:701–16.

258. Araki T, Shinoda S, Schindler CK, Quan-Lan J, Meller R, Taki W, et al. Expression, interaction, and proteolysis of death-associated protein kinase and p53 within vulnerable and resistant hippocampal subfields following seizures. Hippocampus. 2004;14:326–36.

259. Lin Y, Stevens C, Hupp T. Identification of a dominant negative functional domain on DAPK-1 that degrades DAPK-1 protein and stimulates TNFR-1-mediated apoptosis. J Biol Chem. 2007;282:16792–802.

260. Jin Y, Blue EK, Dixon S, Shao Z, Gallagher PJ. A death-associated protein kinase (DAPK)-interacting protein, DIP-1, is an E3 ubiquitin ligase that promotes tumor necrosis factor-induced apoptosis and regulates the cellular levels of DAPK. J Biol Chem. 2002;277:46980–6.

261. Lee Y-R, Yuan W-C, Ho H-C, Chen C-H, Shih H-M, Chen R-H. The Cullin 3 substrate adaptor KLHL20 mediates DAPK ubiquitination to control interferon responses. EMBO J. 2010;29:1748–61.

262. Jin Y, Blue EK, Gallagher PJ. Control of death-associated protein kinase (DAPK) activity by phosphorylation and proteasomal degradation. J Biol Chem. 2006;281:39033–40.

263. Zhang L, Nephew KP, Gallagher PJ. Regulation of death-associated protein kinase. Stabilization by HSP90 heterocomplexes. J Biol Chem. 2007;282:11795–804.

264. Lin Y, Henderson P, Pettersson S, Satsangi J, Hupp T, Stevens C. Tuberous sclerosis-2 (TSC2) regulates the stability of death-associated protein kinase-1 (DAPK) through a lysosome-dependent degradation pathway. FEBS J. 2011;278:354–70.

265. Lin Y, Stevens C, Harrison B, Pathuri S, Amin E, Hupp TR. The alternative splice variant of DAPK-1, s-DAPK-1, induces proteasome-independent DAPK-1 destabilization. Mol Cell Biochem. 2009;328:101–7.

266. Benderska N, Schneider-Stock R. Transcription control of DAPK. Apoptosis. 2014;19:298–305.

267. Martoriati A, Doumont G, Alcalay M, Bellefroid E, Pelicci PG, Marine J-C. *dapk1*, encoding an activator of a $p19^{ARF}$-p53-mediated apoptotic checkpoint, is a transcription target of p53. Oncogene. 2005;24:1461–6.

268. Xuan F, Huang M, Liu W, Ding H, Yang L, Cui H. Homeobox C9 suppresses Beclin1-mediated autophagy in glioblastoma by directly inhibiting the

transcription of death-associated protein kinase 1. Neuro-oncology. 2016;18:819–29.

269. Chen H-Y, Lin Y-M, Chung H-C, Lang Y-D, Lin C-J, Huang J, et al. miR-103/107 promote metastasis of colorectal cancer by targeting the metastasis suppressors DAPK and KLF4. Cancer Res. 2012;72:3631–41.

270. Su Y, Deng M-F, Xiong W, Xie A-J, Guo J, Liang Z-H, et al. MicroRNA-26a/Death-Associated Protein Kinase 1 Signaling Induces Synucleinopathy and Dopaminergic Neuron Degeneration in Parkinson's Disease. Biol Psychiatry. 2018.

271. Oueslati A. Implication of Alpha-Synuclein Phosphorylation at S129 in Synucleinopathies: What Have We Learned in the Last Decade? J Parkinsons Dis. 6:39–51.

272. Zalckvar E, Berissi H, Mizrachy L, Idelchuk Y, Koren I, Eisenstein M, et al. DAP-kinase-mediated phosphorylation on the BH3 domain of beclin 1 promotes dissociation of beclin 1 from Bcl-XL and induction of autophagy. EMBO Rep. 2009;10:285–92.

273. Zalckvar E, Berissi H, Eisenstein M, Kimchi A. Phosphorylation of Beclin 1 by DAP-kinase promotes autophagy by weakening its interactions with Bcl-2 and Bcl-XL. Autophagy. 2009;5:720–2.

274. Schumacher AM, Schavocky JP, Velentza AV, Mirzoeva S, Watterson DM. A calmodulin-regulated protein kinase linked to neuron survival is a substrate for the calmodulin-regulated death-associated protein kinase. Biochemistry. 2004;43:8116–24.

275. You M-H, Kim BM, Chen C-H, Begley MJ, Cantley LC, Lee TH. Death-associated protein kinase 1 phosphorylates NDRG2 and induces neuronal cell death. Cell Death Differ. 2017;24:238–50.

276. Lee TH, Chen C-H, Suizu F, Huang P, Schiene-Fischer C, Daum S, et al. Death-associated protein kinase 1 phosphorylates Pin1 and inhibits its prolyl isomerase activity and cellular function. Mol Cell. 2011;42:147–59.

277. Tian J-H, Das S, Sheng Z-H. Ca2+-dependent Phosphorylation of Syntaxin-1A by the Death-associated Protein (DAP) Kinase Regulates Its Interaction with Munc18. J Biol Chem. 2003;278:26265–74.

278. Kim BM, You M-H, Chen C-H, Suh J, Tanzi RE, Ho Lee T. Inhibition of death-associated protein kinase 1 attenuates the phosphorylation and amyloidogenic processing of amyloid precursor protein. Hum Mol Genet. 2016;25:2498–513.

279. Kang BN, Ahmad AS, Saleem S, Patterson RL, Hester L, Doré S, et al. Death-associated protein kinase-mediated cell death modulated by interaction with DANGER. J Neurosci. 2010;30:93–8.

280. Wu P-R, Tsai P-I, Chen G-C, Chou H-J, Huang Y-P, Chen Y-H, et al. DAPK activates MARK1/2 to regulate microtubule assembly, neuronal differentiation, and tau toxicity. Cell Death Differ. 2011;18:1507–20.

281. Eisenberg-Lerner A, Kimchi A. DAP kinase regulates JNK signaling by binding and activating protein kinase D under oxidative stress. Cell Death Differ. 2007;14:1908–15.

282. Omkumar RV, Kiely MJ, Rosenstein AJ, Min KT, Kennedy MB. Identification of a phosphorylation site for calcium/calmodulindependent protein kinase II in the NR2B subunit of the N-methyl-D-aspartate receptor. J Biol Chem. 1996;271:31670–8.

283. Strack S, McNeill RB, Colbran RJ. Mechanism and regulation of calcium/calmodulin-dependent protein kinase II targeting to the NR2B subunit of the N-methyl-D-aspartate receptor. J Biol Chem. 2000;275:23798–806.

284. Raveendran R, Devi Suma Priya S, Mayadevi M, Steephan M, Santhoshkumar TR, Cheriyan J, et al. Phosphorylation status of the NR2B subunit of NMDA receptor regulates its interaction with calcium/calmodulin-dependent protein kinase II. J Neurochem. 2009;110:92–105.

285. Lisman J, Schulman H, Cline H. The molecular basis of CaMKII function in synaptic and behavioural memory. Nat Rev Neurosci. 2002;3:175–90.

286. Roskoski R. ERK1/2 MAP kinases: structure, function, and regulation. Pharmacol Res. 2012;66:105–43.

287. Stevens C, Lin Y, Sanchez M, Amin E, Copson E, White H, et al. A germ line mutation in the death domain of DAPK-1 inactivates ERK-induced apoptosis. J Biol Chem. 2007;282:13791–803.

288. Gladding CM, Fan J, Zhang LYJ, Wang L, Xu J, Li EHY, et al. Alterations in Striatal-Enriched Protein Tyrosine Phosphatase (STEP) Expression, Activation and Downstream Signaling in Early and Late Stages of the YAC128 Huntington's Disease Mouse Model. J Neurochem. 2014;130:145–59.

289. Drubin DG, Kirschner MW. Tau protein function in living cells. J Cell Biol. 1986;103 6 Pt 2:2739–46.

290. Weingarten MD, Lockwood AH, Hwo SY, Kirschner MW. A protein factor essential for microtubule assembly. Proc Natl Acad Sci USA. 1975;72:1858–62.

291. Kim BM, You M-H, Chen C-H, Lee S, Hong Y, Hong Y, et al. Death-associated protein kinase 1 has a critical role in aberrant tau protein regulation and function. Cell Death Dis. 2014;5:e1237.

292. Lu PJ, Wulf G, Zhou XZ, Davies P, Lu KP. The prolyl isomerase Pin1 restores the function of Alzheimer-associated phosphorylated tau protein. Nature. 1999;399:784–8.

293. Zhou XZ, Kops O, Werner A, Lu PJ, Shen M, Stoller G, et al. Pin1-dependent prolyl isomerization regulates dephosphorylation of Cdc25C and tau proteins. Mol Cell. 2000;6:873–83.

294. Sultana R, Boyd-Kimball D, Poon HF, Cai J, Pierce WM, Klein JB, et al. Oxidative modification and down-regulation of Pin1 in Alzheimer's disease hippocampus: A redox proteomics analysis. Neurobiol Aging. 2006;27:918–25.

295. Butterfield DA, Poon HF, St Clair D, Keller JN, Pierce WM, Klein JB, et al. Redox proteomics identification of oxidatively modified hippocampal proteins in mild cognitive impairment: insights into the development of Alzheimer's disease. Neurobiol Dis. 2006;22:223–32.

296. Butterfield DA, Abdul HM, Opii W, Newman SF, Joshi G, Ansari MA, et al. Pin1 in Alzheimer's disease. J Neurochem. 2006;98:1697–706.

297. Nakamura K, Zhou XZ, Lu KP. Distinct functions of cis and trans phosphorylated tau in Alzheimer's disease and their therapeutic implications. Curr Mol Med. 2013;13:1098–109.

298. Biernat J, Gustke N, Drewes G, Mandelkow EM, Mandelkow E. Phosphorylation of Ser262 strongly reduces binding of tau to microtubules: distinction between PHF-like immunoreactivity and microtubule binding. Neuron. 1993;11:153–63.

299. Bingol B, Wang C-F, Arnott D, Cheng D, Peng J, Sheng M. Autophosphorylated CaMKIIalpha acts as a scaffold to recruit proteasomes to dendritic spines. Cell. 2010;140:567–78.

300. Hell JW. CaMKII: Claiming Center Stage in Postsynaptic Function and Organization. Neuron. 2014;81:249–65.

301. Velentza AV, Wainwright MS, Zasadzki M, Mirzoeva S, Schumacher AM, Haiech J, et al. An aminopyridazine-based inhibitor of a pro-apoptotic protein kinase attenuates hypoxia-ischemia induced acute brain injury. Bioorg Med Chem Lett. 2003;13:3465–70.

302. Okamoto M, Takayama K, Shimizu T, Ishida K, Takahashi O, Furuya T. Identification of death-associated protein kinases inhibitors using structure-based virtual screening. J Med Chem. 2009;52:7323–7.

303. Wilbek TS, Skovgaard T, Sorrell FJ, Knapp S, Berthelsen J, Strømgaard K. Identification and characterization of a small-molecule inhibitor of death-associated protein kinase 1. Chembiochem. 2015;16:59–63.

304. Henshall DC, Araki T, Schindler CK, Shinoda S, Lan J-Q, Simon RP. Expression of death-associated protein kinase and recruitment to the tumor necrosis factor signaling pathway following brief seizures. J Neurochem. 2003;86:1260–70.

305. Gao X, Wang H, Pollok KE, Chen J, Cohen-Gadol AA. Activation of death-associated protein kinase in human peritumoral tissue: A potential therapeutic target. J Clin Neurosci. 2015;22:1655–60.

306. Schumacher AM, Velentza AV, Watterson DM, Wainwright MS. DAPK catalytic activity in the hippocampus increases during the recovery phase in an animal model of brain hypoxic-ischemic injury. Biochim Biophys Acta. 2002;1600:128–37.

307. Tang N, Wu J, Zhu H, Yan H, Guo Y, Cai Y, et al. Genetic Mutation of GluN2B Protects Brain Cells Against Stroke Damages. Mol Neurobiol. 2018;55:2979–90.

308. Xiong W, Wu Y, Xian W, Song L, Hu L, Pan S, et al. DAPK1-ERK signal mediates oxygen glucose deprivation reperfusion induced apoptosis in mouse N2a cells. J Neurol Sci. 2018;387:210–9.

309. Liu S, Zhang N, Guo Y, Zhao R, Shi T, Feng S, et al. G-protein-coupled receptor 30 mediates rapid neuroprotective effects of estrogen via depression of NR2B-containing NMDA receptors. J Neurosci. 2012;32:4887–900.

310. Shu S, Zhu H, Tang N, Chen W, Li X, Li H, et al. Selective Degeneration of Entorhinal-CA1 Synapses in Alzheimer's Disease via Activation of DAPK1. J Neurosci. 2016;36:10843–52.

311. Duan D-X, Chai G-S, Ni Z-F, Hu Y, Luo Y, Cheng X-S, et al. Phosphorylation of tau by death-associated protein kinase 1 antagonizes the kinase-induced cell apoptosis. J Alzheimers Dis. 2013;37:795–808.

312. Li Y, Grupe A, Rowland C, Nowotny P, Kauwe JSK, Smemo S, et al. DAPK1 variants are associated with Alzheimer's disease and allele-specific expression. Hum Mol Genet. 2006;15:2560–8.

313. Hu Y, Cheng L, Zhang Y, Bai W, Zhou W, Wang T, et al. Rs4878104 contributes to Alzheimer's disease risk and regulates DAPK1 gene expression. Neurol Sci. 2017;38:1255–62.

314. Li S-X, Han Y, Xu L-Z, Yuan K, Zhang R-X, Sun C-Y, et al. Uncoupling DAPK1 from NMDA receptor GluN2B subunit exerts rapid antidepressant-like effects. Mol Psychiatry. 2018;23:597–608.

315. Schori H, Yoles E, Wheeler LA, Raveh T, Kimchi A, Schwartz M. Immune-related mechanisms participating in resistance and susceptibility to glutamate toxicity. Eur J Neurosci. 2002;16:557–64.

316. Tian J, Cheng J, Zhang J, Ye L, Zhang F, Dong Q, et al. Protection of Pyruvate against Glutamate Excitotoxicity Is Mediated by Regulating DAPK1 Protein Complex. PLoS One. 2014;9. doi:10.1371/journal.pone.0095777.

317. Wang X, Pei L, Yan H, Wang Z, Wei N, Wang S, et al. Intervention of death-associated protein kinase 1-p53 interaction exerts the therapeutic effects against stroke. Stroke. 2014;45:3089–91.

318. Yamamoto M, Hioki T, Ishii T, Nakajima-Iijima S, Uchino S. DAP kinase activity is critical for C2-ceramide-induced apoptosis in PC12 cells. European Journal of Biochemistry. 269:139–47.

319. Kishino M, Yukawa K, Hoshino K, Kimura A, Shirasawa N, Otani H, et al. Deletion of the kinase domain in death-associated protein kinase attenuates tubular cell apoptosis in renal ischemia-reperfusion injury. J Am Soc Nephrol. 2004;15:1826–34.

320. McQueen J, Ryan TJ, McKay S, Marwick K, Baxter P, Carpanini SM, et al. Pro-death NMDA receptor signaling is promoted by the GluN2B C-terminus independently of Dapk1. Elife. 2017;6.

321. He C, Stroink AR, Wang CX. The role of DAPK-BimEL pathway in neuronal death induced by oxygen-glucose deprivation. Neuroscience. 2014;258:254–62.

322. Bieging KT, Mello SS, Attardi LD. Unravelling mechanisms of p53-mediated tumour suppression. Nature Reviews Cancer. 2014;14:359–70.

323. Stocker H, Möllers T, Perna L, Brenner H. The genetic risk of Alzheimer's disease beyond APOE ε4: systematic review of Alzheimer's genetic risk scores. Translational Psychiatry. 2018;8:166.

324. Hainsworth AH, Allsopp RC, Jim A, Potter JF, Lowe J, Talbot CJ, et al. Death-associated protein kinase (DAPK1) in cerebral cortex of late-onset Alzheimer's disease patients and aged controls. Neuropathol Appl Neurobiol. 2010;36:17–24.

325. Lee M-S, Kao S-C, Lemere CA, Xia W, Tseng H-C, Zhou Y, et al. APP processing is regulated by cytoplasmic phosphorylation. J Cell Biol. 2003;163:83–95.

326. Ates-Alagoz Z, Adejare A. NMDA Receptor Antagonists for Treatment of Depression. Pharmaceuticals (Basel). 2013;6:480–99.

327. Zhang L, Xu T, Wang S, Yu L, Liu D, Zhan R, et al. NMDA GluN2B receptors involved in the antidepressant effects of curcumin in the forced swim test. Progress in Neuro-Psychopharmacology and Biological Psychiatry. 2013;40:12–7.

328. Miller OH, Yang L, Wang C-C, Hargroder EA, Zhang Y, Delpire E, et al. GluN2B-containing NMDA receptors regulate depression-like behavior and are critical for the rapid antidepressant actions of ketamine. eLife. 2014. doi:10.7554/eLife.03581.

329. Tizabi Y, Bhatti BH, Manaye KF, Das JR, Akinfiresoye L. Antidepressant-like effects of low ketamine dose is associated with increased hippocampal AMPA/NMDA receptor density ratio in female Wistar-Kyoto rats. Neuroscience. 2012;213:72–80.

330. Bayram-Weston Z, Stone TC, Giles P, Elliston L, Janghra N, Higgs GV, et al. Similar striatal gene expression profiles in the striatum of the YAC128 and HdhQ150 mouse models of Huntington's disease are not reflected in mutant Huntingtin inclusion prevalence. BMC Genomics. 2015;16. doi:10.1186/s12864-015-2251-4.

331. Fan MMY, Zhang H, Hayden MR, Pelech SL, Raymond LA. Protective up-regulation of CK2 by mutant huntingtin in cells co-expressing NMDA receptors. J Neurochem. 2008;104:790–805.

332. White E. The role for autophagy in cancer. J Clin Invest. 2015;125:42–6.

333. Pouladi MA, Hayden MR. Polyglutamine diseases and the risk of cancer. The Lancet Oncology. 2012;13:569–71.

334. Ji J, Sundquist K, Sundquist J. Cancer incidence in patients with polyglutamine diseases: a population-based study in Sweden. The Lancet Oncology. 2012;13:642–8.

335. McNulty P, Pilcher R, Ramesh R, Necuiniate R, Hughes A, Farewell D, et al. Reduced Cancer Incidence in Huntington's Disease: Analysis in the Registry Study. J Huntingtons Dis. 2018;7:209–22.

336. Cepeda C, Wu N, André VM, Cummings DM, Levine MS. The corticostriatal pathway in Huntington's disease. Prog Neurobiol. 2007;81:253–71.

337. Tyebji S, Hannan AJ. Synaptopathic mechanisms of neurodegeneration and dementia: Insights from Huntington's disease. Prog Neurobiol. 2017;153:18–45.

338. Estrada-Sánchez AM, Rebec GV. Role of cerebral cortex in the neuropathology of Huntington's disease. Front Neural Circuits. 2013;7. doi:10.3389/fncir.2013.00019.

339. Kemp JM, Powell TP. The structure of the caudate nucleus of the cat: light and electron microscopy. Philos Trans R Soc Lond, B, Biol Sci. 1971;262:383–401.

340. McGeorge AJ, Faull RLM. The organization of the projection from the cerebral cortex to the striatum in the rat. Neuroscience. 1989;29:503–37.

341. Buren C, Tu G, Parsons MP, Sepers MD, Raymond LA. Influence of cortical synaptic input on striatal neuronal dendritic arborization and sensitivity to excitotoxicity in corticostriatal coculture. J Neurophysiol. 2016;116:380–90.

342. Kaufman AM, Milnerwood AJ, Sepers MD, Coquinco A, She K, Wang L, et al. Opposing roles of synaptic and extrasynaptic NMDA receptor signaling in cocultured striatal and cortical neurons. J Neurosci. 2012;32:3992–4003.

343. Segal M, Greenberger V, Korkotian E. Formation of dendritic spines in cultured striatal neurons depends on excitatory afferent activity. Eur J Neurosci. 2003;17:2573–85.

344. Cheng C, Trzcinski O, Doering LC. Fluorescent labeling of dendritic spines in cell cultures with the carbocyanine dye "DiI." Front Neuroanat. 2014;8. doi:10.3389/fnana.2014.00030.

345. Bayram-Weston Z, Olsen E, Harrison DJ, Dunnett SB, Brooks SP. Optimising Golgi–Cox staining for use with perfusion-fixed brain tissue validated in the zQ175 mouse model of Huntington's disease. J Neurosci Methods. 2016;265:81–8.

346. Van Raamsdonk JM, Pearson J, Rogers DA, Lu G, Barakauskas VE, Barr AM, et al. Ethyl-EPA treatment improves motor dysfunction, but not neurodegeneration in the YAC128 mouse model of Huntington disease. Exp Neurol. 2005;196:266–72.

347. Van Raamsdonk JM, Pearson J, Bailey CDC, Rogers DA, Johnson GVW, Hayden MR, et al. Cystamine treatment is neuroprotective in the YAC128 mouse model of Huntington disease. J Neurochem. 2005;95:210–20.

348. Van Raamsdonk JM, Pearson J, Rogers DA, Bissada N, Vogl AW, Hayden MR, et al. Loss of wild-type huntingtin influences motor dysfunction and survival in the YAC128 mouse model of Huntington disease. Hum Mol Genet. 2005;14:1379–92.

349. van Dellen A, Welch J, Dixon RM, Cordery P, York D, Styles P, et al. N-Acetylaspartate and DARPP-32 levels decrease in the corpus striatum of Huntington's disease mice. Neuroreport. 2000;11:3751–7.

350. Bibb JA, Yan Z, Svenningsson P, Snyder GL, Pieribone VA, Horiuchi A, et al. Severe deficiencies in dopamine signaling in presymptomatic Huntington's disease mice. Proc Natl Acad Sci USA. 2000;97:6809–14.

351. Kolodziejczyk K, Raymond LA. Differential changes in thalamic and cortical excitatory synapses onto striatal spiny projection neurons in a Huntington disease mouse model. Neurobiol Dis. 2016;86:62–74.

352. Kassubek J, Juengling FD, Ecker D, Landwehrmeyer GB. Thalamic atrophy in Huntington's disease co-varies with cognitive performance: a morphometric MRI analysis. Cereb Cortex. 2005;15:846–53.

353. Miller BR, Bezprozvanny I. Corticostriatal circuit dysfunction in Huntington's disease: intersection of glutamate, dopamine and calcium. Future Neurol. 2010;5:735–56.

354. Wang N, Gray M, Lu X-H, Cantle JP, Holley SM, Greiner E, et al. Neuronal Targets of Mutant Huntingtin Genetic Reduction to Ameliorate Huntington's Disease Pathogenesis in Mice. Nat Med. 2014;20:536–41.

355. Estrada-Sánchez AM, Burroughs CL, Cavaliere S, Barton SJ, Chen S, Yang XW, et al. Cortical efferents lacking mutant huntingtin improve striatal neuronal activity and behavior in a conditional mouse model of Huntington's disease. J Neurosci. 2015;35:4440–51.

356. Sauvageot CM, Stiles CD. Molecular mechanisms controlling cortical gliogenesis. Current Opinion in Neurobiology. 2002;12:244–9.

357. Gomperts SN, Rao A, Craig AM, Malenka RC, Nicoll RA. Postsynaptically silent synapses in single neuron cultures. Neuron. 1998;21:1443–51.

358. Ferrante RJ. Mouse Models of Huntington's Disease and Methodological Considerations for Therapeutic Trials. Biochim Biophys Acta. 2009;1792:506–20.

359. Guo Z, Rudow G, Pletnikova O, Codispoti K-E, Orr BA, Crain BJ, et al. Striatal neuronal loss correlates with clinical motor impairment in Huntington's disease. Mov Disord. 2012;27:1379–86.

360. Lai TW, Zhang S, Wang YT. Excitotoxicity and stroke: identifying novel targets for neuroprotection. Prog Neurobiol. 2014;115:157–88.

361. Ikonomidou C, Turski L. Why did NMDA receptor antagonists fail clinical trials for stroke and traumatic brain injury? Lancet Neurol. 2002;1:383–6.

362. Shonesy BC, Jalan-Sakrikar N, Cavener VS, Colbran RJ. CaMKII: a molecular substrate for synaptic plasticity and memory. Prog Mol Biol Transl Sci. 2014;122:61–87.

363. Coultrap SJ, Vest RS, Ashpole NM, Hudmon A, Bayer KU. CaMKII in cerebral ischemia. Acta Pharmacol Sin. 2011;32:861–72.

364. Waldvogel HJ, Kim EH, Tippett LJ, Vonsattel J-PG, Faull RLM. The Neuropathology of Huntington's Disease. Curr Top Behav Neurosci. 2015;22:33–80.

365. Carroll JB, Lerch JP, Franciosi S, Spreeuw A, Bissada N, Henkelman RM, et al. Natural history of disease in the YAC128 mouse reveals a discrete signature of pathology in Huntington disease. Neurobiol Dis. 2011;43:257–65.

366. Mondragón-Rodríguez S, Trillaud-Doppia E, Dudilot A, Bourgeois C, Lauzon M, Leclerc N, et al. Interaction of Endogenous Tau Protein with Synaptic Proteins Is Regulated by *N* -Methyl-d-aspartate Receptor-dependent Tau Phosphorylation. Journal of Biological Chemistry. 2012;287:32040–53.

367. Sun S, Zhang H, Liu J, Popugaeva E, Xu N-J, Feske S, et al. Reduced synaptic STIM2 expression and impaired store-operated calcium entry cause destabilization of mature spines in mutant presenilin mice. Neuron. 2014;82:79–93.

368. Tang T-S, Tu H, Chan EYW, Maximov A, Wang Z, Wellington CL, et al. Huntingtin and huntingtin-associated protein 1 influence neuronal calcium signaling mediated by inositol-(1,4,5) triphosphate receptor type 1. Neuron. 2003;39:227–39.

369. Chen X, Wu J, Lvovskaya S, Herndon E, Supnet C, Bezprozvanny I. Dantrolene is neuroprotective in Huntington's disease transgenic mouse model. Mol Neurodegener. 2011;6:81.

370. Suzuki M, Nagai Y, Wada K, Koike T. Calcium leak through ryanodine receptor is involved in neuronal death induced by mutant huntingtin. Biochem Biophys Res Commun. 2012;429:18–23.

371. Rinaldi C, Wood MJA. Antisense oligonucleotides: the next frontier for treatment of neurological disorders. Nature Reviews Neurology. 2018;14:9–21.

372. Wu H, Lima WF, Zhang H, Fan A, Sun H, Crooke ST. Determination of the role of the human RNase H1 in the pharmacology of DNA-like antisense drugs. J Biol Chem. 2004;279:17181–9.

373. Evers MM, Toonen LJA, van Roon-Mom WMC. Antisense oligonucleotides in therapy for neurodegenerative disorders. Advanced Drug Delivery Reviews. 2015;87:90–103.

374. Hagedorn PH, Persson R, Funder ED, Albæk N, Diemer SL, Hansen DJ, et al. Locked nucleic acid: modality, diversity, and drug discovery. Drug Discovery Today. 2018;23:101–14.

375. Lee HJ, Boado RJ, Braasch DA, Corey DR, Pardridge WM. Imaging gene expression in the brain in vivo in a transgenic mouse model of Huntington's disease with an antisense radiopharmaceutical and drug-targeting technology. J Nucl Med. 2002;43:948–56.

376. Van Raamsdonk JM, Pearson J, Slow EJ, Hossain SM, Leavitt BR, Hayden MR. Cognitive dysfunction precedes neuropathology and motor abnormalities in the YAC128 mouse model of Huntington's disease. J Neurosci. 2005;25:4169–80.

377. Garcia-Miralles M, Geva M, Tan JY, Yusof NABM, Cha Y, Kusko R, et al. Early pridopidine treatment improves behavioral and transcriptional deficits in YAC128 Huntington disease mice. JCI Insight. 2. doi:10.1172/jci.insight.95665.

378. Sakamoto K, Karelina K, Obrietan K. CREB: a multifaceted regulator of neuronal plasticity and protection. J Neurochem. 2011;116:1–9.

379. Swayze EE, Siwkowski AM, Wancewicz EV, Migawa MT, Wyrzykiewicz TK, Hung G, et al. Antisense oligonucleotides containing locked nucleic acid improve potency but cause significant hepatotoxicity in animals. Nucleic Acids Res. 2007;35:687–700.

380. Geary RS, Norris D, Yu R, Bennett CF. Pharmacokinetics, biodistribution and cell uptake of antisense oligonucleotides. Advanced Drug Delivery Reviews. 2015;87:46–51.

381. Burdick AD, Sciabola S, Mantena SR, Hollingshead BD, Stanton R, Warneke JA, et al. Sequence motifs associated with hepatotoxicity of locked nucleic acid--modified antisense oligonucleotides. Nucleic Acids Res. 2014;42:4882–91.

382. Kasuya T, Hori S, Watanabe A, Nakajima M, Gahara Y, Rokushima M, et al. Ribonuclease H1-dependent hepatotoxicity caused by locked nucleic acid-modified gapmer antisense oligonucleotides. Scientific Reports. 2016;6:30377.

383. Burel SA, Hart CE, Cauntay P, Hsiao J, Machemer T, Katz M, et al. Hepatotoxicity of high affinity gapmer antisense oligonucleotides is mediated by RNase H1 dependent promiscuous reduction of very long pre-mRNA transcripts. Nucleic Acids Res. 2016;44:2093–109.

384. Seth PP, Siwkowski A, Allerson CR, Vasquez G, Lee S, Prakash TP, et al. Short antisense oligonucleotides with novel 2'-4' conformationaly restricted nucleoside analogues show improved potency without increased toxicity in animals. J Med Chem. 2009;52:10–3.

385. Kamola PJ, Maratou K, Wilson PA, Rush K, Mullaney T, McKevitt T, et al. Strategies for In Vivo Screening and Mitigation of Hepatotoxicity Associated with Antisense Drugs. Molecular Therapy - Nucleic Acids. 2017;8:383–94.

386. Shen W, De Hoyos CL, Migawa MT, Vickers TA, Sun H, Low A, et al. Chemical modification of PS-ASO therapeutics reduces cellular protein-binding and improves the therapeutic index. Nat Biotechnol. 2019;37:640–50.

387. Parker D, Ferreri K, Nakajima T, LaMorte VJ, Evans R, Koerber SC, et al. Phosphorylation of CREB at Ser-133 induces complex formation with CREB-binding protein via a direct mechanism. Mol Cell Biol. 1996;16:694–703.

388. Lee B, Butcher GQ, Hoyt KR, Impey S, Obrietan K. Activity-dependent neuroprotection and cAMP response element-binding protein (CREB): kinase coupling, stimulus intensity, and temporal regulation of CREB phosphorylation at serine 133. J Neurosci. 2005;25:1137–48.

389. Murphy DD, Segal M. Morphological plasticity of dendritic spines in central neurons is mediated by activation of cAMP response element binding protein. Proc Natl Acad Sci U S A. 1997;94:1482–7.

390. Pignataro A, Borreca A, Ammassari-Teule M, Middei S. CREB Regulates Experience-Dependent Spine Formation and Enlargement in Mouse Barrel Cortex. Neural Plast. 2015;2015. doi:10.1155/2015/651469.

391. Sargin D, Mercaldo V, Yiu AP, Higgs G, Han J-H, Frankland PW, et al. CREB regulates spine density of lateral amygdala neurons: implications for memory allocation. Front Behav Neurosci. 2013;7. doi:10.3389/fnbeh.2013.00209.

392. Middei S, Spalloni A, Longone P, Pittenger C, O'Mara SM, Marie H, et al. CREB selectively controls learning-induced structural remodeling of neurons. Learn Mem. 2012;19:330–6.

393. Tan Y-W, Hoffmann T, Bading H. Increasing levels of wild-type CREB up-regulates several activity-regulated inhibitor of death (AID) genes and promotes neuronal survival. BMC Neurosci. 2012;13:48.

394. Jiang H, Poirier MA, Liang Y, Pei Z, Weiskittel CE, Smith WW, et al. Depletion of CBP is directly linked with cellular toxicity caused by mutant huntingtin. Neurobiol Dis. 2006;23:543–51.

395. Cong S-Y, Pepers BA, Evert BO, Rubinsztein DC, Roos RAC, van Ommen G-JB, et al. Mutant huntingtin represses CBP, but not p300, by binding and protein degradation. Mol Cell Neurosci. 2005;30:560–71.

396. Lee J, Kim C-H, Simon DK, Aminova LR, Andreyev AY, Kushnareva YE, et al. Mitochondrial Cyclic AMP Response Element-binding Protein (CREB)

Mediates Mitochondrial Gene Expression and Neuronal Survival. J Biol Chem. 2005;280:40398–401.

397. Simpkins KL, Guttmann RP, Dong Y, Chen Z, Sokol S, Neumar RW, et al. Selective activation induced cleavage of the NR2B subunit by calpain. J Neurosci. 2003;23:11322–31.

398. Coultrap SJ, Freund RK, O'Leary H, Sanderson JL, Roche KW, Dell'Acqua ML, et al. Autonomous CaMKII mediates both LTP and LTD using a mechanism for differential substrate site selection. Cell Rep. 2014;6:431–7.

399. Yan X, Liu J, Ye Z, Huang J, He F, Xiao W, et al. CaMKII-Mediated CREB Phosphorylation Is Involved in Ca2+-Induced BDNF mRNA Transcription and Neurite Outgrowth Promoted by Electrical Stimulation. PLoS One. 2016;11. doi:10.1371/journal.pone.0162784.

400. Sun P, Enslen H, Myung PS, Maurer RA. Differential activation of CREB by Ca2+/calmodulin-dependent protein kinases type II and type IV involves phosphorylation of a site that negatively regulates activity. Genes Dev. 1994;8:2527–39.

401. Sotrel A, Williams RS, Kaufmann WE, Myers RH. Evidence for neuronal degeneration and dendritic plasticity in cortical pyramidal neurons of Huntington's disease: a quantitative Golgi study. Neurology. 1993;43:2088–96.

402. Marco S, Murillo A, Pérez-Otaño I. RNAi-Based GluN3A Silencing Prevents and Reverses Disease Phenotypes Induced by Mutant huntingtin. Mol Ther. 2018;26:1965–72.

403. Lu F, Shao G, Wang Y, Guan S, Burlingame AL, Liu X, et al. Hypoxia-ischemia modifies postsynaptic GluN2B-containing NMDA receptor complexes in the neonatal mouse brain. Exp Neurol. 2018;299 Pt A:65–74.

404. Akhtar MW, Sanz-Blasco S, Dolatabadi N, Parker J, Chon K, Lee MS, et al. Elevated glucose and oligomeric β-amyloid disrupt synapses via a common pathway of aberrant protein *S*-nitrosylation. Nature Communications. 2016;7:10242.

405. Lee C-T, Bendriem RM, Wu WW, Shen R-F. 3D brain Organoids derived from pluripotent stem cells: promising experimental models for brain development and neurodegenerative disorders. Journal of Biomedical Science. 2017;24:59.

406. Armañanzas R, Ascoli GA. Towards the automatic classification of neurons. Trends in Neurosciences. 2015;38:307–18.

407. Vasques X, Vanel L, Villette G, Cif L. Morphological Neuron Classification Using Machine Learning. Front Neuroanat. 2016;10. doi:10.3389/fnana.2016.00102.

408. Gratuze M, Cisbani G, Cicchetti F, Planel E. Is Huntington's disease a tauopathy? Brain. 2016;139:1014–25.

409. Gratuze M, Noël A, Julien C, Cisbani G, Milot-Rousseau P, Morin F, et al. Tau hyperphosphorylation and deregulation of calcineurin in mouse models of Huntington's disease. Hum Mol Genet. 2015;24:86–99.

410. Baskota SU, Lopez OL, Greenamyre JT, Kofler J. Spectrum of tau pathologies in Huntington's disease. Lab Invest. 2018.

411. Fernández-Nogales M, Cabrera JR, Santos-Galindo M, Hoozemans JJM, Ferrer I, Rozemuller AJM, et al. Huntington's disease is a four-repeat tauopathy with tau nuclear rods. Nature Medicine. 2014;20:881–5.

412. Kordasiewicz HB, Stanek LM, Wancewicz EV, Mazur C, McAlonis MM, Pytel KA, et al. Sustained therapeutic reversal of Huntington's disease by transient repression of huntingtin synthesis. Neuron. 2012;74:1031–44.

413. Southwell AL, Skotte NH, Kordasiewicz HB, Østergaard ME, Watt AT, Carroll JB, et al. In Vivo Evaluation of Candidate Allele-specific Mutant Huntingtin Gene Silencing Antisense Oligonucleotides. Mol Ther. 2014;22:2093–106.

414. Singh P, Ravanan P, Talwar P. Death Associated Protein Kinase 1 (DAPK1): A Regulator of Apoptosis and Autophagy. Front Mol Neurosci. 2016;9. doi:10.3389/fnmol.2016.00046.

415. Bermejo MK, Milenkovic M, Salahpour A, Ramsey AJ. Preparation of Synaptic Plasma Membrane and Postsynaptic Density Proteins Using a Discontinuous Sucrose Gradient. J Vis Exp. 2014. doi:10.3791/51896.

416. Lin R, Duan Z, Sun H, Fung M-L, Chen H, Wang J, et al. Kinesin-1 Regulates Extrasynaptic Targeting of NMDARs and Neuronal Vulnerability Toward Excitotoxicity. iScience. 2019;13:82–97.

417. Singh P, Talwar P. Exploring putative inhibitors of Death Associated Protein Kinase 1 (DAPK1) via targeting Gly-Glu-Leu (GEL) and Pro-Glu-Asn (PEN) substrate recognition motifs. J Mol Graph Model. 2017;77:153–67.

418. Temmerman K, de Diego I, Pogenberg V, Simon B, Jonko W, Li X, et al. A PEF/Y substrate recognition and signature motif plays a critical role in DAPK-related kinase activity. Chem Biol. 2014;21:264–73.